Identification of a gene signature as a predictive biomarker for successful MEK inhibition in colorectal cancer

Dissertation

zur Erlangung des Doktorgrades

der Naturwissenschaften

vorgelegt beim Fachbereich Biowissenschaften

der Johann Wolfgang von Goethe - Universität

in Frankfurt am Main

von

Ulrike Pfohl

aus Berlin

Frankfurt am Main 2021

(D30)

vom Fachbereich Biowissenschaften (FB15) der

Johann Wolfgang Goethe - Universität als Dissertation angenommen.

Dekan: Prof. Dr. Sven Klimpel

Gutachter: Prof. Dr. Michaela Müller-McNicoll

Prof. Dr. Ritva Tikkanen

Datum der Disputation: 16.09.2022

This study was conducted at the CELLphenomics GmbH in Berlin under supervision of Dr. Christian Regenbrecht.

To my parents.

I. TABLE OF CONTENTS

II. ZUSAMMENFASSUNG

Krebs ist eine lebensbedrohliche Krankheit mit steigender Inzidenz. Nach einer Prognose der WHO aus dem Jahr 2018 wird sich die Krebsinzidenz bis zum Jahr 2040 auf etwa 37 Millionen neue Krebsfälle verdoppeln.

Heutzutage basiert die klinische Behandlung von Krebs auf einer eher einheitlichen Strategie. Hierbei werden die meisten Krebserkrankungen nach wie vor durch eine chirurgische Therapie und eine anschließende adjuvante (ergänzende oder unterstützende) oder eine neoadjuvante (neue ergänzende) Chemotherapie auf der Grundlage recht strenger Leitlinien (S3-Leitlinien in Europa) behandelt. Dieser Ansatz hat insgesamt zu einem erheblichen Anstieg des progressionsfreien Überlebens und des Gesamtüberlebens bei vielen Betroffenen geführt. Dennoch gibt es viele Patienten, bei denen das Behandlungsschema nicht zu einer Verbesserung führt.

Ein Grund hierfür ist die intra-tumorale Heterogenität, welche das Vorhandensein von genetisch unterschiedlichen Zellsubpopulationen in einem Tumor beschreibt. Dies hat zur Folge, dass Krebspatienten aufgrund verschiedener Mutationsmuster unterschiedlich auf bestimmte Medikamente ansprechen.

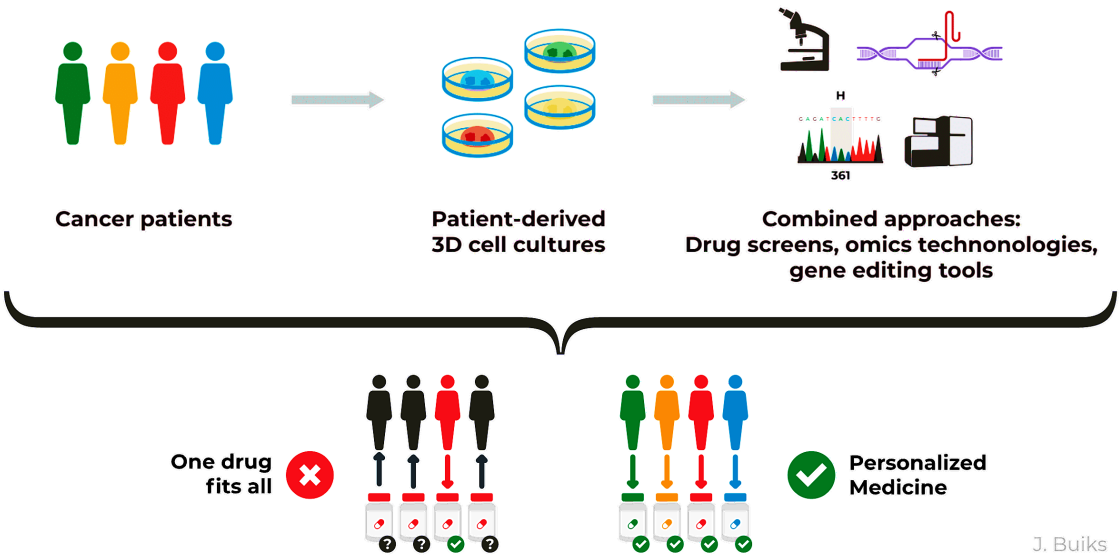

Die Heterogenität von Krebs erfordert einen personalisierten Behandlungsansatz.
Eine geeignete Kombination aus vom Patienten stammenden 3D-Zellkulturmodellen und verschiedenen *„Omics“*-Technologien liefert ein umfassendes Bild der biologischen Prozesse im Tumor eines Patienten und ermöglicht eine umfassende Analyse der Heterogenität innerhalb des Tumors auf mehreren Ebenen, einschließlich Genom-, Transkriptom-, Epigenom- und Metabolom-Ebene. Ein klinisch und molekular heterogener Tumor lässt sich wahrscheinlich nicht mit einem einzigen Medikament für alle erfolgreich behandeln, sondern erfordert einen personalisierten Ansatz, der speziell auf die individuellen Dysregulationen abzielt.

Die Therapie gegen Krebs sollte daher für Patienten so spezifisch und zielgerichtet wie möglich sein. Könnten Patienten im Voraus auf zuverlässige und aussagekräftige prognostische Krebs-Biomarker untersucht werden, die anzeigen, ob sie auf eine bestimmte Therapie ansprechen, würde dies nicht nur die Wahrscheinlichkeit einer erfolgreichen Behandlung erhöhen, sondern auch das Gesundheitssystem finanziell entlasten.

Die dritthäufigste diagnostizierte Krebsart weltweit ist das kolorektale Karzinom (engl. *colorectal cancer* = CRC). Die Haupttodesursache beim CRC ist eine metastasierende Erkrankung, die bei 20 % der Patienten auftritt und sich bei mehr als 30 % der Patienten schon im Frühstadium entwickelt. Die metastasierte Erkrankung ist in der Regel refraktär gegenüber der Erstlinientherapie. Dies spiegelt sich auch in dem unveränderten progressionsfreien Überleben der Patienten in den letzten zehn Jahren wider. Durch die Einführung zytotoxischer Wirkstoffe und zielgerichteter Therapien (Zweitlinientherapien) konnte die mediane Überlebenszeit auf mehr als 30 Monate gesteigert werden.
Die große Heterogenität bei CRC ist durch die Veränderungen in mehreren molekularen Signaltransduktionswegen, welche zelluläre Eigenschaften, wie die Proliferation oder die Apoptose beeinflussen, gekennzeichnet. Häufig betroffene Signalwege sind unter anderem der MAPK- und der TGF-β/BMP-Signalweg (MAPK = *mitogen-activated protein kinase*, TGF-β/BMP = *transforming growth factor-β/bone morphogenetic protein*).
Veränderungen im TGF-β/BMP-Signalweg, z.B. durch Mutationen im SMAD4-Gen (*mothers against decapentaplegic homolog 4*), sind nicht nur mit einem unterschiedlichen Therapieansprechen verbunden, sondern fördern auch Resistenzen gegenüber Chemotherapie. Darüber hinaus stehen sie mit einer höheren Rezidivrate in Verbindung. SMAD4-Mutationen kommen in bis zu 15 % der CRC vor und gehören damit zu den häufigsten krebsfördernden Mutationen. Daher besteht ein dringender Bedarf an therapeutischen Wirkstoffen, die spezifisch auf SMAD4-mutierte Tumore abzielen können.

Das Ziel der vorliegenden Arbeit war zum einen die Untersuchung der klinischen Relevanz und zum anderen der Prüfung der Eignung des SMAD4-Gens als potenziellen Biomarker in CRC.

Hierfür habe ich Geschwister-3D-Zellkulturen, die aus unterschiedlichen Regionen eines CRC-Tumors etabliert wurden, untersucht. Bei diesen Geschwister-3D-Zellkulturen handelt es sich um Patienten abgeleitete Organoide (engl. *patient-derived organoids* (PDO)), die die Architektur des Ursprungsgewebes zuverlässig rekapitulieren, sowie den genomischen Hintergrund und die intra-tumorale Heterogenität bewahren.

Die Geschwister-PDO-Modelle ($R1^{R361H}$ und $R4^{wt}$) teilen die häufigsten CRC-Mutationen, wie $KRAS^{G12D}$ (*kirsten rat sarcoma*), $PIK3CA^{H1047R}$ (*phosphatidylinositol-4,5-bisphosphate 3-kinase, catalytic subunit alpha*) und $TP53^{C242F}$ (*tumor protein 53*), unterschieden sich allerdings in einer $SMAD4^{R361H}$-Mutation und zeigten ein unterschiedliches Therapieansprechen. Die Einzelnukleotidvariante R361H des SMAD4-Gens gehört zu den häufigsten pathogenen Veränderungen bei verschiedenen Krebsarten, einschließlich CRC. Beide PDO-Modelle ($R1^{R361H}$ und $R4^{wt}$) zeigen dabei signifikante Unterschiede im Ansprechen auf Zweitlinientherapien mit MEK-Inhibitoren (Cobimetinib, Trametinib und Selumetinib), welche auf den MAPK-Signalweg abzielen.

MEK-Inhibitoren (MEK = *mitogen-activated protein kinase kinase*) sind für die Therapie des malignen Melanoms zugelassen und befinden sich zurzeit in klinischen Phase-III-Studien zur Behandlung von Patienten mit metastasiertem CRC. Sie sind antineoplastische Mittel, die die Funktion der MAPK-Kinasen MEK1 und MEK2 hemmen und somit die Phosphorylierung von Transkriptionsfaktoren verhindern. Dies führt zur Hemmung der Proliferation von Tumorzellen.

Zur Untersuchung, ob $SMAD4^{R361H}$ für die Sensitivität gegenüber MEK-Inhibitoren verantwortlich ist und deshalb einen möglichen Biomarker darstellen könnte, habe ich drei syngene, $SMAD4^{R361H}$-mutationtragende PDO-Modelle mithilfe der CRISPR/Cas9-Methode etabliert. Alle CRISPR-PDO-Modelle waren, wie auch $R1^{R361H}$, signifikant sensitiver gegenüber den getesteten MEK-Inhibitoren im Vergleich zu $R4^{wt}$. Ich habe damit gezeigt, dass die $SMAD4^{R361H}$-Mutation für die Empfindlichkeit gegenüber MEK-Inhibitoren in CRC-PDO-Modellen verantwortlich ist und ein prädiktiver Biomarker sein könnte.

Zur Überprüfung dieser Hypothese habe ich 62 CRC PDO-Modelle untersucht und mit den MEK-Inhibitoren behandelt. Alle Modelle, die eine pathogene Mutation im SMAD4-Gen aufwiesen (15 %), reagierten empfindlich auf Cobimetinib, 10 % der Modelle waren empfindlich gegenüber Trametinib und 8 % gegenüber Selumetinib.

Transkriptom- und Proteomdaten mittels RNA-Sequenzierung und DigiWest® stützen die Beobachtung, dass die MEK-Inhibition vor allem SMAD4^{R361H} PDO-Modelle betrifft. Die Hauptkomponentenanalyse zeigte, dass alle CRISPR-PDO-Modelle und R1^{R361H} sowohl in der unbehandelten als auch der behandelten Gruppe (Trametinib) im Vergleich zu R4^{wt} geclustert vorlagen. Die Analyse der Genanreicherung (*Gene enrichment analysis*) zeigte, dass die meisten der signifikant veränderten biologischen Prozesse in SMAD4^{R361H} PDO-Modelle jene waren, die mit der DNA-Replikation und der Zellzyklusprogression zusammenhängen. Die SMAD4^{wt}-PDO-Modelle wiederum zeigten in der digitalen Western Blot-Analyse (DigiWest®) eine Aktivierung im BMP-Signalweg, die für die Resistenz gegenüber MEK-Inhibitoren verantwortlich zu sein scheint. Das heißt, eine genetische Veränderung im BMP-Signalweg, über SMAD4 hinaus, könnte zur Sensitivität gegenüber MEK-Inhibitoren führen.

Ich habe vier Gene identifiziert, die im Zusammenhang mit dem BMP-Signalweg stehen und häufig mutiert auftreten. Hierbei handelt es sich um die Gene SMAD4, FBXW7 (*F-box/WD repeat-containing protein 7*), ARID1A (*AT-rich interactive domain-containing protein 1A*) und BMPR2 (*Bone morphogenetic protein receptor type II*), welche von mir als SFAB-Signatur zusammengefasst wurden. Klinische Daten zeigen, dass etwa 36 % der CRC Patienten mindestens eine pathogene Mutation in diesen Genen aufweisen.

Ich habe die CRC PDO-Modelle auf die SFAB-Signatur untersucht. Die Verteilung der Gene in den PDO-Modellen ist repräsentativ zu CRC Patientenkohorten aus klinischen Studien. Unter Verwendung einer Kontingenzanalyse habe ich eine signifikante Vorhersage der SFAB-Signatur auf die Sensitivität gegenüber den MEK-Inhibitoren Cobimetinib (95 %) und Selumetinib (70 %) gezeigt. Auch Trametinib zeigte einen ähnlichen Trend. Darüber hinaus wurden ausgewählte PDO-Modelle mit dem neuen, für Krebs zugelassenen MEK-Inhibitor Binimetinib getestet und sprachen in ähnlicher Weise an. Daher hat die SFAB-Signatur eine hohe Vorhersagekraft für das Ansprechen auf MEK-Inhibitoren und kann als prädiktives Biomarker-Panel verwendet werden.

Die derzeit klinisch verwendeten Krebs-Biomarker im CRC basieren auf dem Mutationsstatus von KRAS und BRAF, die bis zu 50 % und 10 % im CRC vorkommen und als krebsfördernde Gene bekannt sind. Die Untersuchung der molekularen Veränderungen bei CRC ergab, dass Mutationen im KRAS-Gen, das dem EGF-Rezeptor (*epidermal growth factor receptor*) im MAPK-Signalweg nachgeschaltet ist, eine Therapie

mit einem Anti-EGF-Rezeptor-Antikörper (z.B. Cetuximab) beeinträchtigen. Cetuximab ist daher nur für RAS-Wildtyp-Tumore relevant. Dennoch sprechen rund 40 % der Patienten mit RAS-Wildtyp-Status nicht auf diese Behandlung an. Ich habe eine zusätzliche Kontingenzanalyse durchgeführt, um zu untersuchen, ob der RAS-Status die Empfindlichkeit gegenüber MEK-Inhibition vorhersagen kann. Etwa 53 % der CRC PDO-Modelle tragen eine pathogene RAS-Mutation und ca. 10 % weisen eine pathogene BRAF-Mutation (*B-rapidly accelerated fibrosarcoma*) auf. Sowohl der RAS/RAF-Status allein als auch die Kombination des RAS/RAF-Status mit der SFAB-Signatur zeigten keine verbesserte Vorhersage der Empfindlichkeit gegenüber MEK-Inhibition.

Folglich habe ich eine neue RAS/RAF-unabhängige Biomarker-Signatur identifiziert, die mit hoher Wahrscheinlichkeit die Empfindlichkeit der MEK-Inhibition *in vitro* vorhersagt. Die SFAB-Signatur wurde im März 2021 patentiert und könnte als möglicher prädiktiver Biomarker für die Krebstherapie dienen. Damit wurde die Grundlage für eine spätere klinische Anwendung gelegt. Retrospektive klinische Studien an Tumorentitäten mit bekannten Mutationsstati sind geplant, um die neuartige SFAB-Signatur zu validieren. Prospektive klinische Studien sind erforderlich, damit Krebspatienten so bald wie möglich davon profitieren können.

III. SUMMARY

Despite all advancements in cancer research and clinical practice, cancer remains a life-threatening disease with an increasing incidence. According to a 2018 WHO forecast, cancer incidence will double to approximately 37 million new cancer cases by 2040.

Today, clinical management of cancer is based on a "one-fits-all" strategy. Most cancers are still treated by surgical therapy followed by adjuvant or neoadjuvant chemotherapy based on rather strict guidelines (S3 guidelines in Europe) which are based on studies of large cohorts of patients with the same tumor entity. While this approach has led to substantial increases in progression-free survival and overall patient survival, most patients do not benefit from the administered treatment regimen. One reason for this is intra-tumor heterogeneity, which results from clonal evolution between cancer cells and their environment. This means that cancer patients may respond differently to a particular drug due to the different mutation patterns of their tumor cells. Therefore, patients should be screened in advance for reliable cancer biomarkers that definitively predict whether they will respond to a particular therapy. This would increase the probability of a successful treatment.

Colorectal cancer (CRC) is the third most diagnosed cancer and the second leading cause of cancer deaths worldwide. The main cause of death in CRC is a metastatic disease, which is presented in 20 % of patients and eventually develops in more than 30 % of early-stage patients. Despite the significant increase (to more than 30 months) in median survival with the development of cytotoxic agents and the introduction of targeted therapy, the progression-free survival in the first-line setting has remained largely unchanged over the past decade.

The heterogeneity in CRC is characterized by alterations in multiple signaling pathways that affect cellular functions such as cell proliferation or apoptosis. Commonly affected signaling pathways include the mitogen-activated protein kinase (MAPK)- and the transforming growth factor-β/bone morphogenetic protein (TGF-β/BMP)-pathway.

Alterations in the TGF-β/BMP pathway, due to mutations in the SMAD4 gene (mothers against decapentaplegic homolog 4), are associated with different drug response and promote resistance to chemotherapy. In addition, they are associated with a higher recurrence rate.

SMAD4 is one of the most common cancer driver genes, and mutations occur in up to 15 % of CRC cases. Therefore, there is an urgent need for therapeutic agents that can specifically target SMAD4-mutated tumors.

The aim of the present study was the identification of the clinical relevance of the SMAD4 gene and the investigation of its suitability as a potential biomarker in CRC.

For this purpose, I investigated sibling patient-derived organoids (PDOs) derived from different regions of a chemo-naïve CRC tumor. PDOs are 3D cell cultures that reliably recapitulate the architecture of the tissue of origin, as well as preserve the genomic background and intra-tumor heterogeneity. The sibling PDOs ($R1^{R361H}$ and $R4^{wt}$) shared the most common CRC mutations, such as $KRAS^{G12D}$ (kirsten rat sarcoma), $PIK3CA^{H1047R}$ (phosphatidylinositol-4,5-bisphosphate 3-kinase, catalytic subunit alpha), and $TP53^{C242F}$ (tumor protein 53), but differed in a $SMAD4^{R361H}$ mutation and showed a different drug response. The single nucleotide variant R361H of the SMAD4 gene is among the most common pathogenic alterations in various cancers, including CRC.

The sibling PDOs showed significant differences in response to the MEK-inhibitors cobimetinib, trametinib, and selumetinib. MEK-inhibitors are antineoplastic agents that inhibit the function of MEK1 and MEK2, preventing phosphorylation of transcription factors, which leads to inhibition of tumor cell proliferation. MEK-inhibitors are approved for the treatment of malignant melanoma. Currently, they are in phase-III clinical trials for the treatment of patients with metastatic CRC.

To investigate whether $SMAD4^{R361H}$ is responsible for sensitivity to MEK-inhibitors, I established three syngeneic PDOs harboring a $SMAD4^{R361H}$ mutation using the CRISPR/Cas9 genome editing system. All CRISPR-PDOs were significantly more sensitive to the MEK-inhibitors, compared to $R4^{wt}$. I have shown that the $SMAD4^{R361H}$ mutation is responsible for sensitivity to MEK inhibition in CRC models and may be a predictive biomarker.

To test this hypothesis, I examined 62 CRC PDO models and treated them with the MEK-inhibitors cobimetinib, trametinib, and selumetinib. All models that had a pathogenic mutation or deletion in the SMAD4 gene (15 %) were sensitive to cobimetinib, 10 % of models were sensitive to trametinib, and 8 % were sensitive to selumetinib.

I performed transcriptome (RNA sequencing) and proteome analyses using the DigiWest® method to investigate the mechanism underlying MEK-inhibitor sensitivity.

DigiWest® is a Luminex® bead-based analysis that allows the simultaneous analysis of over 100 (phospho-)proteins. The transcriptome and proteome data support the observation that MEK inhibition primarily affects SMAD4^{R361H} PDOs. Furthermore, I have shown that activation of the BMP signaling pathway in organoids with wild-type SMAD4 appears to be responsible for resistance to MEK-inhibitors. Thus, a genetic alteration in the BMP signaling pathway, beyond SMAD4, could lead to sensitivity to MEK-inhibitors.

I identified four genes involved in the TGF-β/BMP signaling pathway that are frequently mutated in CRC and grouped them into the so-called SFAB-signature (SMAD4, FBXW7 (F-box/WD repeat-containing protein 7), ARID1A (AT-rich interactive domain-containing protein 1A), or BMPR2 (Bone morphogenetic protein receptor type II). Clinical data show that approximately 36 % of CRC patients have at least one pathogenic mutation in these genes.

I tested all 62 CRC PDO models and found a significant positive prediction for sensitivity to cobimetinib (95 %) and selumetinib (70 %) for the SFAB-signature. Trametinib and the newly approved MEK-inhibitor binimetinib showed a similar trend. Therefore, the SFAB-signature has high predictive power for response to MEK-inhibitors and could be used as a predictive biomarker panel.

The current clinically used biomarkers for CRC are based on the mutation status of driver genes KRAS and BRAF, which are present in up to 50 % and 10 % of CRC, respectively. Investigation of molecular alterations in CRC revealed that mutations in the KRAS gene, which is downstream of EGFR (epidermal growth factor receptor) in the MAPK-pathway, interfere with an anti-EGFR-antibody therapy (e.g., cetuximab). Therefore, cetuximab is only relevant for RAS wild-type tumors. However, approximately 40 % of patients with RAS wild-type status do not respond to this treatment.

About 53 % of CRC PDO models carry a pathogenic RAS mutation, about 10 % harbor a pathogenic BRAF mutation. Both, the RAS and RAF status alone as well as the combination of RAS and RAF status with SFAB-signature did not provide a better prediction of sensitivity to MEK inhibition.

Consequently, I identified a novel RAS/RAF-independent biomarker signature that is highly predictive of MEK inhibition sensitivity *in vitro*. The SFAB-signature was patented in March 2021 and could serve as a potential predictive biomarker for cancer therapy. This laid the groundwork for later clinical application. Retrospective clinical studies in tumor entities with known mutation status are planned to validate the novel SFAB-signature. Prospective clinical studies are required to allow cancer patients to benefit as soon as possible.

IV. LIST OF FIGURES

V. LIST OF TABLES

VI. LIST OF SUPPLEMANTARY FIGURES

VII. LIST OF SUPPLEMANTARY TABLES

VIII. ABBREVIATIONS

2D /3D	two-dimensional / three-dimensional
AACR	American Association for Cancer Research
AJCC	American Joint Committee on Cancer
APC	Adenomatous polyposis coli
ARID1A	AT-rich interactive domain-containing protein 1A
ATCC	American Type Culture Collection
BCA	Bicinchoninic Acid
bFGF	(basic) Fibroblast growth factor
BFP	Blue fluorescent protein
BMP	Bone morphogenetic protein
BMPR2	Bone morphogenetic protein receptor type II
bp	Base pair
BRAF	B-rapidly accelerated fibrosarcoma
°C	Degrees Celsius
Cas9	CRISPR-associated protein 9
CCLE	Cancer Cell Line Encyclopedia
CDKN1A	Cyclin dependent kinase inhibitor 1A
cDNA	Complementary deoxyribonucleic acid
CMS	Consensus molecular subtypes
CRC	Colorectal cancer
CRIS	CRC intrinsic subtypes
CRISPR	Clustered regularly interspaced short palindromic repeats
ctDNA	Circulating tumor DNA
d	Day
DAPI	4′,6-diamidino-2-phenylindole
dH_2O	Distilled water
DMEM	Dulbecco's modified Eagle's medium
dMMR	DNA mismatch Repair
DMSO	Dimethyl sulfoxide
DNA	Deoxyribonucleic acid
dNTP	Deoxyribonucleoside triphosphate
DPBS	Dulbecco's phosphate-buffered saline
E. coli	*Escherichia coli*
e.g.	*exempli gratia* (for example)
EGF	Epidermal growth factor receptor
EGFR	Epidermal growth factor receptor
EMA	European Medicines Agency
EMT	Epithelial-mesenchymal transition
ERK	Extracellular-signal related kinase
FACS	Fluorescence-activated cell sorting
FBS	Fetal bovine serum
FBXW7	F-box/WD repeat-containing protein 7
FDA	Food and Drug Administration
FOLFIRI	5-Fluorouracil + folinic acid + irinotecan
FOLFOX	5-Fluorouracil + folinic acid + oxaliplatin
5-FU	5-Fluoruracil + folinic acid + oxaliplatin
g	Gram
GAPDH	Glyceraldehyde 3-phosphate dehydrogenase
GDP	Guanosine diphosphate
GFP / eGFP	Green fluorescent protein / enhanced green fluorescent protein
GLOBOCAN	Global cancer statistics
GO	Gene ontology
GrB2	Growth factor receptor-bound protein 2
gRNA	Guide RNA
GSK	Glycogen synthase kinase 3
GTP	guanosine triphosphate
h	Hour(s)
HDR	Homology-directed repair
HEK	Human Embryonic Kidney
HER2	Human epidermal growth factor receptor 2
HGMD®	Human Gene Mutation Database
HRP	Horseradish peroxidase
i.e.	*id est* (= Latin for "that is")
i.v.	Intravenous
indel	Insertion or deletion
ITH	Intra-tumor heterogeneity
kDa	Kilo Dalton
KRAS	Kirsten rat sarcoma
l	Liter
LCC	Left-sided colon cancer
M	Molar
mAb	Monoclonal antibody
MAPK	Mitogen-activated protein kinase
MDC	Max-Delbrück-Centrum (Berlin, Germany)
MEK	Mitogen-activated protein kinase kinase
MH1	Mad Homology 1 domain
MH2	Mad Homology 2 domain
min	Minute
(m)RTK	(multi)-Receptor tyrosine kinases
MSI	Microsatellite instability
mTOR	Mammalian target of rapamycin
mut	Mutant allele(s)
n/ µ/ m	nano / micro / milli
NCBI	National Center for Biotechnology Information
NCCN	National Comprehensive Cancer Network
NCI	National Cancer Institute
NDA	New Drug Application
NEB	New England Biolabs
NMI	Natural and Medical Sciences Institute

NRAS	Neuroblastoma rat sarcoma
nt	Nucleotides
OS	Overall survival
P/S	Penicillin streptomycin
P4	Predictive, personalized, preventive, participatory
PAM	Protospacer-adjacent motif
PCR	Polymerase chain reaction
PDO	Patient-tumor organoid
PDX	Patient derived xenograft
PFS	Progression-free survival
pH	*potentia hydrogenii*
PIK3CA	Phosphatidylinositol-4,5-bisphosphate 3-kinase, catalytic subunit alpha
PVDF	Polyvinylidene fluoride
R361H	Arginine 361 Histidine
RCC	Right-sided colon cancer
RCF	Relative centrifugal force
RNA	Ribonucleic acid
ROCK	Rho-associated Kinase
RT	Room temperature
SDS	Sodium dodecyl sulphate
sec	Second(s)
SFAB	SMAD4, FBXW7, ARID1A, or BMPR2
sgRNA	Single guide ribonucleic acid
SH2/SH3	Src homology 2 / src homology 3
SMAD4	Mothers against decapentaplegic homolog 4
SOS	Son of sevenless
TAE	Tris/acetic acid/EDTA
TCGA	The Cancer Genome Atlas
TGF-β	Transforming growth factor beta
TP53	Tumor protein 53
u	Units
UCSC	University of California Santa Cruz
v	Volume
V	Volts
v/v	Volume per volume (volume concentration of a solution)
V600E	Valine 600 glutaminic acid
VEGF	Vascular endothelial growth factor
VEGFR	Vascular endothelial growth factor receptor
vs.	*versus*
W	Watt
w/v	Weight per volume (mass concentration of a solution)
WHO	World Health Organization
WNT	Wingless and Int-1 gene
wt	Wild-type allele(s)

1. INTRODUCTION

Despite all the advances in research and clinical practice, cancer remains a life-threatening disease with increasing incidence. In a forecast by the WHO in 2018, cancer incidence is expected to double to about 37 million new cancer cases by 2040 [1].

Today, the clinical management for cancer based on guideline therapies deduced from large cohort studies. Predictive, personalized, preventive, participatory (P4)-guided approaches [2] for cancer medicine are far from clinical routine. Following the strict guidelines (S3 guidelines in Europe), most solid cancers are still treated by surgical removal of the tumor combined with a (neo-)adjuvant chemotherapy, mainly to reduce the tumor size. While this approach has resulted in a significant prolongation of patients' progression-free survival (PFS) and overall survival (OS), only a few patients have improved treatment outcomes. A specific cancer treatment that may improve the disease burden of one patient may be ineffective in another patient diagnosed with the same type of cancer. The reason is that cancer is a multifactorial disease associated with a specific, almost individual mutational landscape. Although, sequencing technologies have led to a better understanding of the cancer genome, only 10-15 % of all cancer patients benefit from therapies guided by sequencing results [3].

The hallmarks of cancer cells include maintenance of proliferative signaling, evasion of growth suppressors, activation of invasion and metastasis, facilitation of replicative immortality, induction of angiogenesis, and resistance to cell death, which are primarily caused by genetic mutations [4]. These mutations occur in several genes (so-called "cancer driver genes"), whose mutated forms impair the homeostatic development of key cellular functions, such as cell division, cell replication, or cell metabolism, among others [5]. Alterations in cancer driver genes can lead to dysregulated transcriptional programs [6]. These dysregulated programs can render cancer cells highly dependent on specific regulators of gene expression than normal cells [6,7]. This phenomenon is called oncogene addiction and explains how cancers are dependent or "addicted" to one or a few driver genes to maintain both the malignant phenotype and cell survival [6,8]. Thus, reversing only one or a few of these abnormalities can inhibit cancer cell growth and, in some cases, lead to improved survival rates [8].

A major clinical challenge in oncology is that tumors are diagnosed relatively late in their development. By the time a typical neoplasm is diagnosed, it often already contains more than a billion cells, including normal cells in the supporting tissue (Figure 1) [9]. This heterogeneity is reflected on many levels, including cellularity, different genetic alterations, and different clinical behavior [10].

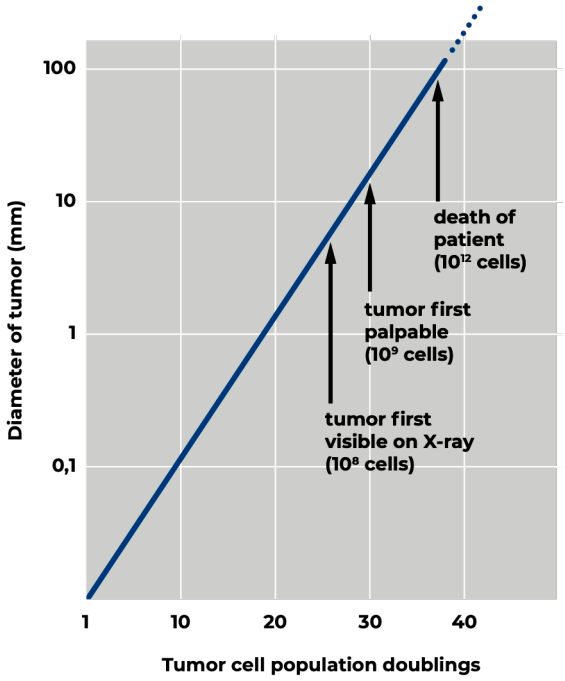

Figure 1: Increase in cell number in a typical human tumor.
The x-axis indicates the population doublings of cells in a tumor, while the y-axis represents the diameter of the tumor on a logarithmic scale (adapted from Albert et al., 1994 *[9]*).

P4-guided cancer medicine would be advantageous to be able to estimate the probability of successful treatment with a diagnostic procedure before the initial treatment and to tailor the medication individually to each patient. For instance, if patients could be screened in advance for cancer biomarkers that predict response to a particular therapy, this would not only increase the likelihood of successful treatment, but also reduce the number of unsuccessful treatments, thereby improving patients' quality of life and saving the healthcare system a lot of money. The stratification of patients based on the reliable and powerful prognostic or predictive biomarkers could significantly improve the outcomes and allow for individually tailored therapeutic approach or precision medicine.

1.1. Role of biomarkers in cancer therapy

The National Cancer Institute defines a biomarker as "a biological molecule found in blood, other body fluids, or tissues that is a sign of a normal or abnormal process or of a condition or disease", such as cancer (NCI, Table 16). Parameters used as biomarkers range from body temperature and body fluids, proteins (enzymes, receptors), nucleic acids (RNA, DNA), antibodies, and peptides, among others. Biomarkers can be used for patient assessment in a variety of clinical settings, including estimating the risk of disease, screening for cancers, distinguishing between benign and malignant conditions, or between one type of malignancy and another [11].

The US Food and Drug Administration (FDA) and the European Medicines Agency (EMA) rarely do approve drugs without a mode-of-action analysis based on predictive and prognostic biomarkers, respectively [12,13]. Both have also developed definitions for different categories of biomarkers. Prognostic biomarkers determine the probable course of disease while predictive biomarkers indicate the probable response to a particular drug [14] (Figure 2).

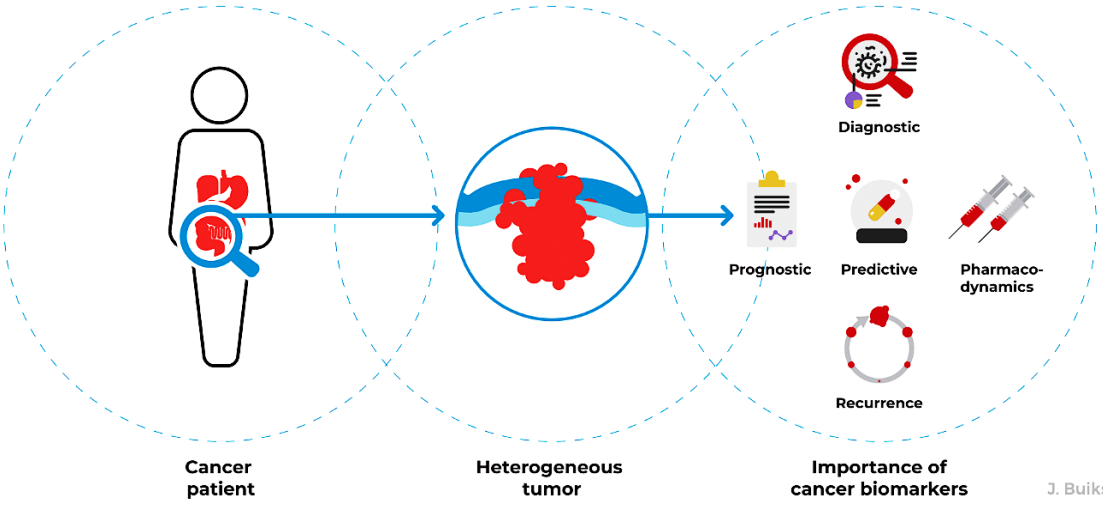

Figure 2: Importance of cancer biomarkers.
Biomarkers are cellular, biochemical, or molecular changes that are measurable in biological media such as human tissues, cells, or fluids *[15]*. Biomarkers have many potential applications in oncology, including risk assessment, screening, differential diagnosis, determining prognosis, predicting response to treatments, and monitoring disease progression.

1.2. Colorectal cancer

1.2.1. Incidence

Colorectal cancer (CRC) is third most diagnosed cancer and causes the second highest number cancer-related deaths worldwide [16] (Figure 3). The global burden of CRC is expected to increase by 60 %, to over 2.2 million new cases and 1.1 million annual deaths, by 2030. CRC incidence has steadily increased worldwide especially in developing nations [17].

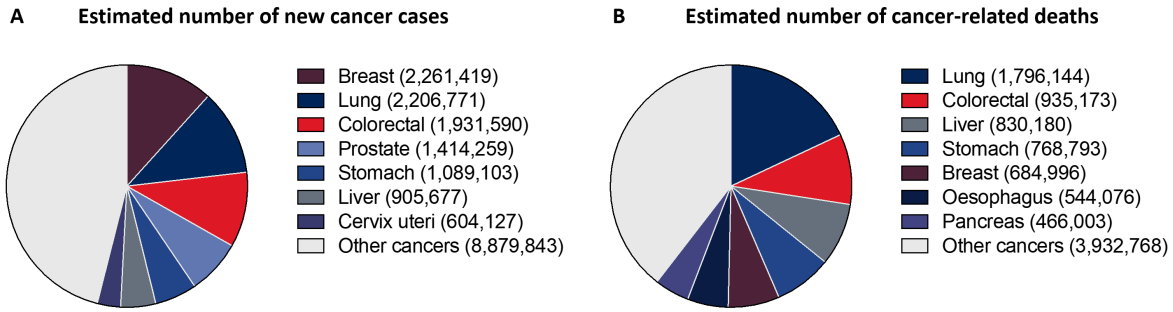

Figure 3: Estimates and proportion of new cancer cases and deaths from major cancer types in both sexes worldwide in 2020 [18].
(A) Estimated number of new cancer cases worldwide in 2020. (B) Estimated number of cancer-related deaths worldwide in 2020 (source: Global Burden of Disease Study (GLOBOCAN) 2020).

1.2.2. Colorectal cancer carcinogenesis

CRC is a heterogeneous disease that arises from the glandular epithelial cells of the colon and develops when certain cells of the epithelium acquire a series of genetic or epigenetic alterations [19] that give them a selective advantage which can develop a carcinoma and metastasize over decades [20].

CRC can develop from one or a combination of three different mechanisms, namely chromosomal instability (CIN), CpG island methylator phenotype (CIMP), and microsatellite instability (MSI) [21].

The classical CIN pathway begins with an inactivating mutation of the APC (adenomatous polyposis coli) tumor suppressor gene leading to an hyperactivation of the WNT-pathway (Wingless and Int-1 genes), followed by mutational activation of the oncogene KRAS (kirsten rat sarcoma) [22–24].

Subsequent malignant transformation is driven by additional mutations in TP53 (tumor protein 53), SMAD2/4 (mothers against decapentaplegic homologs 2/4) and PIK3CA

(catalytic subunit p110α of phosphoinositide 3-kinase) [24–27]. CIN is the most common genomic instability, comprising 50 - 85 % of all CRCs [28].

The CIMP pathway is characterized by hypermethylation of the promoter of several tumor suppressor genes, such as MGMT (O-6-methylguanine-DNA methyltransferase) and MLH1 (mutL homolog 1), often associated with BRAF (B-rapidly accelerated fibrosarcoma) mutation and MSI [29]. Approximately 35 - 40 % of sporadic CRCs, i.e., without genetic predisposition or family history, are CIMP-positive [28].

The MSI pathway involves inactivation of genetic alterations in short repetitive sequences that occur in DNA mismatch repair (MMR) genes [30,31]. MSI tumors account for 15 % of CRC [32] and are commonly associated with proximal colon and poor differentiation but have a better prognosis [33]. The three mechanisms often overlap in CRC (Figure 4).

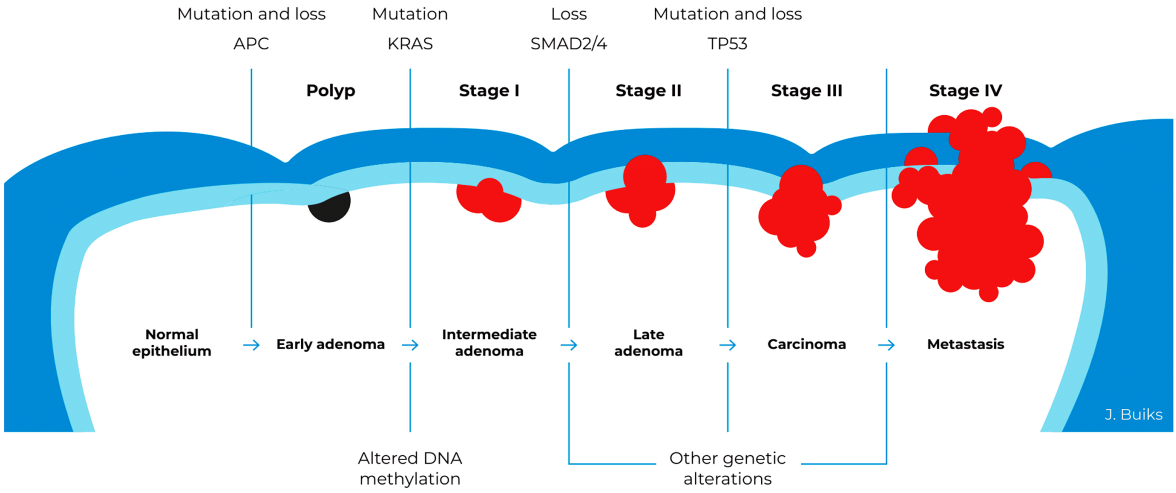

Figure 4: Colorectal cancer (CRC) stages and the classical carcinogenesis caused by driver genes.
Progression from normal epithelium through adenoma to CRC is characterized by accumulation of genetic abnormalities *[34]*. Early adenoma starts with a polyp. Intermediate adenoma (stage I) is present in several cell layers, but there is no breakthrough of the entire intestinal wall. In the late adenoma (stage II), the tumor has grown throughout the entire intestinal wall but has not spread to local lymph nodes. A carcinoma (stage III) spreads to local lymph nodes, but not to other organs. In stage IV metastases occur in other organs (e.g., liver or lung). A mutation in the APC tumor suppressor gene is the initiation event, followed by the sequential accumulation of other epigenetic and genetic changes that result in the progression from a normal cell to a metastatic tumor *[35]*. (APC = adenomatous polyposis coli, KRAS = kirsten rat sarcoma, SMAD2/4 = mothers against decapentaplegic homolog 2/4, TP53 = tumor protein 53).

1.2.3. Staging and grading of colorectal cancer

CRC is staged using tumor/node/metastasis (TNM) classification and staging system. In this system, stages are assigned based on the characteristics of the primary tumor (T) and the extent of regional lymph node involvement (N) and distant metastasis (M) [36]. The staging of CRC is further standardized by the WHO (World Health Organization) as shown in Table 1.

Table 1: Overview of colorectal cancer stages.
(American Joint Committee on Cancer. Chapter 20 - Colon and Rectum. In: AJCC Cancer Staging Manual. 8th ed. New York, NY: Springer; 2017.)

Stage	Description
Carcinoma in situ	Early adenoma: the cancer affects only the mucosa of the colon or rectum and is confined to one or more polyps.
I	Stage I CRC affects more than just the inner lining of the colon. The polyp has developed into a tumor and invades the wall of the colon or rectum.
II	Stage II CRC has spread beyond the colon to the tissue surrounding the colon, but not to lymph nodes.
III	Stage III CRC has spread outside the intestine to the lymph nodes. At this stage, the cancer has not yet spread to other organs in the body.
IV	Stage IV CRC has spread to other organs of the body such as the lungs or liver.

The grading of CRC indicates how closely the cancer resembles normal intestinal tissue when seen under the microscope [37]. The scale for grading CRC ranges from G1 (the cancer resembles normal intestinal tissue) to G4 (the cancer has an extremely abnormal appearance) [38]. The grade is often simplistically described as "low-grade" (G1 or G2) or "high-grade" (G3 or G4) [38]. Low-grade cancers tend to grow and proliferate more slowly than high-grade cancers [37].

1.2.4. Current biomarkers clinically used in colorectal cancer

Recently, new guidelines have been established for the investigation of molecular biomarkers in CRC tumor tissue to support disease prognosis, surveillance, and treatment [39]. Most of the currently used biomarkers are based on the mutational status of genes known to play a role in CRC carcinogenesis (KRAS, NRAS, BRAF) or are associated with defects in the DNA mismatch repair (MMR) system (MSI status) [39] (Table 2).

Table 2: Current clinical used molecular biomarkers in colorectal cancer (CRC) adopted from Koncina et al. [39].
(BRAF = B-rapidly accelerated fibrosarcoma, EGRF = epidermal growth factor receptor, 5-FU = 5-Fluorouracil, FOLFOX = 5-FU + folinic acid + oxaliplatin, KRAS = kirsten rat sarcoma, MSI = microsatellite instability, NRAS = neuroblastoma rat sarcoma).

Biomarker	Prevalence	Prognostic value	Predictive value		References
			Non-Metastatic	Metastatic	
MSI status	All CRC: 15 % Stage II/III: 15 % Stage IV: 4.5 %	Increased overall survival in stage II	X 5-FU monotherapy (stage II) ✓ FOLFOX (stage III)	✓ Immunotherapy	[31,33,40,41]
KRAS / NRAS mutation	45 %	Poor prognosis	No impact on treatment	X Anti-EGFR therapy	[42–53]
BRAF mutation	7- 10 %	Poor prognosis	Currently not impact on treatment	X Anti-EGFR therapy (conflicting data) ✓ Combi therapy: Anti-BRAF/Anti-EGFR	[54–58]

Benefit: ✓ ; No benefit: X

1.2.5. Mutational status of RAS and RAF in colorectal cancer

In CRC, KRAS mutations are present in more than 40 % of metastatic tumors and approximately 15-37 % of early-stage tumors [42]. KRAS acts as a central element in the mitogen-activated protein kinases (MAPK)-pathway (Figure 5) that regulates physiological processes, such as cell proliferation, differentiation, survival, and apoptosis [59].

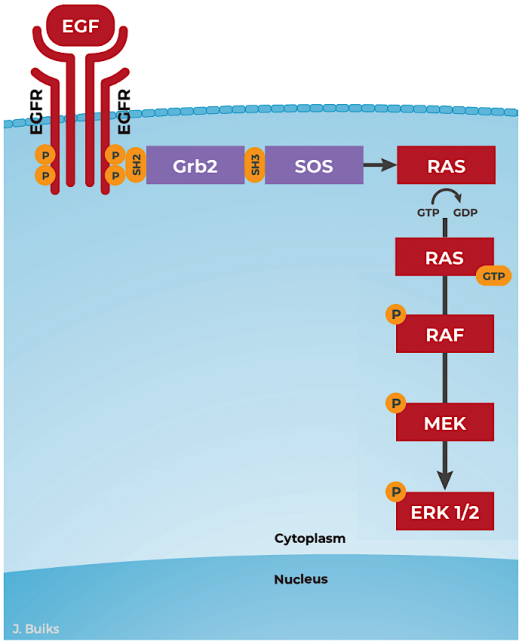

Figure 5: Schematic representation of the MAPK signaling pathway.
Binding of epidermal growth factor (EGF) activates epidermal growth factor receptor (EGFR) and provides docking sites for the SH2 (src homology 2) domain-containing adaptor protein Grb2 (growth factor receptor-bound protein 2). SOS (son of sevenless) is coupled to the receptor via the SH3 (src homology 3) domain, allowing it to activate (K)RAS (kirsten rat sarcoma) by facilitating exchange of GDP to GTP. GTP-bound RAS activates the RAF (rapid accelerated fibrosarcoma)-MEK (MAPK/ERK kinase)-ERK (extracellular signal-regulated kinase) kinase cascade. Phosphorylated ERK migrates to the nucleus and activates transcription factors such as ATF (activating transcription factor), leading to the expression of target genes *[60]*.

Other components of this pathway that can confer sustained signaling activity upon mutation include NRAS (neuroblastoma RAS viral oncogene homolog) and BRAF (B-rapidly accelerated fibrosarcoma), which are mutated in up to 12 % and 6 - 10 % of metastatic CRC, respectively [43,60].

BRAF-activating mutations most frequently occur in codon 600 (BRAF p.V600), which represents almost 90 % of all BRAF mutations [54] and are often associated with reduced overall survival in stage III and IV CRC [55]. Until recently, BRAF p.V600 mutation status testing was exclusively a prognostic marker for stage III-IV CRC, with little impact on treatment decisions [61]. For this reason, the National Comprehensive Cancer Network (NCCN) guidelines recommend routine testing of BRAF mutation status in advanced metastatic CRC [62].

1.2.6. Targeted therapy in colorectal cancer

In contrast to systemic (chemo)therapies, targeted cancer therapeutics aim to selectively act on aberrantly expressed or folded key proteins of the tumor ideally sparing normal cells and thus severe side effects on the patient [63,64].

Molecularly targeted agents have been included as standard-of-care treatment for CRC patients in combination with conventional fluoropyrimidine-based chemotherapy [65] (Figure 6).

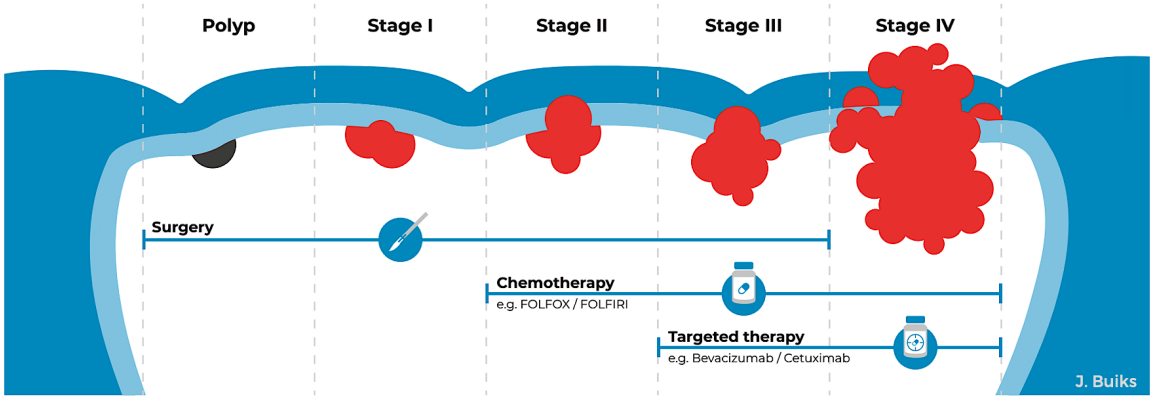

Figure 6: Therapy of colorectal cancer depending on stage.
Polyps and colorectal cancer (CRC) stage I-III are treated with surgery; stage II-III usually include chemotherapy with FOLFOX (5-Fluorouracil + folinic acid + oxaliplatin) or FOLFIRI (5-Fluorouracil + folinic acid + irinotecan); stage III might include additional targeted agents, such as bevacizumab (vascular endothelial growth factor (VEGF)-inhibitor) or cetuximab (epidermal growth factor receptor (EGFR)-inhibitor). For CRC stage IV, surgery is contraindicated, chemotherapy alone, similar to stage III, is used.

Targeting the MAPK-pathway has shown promising results in multiple cancer types, including CRC [66]. Monoclonal antibodies targeting the MAPK-pathway by blocking the epidermal growth factor receptor (EGFR) (e.g., cetuximab and panitumumab) or angiogenesis by blocking the vascular endothelial growth factor/receptor (VEGF/VEGFR) (e.g., bevacizumab and ramucirumab) (Figure 7) prolonged median survival up to 30 months when given concurrently with chemotherapy to CRC patients [67,68].

Although, the phase III CRYSTAL trial showed that cetuximab in combination with the chemotherapeutic regimen FOLFIRI (5-Fluorouracil + folinic acid + irinotecan) resulted in better median progression-free survival (PFS) (8.9 vs. 8 months) than FOLFIRI alone, the overall survival (OS) was not significantly different [45]. Moreover, several trials evaluating cetuximab in combination with FOLFOX (5-Fluorouracil + folinic acid + oxaliplatin) in unstratified cohorts of metastatic CRC patients failed to significantly improve PFS and OS [46,47,69]. It was shown that only 10–20 % of CRC patients are responsive to anti-EGFR treatment [48].

Examination of molecular alterations indicated that mutations in KRAS interfered with anti-EGFR therapy [49–51]. Therefore, cetuximab can only act in RAS wild-type tumors [45,52,53] – an important discovery for the CRC therapy.

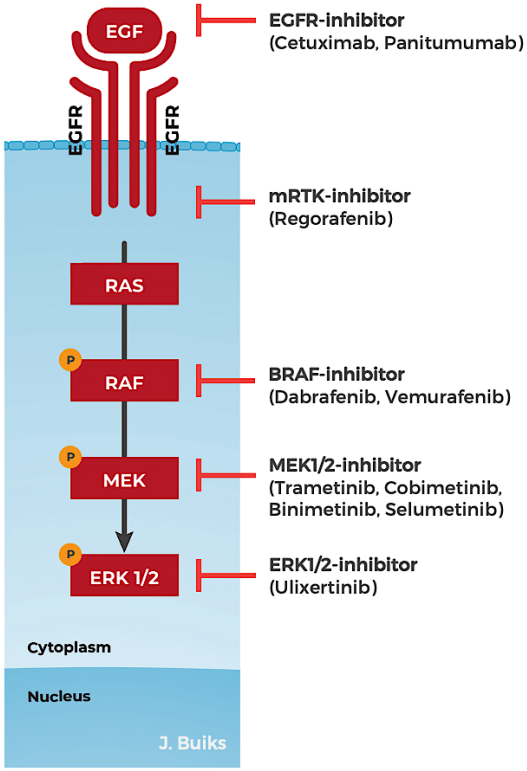

Figure 7: Schematic representation of the MAPK -pathway and targeted therapeutics.
(BRAF = B-rapidly accelerated fibrosarcoma, EGRF = epidermal growth factor receptor, ERK = extracellular-signal related kinase, (K)RAS = Kirsten rat sarcoma, MEK = mitogen-activated protein kinase kinase, mRTK = multi-receptor tyrosine kinases).

Following the success of cetuximab, other small molecules, biosimilars and monoclonal antibodies were invented and taken into the clinic, such as mitogen-activated protein kinase kinase (MEK)-inhibitors. MEK-inhibitors are small molecules that target the MAPK signaling pathway downstream of RAS inhibiting cell proliferation and inducing apoptosis [70]. They have the potential in clinical use for cancer treatment, especially for those cancers induced by RAS/RAF dysfunction [70]. Almost all major pharma companies have invested big efforts to develop highly specific and potent MEK1/2-inhibitors, which have been or currently are evaluated in clinical trials [70]. Therefore, tremendous efforts have been made in the past decades to develop highly specific and potent MEK1/2-inhibitors, which have been evaluated in clinical trials [71]. MEK-inhibitors have shown promising results in combination with BRAF-inhibitors for patients with unresectable or metastatic melanoma with common $BRAF^{V600E}$ or $BRAF^{V600K}$ mutations [72,73].

Despite the critical role of MEK in RAS- and/or RAF-mediated carcinogenesis, only three MEK-inhibitors have been approved for clinical use in cancer patients in the U.S. and Europe in the last decade: trametinib [74], cobimetinib [75] and binimetinib [76]. Another MEK-inhibitor, selumetinib [77], also demonstrated synergistic growth suppression and delay in the emergence of resistance when combined with BRAF-inhibitors and has been clinically approved for melanoma [78–81].

Based on the promising results of MEK-inhibitors in skin cancer, researchers are actively engaged in the development of MEK-inhibitors to expand their use to other invasive cancer indications, such as CRC. It was previously reported that MEK inhibition suppress cell proliferation and induce apoptosis in CRC in patient-derived xenograft models and CRC cell lines [82,83]. Currently, MEK-inhibitors are in a phase III study for the treatment of patients suffering from $BRAF^{V600E}$-mutated metastatic CRC and have already shown a beneficial effect [61].

1.2.7. TGF-β and BMP signaling in colorectal cancer

The transforming growth factor-β / bone morphogenetic protein (TGF-β/BMP)-pathway regulates the adhesion-dependent growth behavior of cells, which has an influence on wound healing and inflammation processes, cell differentiation and apoptosis [84,85]. In the malignant transformation of cells, it initiates cancer progression [86].

TGF-β has a dual role in tumor development. TGF-β acts as a tumor suppressor in normal epithelial cells and in the early stages of tumor progression [84]. In advanced cancers, the growth inhibitory function of TGF-β is selectively lost and TGF-β induces many activities leading to cancer cell growth, invasion, and metastasis [87]. TGF-β influences tumor growth directly (intrinsic effect) or indirectly (extrinsic effect) by promoting epithelial-mesenchymal transition (EMT), blocking immune response against tumor, activating tumor-associated fibrosis, and promoting angiogenesis [88,89].

When the TGF-β-pathway is activated, the TGF-β type I/II receptor (TGF-βRI/ TGF-βRII) complex phosphorylates SMAD2 and SMAD3 [90] while the other R-SMADs SMAD1/5/8, participate in the BMP-pathway, after being phosphorylated by the BMP type I/II receptor (BMPR I/BMPR II) complex [91] (Figure 8).

The phosphorylated R-SMADs usually form a heteromeric complex with SMAD4 (co-SMAD), and translocate into the nucleus, where they activate or repress gene expression in conjunction with other transcription factors, transcriptional coactivators or corepressors [92,93], such as c-JUN (JUN proto-oncogene, activator portein-1 (AP-1) transcription factor subunit) [94] or MYC (myelocytomatosis, proto-oncogene) [95] (Figure 8).

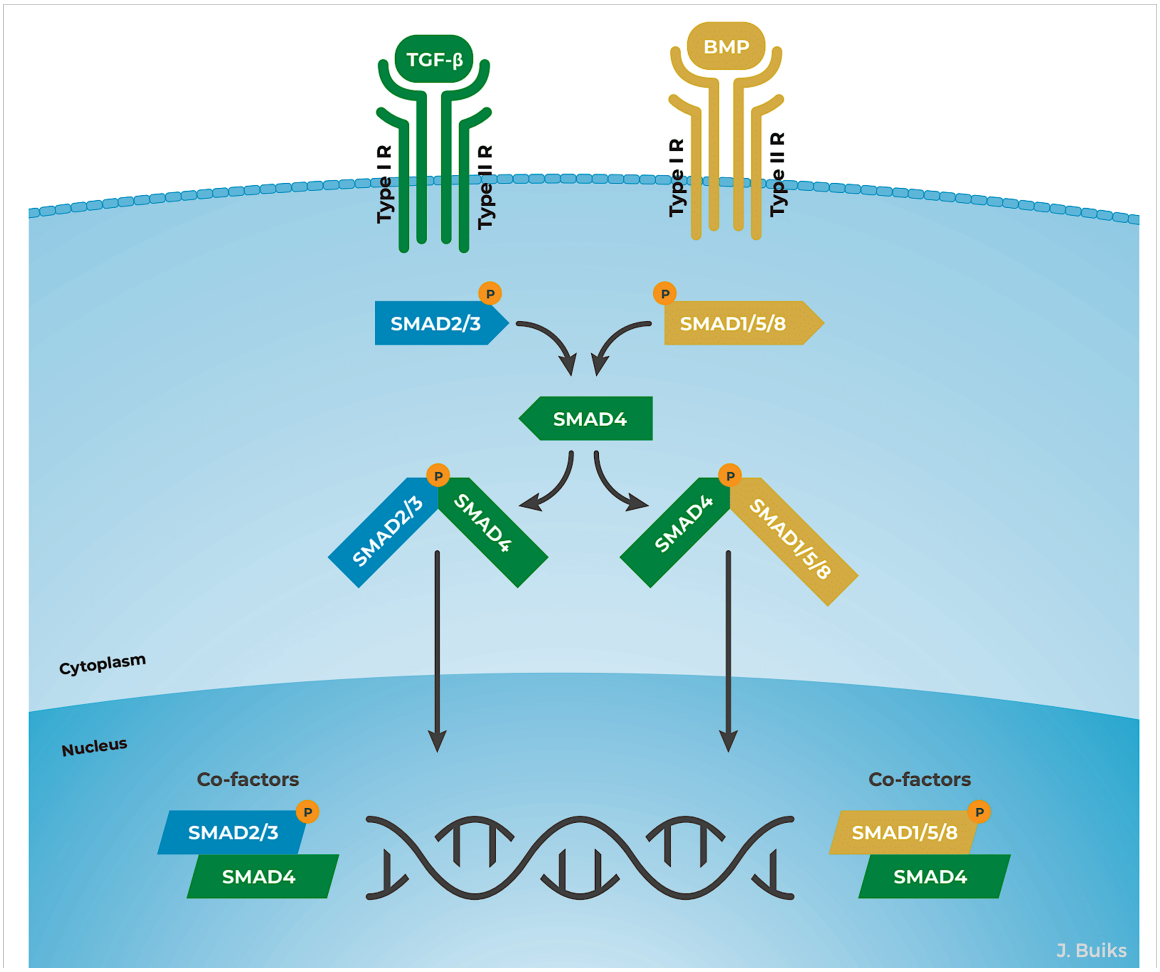

Figure 8: Schematic representation of TGF-β/BMP signaling pathway.
After ligand binding to type II receptors, they form a heterotetrametric complex with type I receptors, which then phosphorylate receptor-activated R-SMADs (for the TGF-β arm SMAD2/3 and for the BMP arm SMAD1/5/8). R-SMADs form a complex with the co-SMAD, SMAD4, and migrate into the nucleus. TGF-β can also induce noncanonical signaling pathways such as phospho-inositide-3'-kinase (PI3K), mitogen-activated protein kinase (MEK/ERK), and small GTPase (RhoA), which can lead to activation of the other transcription factors that act as cofactors for the SMAD complexes. Together, the transcription co-factors and SMADs can regulate the expression of various genes by either inducing or repressing their expression *[90–92]*.

Role of SMAD4 in colorectal cancer

Out of all members of the SMAD (mothers against decapentaplegic homolog 4) family, SMAD4 is the most frequently mutated gene in different cancer types such as pancreatic cancer (~20 %), CRC (~15 %), and stomach cancer (~10 %) [86]. Mutations in SMAD2 and SMAD3 are found in approximately 5 % of CRC patients respectively [96–98].

SMAD4 mutations have previously been shown to associate with distant metastases and decreased overall survival in CRC [99–103] (Figure 9). Moreover, functional loss of SMAD4 promotes chemoresistance in multiple cancer types, including CRC [86,102].

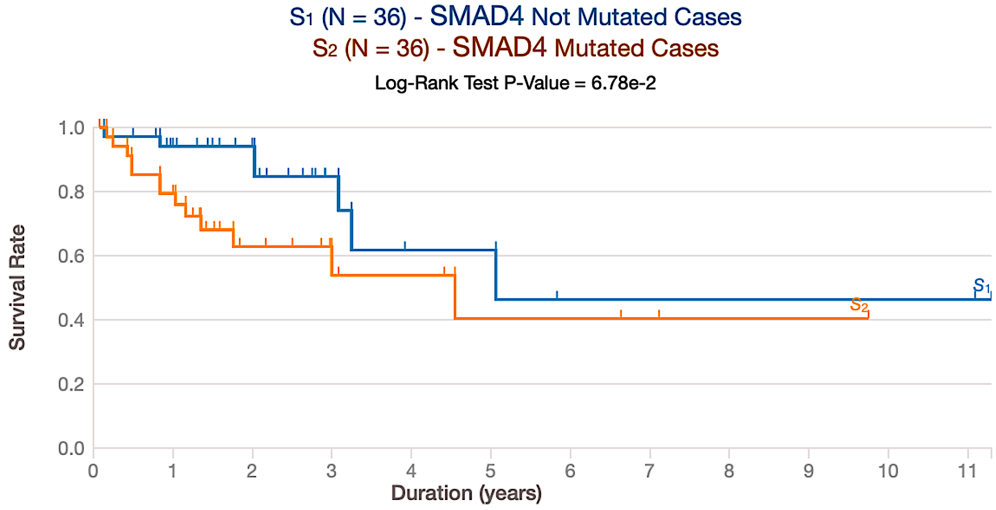

Figure 9: Overall survival plot of colorectal cancer patients (n = 36) with or without SMAD4 mutations.
(Data from TCGA-COAD, 2020).

The SMAD4 protein consists of three domains: the Mad Homology 1 domain (MH1) at the N-terminus, the Mad Homology 2 domain (MH2) at the C-terminus, and a linker region between the MH1 and MH2 domains [104,105].

The MH1 domain exhibits sequence-specific DNA-binding activity and negatively regulates the functions of the MH2 domain [106].

MH2 domain is responsible for receptor recognition, transactivation, interaction with transcription factors, and homo- and hetero-oligomerization between SMADs and is required for the formation of the R-SMAD/co-SMAD complex, largely encoded by exon 8 and exon 11 and entirely by exon 9 to exon 10 [107,108].

Missense mutations in the MH2 domain (Mad Homology 2 domain) especially at position 361 has been identified in several individuals with juvenile polyposis syndrome with an autosomal-dominant inherited predisposition to multiple gastrointestinal polyps and cancer [109–112].

The single nucleotide variant R361H of the SMAD4 gene has the designation SMAD4 c.1082G>A at the cDNA level, p.Arg361His at the protein level, and results in the exchange of an arginine for a histidine at position 361 of the SMAD4 protein (ClinVar, Table 16). R361H is the most common alteration in various cancer types, including CRC (Figure 10) [112,113]. It has been shown to inhibit the binding of SMAD4 to SMAD2 and associated with enhanced tumor growth and metastasis [108,112,113].

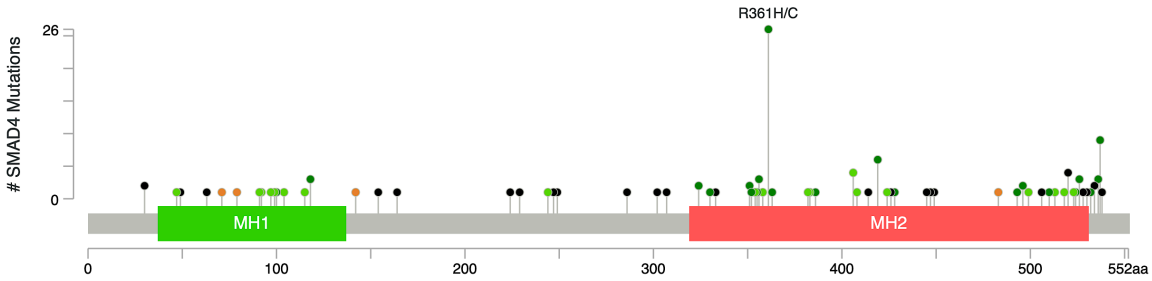

Figure 10: Lollipop plot of common SMAD4 mutations in colorectal cancer.
The prevalence and spectrum of SMAD4 mutations are shown (n = 117) (cBioPortal (access on 06/10/ 2021) *[114]*. Out of 117 patients with colon adenocarcinoma and colorectal adenocarcinoma, there are 15 cases with R361H mutation (p.Arg361His) and 11 cases with R361C (p.Arg361Cys) mutation. (MH1 = Mad Homology 1 domain, MH2 = Mad Homology 2 domain).

It was previously shown that the R361H mutation in the SMAD4 gene can cause differential drug response or even drug resistance within a colorectal tumor [115]. In head and neck cancer, pathogenic SMAD4 mutations have been shown to cause resistance to cetuximab [116,117].

The loss-of-function variant R361H prevents of the binding of SMAD4 to SMAD2. R361H is the most common pathogenic alteration in various cancer types, including CRC [112,113]. Therefore, SMAD4 or rather the TGF-β/BMP-pathway poses a promising target for pharmacological intervention in CRC.

1.3. Patient-derived organoids are suitable models for biomarker discovery

Given the broad spectrum of biomarkers (see 1.2.4.), the range of biomarker discovery strategies is enormous. The generation of human cancer cell lines has added to the discovery of biomarkers, moving away from measuring parameters directly at the patient to discovering biomarkers *ex vivo*.

Since the first human cancer cell line (HeLa, [118]) was generated and allowed to investigate the biology of cancer, the range of suitable *ex situ* models extends from mouse monoclonal generic cell lines to patient-derived xenografts (PDX) models and complex patient-derived 3D cell cultures (PD3D® or PDO (patient-derived organoids)) [119]. These cancer models are naturally occurring or artificially created systems that share the same characteristics as human cancers and are described in detail by Sajjad et al. [120].

PDO models have been shown to reliably recapitulate the architecture of the donor tissue and to preserve its genomic background, including its intra-tumor heterogeneity (ITH) [115,121]. Schütte et al. compared patient CRC tissue with matched PDX and PDO models with both models used to test clinically relevant drugs. They have shown that these models recapitulate many of the genetic and transcriptomic features of donor tumors whereas clonal discordances found at early passages were attributed to ITH and MSI [121]. This approach not only allows identification of functionally effective compounds for the individual patient tumor, but also reveals the tumor's molecular characteristics driving its therapy sensitivity or resistance [121]. PDOs are suitable and convenient models not only for the study of ITH, but also for the application of high-throughput drug screening to evaluate the response of a tumor to potential drug treatment considering ITH [115,122,123].

In Figure 11, a PDO approach is compared with a PDX approach aiming to test the same number of tumor samples and compounds to illustrate the time- and cost-effectiveness of the organoid system [124].

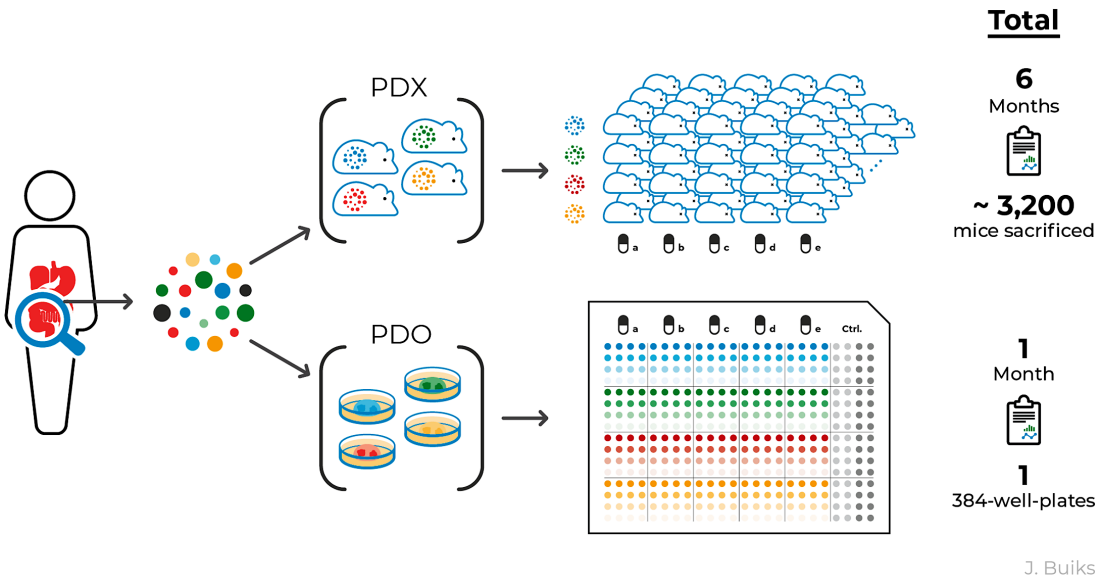

Figure 11: Patient-derived xenograft (PDX) vs. patient-derived organoid (PDO) cancer models to study a tumor's drug response incorporating intra-tumor heterogeneity.
Multi-regional sampling of a tumor is required to take ITH into account when assessing the tumor's drug response. Multi-regional PDO-based pre-therapeutic drug screenings are significantly more time- and cost-effective compared to multi-regional PDX models. PDO-based screenings, in addition to amplicon sequencing, combined with targeted proteomic approaches, are both feasible and available within a timeframe that allows discussing guided treatment options *[124]*.

Moreover, PDOs can be used in combination with multiple molecular technologies, such as CRISPR/Cas9 genome editing system, omics-approaches (e.g., genomics, proteomics, transcriptomics), and organ-on-a-chip [125,126] (Figure 12).

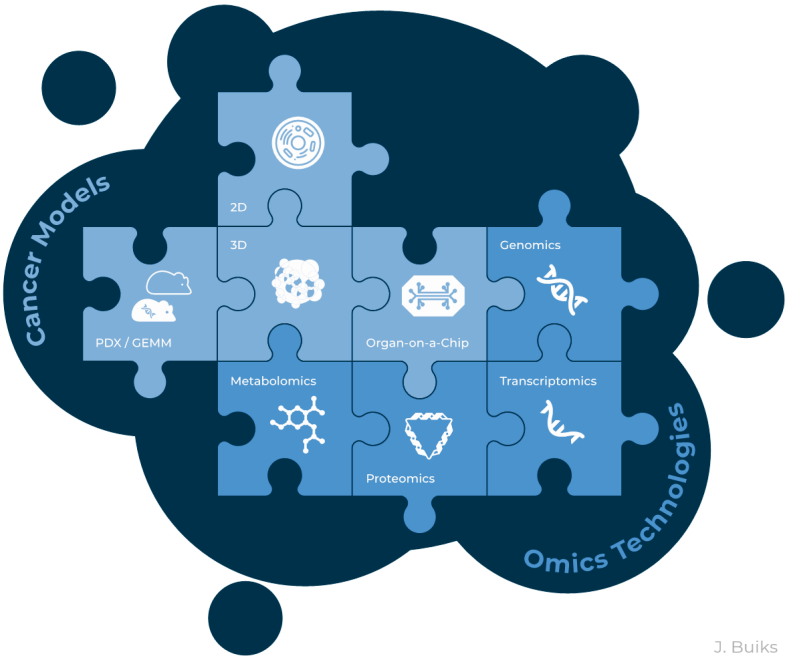

Figure 12: Cancer models and omics technologies to obtain a comprehensive picture of biological processes within a patient's tumor.
An appropriate combination of different omics technologies and relevant tumor models allows for a more comprehensive analysis of an intra-tumor heterogeneity, crucial for improvement of the patient treatment. (PDX = patient-derived xenograft, GEMM = genetically engineered mouse models, 2D = two-dimensional cell culture, 3D = three-dimensional cell culture) [124].

PDOs are useful for many applications, but they also have relevant technical and conceptual limitations, for example, lack of liver or kidney clearance or liver pro-drug activation mechanism [124]. They are also limited in their ability to account for the effects of environmental influences and organism aging on human organs *in vivo* [127].

However, PDO models are invaluable in preclinical research to our current understanding of cancer biology, but they are also moving into focus with respect to their potential use for cancer precision medicine.

1.4. Aims of the present study

Patient stratification is a critical prerequisite for personalized treatment regimen. So far, only RAS wild-type tumors respond to anti-EGFR therapy [45,52,53], leaving over 40 % of CRC patients [128].

In CRC, mutations in the TGF-β/BMP-pathway, especially in the SMAD4 gene have been correlated with decreased overall survival and are suspected to modulate chemoresistance [102]. Thus, there is a critical need for the identification of therapeutic agents capable of targeting SMAD4 mutated tumors. Given the medical need, this study was designed with two main objectives, and three secondary objectives for the dissertation:

1. **Investigation of the clinical relevance of SMAD4 gene in CRC by:**
    a. establishment of syngeneic patient-derived organoids harboring SMAD4^{R361H} mutation.
    b. investigation of the effects of SMAD4^{R361H} mutation on drug response in patient-derived organoids from CRC patients.
    c. examination of molecular signaling pathways that are potentially induced using multi-omics technologies.
2. **Identification of potential biomarkers for improved treatment outcomes in CRC.**

2. MATERIALS

2.1. Patient-derived organoid (PDO) models

Table 3: Colorectal cancer PDO models (source CELLphenomics GmbH).
*Staging data not available. **Tumor location of metastasis unknown.

PDO models	Tumor origin	Tumor location	Type	Gender	Stage
R1R361H	colon	colon	primary	f	IV
R4wt	colon	colon	primary	f	IV
Co-P-58-m-PUL-C	colon	lung	metastasis	f	IV
Co-P-58-m-PUL-D	colon	lung	metastasis	f	IV
Co-P-59-m-PUL	colon	lung	metastasis	f	IV
Co-P-71	colon	colon	primary	m	II
Co-P-72	colon	liver	metastasis	m	IV
Co-P-73	colon	rectum	primary	m	IV
Co-P-74	rectum	liver	metastasis	m	IV
Co-P-75	colon	colon	primary	m	III
Co-P-76	colon	colon	primary	f	III
Co-P-78	colon	colon	primary	f	II
Co-P-79	colon	colon	primary	f	I
Co-P-80	colon	colon	primary	m	IV
Co-P-82	colon	colon	primary	m	III
Co-P-84	colon	colon	primary	m	II
Co-P-85	colon	colon	primary	f	IV
Co-P-86	rectum	rectum	metastasis	m	IV
Co-P-87	rectum	rectum	primary	m	II
Co-P-88	colon	colon	primary	f	IV
Co-P-89	colon	colon	primary	m	II
Co-P-90	colon	colon	primary	f	IV
Co-P-91	colon	colon	primary	f	IV
Co-P-92	colon	colon	primary	f	II
Co-P-93	colon	colon	primary	m	IV
Co-P-95	colon	colon	primary	f	I
Co-P-96	colon	colon	primary	m	II
Co-P-97	colon	colon	primary	m	III
Co-P-98	colon	colon	primary	m	II
Co-P-99	colon	colon	primary	m	II
Co-P-100	colon	colon	primary	m	I
Co-P-101	colon	liver	metastasis	f	IV
Co-P-102	colon	colon	primary	m	II
Co-P-104	colon	colon	primary	m	I

PDO models	Tumor origin	Tumor location	Type	Gender	Stage
Co-P-105	colon	colon	primary	f	II
Co-P-106	rectum	rectum	metastasis	m	IV
Co-P-108	colon	**	metastasis	f	IV
Co-P-126	colon	colon	primary	f	II
Co-P-132	colon	colon	primary	f	*
Co-P-132-m-PER	colon	peritoneum	metastasis	f	*
Co-P-133	rectum	rectum	primary	m	III
Co-P-133-m-HEP	rectum	liver	metastasis	m	III
Co-P-134	rectum	rectum	primary	m	*
Co-P-134-m-HEP	rectum	liver	metastasis	m	*
Co-P-135	colon	colon	primary	f	*
Co-P-138-m-BRA	colon	brain	metastasis	f	*
Co-P-149-B	colon	colon	primary	f	IV
Co-P-153	colon	colon	primary	f	I
Co-P-154	colon	colon	primary	m	IV
Co-P-155	colon	**	metastasis	f	IV
Co-P-156	colon	colon	metastasis	f	IV
Co-P-157	colon	colon	primary	m	II
Co-X-37	colon	peritoneum	metastasis	f	IV
Co-X-38-A	colon	peritoneum	metastasis	m	IV
Co-X-38-B	colon	peritoneum	metastasis	m	IV
Co-X-40	colon	peritoneum	metastasis	m	IV
Co-X-41	colon	peritoneum	metastasis	m	IV
Co-X-44	colon	peritoneum	metastasis	f	IV
Co-X-69	colon	colon	primary	m	III
Co-X-70	colon	colon	primary	f	IV
Co-X-77	colon	colon	primary	f	I

2.2. Cell lines and organisms

Table 4: List of 2D cell lines and organisms.

Cell line/Organism	Entity/Name	Source
HEK-293T	Embryonic human kidney	CELLphenomics GmbH Berlin, Germany
E.coli	DH5α	Ralf Kühn, Max-Delbrück Center Berlin, Germany

2.3. Chemicals

Table 5: List of chemicals and commercial solution.

Chemicals and commercial solutions	Vendor
Acetic acid	Sigma-Aldrich Chemie GmbH, Steinheim, Germany
Advanced Dulbecco's modified Eagle's medium /Ham's F-12	Gibco™ by Life Technologies| ThermoFisher Scientific, Waltham, MA, USA
Amphotericin B	Sigma-Aldrich Chemie GmbH, Steinheim, Germany
4′,6-Diamidino-2-phenylindole dihydrochloride (DAPI)	AppliChem, Darmstadt, Germany
Agarose NEEO Ultra-Qualität Roti®garose	Carl Roth, Karlsruhe, Germany
Carbenicillin 25 mg/ml	Carl Roth, Karlsruhe, Germany
Cell recovery solution	Corning Life Science, Tewksbury, MA, USA
Collagenase IV	Sigma-Aldrich Chemie GmbH, Steinheim, Germany
B-27 Supplement (50X)	Gibco™ by Life Technologies| ThermoFisher Scientific, Waltham, MA, USA
Blocking Reagent (Roche)	Sigma-Aldrich Chemie GmbH, Steinheim, Germany
Blue BANDit™	VWR Internation GmbH, Darmstadt, Germany
Bovine Serum Albumin (BSA)	Sigma-Aldrich Chemie GmbH, Steinheim, Germany
CutSmart Buffer 10X	Sigma-Aldrich Chemie GmbH, Steinheim, Germany
Cultrex® 3D RGF BME	R&D Systems, Abingdon, UK
4′,6-Diamidino-2-phenylindole dihydrochloride (DAPI)	AppliChem, Darmstadt, Germany
Dimethyl sulfoxide (DMSO), sterile for cell culture	Sigma-Aldrich Chemie GmbH, Steinheim, Germany
Dispase	StemCell Technologies, Cologne, Germany
Dithiothreitol (DTT)	Carl Roth, Karlsruhe, Germany
DNAse I	AppliChem, Darmstadt, Germany
DNA-Marker 1 kb	New England BioLabs, Ipswich, Massachusetts, USA
DNA-Marker 1 kb GeneRuler	ThermoFisher Scientific, Waltham, MA, USA
DNA-Marker GeneRuler 100 bp	ThermoFisher Scientific, Waltham, MA, USA
DNA-Marker GeneRuler 100 bp Plus	ThermoFisher Scientific, Waltham, MA, USA
DNA-Marker GeneRuler Low Range DNA Ladder	ThermoFisher Scientific, Waltham, MA, USA
6x DNA Loading dye	New England BioLabs, Ipswich, MA, USA
6x TriTrack DNA Loading Dye	ThermoFisher Scientific, Waltham, MA, USA
Escherichia coli strain DH5α	Invitrogen | ThermoFisher Scientific, Waltham, MA, USA
dNTPs Mix (10 mM)	ThermoFisher Scientific, Waltham, MA, USA
DreamTaq DNA Polymerase	ThermoFisher Scientific, Waltham, MA, USA
Dulbecco's phosphate-buffered saline (DPBS), no calcium, no magnesium	Gibco™ by Life Technologies| ThermoFisher Scientific, Waltham, MA, USA
ECL Western substrate	ThermoFisher Scientific, Waltham, MA, USA
EDTA (Ethylenediaminetetraacetic acid)	Merck, Darmstadt, Germany
Ethanol	Merck, Darmstadt, Germany
Ethidium bromide	Carl Roth, Karlsruhe, Germany
Fetal bovine serum (FBS)	Sigma-Aldrich Chemie GmbH, Steinheim, Germany
Formalin solution	Sigma-Aldrich Chemie GmbH, Steinheim, Germany

Gel Loading Dye purple (6X)	New England BioLabs, Ipswich, MA, USA
Gentamicin solution (G1397, 50 mg/ml)	Sigma-Aldrich Chemie GmbH, Steinheim, Germany
Glacial acetic acid	Sigma-Aldrich Chemie GmbH, Steinheim, Germany
GlutaMAX™ Supplement (100X)	Gibco™ by Life Technologies| ThermoFisher Scientific, Waltham, MA, USA
Glycerol	ThermoFisher Scientific, Waltham, MA, USA
Glycine	Merck, Darmstadt, Germany
Hanks' balanced salt solution (HBSS)	Gibco™ by Life Technologies| ThermoFisher Scientific, Waltham, MA, USA
HEPES buffer	Gibco™ by Life Technologies| ThermoFisher Scientific, Waltham, MA, USA
Human Epidermal Growth Factor (hEGF)	Sigma-Aldrich Chemie GmbH, Steinheim, Germany
Human Fibroblast Growth Factor-Basic (hFGF)	PeproTech, East Windsor, NJ, USA
Iso-propanol (2-propanol)	Carl Roth, Karlsruhe, Germany
LB medium	Carl Roth, Karlsruhe, Germany
Matrigel® Basement Membrane Matrix, Growth Factor reduced, Phenol Red-Free	Corning Life Science, Tewksbury, MA, USA
Methanol	Merck, Darmstadt, Germany
β-mercaptoethanol	Sigma-Aldrich Chemie GmbH, Steinheim, Germany
Milk powder (MP # T145.2)	Carl Roth, Karlsruhe, Germany
Mounting Medium	Ibidi GmbH, Gräfelfing, Germany
N-2 Supplement (100X)	Gibco™ by Life Technologies| ThermoFisher Scientific, Waltham, MA, USA
N-Acetyl-L-cysteine	Sigma-Aldrich Chemie GmbH, Steinheim, Germany
NHS-PEG12-Biotin	ThermoFisher Scientific, Waltham, MA, USA
NEB buffer 10X	New England BioLabs, Ipswich, MA, USA
Nuclei Lysis Solution	Promega, Madison, WI, USA
NuPAGE Transfer Buffer (20x)	ThermoFisher Scientific, Waltham, MA, USA
Opti-MEM® I Reduced Serum Medium	Gibco™ by Life Technologies| ThermoFisher Scientific, Waltham, MA, USA
Penicillin Streptomycin (P/S) (100X)	Gibco™ by Life Technologies| ThermoFisher Scientific, Waltham, MA, USA
Phusion GC Buffer 5X	New England BioLabs, Ipswich, MA, USA
Phusion® High-Fidelity DNA Polymerase	New England BioLabs, Ipswich, MA, USA
Polybrene (hexadimethrine bromide)	Sigma-Aldrich Chemie GmbH, Steinheim, Germany
Ponceau S	Merck, Darmstadt, Germany
2-Propanol	Carl Roth, Karlsruhe, Germany
Protein Precipitation Solution	Promega, Madison, WI, USA
Puromycin 10 mg/ml	Gibco™ by Life Technologies| ThermoFisher Scientific, Waltham, MA, USA
Recovery™ Cell Culture Freezing Medium	Gibco™ by Life Technologies| ThermoFisher Scientific, Waltham, MA, USA
Restriction endonuclease SspI-HF® (20 U/µl)	New England BioLabs, Ipswich, MA, USA
Rho-associated Kinase inhibitor, Y27632	Miltenyi Biotec, Bergisch Gladbach, Germany
RPMI1640 medium	Gibco™ by Life Technologies| ThermoFisher Scientific, Waltham, MA, USA
RLT buffer	QIAGEN, Venlo, The Netherlands
Running buffer	BioRad, Hercules, CA, USA

S.O.C. medium	ThermoFisher Scientific, Waltham, MA, USA
Sodium azide	Sigma-Aldrich Chemie GmbH, Steinheim, Germany
Sodium chloride	Merck, Darmstadt, Germany
Sodium Dodecyl Sulfate (SDS)	Sigma-Aldrich Chemie GmbH, Steinheim, Germany
T4 DNA Ligase	New England BioLabs, Ipswich, MA, USA
T4 Ligase Buffer10X	New England BioLabs, Ipswich, MA, USA
TransIT®-2020 TransfectionReagent	Mirus Bio, Madison, WI, USA
TransIT®-LT1 TransfectionReagent	Mirus Bio, Madison, WI, USA
TransIT®-X2® Dynamic Delivery System	Mirus Bio, Madison, WI, USA
Tris(hydroxymethyl)aminomethan hydrochlorid (Tris-HCl)	Merck, Darmstadt, Germany
Tris Base	Merck, Darmstadt, Germany
Triton X-100	ThermoFisher Scientific, Waltham, MA, USA
Trypan Blue Staining Solution (0.4%)	Gibco™ by Life Technologies| ThermoFisher Scientific, Waltham, MA, USA
TrypLE™ Express Enzyme (1X) without phenolred	Gibco™ by Life Technologies| ThermoFisher Scientific, Waltham, MA, USA
Trypsin-EDTA 0.25% without phenol red	Gibco™ by Life Technologies| ThermoFisher Scientific, Waltham, MA, USA
Tween®20 Detergent	Merck, Darmstadt, Germany
Water Bioperformance certified	Sigma-Aldrich Chemie GmbH, Steinheim, Germany

2.4. Culture media

Table 6: List of culture media.

Solution / Medium	Composition
DMEM	Advanced DMEM/F12, 10 % FBS, 1x P/S
RPMI1640	RPMI1640, 10 % FBS, 1x P/S
P/S medium	Advanced DMEM/F12, 1x P/S, 10 mM HEPES buffer
Complete medium	Advanced DMEM/F12, 1x GlutaMAX, 1x P/S, 10 mM HEPES buffer, 1x N2 Supplement, 1x B27 Supplement, 1 mM N-Acetyl-L-cysteine, 20 ng/ml bFGF, 50 ng/ml EGF
XY-medium	Complete medium, 10 µM ROCK-II inhibitor Y27632

2.5. Kits

Table 7: List of kits.

Kit	Vendor
Amersham™ ECL Select™ Western Blotting Detection Reagent	GE Healthcare, Chalfont Saint Giles, UK
CellTiter-Glo® Luminescent Cell Viability Assay	Promega, Madison, WI, USA
CloneJET PCR Cloning Kit	ThermoFisher Scientific, Waltham, MA, USA
GeneJET Gel Extraction Kit	ThermoFisher Scientific, Waltham, MA, USA
GeneJET Plasmid Miniprep Kit	ThermoFisher Scientific, Waltham, MA, USA
GeneJET PCR Purification Kit	ThermoFisher Scientific, Waltham, MA, USA
Ion AmpliSeq™ Library Kit 2.0	ThermoFisher Scientific, Waltham, MA, USA
MycoAlert PLUS detection kit (50 test)	LONZA, Basel, Switzerland
NEB Next Ultra DNA Library Prep kit	New England BioLabs, Ipswich, MA, USA
NEB Next Multiplex Oligos (NEB, E7335S)	New England BioLabs, Ipswich, MA, USA
Pierce™ BCA Protein Assay Kit	ThermoFisher Scientific, Waltham, MA, USA
Trans-Blot® TurboTM RTA Midi PVDF Transfer Kit	BioRad, Hercules, CA, USA
QIAamp DNA Mini Kit	QIAGEN, Venlo, The Netherlands
QIAGEN Plasmid Maxi Kit (25)	QIAGEN, Venlo, The Netherlands
Wizard Kit for DNA isloation	Promega, Madison, WI, USA

2.6. Buffers and solutions

Table 8: List of buffers and solutions.

Buffer	Formulation
Assay buffer	Roche blocking reagent, 0.05 % sodium azide, 0.2 % milk powder
Dilution buffer	5 % BSA in PBS, 0.02 % sodium azide, 0.05 % Tween-20
Elution buffer	8 M urea, 1 % Triton-X100 in 100 mM Tris-HCl, pH 9.5
LDS buffer	741 mM Tris, 6 % LDS, 1.53 mM EDTA
lysis buffer	1x complete™, 1x PhoSTOP™ add 50-100 µl M-PER™
loading buffer	6x SDS (0.375 M Tris pH 6.8, 12 % SDS, 60 % glycerol, 0.6 M DTT, 0.06 % bromophenol blue)
running buffer 5x	15.1 g Tris Base (25 mM), 72 g Glycine (192 mM), 5 g 1x SDS in 1 l ddH_2O
blotting buffer 2.5x	14.53 g Tris Base (25 mM), 7.33 g Glycine (192 mM), 4.69 g 20 % SDS, 500 ml methanol, in 1 l ddH_2O
blocking buffer	5 % (w/v) non-fat dry milk, 1x TBS
PBST	PBS with 0.1% Tween®20
Ponceau S solution	0.1 % (w/v) Ponceau S in 1 % acetic acid in ddH2O
Primary antibody dilution buffer	1 % BSA in 1x TBS, 0.1% Tween®20
Secondary antibody dilution buffer	5 % (w/v) non-fat dry milk, 1x TBS, 0.1 % Tween®20
Storage buffer	1 % BSA, 0.05 % Tween®20, 0.05 % sodium azide in PBS
50x TAE (pH 8.0)	242.2 g Tris Base, 57.1 ml glacial acetic acid, 100 ml 0.5 M EDTA in 1 L ddH_2O
TBS	0.1 M Tris, 1.50 M sodium chloride in 1 L ddH2O, pH 7.4
TE buffer	10 mM Tris-HCl, 1 mM EDTA (pH 8.0)
Transfer buffer	NuPAGE Transfer Buffer (20x)
Wash buffer (TBST for DigiWest®)	0.1 % (v/v) Tween®20 in 100 ml TBS
Wash buffer (TBST for Western Blot)	50 mM Tris-HCl, 150 mM sodium chloride, 0.05 % Tween®20, pH 7

2.7. Consumables

Table 9: List of consumables.

Consumables	Vendor
0.5 µl PCR tubes	Biozym, Oldendorf, Germany
10 µl, 100 µl, 300 µl, 1250 µl filter tips	Greiner Bio-One, Frickenhausen, Germany
10 µl, 100 µl, 300 µl, 1250 µl pipet tips	Eppendorf, Hamburg, Germany
5 ml, 10 ml, 25 ml, 50 ml serological pipets	Corning Life Science, Tewksbury, MA, USA
24-well plates	Corning Life Science, Tewksbury, MA, USA
24-well plates (ultra-low attachment)	Greiner Bio-One, Frickenhausen, Germany
96-well plates (F-bottom, transparent)	Corning Life Science, Tewksbury, MA, USA
96-well plates (U-bottom)	Greiner Bio-One, Frickenhausen, Germany
384-well plates (F-bottom, µCLEAR®, black)	Greiner Bio-One, Frickenhausen, Germany
AP96 TIPS, P20 sterile	Beckman Coulter, Brea, CA, USA
AP96 TIPS, P250 sterile	Beckman Coulter, Brea, CA, USA
Cell culture flasks 25 cm^2	Greiner Bio-One, Frickenhausen, Germany
Cell culture flasks 75 cm^2	Greiner Bio-One, Frickenhausen, Germany
Cell culture flasks 175 cm^2	Greiner Bio-One, Frickenhausen, Germany
Cell culture flasks	Greiner Bio-One, Frickenhausen, Germany
CL-Xposure Films (Pierce)	ThermoFisher Scientific, Waltham, MA, USA
Cryovials (2 ml)	Greiner Bio-One, Frickenhausen, Germany
Falcon® 12x75mm tube with cell strainer cap (35 µm)	Corning Life Science, Tewksbury, MA, USA
Laboratory glassware	SIMAX, Sázava, Czech Republic
MagPlex Microspheres	Luminex Corporation, Austin, TX, USA
NuPAGE Novex 4-12 % Bis-Tris Gels 1 mm x 12 well or 1 mm x 17 well	ThermoFisher Scientific, Waltham, MA, USA
Pasteur pipets (230 mm)	Carl Roth, Karlsruhe, Germany
Petri dishes 10 cm	Corning Life Science, Tewksbury, MA, USA
PVDF membrane, 0.45 µm, 7.5 cm x 8.5 cm	Merck Millipore, Billerica, USA
Reaction tubes 1.5 ml, 2 ml	ThermoFisher Scientific, Waltham, MA, USA
Reaction tubes 15 ml, 50 ml	Greiner Bio-One, Frickenhausen, Germany
Reservoirs	ThermoFisher Scientific, Waltham, MA, USA
Scalpel Aesculap®, 11 (B.Braun)	Carl Roth, Karlsruhe, Germany
Scalpel Aesculap®, 21 (B.Braun)	Carl Roth, Karlsruhe, Germany
Strainer MACS® Smart, 30 µm, 100 µm	Miltenyi Biotec, Germany
Syringe filter 0.45 µm	Carl Roth, Karlsruhe, Germany
Whatman paper 7.5 cm x 8.5 cm, 0.34 mm	GE Healthcare, Little Chalfont, UK

2.8. Devices

Table 10: List of technical laboratory equipment.

Device	Vendor
Autoclave 5075 ELV	Systec, Linden, Germany
Balance Practum 124-1S	Sartorius AG, Göttingen, Germany
Bath Water Precision GP 10	ThermoFisher Scientific, Waltham, MA, USA
Benchmark myFuge mini	Benchmark Scientific, Inc., Sayreville, NJ, USA
Biomek FX^{P} Automated Liquid Handling Solutions	Beckman Coulter, Brea, CA, USA
Biological Safety Cabinets, type Safe 2020 1.8	ThermoFisher Scientific, Waltham, MA, USA
Biological Safety Cabinets, type Safe 2020 1.2	ThermoFisher Scientific, Waltham, MA, USA
Camera Leica DFC 320	Leica Microsystems, Wetzlar, Germany
Centrifuge 5424	Eppendorf, Hamburg, Germany
Centrifuge 5810R	Eppendorf, Hamburg, Germany
Centrifuge Mini Sprout®	Heathrow Scientific, Vernon Hills, IL, USA
Centrifuge Sorvall Lynx 6000	ThermoFisher Scientific, Waltham, MA, USA
Centrifuges VWR GalaXY Mini	VWR® International, Radnor, PA, USA
Centrifuge for plates Universal 320	Hettich GmbH, Tuttlingen, Germany
Confocal microscope CSU-W1	Nikon Instruments Inc., Melville, NY, USA
CryoCube (-80°C)	Eppendorf, Hamburg, Germany
Cryo plus - Liquid nitrogen cryostorage systems	ThermoFisher Scientific, Waltham, MA, USA
FACSAria™	BD Biosciences, Franklin Lakes, NJ, USA
FLEXMAP 3D	Luminex Corporation, Austin, TX, USA
FUSION Solo6s Western Blot Imaging	Vilber Lourmat, Collégien, France
Gel Documentation Imaging Quantum ST5	Vilber Lourmat, Collégien, France
Ice machine	Ziegra, Isernhagen, Germany
IncuCyte® S3 Live-Cell Analysis System	Satorius | Essen BioScience, Royston, UK
IKA Vortex 2	IKA, Staufen, Germany
Incubator Shaker Series Innova™ 42	New Brunswick Scientific™, Nürtingen, Germany
Lable printer Zebra GK420d	Zebra Technologies Corporation, Lincolnshire, IL, USA
Nanodrop ND-2000 Spectrophotometer	ThermoFisher Scientific, Waltham, MA, USA
NuPage® Novex® Gel System	ThermoFisher Scientific, Waltham, MA, USA
Microscope DM IL LED Fluo	Leica Microsystems, Wetzlar, Germany
Microscope DMi 1	Leica Microsystems, Wetzlar, Germany
MiSeq™-System	Illumina, San Diego, Ca, USA
Pipettes single channel (10 µl, 20 µl, 100 µl, 200 µl, 1000 µl)	Eppendorf, Hamburg, Germany
Pipettes multi-channel (300 µl)	Eppendorf, Hamburg, Germany
PeqPower 300V	VWR® International, Radnor, PA, USA
Platereader SpectraMax i3x	Molecular Devices, San Jose, CA, USA
Printer Mitsubishi P35	Mitsubishi Electric, Tokio, Japan
Refrigerator (4°C)	Liebherr, Kempten, Germany
Refrigerator (-20°C)	Bosch GmbH, Stuttgart, Germany
Shaker for plates (MTS4)	IKA® Werke GmbH, Staufen, Germany
Silhouette cutting tool	Silhouette America, Orem, USA
Synergy® UV Water Purification System	Merck, Darmstadt, Germany

Thermocycler Professional Trio	Analytik Jena, Jena, Germany
Thermomixer F1.2	Eppendorf, Hamburg, Germany
UV Transilluminator	VWR® International, Radnor, PA, USA
Vacuum concentrator	Bachofer GmbH, Reutlingen, Germany
Vacusafe	Integra Biosciences, Biebertal, Germany
XCell SureLock Mini-Cell Electrophoresis System	ThermoFisher Scientific, Waltham, MA, USA

2.9. Compounds

Table 11: List of compounds.

Compound	Target(s)	Cat. No.	Vendor
5-Fluorouracil (5-FU)	pyrimidine analog	F6627	Sigma-Aldrich Chemie GmbH, Steinheim, Germany
Binimetinib	MEK1/2	HY-15202	MedChemExpress, Monmouth Junction, NJ, USA
Cobimetinib	MEK1/2	HY-13064	MedChemExpress, Monmouth Junction, NJ, USA
Dabrafenib	BRAF	S2807	Selleck Chemicals, Houston, USA
Regorafenib	VEGFR1/2/3, PDGFRβ, KIT, RET and Raf-1	S1178	Selleck Chemicals, Houston, TX, USA
Selumetinib	MEK1, ERK1/2 phosphorylation	HY-50706	MedChemExpress, Monmouth Junction, NJ, USA
Staurosporine	Protein kinase C	S1421	Selleck Chemicals, Houston, TX, USA
Trametinib	MEK 1/2	S2673	Selleck Chemicals, Houston, TX, USA
Ulixertinib	ERK	HY-15816	MedChemExpress, Monmouth Junction, NJ, USA

2.10. Plasmids

Table 12: List of plasmids.

Plasmid	Cat. No. / depositor with reference	Vendor
pU6chimRNA-CAG-Cas9(D10A)-venus-bpA	#134	Ralf Kühn, Max-Delbrück-Centrum, Berlin, Germany
CAG-i53-EfI-BFP	#602	Ralf Kühn, Max-Delbrück-Centrum, Berlin, Germany
pCAG-Cas9v2-PGK-Venus-bpA	#65	Ralf Kühn, Max-Delbrück-Centrum, Berlin, Germany
pHAGE SMAD4	#116791 / Ng et al Cancer Cell. 2018 Mar 12;33(3):450-462.e	Addgene, Watertown, MA, USA
pHAGE puro	#118692 / Lu et al Cancer Cell. 2018 Dec 10;34(6):970-981.e	Addgene, Watertown, MA, USA
pRSV-REV	#12253 / Dull et al J Virol. 1998 Nov . 72(11):8463-71.	Addgene, Watertown, MA, USA
pMDLg/pRRE	#12251 / Dull et al J Virol. 1998 Nov . 72(11):8463-71.	Addgene, Watertown, MA, USA
pCMV-VSV-G	#8454 / Stewart et al RNA 2003 Apr;9(4):493-501.	Addgene, Watertown, MA, USA

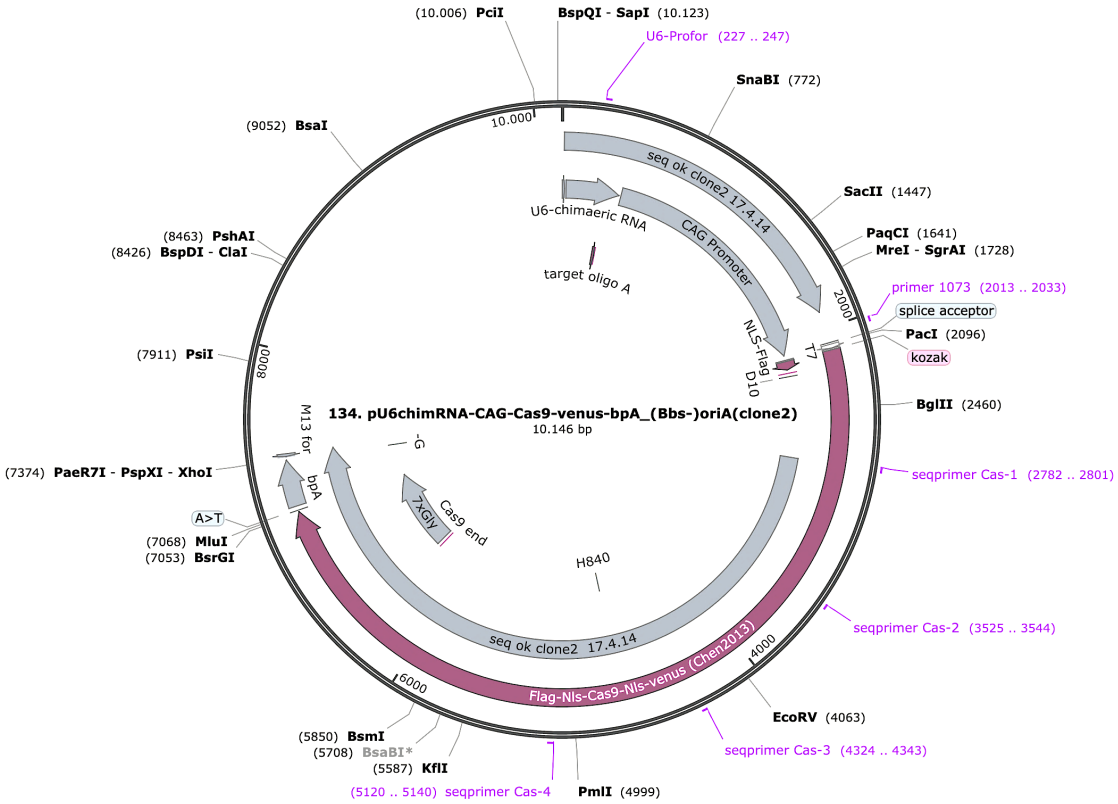

Figure 13: Vector map of pU6chimRNA-CAG-Cas9(D10A)-venus-bpA.
The plasmid was kindly provided by Ralf Kühn (MDC Berlin). Vector map image created with SnapGene Viewer.

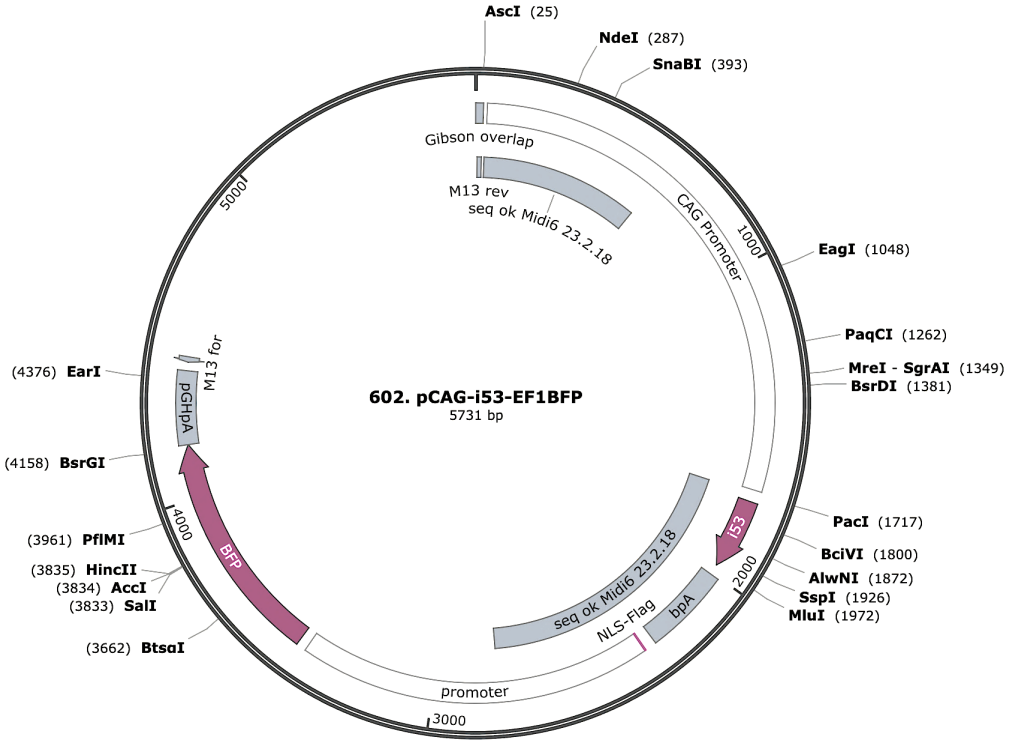

Figure 14: Vector map of CAG-i53-EfI-BFP.
The plasmid was kindly provided by Ralf Kühn (MDC Berlin). Vector map image created with SnapGene Viewer.

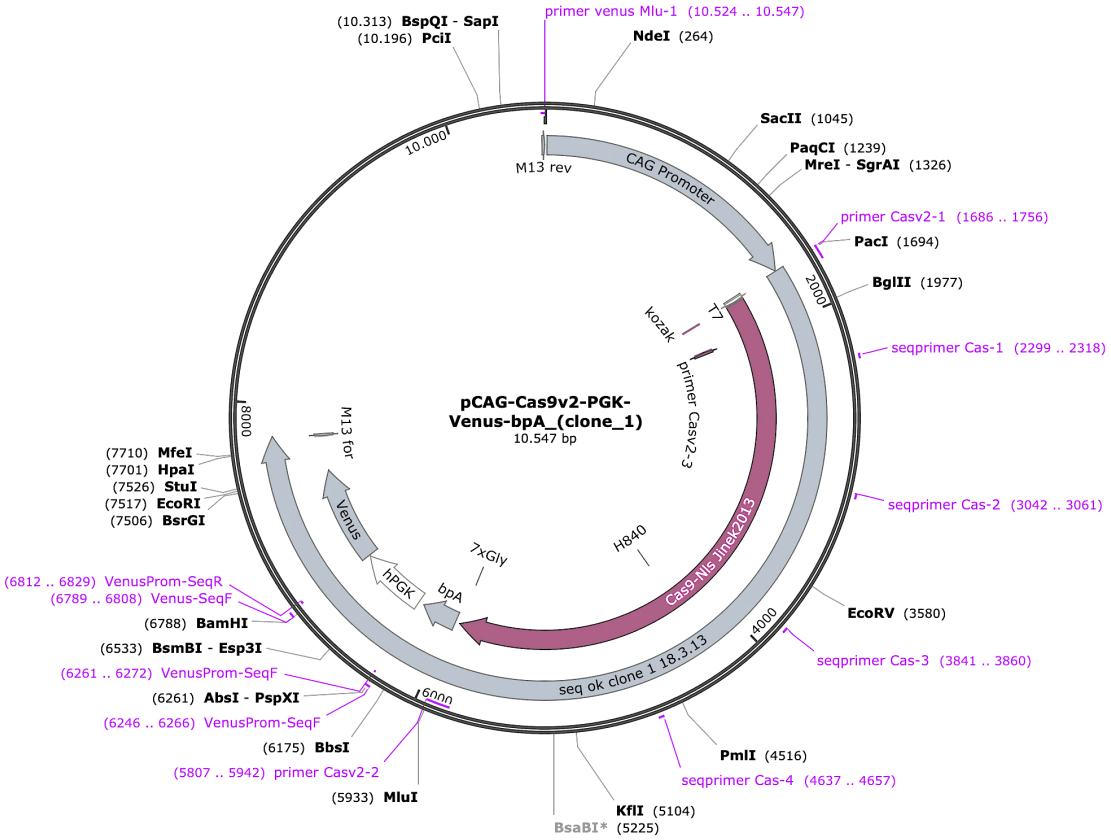

Figure 15: Vector map of CAG-Cas9uPUK-Venus.
The plasmid was kindly provided by Ralf Kühn (MDC Berlin). Vector map image created with SnapGene Viewer.

2.11. Restriction enzymes

Table 13: List of restriction enzymes.

Enzyme	Vendor
EcoRI-HF	New England BioLabs, Ipswich, MA, USA
EcoRV	New England BioLabs, Ipswich, MA, USA
FspI	ThermoFisher Scientific, Waltham, MA, USA
ScaI	New England BioLabs, Ipswich, MA, USA
XbaI	New England BioLabs, Ipswich, MA, USA
XhoI	New England BioLabs, Ipswich, MA, USA

2.12. Antibodies

Table 14: List of primary antibodies used for the DigiWest® experiment.
(Species rb = rabbit, ms = mouse, gt = goat)

Analyte	Modification site	Pathway / function	Molecular weight	Species	UniProt ID	Product No. #	Supplier
Akt		PI3K / Akt signaling	60	rb	P31749	4685	Cell Signaling
Akt - phospho Ser473	Ser473	PI3K / Akt signaling	60	rb	P31749	4060	Cell Signaling
Akt1		PI3K / Akt signaling	60	ms	P31749	2967	Cell Signaling
Akt1 - phospho Ser473	Ser473	PI3K / Akt signaling	55	rb	P31749	9018	Cell Signaling
Akt2 - phospho Ser474	Ser474	PI3K / Akt signaling	60	rb	P31751	8599	Cell Signaling
Akt3		PI3K / Akt signaling	60	rb	Q9Y243	3788	Cell Signaling
Annexin II		Cytoskeleton	36	ms	P07355	A14020 (new: BD #610068)	Transduction Laboratories
Aurora A (AIK)		Proliferation	48	rb	O14965	4718	Cell Signaling
Aurora A/B/C - phospho	Thr288/Thr232/Thr198	Proliferation	35, 40, 48	rb	O14965, Q96GD4, Q9UQB9	2914	Cell Signaling
Aurora B (AIM1)		Proliferation	40	rb	Q96GD4	3094	Cell Signaling
Bcl2		Apoptosis	26	rb	P10415	2870	Cell Signaling
Bcl-xL		Apoptosis	30	rb	Q07817	2764	Cell Signaling
beta-Actin		Cytoskeleton	42	ms	P60709	A1978	Sigma
beta-Catenin		Wnt signaling	92	rb	P35222	8480	Cell Signaling
beta-Catenin- active (non-phospho Ser33/37/Thr41)		Wnt signaling	92	rb	P35222	8814	Cell Signaling
beta-Catenin - phospho Ser552	Ser552	Wnt signaling	92	rb	P35222	9566	Cell Signaling
beta-Catenin - phospho Ser675	Ser675	Wnt signaling	92	rb	P35222	9567S	Cell Signaling
Bmi1		TGF-beta / Smad signaling	41, 43	rb	P35226	6964	Cell Signaling
BMP4		TGF-beta / Smad signaling	46	rb	P12644	5163-1	Epitomics
B-Raf - phospho Ser445	Ser445	MAPK signaling	86	rb	P15056	2696	Cell Signaling
C/EBP beta	Thr235	Transcription factor	42, 28	rb		3084	Cell Signaling
Caseinkinase 1 epsilon		Wnt signaling	47	rb	P49674	487600	Invitrogen
Caspase 3 - full length		Apoptosis	17, 19, 35	rb	P42574	9662	Cell Signaling
Caspase 8 - full length		Apoptosis	18, 43, 57	ms	Q14790	9746	Cell Signaling
Caspase 9 - full length		Apoptosis	35, 37, 47	rb	P55211	9502	Cell Signaling
CD133		Stem	97	rb	O43490	3663	Cell Signaling
CDKN2B (p15 INK4B, CDN2B, MTS2)		p53 pathway	15	ms	P42772	MAB6798	Bio-Techne
c-Jun	Ser63	Transcription factor	48	rb	P05412	2361	Cell Signaling
c-myc		Transcription factor	57-70	rb	P01106	9402	Cell Signaling
c-myc	Thr58/Ser62	Transcription factor	57	rb	P01106	ab32029 (1203-1)	abcam (Epitomics)
c-Raf		MAPK signaling	65-75	rb	P04049	9422	Cell Signaling
c-Raf - phospho Ser259	Ser259	MAPK signaling	74	rb	P04049	9421	Cell Signaling
Cyclin B1		Cell cycle	58	rb	P14635	ab32053 (1495-1)	abcam (Epitomics)
Cytokeratin 18		Tumor marker	46	ms	P05783	4548	Cell Signaling
Cytokeratin 19		Tumor marker	40	ms	P08727	4558	Cell Signaling
Cytokeratin 8 - phospho Ser23 (49 kDa peak)	Ser23	Tumor marker	52	rb	P05787	2147-1	Epitomics
Cytokeratin 8/18		Tumor marker	46, 55	ms	P05787, P05783	4546	Cell Signaling
Cytokeratin - pan (4,5,6,8,10,13,18)		Tumor marker	46, 55	ms	P19013, P13647, P02538, P05787, P13645, P13646, P05783	4545	Cell Signaling
DUSP6		MAPK signaling	42	rb	Q16828	ab76310 (2138-1)	abcam (Epitomics)
E-Cadherin		EMT	135	gt	P12830	AF748	R&D
E-Cadherin - phospho Ser838/Ser840	Ser838/Ser840	EMT	135	rb	P12830	2239-1	Epitomics
Elk-1		Transcription factor	46	rb	P19419	9182	Cell Signaling
Elk-1 - phospho Ser383	Ser383	MAPK signaling	47	ms	P19419	9186	Cell Signaling
Erk1		MAPK signaling	42, 44	rb	P27361, P28482	4695 B	Cell Signaling
Erk2 - phospho Thr202/Tyr204		MAPK signaling	42, 44	rb	P27361, P28482	4695 B	Cell Signaling

Erk2 - phospho Thr202/Tyr204	Thr202/Tyr204	MAPK signaling	42, 44	ms	P27361, P28482	4370B	Cell Signaling
Ezh2		Chromatin reg. / Epigenetics	98	rb	Q15910	5246S	Cell Signaling
FGF-1		Tyrosine kinase	17	rb	P05230	ab179455 (8504-1)	abcam (Epitomics)
GADD45 alpha		Cell cycle	22	rb	P24522	4632	Cell Signaling
GAPDH		Glucose metabolism	37	rb	P04406	5174	Cell Signaling
Glutamine synthetase		Tumor marker	45	rb	P15104	G2781	Sigma
GSK3 alpha/beta - phospho Ser21/Ser9 (51 kDa peak of GSK3 alpha)	Ser21/Ser9	Wnt signaling	46, 51	rb	P49840, P49841	9331	Cell Signaling
GSK3 alpha/beta - phospho Tyr279/Tyr216	Tyr279/Tyr216	Wnt signaling	47, 51	rb	P49840, P49841	ab68476 (2309-1)	abcam (Epitomics)
GSK3 beta		Wnt signaling	46	rb	P49841	9315	Cell Signaling
GSK3 beta - phospho Ser9	Ser9	Wnt signaling	46	rb	P49841	9336	Cell Signaling
Ha-ras		MAPK signaling	21	rb	P01112	05-775	Upstate
Her2		Tyrosine kinase	185	rb	P04626	A0485	Dako
HGF		Tyrosine kinase	83	gt	P14210	AF2207	R&D
HSP 27 - phospho Ser15	Ser15	Protein folding / Chaperones	27	rb	P04792	2231-1	Epitomics
IDH1		Metabolism	46	rb	O75874	8137	Cell Signaling
IGFBP-1		IGF signaling	36	gt	P08833	sc-6000	Santa Cruz
JAK1		Jak/Stat signaling	130	rb	P23458	3344	Cell Signaling
JNK/SAPK 1/2/3 - phospho Tyr185/Tyr223	Tyr185/Tyr223	MAPK signaling	46	rb	P45983, P45984, P53779	2155-1	Epitomics
MCM2		Cell cycle	125	rb	P49736	3619	Cell Signaling
MEK1		MAPK signaling	45	rb	Q02750	9124	Cell Signaling
MEK1/2 - phospho Ser217/Ser221	Ser217/Ser221	MAPK signaling	45	rb	Q02750, P36507	9154	Cell Signaling
MEK2		MAPK signaling	45	rb	P36507	9125	Cell Signaling
MEKK3		MAPK signaling	71	rb	Q99759	1673-1	Epitomics
mTor - phospho	Ser2448	mTOR signaling	288	rb	P42345	5536	Cell Signaling
mTOR		mTOR signaling	289	rb	P42345	2983	Cell Signaling
mTOR (FRAP)- phospho	Ser2481	mTOR signaling	289	rb	P42345	2974	Cell Signaling
p38 MAPK		MAPK signaling	43	rb	Q16539	9212	Cell Signaling
p38 MAPK - phospho Thr180/Tyr182	Thr180/Tyr182	MAPK signaling	43	rb	Q16539	4511	Cell Signaling
p53		DNA damage / TSG	53	gt	P04637	af1355	R&D
p53 - acetyl Lys305	Lys305	DNA damage / TSG	44	rb	P04637	ab109396 (3308-1)	abcam (Epitomics)
p70 S6 kinase		Translational control	70, 85	rb	P23443	2708	Cell Signaling
PAK 4/5/6 - phospho Ser474/Ser602/Ser560	Ser474/Ser602/Ser560	Cytoskeleton	72 (PAK4), 82 (PAK6), 90 (PAK5)	rb	O96013, Q9NQU5, Q9P286	3241	Cell Signaling
PARP - full length		Apoptosis	116, 89	rb	P09874	9532	Cell Signaling
PARP - cleaved Asp214	Asp214	Apoptosis	89	rb	P09874	9541	Cell Signaling
PDGFR beta		Tyrosine kinase	190	rb	P09619	3169	Cell Signaling
PI3 Kinase - p110 beta		PI3K / Akt signaling	110	rb	P42338	04-400	Millipore
PI3 Kinase - p85		PI3K / Akt signaling	85	rb		4292	Cell Signaling
PI3 Kinase - p85 alpha		PI3K / Akt signaling	85	rb	P27986	1675-1	Epitomics
PP2A C - phospho	Tyr307	Wnt signaling	36	rb	P67775	AF3989	R&D
PTEN		PI3K / Akt signaling	54	rb	P60484	9552	Cell Signaling
PTEN - phospho Ser380	Ser380	PI3K / Akt signaling	54	rb	P60484	9551	Cell Signaling
Ras		MAPK signaling	21	rb	P01116	8955	Cell Signaling
Rb		Cell cycle	110	ms	P06400	9309	Cell Signaling
Rb - phospho Ser807/Ser811	Ser807/Ser811	Cell cycle	110	rb	P06400	8516	Cell Signaling
RSK 1 (p90RSK)		MAPK signaling	90	rb	Q15418	2004-1	Epitomics
RSK1 p90 - phospho Thr573	Thr573	MAPK signaling	83	rb	Q15418	ab62324 (2185-1)	abcam (Epitomics)
S6 ribosomal protein		Translational control	32	ms	P62753	2217	Cell Signaling
S6 ribosomal protein - phospho Ser235/Ser236	Ser235/Ser236	Translational control	32	rb	P62753	2211	Cell Signaling
S6 ribosomal protein - phospho Ser240/Ser244	Ser240/Ser244	Translational control	32	rb	P62753	2215	Cell Signaling
SHP-2		Tyrosine phosphatase	72	rb	Q06124	1609-1	Epitomics
Smad1		TGF-beta / BMP signaling	60	rb	Q15797	6944	Cell Signaling
Smad2		TGF-beta / BMP signaling	60	rb	Q15796	5339	Cell Signaling
Smad3		TGF-beta / BMP signaling	52	rb	P84022	9523	Cell Signaling
SMAD4		TGF-beta / BMP signaling	70	rb	Q13485	9515	Cell Signaling

Smad5		TGF-beta / BMP signaling	60	rb	Q99717	9517	Cell Signaling
Smad9 (Smad8)		TGF-beta / BMP signaling	52	gt	O15198	AF2309	R&D
Smad1/5 - phospho	Ser463/Ser465	TGF-beta / BMP signaling	60	rb	Q15797/Q99717	9516	Cell Signaling
Smad2 - phospho	Ser245/Ser250/Ser255	TGF-beta / BMP signaling	60	rb	Q15796	3104	Cell Signaling
Smad2/3 - phospho	Ser465/467 (Smad2) Ser423/425 (Smad3)	TGF-beta / BMP signaling	52, 60	rb	Q15796/P84022	8828	Cell Signaling
SPRY1		MAPK signaling	35	rb	O43609	AV50521	Sigma (aviva systems biology)
SPRY2		MAPK signaling	35-40	rb	O43597	07-524	Millipore
SPRY3		MAPK signaling	31	rb	O43610	AV50519	Sigma
Src - phospho Tyr527 (55 kDa peak)	Tyr527	Tyrosine kinase	59	rb	P12931	2105	Cell Signaling
Src - phospho Tyr527 (60 kDa peak)	Tyr527	Tyrosine kinase	60	rb	P12931	2105	Cell Signaling
STAT 1		Jak/Stat signaling	84, 91	rb	P42224	9175	Cell Signaling
STAT 3		Jak/Stat signaling	79, 86	rb	P40763	4904	Cell Signaling
STAT 3 alpha		Jak/Stat signaling	86	rb	P40763	8768	Cell Signaling
STAT 5		Jak/Stat signaling	90	rb	P42229	9363	Cell Signaling
STAT 5 alpha		Jak/Stat signaling	92	rb	P42229	ab32043 (1289-1)	abcam (Epitomics)
TCF1		Transcription factor	28-50	rb		2206	Cell Signaling
TCF4		Transcription factor	58, 79	rb	Q9NQB0	2565	Cell Signaling
Twist		EMT	28	rb	Q15672	sc-15393	Santa Cruz
Vimentin		Cytoskeleton	57	rb	P08670	5741	Cell Signaling
Wnt3A		Wnt signaling	40	rb	P56704	09-162	Millipore

2.13. Primer and oligonucleotides

Table 15: List of primer and oligonucleotides.

Single stranded oligonucleotides (ssODN) were used as repair templates in the CRISPR experiments. The point mutation is highlighted in red.

Region	Sequence 5’ - 3’	Manufacturer
SMAD4-I A (sgRNA)	CACCGATGGATACGTGGACCCTTC	BioTEZ GmbH, Berlin, Germany
SMAD4-I B (sgRNA)	AAACGAAGGGTCCACGTATCCATC	BioTEZ GmbH, Berlin, Germany
SMAD4-II A (sgRNA)	CACCGGATACGTGGACCCTTCTGG	BioTEZ GmbH, Berlin, Germany
SMAD4-II B (sgRNA)	AAACCCAGAAGGGTCCACGTATCC	BioTEZ GmbH, Berlin, Germany
SMAD4 ssODN1	TCCTTCAAGCTGCCCTATTGTTACTGTTGATGGATACGTGGACCCTTCTGGAGGAGATC**G**CTTTTGTTTGGGTCAACTCTCCAATGTCCACAGGACAGAAGCCATTGAGAGAGCAAGGT	BioTEZ GmbH, Berlin, Germany
SMAD4 ssODN2	ACCTTGCTCTCTCAATGGCTTCTGTCCTGTGGACATTGGAGAGTTGACCCAAACAAAAG**C**GATCTCCTCCAGAAGGGTCCACGTATCCATCAACAGTAACAATAGGGCAGCTTGAAGGA	BioTEZ GmbH, Berlin, Germany
SMAD4 ssODN3	TCCTTCAAGCTGCCCTATTGTTACTGTTGATGGATACGTGGACCCTTCTGGAGGAGATC**A**CTTTTGTTTGGGTCAACTCTCCAATGTCCACAGGACAGAAGCCATTGAGAGAGCAAGGT	BioTEZ GmbH, Berlin, Germany
SMAD4 ssODN4	ACCTTGCTCTCTCAATGGCTTCTGTCCTGTGGACATTGGAGAGTTGACCCAAACAAAAG**T**GATCTCCTCCAGAAGGGTCCACGTATCCATCAACAGTAACAATAGGGCAGCTTGAAGGA	BioTEZ GmbH, Berlin, Germany
SMAD4 fw	AAATTCTCAGTTGACCTGGTCC	BioTEZ GmbH, Berlin, Germany

SMAD4 rev	ACCGACAATTAAGATGGAGTGC	BioTEZ GmbH, Berlin, Germany
SMAD4_RE_fw1	ACCTGGACTGGAAGTAGGAC	BioTEZ GmbH, Berlin, Germany
SMAD4_RE_rev1_new	CTGCTGCATCTGTCGATGAC	BioTEZ GmbH, Berlin, Germany
T7prom	TAATACGACTCACTATAGG	Addgene, Watertown, MA, USA
pEFmyccyto-F	TCTCAAGCCTCAGACAGT	Addgene, Watertown, MA, USA
U6 primer	GAGGGCCTATTTCCCATG	BioTEZ GmbH, Berlin, Germany

2.14. Databases, online tools, bioinformatic tools, and software

Table 16: List of databases, online tools, and software.

Name	Version / Year of use	Vendor / Source
ApE (A plasmid Editor)	Version 2.0.51	© M.Wayne Davis
ATCC Database	access 2020	© 2020 ATCC
CCLE Database	access 2021	© 2020 The Broad Institute of MIT & Harvard
CLC Genome Viewer 7	Version 7.8.1.	QIAGEN, Venlo, The Netherlands
ClinVar	access 2021	https://www.ncbi.nlm.nih.gov/clinvar/variation/VCV000024832.7
CRISPOR	Version 4.99	[129]
cBioportal	access 2021	[130,131]
DigiWest® analysis software	Version 3.8.6.1	NMI, Reutlingen, Germany
Ensembl	GRCh38	© EMBL-EBI
Enrichr	access 2021	https://maayanlab.cloud/Enrichr/
FUSION Solo S software	Version 17.01	© Vilber Lourmat, Collégien, France
GraphPad Prism	Prism9	© 2020 GraphPad Software
GO enrichment analysis	access 2021	website https://maayanlab.cloud/Enrichr/
Microsoft Office 2016	Version 16.51	Microsoft Corporation, Redmond, WA, USA
National Cancer Institute	Access 2021	http://www.cancer.gov/dictionary/?CdrID=45618
NIS Element Software	Version 4.0	Nikon Europe BV, Amsterdam, Netherlands
ImageJ	Version 2.1.0/1.53c	Open-source image processing software
InqScape	Version 1.0.1 (c497b03c, 2020-09-10)	© 2020 Inkscape Development Team
IncuCyte® S3 Live-Cell Analysis System Software	Version 2018B	Sartorius | Essen BioScience, Royston, UK
NanoDrop 2000/2000c	Version 1.6	ThermoFisher Scientific, Waltham, MA, USA
LAS X Life Science Microscope	Version 3.6.0.20104	Carl Zeiss Microscopy GmbH, Germany
Primer-BLAST	access 2018	NCBI, Bethesda MD, USA
Primer3Plus	access 2018	[132]

Snap Gene Viewer	Version 5.3.2.	GSL Biotech LLC
Silhouette Studio	Version 4.0.837ss	Silhouette America, Lehi, USA
TCGA Database	access 2021	National Cancer Institute (NCI), USA
UCSC Genome Browser	access 2021	© 2000-2020 The Regents of the University of California
UniPort	access 2018	UniProt consortium members: European Bioinformatics Institute (EMBL-EBI), Cambridge, UK SIB Swiss Institute of Bioinformatics, Geneva, Switzerland Protein Information Resource, Washington, DC, USA
Venn diagrams	access 2021	https://bioinformatics.psb.ugent.be/webtools/Venn/
xPONENT	Version 4.2	Luminex Corporation, Austin, TX, USA

3. METHODS

3.1. Establishment of PDO models

Human colorectal cancer PDO models used in this project (Table 3) were generated and obtained from a previous study [115,121].

In addition, I generated PDO models from fresh frozen human colorectal cancer tissue, kindly provided by Dr. Michael Linnebacher, University Medicine Rostock (Table 3). I performed all *in vitro* experiments under sterile conditions. I maintained cells at 37 °C with a CO_2 concentration of 5 % and a humidity of 95 %. I pre-warmed the cell culture media to room temperature (RT) before use.

3.1.1. Maintenance and propagation of PDO models

Organoid cultures were generated and propagated as previously described [121]. In brief, patient-derived tumor tissues were macro-dissected and necrotic as well as fatty areas were removed. Tissue was then washed twice in Hanks' balanced salt solution (HBSS, Gibco), manually minced (pieces < 1 mm) and enzymatically dissociated by incubating it up to 1 h at 37°C in digestion solution consisting of collagenase IV (Sigma-Aldrich), DNase I (AppliChem) and dispase (StemCell Technologies). Subsequently, the cell suspension was progressively filtered through 100 µm and 30 µm cell strainers (Miltenyi Biotec) and, after red blood cell lysis, 30-100 µm cell clusters were plated in phenol-red free growth factor-reduced Matrigel® (Corning) into 24-well plates (Corning). After incubating the plate for 15-30 min at 37 °C, XY-medium (Table 6) was added. 1.25 µg/ml amphotericin B (Sigma-Aldrich) were added for the first week of culture.

I thawed the fresh frozen patient-derived tumor tissue at 37 °C and washed it three times in P/S medium (Table 6) in a Petri dish (Corning, U.S.A.). I macro-dissected the tumor tissue and transferred it into a 15 ml Falcon tube and centrifuged it at 300 rcf for 5 min. I plated cell clusters in Matrigel® or Cultrex® (R&D Systems) into 24-well plates. After incubating the plate for 15-30 min at 37 °C, I added XY-medium (Table 6) supplemented with 1.25 µg/ml amphotericin B.

I observed the PDO cultures under the microscope (Leica) and cultured them by changing the medium every other day. As soon as organoids reached a diameter of approximately 400 – 600 µm, I splitted the organoids by releasing the cell aggregates from Matrigel® or

Cultrex®, pelleting (300 rcf for 3 minutes) and adding 0.5 ml – 1 ml (depending on pellet size) 1x TrypLE Express solution (Gibco). Depending on the rigidity of the 3D aggregates, I digested the organoids with TrypLE for 10 to 40 minutes. Following digestion, I washed the aggregates with 5 ml P/S medium (Table 6) and re-plated them in a 24-well plate (Greiner Bio-One).

In general, each new batch number of Matrigel® or Cultrex® has been tested before use. Therefore, the same PDO model with the same passage number was cultivated in Matrigel® or Cultrex® from the old and the new batch in parallel and were observed under microscope for at least two weeks.

3.1.2. Freezing and thawing of PDO models

I generated stocks for re-cultivation of all PDO cultures from the lowest possible passage on by pelleting and resuspending 4 wells with 1 ml of Recovery Cell Culture Freezing Medium (Gibco). For re-cultivation, I thawed cell aggregates at 37 °C and transferred them into a 15 ml Falcon tube. I diluted the DMSO-containing Recovery Cell Culture Freezing Medium by slowly adding 5 ml P/S medium (Table 6). After centrifugation at 300 rcf for 3 minutes, I mixed the cells with Matrigel® or Cultrex® and plated droplets (15 µl) in a 24-well plate. 15 min after solidification at 37 °C, I added 750 µl of XY-medium (Table 6).

3.1.3. Fixation of organoids

For fixation, I collected organoids in a 15 ml Falcon tube and carefully loosened them from Matrigel®. I filled up the organoid/Matrigel®/medium mixture to 10 ml with 0.1 % BSA/PBS and centrifuged it at 100 rcf for 3 min. The organoids did not form a flat pellet. I resuspended the Organoid/Matrigel®-Mix with 4 % formalin/PBS solution (100 µl – 1 ml) and incubated it for 1 h at RT. Afterwards, I centrifuged the organoids at 100 rcf for 3 min, resuspended and incubated them in 10 ml 0.1 % BSA/PBS for 10 min to remove fixative. I repeated the washing step three times. For the last washing step, I incubated the organoids in 0.1 % Triton/PBS for better DAPI permeability. For nuclei staining, I incubated the organoids with 1 ml 0.1 % BSA/PBS including 0.2 mg/ml DAPI (AplliChem) for 5 min. I filled up the organoid suspension to 10 ml with 0,1 % BSA/PBS and centrifuged it at 100 rcf for 3 min. I resuspended the stained organoids with 200 µl 0.1 % BSA/PBS and transferred onto a glass slide.

I removed the excess liquid and added mounting media (Ibidi GmbH) for the cover slips. I protected the slides from light and dried them for 1-2 h at RT or over night at 4°C to solidify the mounting media.

3.1.4. Growth assays with PDO models

For the growth assay, I incubated PDO cultures with TrypLE until a single cell suspension was achieved. I added P/S medium (Table 6) to stop trypsinization and counted the cells. I mixed the single cells in Matrigel® or Cultrex® and seeded them at a density of 1250 cells/well, 2500 cells/well and 5000 cells/well in 96-well plates (1 plate per day of measurement). After incubating at 37 °C for 15 min to allow the Matrigel® to solidify, I added 100 µl/well of XY-medium. I detected the cell density using Cell Titer Glo (CTG) assay (Promega) according to manufacturer's protocol after seeding, on days 2, 3, 5 and 7. I repeated the experiments twice with three technical replicates. Afterwards, I calculated the doubling times using exponential growth equation in Prism 9.

3.2. Semi-automated high-throughput drug response assay

For the semi-automated drug screening, I incubated the PDO cultures with TrypLE until a single cell suspension was achieved. I added P/S medium (Table 6) to stop trypsinization and counted the cells. I mixed the single cells in Matrigel® or Cultrex® and seeded them at a density of 1500 cells/well in 384-well plates (Greiner Bio-One) by means of Biomek FX automated workstation (Beckman Coulter). After incubating at 37 °C for 15 min to allow the Matrigel® to solidify, I added 50 µl/well of XY-medium (Table 6). Cells were cultured for three to four days until organoid sizes reached 50 µm in diameter prior to treatment. Subsequently, I performed the drug treatments by removing XY-medium daily and adding 50 µl/well complete medium (Table 6) without ROCK inhibitor, containing drugs by means of Biomek FX automated liquid handler (Beckman Coulter). The concentrations of tested compounds were distributed around the c_{max} (human maximal plasma concentration) values (Table 17) [133]. I plated drugs in 4-point, 6-point, 12-point or 24-point serial dilutions (Table 18). Cells treated with DMSO (Sigma-Aldrich) (0.2 %) were used as "untreated control" while Matrigel® or Cultrex® only was used for background readout. Staurosporine was used as internal positive control.

I performed drug testing experiments with four technical replicates and repeated them at least three times.

After 4 days of treatment, I determined the cell viability by Cell Titer Glo (CTG) assay following the manufacturer's protocol. I measured the intensity of luminescence using a SpectraMax i3x plate reader (Molecular Devices) 30 min after addition of CTG. I used the luminescence intensity data to evaluate the percentage of viability after background subtraction.

Table 17: Compounds used for drug screening.

Clinical dosage, molecular mass and associated c_{max} values are shown. (BRAF = B-rapidly accelerated fibrosarcoma, ERK = extracellular-signal related kinase, MEK = mitogen-activated protein kinase kinase, mRTK = multi-receptor tyrosine kinases)

Compound	Target(s)	Actual clincial dosage	Mass [g/mol]	c_{max} [µM]	Reference
5-FU	pyrimidine analog	400 mg/m² bolus i.v.	130.08	230.627	[134]
Binimetinib	MEK 1/2	45 mg PO	441.23	0.544	[76,135]
Cobimetinib	MEK1/2	60 mg PO	531.31	0.508	[75,133]
Dabrafenib	BRAF	150 mg PO	519.56	1.551	[136,137]
Regorafenib	mRTK	160 mg PO	482.82	8.078	[138]
Selumetinib	MEK1	100 mg PO	457,68	1,062	[77,139]
Staurosporine	protein kinase	-	466.5	0.25	[140]
Trametinib	MEK1/2	2 mg PO	615.39	0.036	[74,136]
Ulixertinib	ERK1/2	600 mg PO	433.33	2.769	[141]

Table 18: 4-point, 6-point, 12-point, and 24-point dilutions (dil) of different compounds [µM] used for drug screening.

4-point dilutions

Compound [µM]	**dil 1**	**dil 2**	**dil 3**	**dil 4**
Trametinib	0.162	0.032	0.006	0.001
Cobimetinib	2.579	0.508	0.094	0.019
Selumetinib	4.261	0.852	0.175	0.044
Regorafenib	51.779	10.356	2.071	0.414
Dabrafenib	19.247	3.849	0.770	0.154
5-FU	1153.137	230.627	46.125	9.225
Ulixertinib	13.846	2.769	0.554	0.111
Staurosporine	1.250	0.250	0.050	0.010

6-point dilutions

Compound [µM]	**dil 1**	**dil 2**	**dil 3**	**dil 4**	**dil 5**	**dil 6**
Trametinib	0.292	0.097	0.032	0.011	0.004	0.001
Cobimetinib	4.574	1.525	0.508	0.169	0.056	0.019
Selumetinib	1.573	0.524	0.175	0.058	0.019	0.006
Staurosporine	1.250	0.417	0.139	0.046	0.015	0.005

12-point dilutions

Compound [µM]	**dil 1**	**dil 2**	**dil 3**	**dil 4**	**dil 5**	**dil 6**	**dil 7**	**dil 8**	**dil 9**	**dil 10**	**dil 11**	**dil 12**
Trametinib	0.341	0.213	0.133	0.083	0.052	0.032	0.020	0.013	0.008	0.005	0.003	0.002
Cobimetinib	5.329	3.330	2.081	1.301	0.813	0.508	0.318	0.199	0.124	0.078	0.048	0.030
Selumetinib	1.833	1.146	0.716	0.447	0.280	0.175	0.109	0.068	0.043	0.027	0.017	0.010
Regorafenib	108.589	67.868	42.417	26.511	16.569	10.356	6.472	4.045	2.528	1.580	0.988	0.617
Dabrafenib	40.364	25.228	15.767	9.854	6.159	3.849	2.406	1.504	0.940	0.587	0.367	0.229
5-FU	2418.303	1511.439	944.649	590.406	369.004	230.627	144.142	90.089	56.305	35.191	21.994	13.746
Binimetinib	5.727	3.580	2.237	1.398	0.874	0.546	0.341	0.213	0.133	0.083	0.052	0.033
Ulixertinib	29.038	18.149	11.343	7.089	4.431	2.769	1.731	1.082	0.676	0.423	0.264	0.165

24-point dilutions

Compound [µM]	**dil 1**	**dil 2**	**dil 3**	**dil 4**	**dil 5**	**dil 6**	**dil 7**	**dil 8**	**dil 9**	**dil 10**	**dil 11**	**dil 12**
Trametinib	0.940	0.671	0.480	0.343	0.245	0.175	0.125	0.089	0.064	0.045	0.032	0.023
	dil 13	**dil 14**	**dil 15**	**dil 16**	**dil 17**	**dil 18**	**dil 19**	**dil 20**	**dil 21**	**dil 22**	**dil 23**	**dil 24**
	0.017	0.012	0.008	0.006	0.004	0.003	0.002	0.002	0.001	0.001	0.001	0.000
Cobimetinib	**dil 1**	**dil 2**	**dil 3**	**dil 4**	**dil 5**	**dil 6**	**dil 7**	**dil 8**	**dil 9**	**dil 10**	**dil 11**	**dil 12**
	14.699	10.499	7.500	5.357	3.826	2.733	1.952	1.394	0.996	0.711	0.508	0.363
	dil 13	**dil 14**	**dil 15**	**dil 16**	**dil 17**	**dil 18**	**dil 19**	**dil 20**	**dil 21**	**dil 22**	**dil 23**	**dil 24**
	0.259	0.185	0.132	0.094	0.067	0.048	0.034	0.025	0.018	0.013	0.009	0.006
Selumetinib	**dil 1**	**dil 2**	**dil 3**	**dil 4**	**dil 5**	**dil 6**	**dil 7**	**dil 8**	**dil 9**	**dil 10**	**dil 11**	**dil 12**
	5.056	3.611	2.580	1.843	1.316	0.940	0.671	0.480	0.343	0.245	0.175	0.125
	dil 13	**dil 14**	**dil 15**	**dil 16**	**dil 17**	**dil 18**	**dil 19**	**dil 20**	**dil 21**	**dil 22**	**dil 23**	**dil 24**
	0.089	0.064	0.046	0.033	0.023	0.017	0.012	0.008	0.006	0.004	0.003	0.002

3.3. Live-cell imaging

I performed live-cell imaging experiments at the Max Planck Institute for Molecular Medicine in Göttingen, Germany. I used live-cell imaging to observe PDO drug response over time. Therefore, I coated the 96-well plates with 50 µl Matrigel® (2.5 mg/ml in cold complete medium) and incubated them for 1 h at 37 °C. I collected the organoids and incubated them with TrypLE until a single cell suspension was achieved. I added P/S medium (Table 6) to stop trypsinization, and cells were counted. I mixed single cells at a density of 2000 cells/well in complete medium (Table 6) and incubated them for 1 h at 37 °C. Afterwards, I removed the medium and covered the cells with 25 µl Matrigel® (2.5 mg/ml in cold complete medium). Finally, I added 75 µl complete medium supplemented with respective drug or drug combination and changed it daily. IncuCyte® Live-Cell Imaging System (Sartorius) took pictures every 30 min for 72 h. I used IncuCyte® Live-Cell Imaging System Software (Sartorius) to analyze the data.

3.4. Standard DNA procedures

3.4.1. Isolation of genomic DNA and total RNA

For DNA preparation, I collected organoids from 4-8 wells of a 24-well plate, centrifuged (300 rcf for 3 min), washed in 1x PBS (Gibco) and stored them at -80 °C for further use.
For isolation of genomic DNA, I used the Wizard Kit (Promega) according to the manufacturer's protocol. I eluted the DNA in 30 µl RNAase free water (Sigma-Aldrich) and stored it at -20 °C for further use.
For total RNA isolation, I collected organoids from 12 wells of a 24-well plate. I removed the Matrigel® by pipetting 10 times up and down and centrifugation (300 rcf for 5 min at 4 °C). For the following steps, I kept all samples ice. I washed the cell pellet with 5 ml sterile ice-cold PBS and centrifuged (300 rcf for 5 min at 4 °C). Afterwards, I resuspended the cell pellet in 600 µl ice-cold RLT buffer (QIAGEN #79216) supplemented with β-mercaptoethanol (Sigma-Aldrich) (1:100). Samples were frozen at -80 °C for further use. Total RNA was isolated (Germany) and quantified using a spectrophotometer (Nanodrop 2000, ThermoFisher) by ATLAS Biolabs GmbH.

3.4.2. Standard PCR

For standard polymerase chain reaction (PCR) [142], I designed primer using the web-interfaces Primer3Plus and Primer-BLAST. The PCR reaction mixture (25 µl) contained 100 ng isolated DNA, 1x Phusion GC buffer (ThermoFisher), 3 % DMSO, 200 µM dNTPs, about 0.5 µM of forward (SMAD4 fw2) and reverse (SMAD4 rev2) primer (Table 15), and about 0.02 U/µl of Phusion DNA polymerase (ThermoFisher). Amplification started with initial denaturation at 95 °C for 5 min. Amplification protocol continued with denaturation at 95 °C for 30 sec, primer annealing at 58 °C for 30 sec and extension at 72 °C for 30 sec. Steps within the amplification protocol were repeated 34 times in an automated DNA thermal cycler (Biometra TRIO, Analytik Jena AG). Final extension was performed at 72 °C for 5 min. I resolved the PCR products on a 2 % agarose gel (prepared in 1x TAE buffer (Table 8)) stained with ethidium bromide (Carl Roth). PCR product (688 bp) was visualized under the UV trans illuminator (VWR®). Molecular size markers (GeneRulerTM100bp DNA Ladder, ThermoFisher) ran concurrently.

3.4.3. Re-isolation and purification of PCR products

I purified the PCR products using the GeneJET PCR purification Kit (ThermoFisher). For re-isolation of the PCR product from agarose gels, I used the GeneJET Gel Extraction Kit (ThermoFisher). I used both kits according to the manufacturer's protocols. I eluted the cleaned or re-isolated PCR products in 30 µl of the respective elution buffers.

3.5. Sequencing Methods

3.5.1. Panel sequencing

Targeted high-depth DNA sequencing was performed (mean depth 1500 reads) for genomic areas comprising 100 genes using a custom-designed CRC panel by Soulafa Mamlouk from Charité Comprehensive Cancer Center (Suppl. Table 1) [143]. A MiSeq device (Illumina) was used. DNA (10 ng) was prepared using the Ion AmpliSeq Library Kit 2.0 (ThermoFisher) for the CRC panel, followed by library preparation using the NEB Next Ultra DNA Library Prep kit (end repair, A-tailing, adaptor ligation and amplification; NEB, E7370S) and NEB Next Multiplex Oligos provided for Illumina (NEB, E7335S). 100 pM of resulting library DNA were pooled. The average read output was 4.6 x 10^6 reads [143].

3.5.2. Sanger sequencing of PCR amplicons

Mutations found via panel sequencing were validated via Sanger sequencing of PCR amplicons using both SMAD4 fw2 and SMAD4 rev2 primer (Table 15). Template DNA for PCR reactions came from the same aliquot used for targeted sequencing as template. I sent aliquots of 20 ng/µl purified PCR product to LGC Genomics GmbH (Germany) for sequencing. I analyzed electropherograms and FASTA files from Sanger sequencing using CLC Genome Viewer (QIAGEN).

3.5.3. Whole transcriptome sequencing

Whole-transcriptome sequencing was performed at ATLAS Biolabs GmbH (Germany). An average of 1 µg total RNA per sample was used to generate barcode-labeled libraries using the Illumina TruSeq Standard mRNA Library preparation kit. Paired-end libraries were sequenced on an Illumina NovaSeq sequencer with 125 bp reads protocol. The RNA-sequencing analysis war performed by Sergei Belanov from the Institute of Biotechnology at the University of Helsinki.

To generate gene expression data, RNA-seq reads were mapped to the latest available annotated reference genome from the Ensembl collection [144] using STAR aligner [145]. Rsubread package [146] and featureCounts tool [147] were used to evaluate read counts and generate expression data matrix. Further differential gene expression analysis was performed using the NOISeq package [148] with the pipeline customized for the replicate simulation analysis. Read counts were normalized using RPKM (Reads per kilo base per million mapped reads) [149] and TMM (Trimmed Mean of M-values) methods [150], low count values were filtered away, ARSyNseq function of NOISeq package used to filter out noise-associated results and unidentified batch effects, to increase a significance of differential expression probability we used parameter q = 0.95 for the NOISeq-sim function. Bioconductor packages org.Hs.eg.db (DOI: 10.18129/B9.bioc.org.Hs.eg.db) and Genomic Features [151] used to annotate results. GO-annotation and functional enrichment analysis was implemented utilizing GOexpress [152] and EnrichR [153,154] packages.

For the comparison, I created a Venn diagram using a Venn diagram online tool (Table 16) and for GO enrichment analysis, I used the website https://maayanlab.cloud/Enrichr/.

3.6. Generating CRISPR-engineered organoids

The clustered regularly interspaced short palindromic repeats (CRISPR)/CRISPR-associated (Cas) system CRISPR/Cas system is an efficient gene editing tool based on nucleic-acid-based adaptive immune systems widely used in bacteria and archaea [155–157]. CRISPR/Cas nucleases perform RNA- guided DNA cleavages to induce targeted genetic modifications [158]. The Cas9 nuclease domain of *Streptococcus pyogenes (S. pyogenes)* performs the DNA cleavage 3 bp upstream (5`) to the PAM sequence, resulting in a blunt cut between the 17th and 18th bases of the target sequence [155,159]. The PAM sequence of Cas9 nuclease from *S. pyogenes* is a 5`-NGG-3` DNA sequence. The created double strand break stimulates the cellular repair mechanisms, non-homologous end-joining (NHEJ) or the homology-directed repair (HDR) for genome editing [160]. The CRISPR/Cas9 system can be directed to any 5`-N20-NGG-3` DNA sequence by simply rearranging the 20 nt of RNA hybrid that confers sequence specificity to the target sequence [161–163].

The CRISPR/Cas9 system can be easily used for gene editing because only a single gRNA (sgRNA) is needed to target a specific sequence [164].

In this study, I generated CRISPR-engineered organoids. Therefore, I inserted SMAD4 sgRNA SMAD4-I-A or SMAD4-II-B (Table 15) into the BbSI site downstream of a human U6 promoter into plasmid pU6sgh-CAG-Cas9-venus-bpA (Figure 13) (kindly provided by Dr. Ralf Kühn (MDC Berlin). For this purpose, plus and minus strand oligos containing the 20 nt guide sequence were annealed for 5 min at 100 °C in 100 µl 1x TE buffer (Table 8) (10 ng/µl) and slowly cooled down to RT. 5 µg of plasmid pU6chimRNA-CAG-Cas9-venus-bpA were digested with restriction enzyme BbsI (NEB #R3539) for 1.5 h in a 37 °C water bath. I loaded the product on a 0.9 % agarose gel (prepared in 1x TAE buffer) and extracted the 10 kb vector band from the gel using GeneJET Gel Extraction Kit (ThermoFisher).

I incubated the mixture of linearized plasmid and inserts (15 µl) with ligase (New England BioLabs) over night at 16 °C followed by transformation into DH5 alpha *E. coli*. I plated the transformed bacteria onto 10 cm agar plates containing LB medium and 100 µg/ml Carbenicillin (Sigma-Aldrich). Growing colonies were picked and incubated in LB medium containing 100 µg/ml Carbenicillin over night at 37 °C for minipreps.

I performed minipreps according to the standard protocol (ThermoFisher). Resulting plasmid was sequenced using the U6 primer (Table 15) before transfection. All primer and single stranded oligonucleotides were synthesized by BioTEz GmbH (Germany).

3.6.1. Transfection for targeted gene editing

I collected and digested the organoids as described above. I plated $2x10^5$ single cells in 500 µl of culture medium into ultra-low attachment 24-well plates (Greiner Bio-One). I used single stranded oligos (ssODNs) for introduction or correction of single nucleotide mutation via homology-directed repair (HDR) at the target site (Table 15). For the transfection, I used TransIT-2020 transfection reagent (Mirus Bio), according to the manufacturer's protocol. To increase HDR, I co-transfected the organoids with a plasmid vector containing i53-bpA (Figure 14), an inhibitor of 53BP1 [165].

I transfected the cells with 700 ng DNA MasterMix, consisting of 250 ng pU6SMAD4-I-CAG-Cas9-venus-bpA or pU6SMAD4-II-CAG-Cas9-venus-bpA (U1 or U2) (Figure 13), 83.3 ng pCAG-i53-EF1BFP (Figure 14), 200 ng pCAG-Cas9-PCK-venus (Figure 15),

166.6 ng ssODN as template bearing either the SMAD4 wild type sequence (ssODN 1 and 2) or R361H point mutation (ssODN 3 and 4).

3.6.2. Cell sorting

After 72 h of transfection, I sorted cells upon using fluorescence-activated cell sorting (FACS). For this purpose, I collected cells by centrifugation at 300 rcf for 5 min and resuspended them in 500 µl TrypLE for 15 min. I washed the single cells in XY-medium (Table 6) and incubated them for 15 min at 37 °C. Afterwards, I washed the cells in 1x PBS (Gibco) and filtered them through 35 µm cell strainer (Corning). I gated single cells for Venus/BFP and sorted them directly in 500 µl of XY-medium (Table 6) containing 10 µg/ml Gentamicin (Sigma-Aldrich) using a BD Aria cell sorter (BD Biosciences). Afterwards, I embedded Venus/BFP-positive cells in Matrigel® (Corning).
After three weeks in culture, I used half of the cells to isolate genomic DNA and performed PCR for genotyping, while using the other half for expansion and clonal selection.

3.6.3. Limited dilution

For limited dilution, I dissociated cells using TrypLE as described above. I prepared a cell solution, at a concentration of 5 cells/ml in 10 ml XY-medium for one 96-well plate (Greiner Bio-One). I transferred 100 µl into a round-bottom 96-well plate (Greiner Bio-One) to achieve an average density of 0.5 cell/well. In the upper left well, I seeded 1000 cells for the later adjustment of the microscope focus when scanning the plates for single cells. I monitored the limited dilution plates under the microscope for monoclonal colonies over time. Individual colonies were allowed to grow until they could be genotyped individually. To confirm gene editing, I used the CloneJET PCR Cloning Kit (ThermoFisher) according to the manufacturer's protocol.

3.7. Establishment of 5-FU resistant PDO models

I cultured PDO models in presence of a sublethal concentration of 5-FU (9.2 µM) for four weeks. Surviving cells were allowed to recover and challenged further with 46.1 µM of 5-FU over four months. Subsequently, I increased the 5-FU concentration to 230 µM (c_{max}) [134] for another three months. Developed 5-FU resistant cells were amplified in XY-medium before the drug treatment experiments (Figure 42).

3.8. Lentiviral gene transfer

To overexpress the SMAD4 wild type gene in SMAD4^{R361H} organoids, I performed lentiviral transduction.

3.8.1. Restriction digest of plasmid used for lentiviral transduction

Both plasmids pHAGE-SMAD4 (addgene #116791) and pHAGE puro (addgene #118692) were sequenced using pEFmyccyto-F and T7prom primer as control (Table 15).
I tested the packing plasmids pRSV-REV (addgene #12253), pMDLg/pRRE (addgene #12251) and pCMV-VSV-G (addgene #8454) by using restriction digestion (Table 13).

3.8.2. Virus formation

I cultured the virus producing cells (HEK293T) in RPMI1640 (Table 6) and plated them in a T75 flask at approximately 40 % confluency the day before transfection (antibiotic-free preferred).
After 24 h, I prepared the transfection mixture, consisting of 10 µg pHAGE-SMAD4 (addgene #116791), 10 µg packaging plasmids (2.5 µg of pRSV-REV (addgene #12253), 4 µg of pMDLg/pRRE (addgene #12251) and 3.5 µg of pCMV-VSV-G (addgene #8454)), 4 µg gfp-plasmid (Table 12), 24 µl transfection reagent Trans IT 2020 (Mirus Bio), which I diluted in 1.2 ml Opti-MEM (Gibco) and incubated for 15 min at RT. As negative control, I used 10 µg pHAGE puro (addgene #118692).
I added the transfection mixture drop-wise to the cells. I collected and pooled the media after 12 h, 24 h, 36 h, 48 h and 72 h. After the last collection, I centrifuged the pooled supernatants at 1000 rcf for 5 min and filtered them through a syringe filter (0.45 µm). Viral particles could then be used for transduction.

3.8.3. Lentiviral transduction

For lentiviral transduction, I collected organoids from four wells of a 24-well plate and released them from Matrigel®, transferred them into a 15 ml Falcon tube and centrifuged them (300 rcf for 5 min). I added 2 ml virus containing medium supplemented with 8 µg/ml polybrene (Sigma-Aldrich) and centrifuged at 1000 rcf for 30 min. Afterwards, I added 3 ml XY-medium (Table 6) and plated organoids into ultra-low attachment 24-well plates and incubated them for 18-20 h at 37 °C.

All steps described above were repeated four times. Following transduction, I re-plated organoids in Matrigel® and selected them with 2 µg/ml puromycin (Gibco). After selection, I expanded organoids for further experiments.

PCR was performed as described above, but I used SMAD4_RE_fw1 as forward and SMAD4_RE_rev1_new and as reverse primer instead (Table 15). Amplification started with initial denaturation at 95 °C for 5 min. Amplification protocol continued with denaturation at 95 °C for 30 sec, primer annealing at 58 °C for 5 sec and extension at 72 °C for 15 sec. Steps within the amplification protocol were repeated 34 times in an automated DNA thermal cycler (Biometra TRIO, Analytik Jena AG). Final extension was performed at 72 °C for 5 min. I verified the PCR products on a 2 % agarose gel (prepared in 1x TAE buffer (Table 8)) stained with ethidium bromide (Carl Roth). PCR product (549 bp) was visualized under the UV trans illuminator (VWR®). Molecular size markers (GeneRulerTM100bp DNA Ladder, ThermoFisher) ran concurrently.

3.9. Protein analysis via DigiWest®

Organoid cultures were subjected to multiplex protein profiling analysis of 120 proteins and some of their phosphorylated forms. Therefore, I subjected organoid cultures to drug treatment prior to protein extraction. Therefore, I plated 3.0 x 10^6 cells (= 4 x 10^4 cells/well in 6 wells of a 24-well plate) per condition, followed by a growth period of 72 h and subsequent treatment with trametinib (0.03 µM) or vehicle control (0.03 % DMSO) for the duration of 0.5 h, 6 h and 24 h. Trametinib concentration was chosen based on clinically achievable plasma concentrations [136]. After treatment, I washed organoids with ice cold PBS and incubated them with cell recovery solution (Corning) on ice for 30 min. Afterwards, I washed them twice with ice cold PBS, centrifuged them (300 rcf for 5 min). The pellet was snap frozen and stored at -80 ˚C until cell lysis.

DigiWest® experiments were conducted by Markus Templin and Patrick Herter at NMI Natural and Medicinal Sciences Institute, University of Tübingen (Reutlingen, Germany). DigiWest® procedure was performed as previously described [166]. The samples were lysed with LDS-buffer (Table 8) at 95 °C. Afterwards the protein concentration was determined. Before performing the SDS-PAGE, cell lysates were concentrated in a vacuum concentrator (Bachofer GmbH) for 2 h.

The proteins were separated through 4 % - 12 % Bis-Tris gels using the NuPAGE SDS-PAGE gel system (ThermoFisher) following the manufacturer's instruction. Blotting onto PVDF membranes (Merck Millipore) was performed under standard conditions. After blotting, the immobilized proteins were biotinylated with sulfo-NHS-biotin (NHS-PEG12-Biotin, ThermoFisher). Then an automated cutting tool (Silhouette) cut each sample lane into 96 stripes, each stripe representing a unique molecular mass fraction between 15 and 250 kDa. For protein elution, each stripe was sorted into a separate well of a 96-well plate, followed by 2 h of incubation with elution buffer (Table 8). After adding 90 µl of dilution buffer (Table 8), 96 different neutravidin-coated Luminex® bead sets (60,000 beads/well) were added to the individual wells, and biotinylated proteins were captured on the bead surface. After overnight incubation, the Luminex® beads were pooled, washed, and stored in a storage buffer (Table 8) at 4 °C. To perform the primary antibody incubation, 0.5 % of the pooled beads were transferred to an assay plate. Afterwards, the primary western blot antibody was added to each well, diluted in 30 µl assay buffer (Table 8), followed by an incubation step overnight. The list of antibodies is shown in Table 14. After incubation, the beads were washed twice with 100 µl PBST (Table 8). Afterwards the secondary species-specific PE labelled antibody was diluted in 30 µl assay buffer and the beads were incubated for 1 h with the diluted secondary antibody. The beads were washed again twice with 100 µl assay buffer. The analyte signals were generated in a FlexMAP 3D instrument (Luminex®). The generated data were analyzed with a DigiWest® analysis tool (NMI, Germany). The tool visualized the fluorescent signals generated by the secondary antibody in a bar chart, which is composed of the signals for the 96 molecular mass fractions. To each of the 96 fractions a relative molecular mass was assigned. The software tool identified specific peaks for each of the 120 used primary antibodies. After background correction, the integral of the analyte specific peak was used to calculate the signal for each analyte. I normalized the values to beta-actin. I calculated increase in protein expression by dividing the treated sample by the untreated control. For phosphorylation status, each phospho-protein was normalized to correspondent protein total level.

3.10. Statistical analysis

I used GraphPad Prism software (version 9) to visualize the data and to perform statistical analysis. All data are presented as means and standard deviations, using the results of at least three independent experiments, unless indicated otherwise.

For comparison of two different groups, I used Student's t-test. For the comparison of three or more different groups, I performed a one-way analysis of variance (ANOVA) and Tukey's post multiple comparison test.

For the comparison of drug effect curves, I applied the extra-sum-of-squares (F) test. For the contingency analyses, I used Fisher's exact test.

All significance tests were two-sided, and I defined p-values of less than 0.05 as statistically significant.

4. RESULTS

4.1. Investigation of the clinical relevance of the SMAD4 gene in colorectal cancer

Patient-derived organoid (PDO) models provide accurate and physiologically relevant models for studying the biology of diseases and support (pre)clinical research as well as clinical decision making. These three-dimensional cultures maintain a typical adenoma-like architecture that retains higher-order organization and apical-basal polarity of the colonic epithelium, as reported earlier [121].

Intra-tumor heterogeneity (ITH) poses a significant problem in anti-cancer therapy, however, in the laboratory it can be used to identify potential biomarkers.

In a previous study, ITH was investigated by using organoid "sibling" culture models, established from separate regions of an individual primary chemo-naïve metastatic CRC tumor [115] (Figure 16). ITH, due to an additional SMAD4^{R361H} mutation in some of the "sibling" cultures leads to a differential drug response [115].

4.1.1. Single gene alteration leads to differential drug response

In the present study, I focused on two representative regions, region 1 (R1) and region 4 (R4) which differ in a homozygous SMAD4^{R361H} mutation [115], a well-known loss of function mutation [167] (Figure 16).

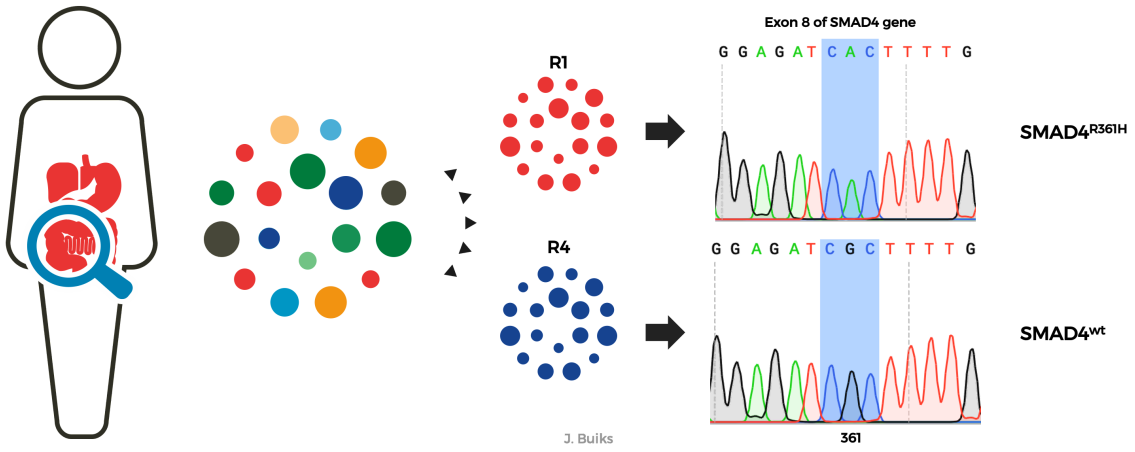

Figure 16: Establishment of the tumor region specific PDO models from surgical specimens of a metastatic colorectal cancer patient (stage IV).
Two representative PDO models are shown (R1 and R4). A CRC panel-sequencing *[143]* showed significant overlap in common mutations (KRAS^{G12D}, PIK3CA^{H1047R}, and TP53^{C242F}). R1 differs from R4 in a homozygous SMAD4^{R361H} loss-of-function mutation.

The panel-sequencing with 94 commonly mutated genes in CRC [143] showed significant overlap in common mutations (KRAS^{G12D}, PIK3CA^{H1047R}, and TP53^{C242F}) and confirmed the homozygous SMAD4^{R361H} mutation in R1 (Table 19). Therefore, R1 is further described as **R1^{R361H}** and R4 as **R4^{wt}**.

Table 19: Colorectal cancer panel sequencing of R1^{R361H} and R4^{wt}.
In total, 94 CRC related genes were sequenced *[143]*. Variant allele frequencies (VAF) of 12 gene are shown. R1^{R361H} and R4^{wt} differ in a homozygous SMAD4^{R361H} loss-of-function mutation.

Gene	VAF	
	R1^{R361H}	R4^{wt}
KRAS_c.12 G>D	60	53
KRAS_c.15 G>A	3	0
POLE_c.252 A>V	40	47
TP53_c.242 C>F	100	100
SMAD4_c.361R>H	100	0
PI4KA_c.702 Y>*	5	4
PI4KA_c.2208 N>K	0	0
MLH1_c.219 I/V	41	0
PIK3CA_c.1047 H>R	32	33
KDR_c.472 Q>H	49	0
HDAC3_c.296 G>V	27	26
HDAC2_c.81-82 SR>RR	0	1

I performed a growth assay, to assess the doubling time of R4^{wt} and R1^{R361H} PDOs, to determine the optimal cell density for further drug screenings (Figure 17). The organoid model R1^{R361H} with SMAD4^{R361H}, tended to proliferate significantly faster with doubling time of 1 day vs. 1.6 days in SMAD4 wild-type model R4^{wt} (Figure 17). For further drug screenings in a 384-well-plate-format, I did choose 1500 cells/well as optimal cell number.

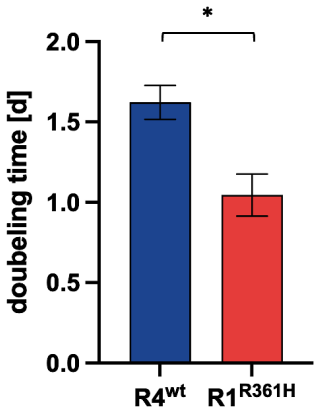

Figure 17: Doubling time of R4^{wt} and R1^{R361H}.
Cell density was measured on day [d] 2, 3, 5, and 7, by measuring cellular ATP content using Cell Titer Glow assay (Student's t-test, *p < 0.05).

It was previously shown that mutations in the SMAD4 gene have been associated with chemoresistance in CRC [102]. Therefore, I treated $R4^{wt}$ and $R1^{R361H}$ with 5-Fluorouracil (5-FU), as a representative first-line drug, which is used in systemic chemotherapy [168]. There was no significant difference in response to 5-FU (Figure 18) between the models. Although tumor cell proliferation was reduced under 5-FU treatment (Figure 18), the absolute IC_{50} (50 % inhibition) values for both models were comparable to the c_{max} value of 5-FU [134].

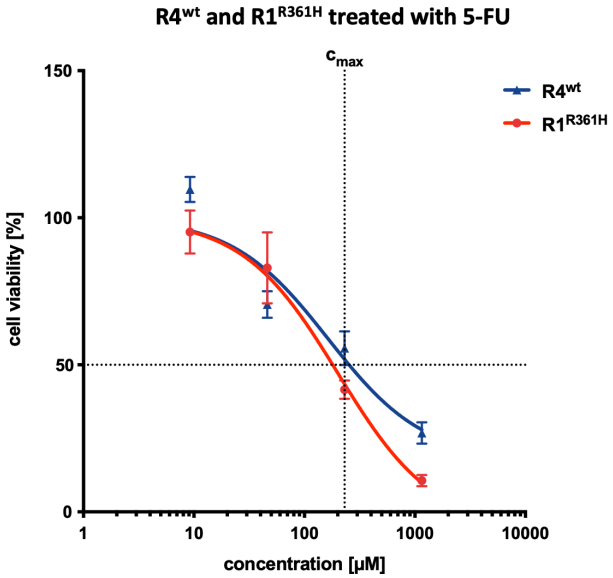

Figure 18: Sibling PDOs ($R4^{wt}$ and $R1^{R361H}$) treated with 5-Fluorouracil (5-FU).
5-FU is the basis of standard first-line chemotherapy for colorectal cancer [168]. Cell viabilities [%] of $R4^{wt}$ and $R1^{R361H}$ treated with 5-FU for 4 days in a 4-point dilution set-up (3 repetitions) are shown. Fitted curve parameters were not significantly different.

However, $R1^{R361H}$ changed their morphology from a round shape to a more spindle like (mesenchymal) cell shape under 5-FU treatment (Figure 19A), in comparison to $R4^{wt}$ (Figure 19B).

Since the MAPK-pathway is altered through activating mutations in RAS in 30-50 % in CRC [169], I treated $R4^{wt}$ and $R1^{R361H}$ with second-line therapeutics targeting the MAPK signaling pathway (Figure 20A). I used DMSO as vehicle control and the protein kinase inhibitor staurosporine as positive control [140].

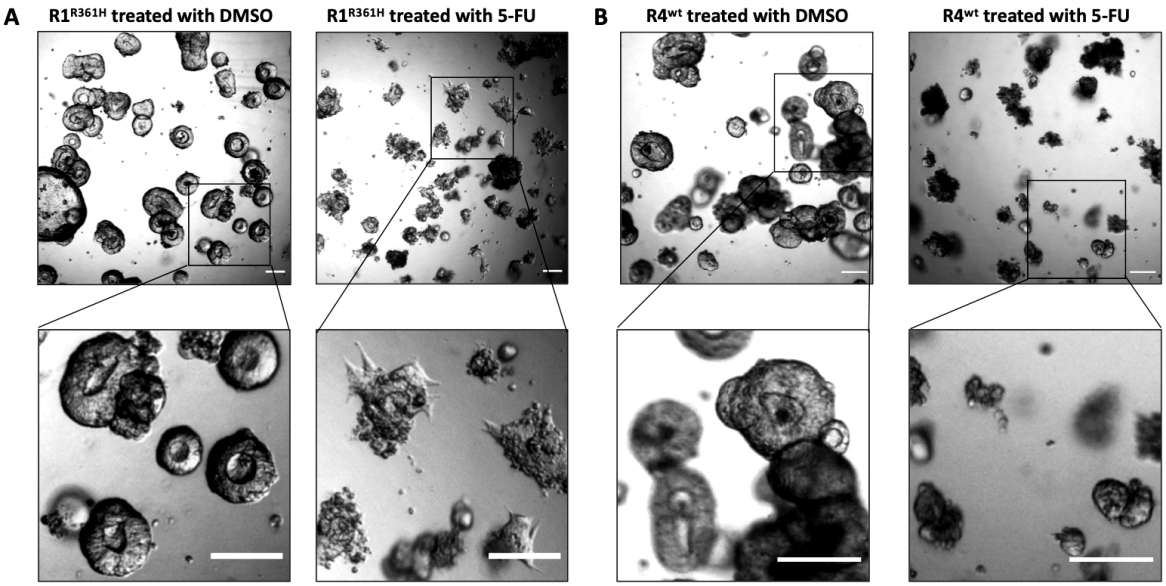

Figure 19: Microscopic pictures of colorectal cancer organoids (R4^{wt} and R1^{R361H}).
Organoids of (A) R1^{R361H} and (B) R4^{wt} were treated with DMSO (0.3 %) and 5-Fluorouracil (5-FU) for 4 days. Scale bars = 100 µm.

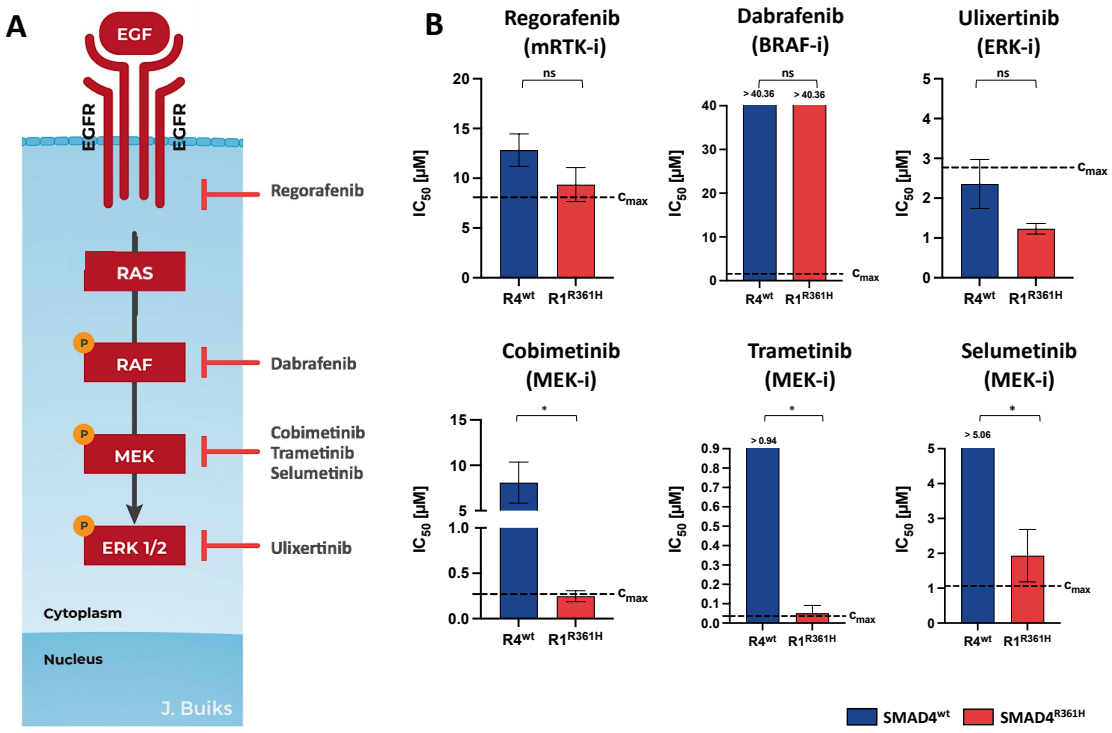

Figure 20: R4^{wt} and R1^{R361H} treated with second-line therapy targeting the MAPK signaling pathway.
(A) Schematic representation of the MAPK signaling pathway and targeted drugs (small molecules). (B) IC_{50} [µM] values of R4^{wt} and R1^{R361H} treated with multi-receptor tyrosine kinase inhibitor (mRTK-i) regorafenib, B-rapidly accelerated fibrosarcoma-inhibitor (BRAF-i) dabrafenib, extracellular-signal related kinase-inhibitor (ERK-i) ulixertinib, and mitogen-activated protein kinase kinase-inhibitors (MEK-i) cobimetinib, trametinib, and selumetinib. Treatment was conducted daily for 4 days in a 4-point, 12-point and 24-point dilution set-up (combined experiments n=6). When IC_{50} was not reached, the highest concentration of the respective drug tested was used for statistical analysis (Student's t-test: *$p < 0.05$).

Both models were sensitive to multi-receptor tyrosine kinase inhibitor regorafenib in the tested concentration range, and resistant to BRAF-inhibitor dabrafenib (Figure 20B, Figure 21). $R1^{R361H}$ exhibited sensitivity to MEK-inhibitors cobimetinib and trametinib (Figure 20B), as well as to selumetinib (Figure 20B). In contrast, $R4^{wt}$ was more resistant to cobimetinib and did not even reach the IC_{50} (50 % inhibition) after treatment with trametinib and selumetinib. Since the extracellular signal-regulated kinases (ERK) are the only known phosphorylation targets of MEK1 and MEK2 [170], I treated $R4^{wt}$ and $R1^{R361H}$ with an ERK1/2-inhibitor [171] to proof MEK specificity. Both models displayed the same sensitivity to ulixertinib (Figure 20B, Figure 21).

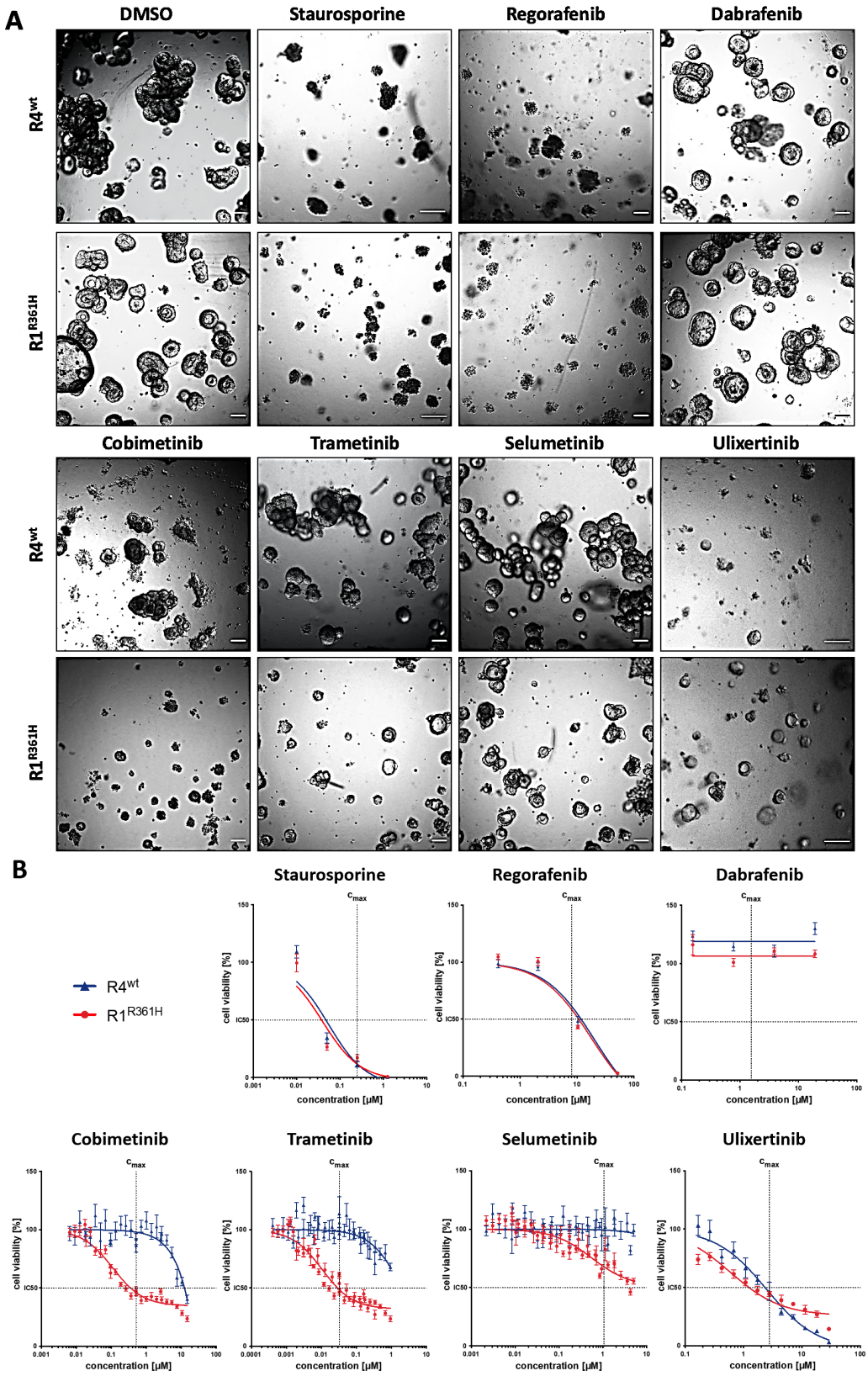

Figure 21: Microscopic pictures and corresponding drug response curves of R4^{wt} and R1^{R361H} treated with second-line therapeutics targeting the MAPK signaling pathway.

(A) Pictures were taken after 4 days of daily treatment with vehicle control: DMSO (0.3%), positive control: staurosporine (0.25 µM), mRTK-inhibitor: regorafenib (10 µM), BRAF-inhibitor: dabrafenib (1.55 µM), MEK-inhibitors: cobimetinib (0,51 µM), trametinib (0.03 µM), selumetinib (1.06 µM), and ERK-inhibitor: ulixertinib (2.77 µM). Scale bars = 100 µm. (B) Corresponding drug response curves of R4^{wt} and R1^{R361H}. For cobimetinib, trametinib and selumetinib, fitted curve parameters were significantly different (extra-sum-of-squares F test, $p < 0.05$).

4.1.2. Generating CRISPR-engineered organoids

In order to investigate whether SMAD4^{R361H} is responsible for the sensitivity towards MEK-inhibitors, I generated syngeneic organoids harboring SMAD4^{R361H} using the CRISPR/Cas9 genome editing system [155,156] (Figure 22B).

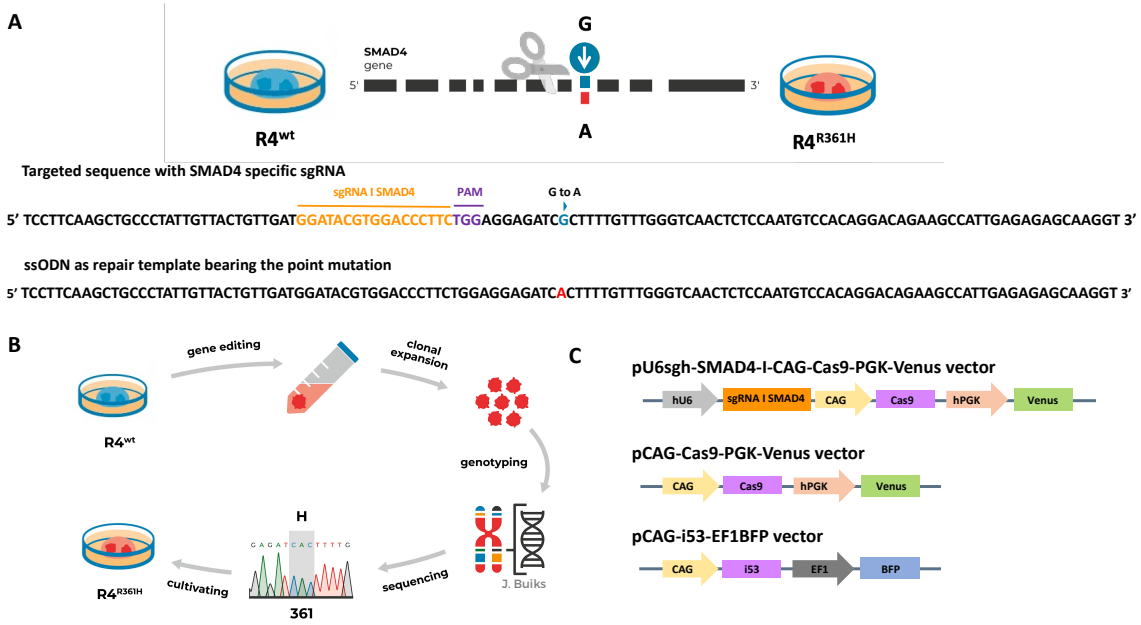

Figure 22: Generation of CRISPR-engineered SMAD4^{R361H} organoids.
(A) In the targeted sequence the SMAD4-specific sgRNA is indicated in orange and the PAM signal is shown in purple, 8 bp upstream from the point mutation. The ssODN includes homology arms (HA) of 60 bp flanking the point mutation. (B) Workflow: R4^{wt} organoids were transfected with vectors, as in C, and ssODN, as in A, to exchange guanine to adenine (G to A), which leads to an amino acid change of arginine to histidine. 72 h after transfection, Venus- and BFP-positive cells were sorted as bulk population. Single clones were isolated via limited dilution and genotyped by locus specific sequencing to confirm the R361H point mutation. (C) Vectors for transient transfection of organoids. SMAD4^{wt} organoids were transfected with an all-in-one vector pU6sgh-SMAD4-I-CAG-Cas9-PGK-Venus (U1) or pU6sgh-SMAD4-II-CAG-Cas9-PGK-Venus (U2) and an additional Cas9-vector (pCAG-Cas9-PGK-Venus). To increase homologous-directed repair, organoids were co-transfected with a plasmid vector containing i53-bpA *[165]*.

For this procedure, I designed sgRNA I (SMAD4-I) and sgRNA II (SMAD4-II) (Table 15) as well as single-stranded oligonucleotides ssODN 3 (forward) and ssODN 4 (reverse) bearing the R361H point mutation (Figure 22A, Suppl. Figure 1).

I cloned sgRNA I (SMAD4-I) and sgRNA II (SMAD4-II) into the pU6sgh-CAG-Cas9-PGK-Venus-bpA vector (Figure 22C, Figure 13) and sequenced it with Primer U6 (Table 15). In parallel, I determined the optimal transfection parameters (ratio of the transfection reagent to DNA and duration).

I transfected SMAD4^{wt} organoids (R4^{wt}) with an all-in-one vector, either pU6sgh-SMAD4-I-CAG-Cas9-PGK-Venus (U1) or pU6sgh-SMAD4-II-CAG-Cas9-PGK-Venus (U2), an additional Cas9-vector (pCAG-Cas9-PGK-Venus), and a ssODN as the repair template bearing the R361H point mutation (ssODN 3 or ssODN 4 (Table 15)) to achieve a single nucleotide exchange (G to A) that leads to an amino acid change of arginine to histidine in the SMAD4 gene.

Under physiological conditions, a DNA double strand break can be repaired via nonhomologous end joining (NHEJ) or homologous repair (HDR) [160]. To enhance HDR, I co-transfected the organoids with a plasmid vector containing i53-bpA to inhibit the NHEJ key molecule 53BP1 [165,172] (Figure 22C).

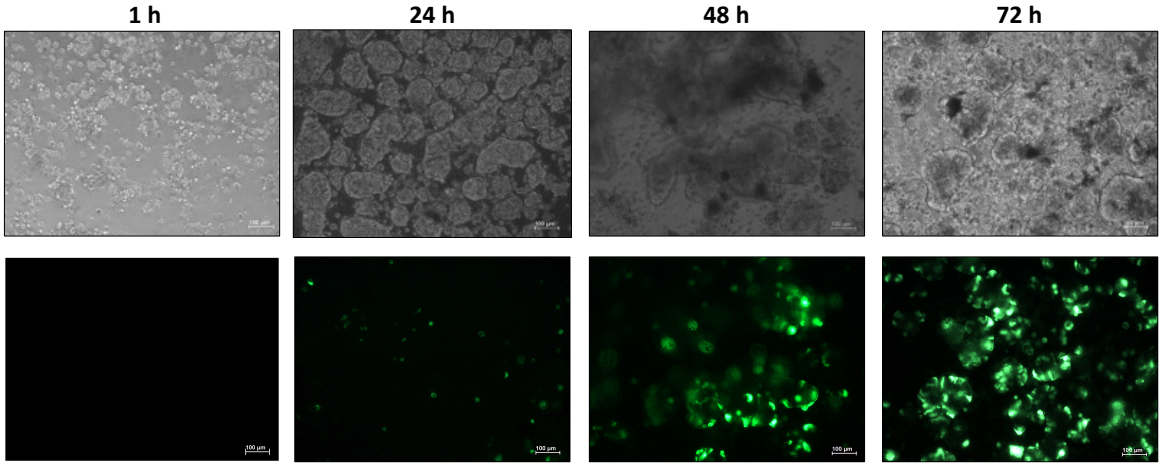

Figure 23: Representative microscopic pictures of transfected R4^{wt} organoids.
R4^{wt} were seeded and transfected as single cells with pU6sgh-SMAD4-I-CAG-Cas9-PGK-Venus (U1) and ssODN4 (U1+4) for 72 h. Bright field (top raw) and fluorescence images (below) are shown. Scale bar = 100 µm.

Based on microscopic analysis of green fluorescence in transfected cells, the highest transfection efficiency was observed at 72h after transfection (Figure 23). Afterwards, I sorted Venus- and BFP-positive cells as bulk population (Figure 24, Suppl. Figure 3). The percentage of Venus- and BFP-positive cells was below 5 % for all transfection approaches with pU6sgh-SMAD4-I-CAG-Cas9-PGK-Venus vector (U1), pU6sgh-SMAD4-II-CAG-Cas9-PGK-Venus (U2) and ssODNs 3 and 4 (U1+3, U1+4, U2+3, and U2+4) (Figure 24A-C). The transfection approach of R4^{wt} plus U1+4 showed with 4.62 % the highest efficiency (Figure 24B-C). I sorted single cells of each approach (Suppl. Figure 3) and subsequently plated them as bulk population in Matrigel® and cultured them for further experiments.

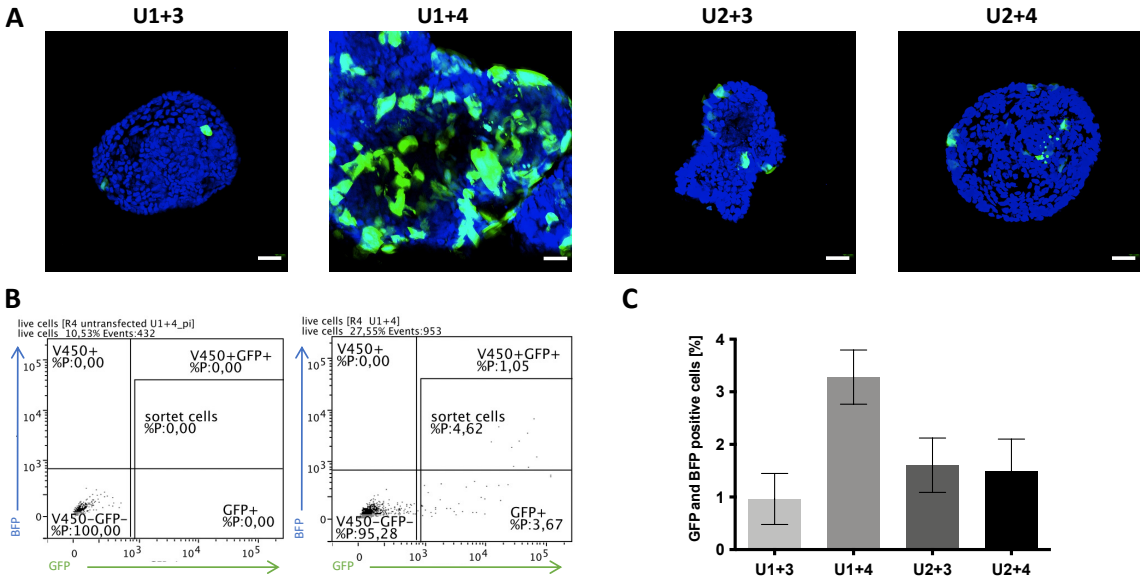

Figure 24: Transfection of R4^{wt} organoids.
(A) Organoids were fixed in 4 % formalin and stained with Dapi (1:10,000) 72 h after transfection. Pictures were taken with spinning disc confocal microscope CSU-W1 (Nikon/Andor) equipped with an iXON888 camera and analyzed with NIS-Elements Software. (B) Representative FACS analysis of R4^{wt} cells untransfected and transfected with U1+4. R4^{wt} cells were sorted as bulk population by gating on GFP+/BFP+. (C) Percentage of Venus- and BFP-positive R4^{wt} cells transfected with Cas9-vector (pCAG-Cas9-PGK-Venus), U1 (pU6sgh-SMAD4-I-CAG-Cas9-PGK-Venus) or U2 (pU6sgh-SMAD4-II-CAG-Cas9-PGK-Venus) and ssODNs 3 or ssODN 4 (U1+3, U1+4, U2+3, U2+4) (3 replicas). Scale bars = 100 µm.

In parallel, I attempted to establish syngeneic CRISPR-engineered SMAD4^{wt} organoids. Therefore, I transfected R1^{R361H} using the same conditions as for R4^{wt}, but ssODN 1 and ssODN 2, bearing the SMAD4^{wt} sequence (Table 15, Figure 25).

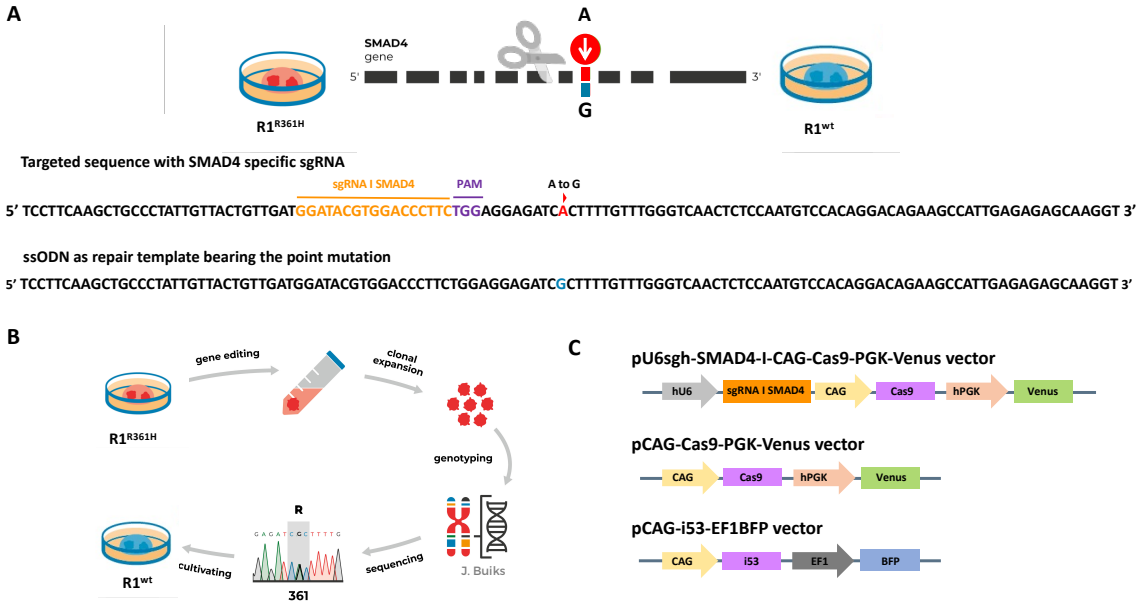

Figure 25: Generation of CRISPR-engineered SMAD4^{wt} organoids.
(A) In the targeted sequence the SMAD4-specific sgRNA is indicated in orange and the PAM signal is shown in purple, 8 bp upstream from the point mutation. The ssODN includes homology arms (HA) of 60 bp flanking the point mutation. (B) Workflow: R4^{wt} organoids were transfected with vectors, as in C, and ssODN, as in A, to exchange adenine to guanine (A to G), which leads to an amino acid change of histidine to arginine. 72 h after transfection, Venus- and BFP-positive cells were sorted as bulk population. Single clones were isolated via limited dilution and genotyped by locus specific sequencing to confirm the R361H point mutation. (C) Vectors for transient transfection of organoids. SMAD4^{R361H} organoids were transfected an all-in-one vector pU6sgh-SMAD4-I-CAG-Cas9-PGK-Venus (U1) or pU6sgh-SMAD4-II-CAG-Cas9-PGK-Venus (U2) and an additional Cas9-vector (pCAG-Cas9-PGK-Venus). To increase homologous-directed repair, organoids were co-transfected with a plasmid vector containing i53-bpA [165].

Based on microscopic analysis of green fluorescence in transfected cells, the highest transfection efficiency was observed at 72h after transfection (Figure 26A). I sorted Venus- and BFP-positive cells as bulk population (Figure 26B). The percentage of Venus- and BFP-positive cells was on average 10-13 % for all transfection approaches with pU6sgh-SMAD4-I-CAG-Cas9-PGK-Venus vector (U1), pU6sgh-SMAD4-II-CAG-Cas9-PGK-Venus (U2) and ssODNs 1 and 2 (U1+1, U1+2, U2+1, and U2+2) (Figure 26B + C, Suppl. Figure 4). I sorted single cells of each approach and subsequently plated them as bulk population in Matrigel® and cultured them for further experiments.

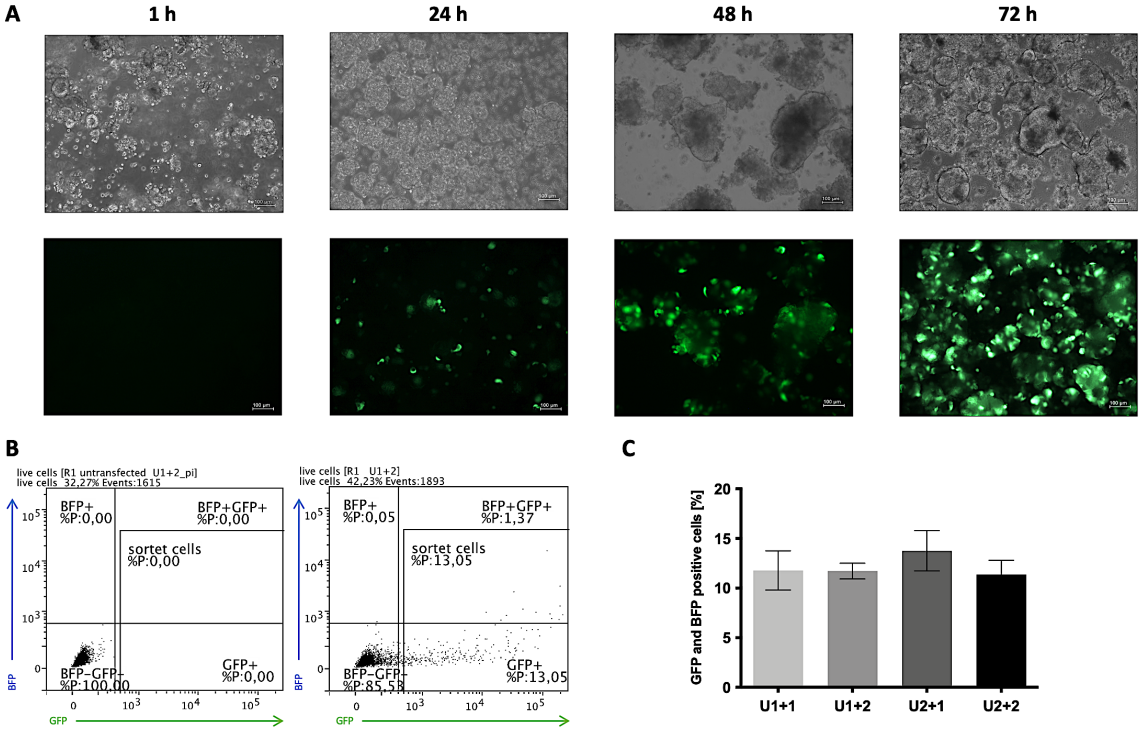

Figure 26: Transfection of R1^{R361H} organoids.
(A) Representative microscopic images of R1^{R361H} seeded and transfected as single cells with U1 (pU6sgh-SMAD4-I-CAG-Cas9-PGK-Venus) and ssODN 2 (U1+2) for 72 h. Bright field (top raw) and fluorescence image (below) are shown. (B) Representative FACS images of R1^{R361H} cells untransfected and transfected with U1+2. R1^{R361H} cells were sorted as bulk population by gating on GFP+/BFP+. (C) Percentage of Venus- and BFP-positive R1^{R361H} transfected with Cas9-vector (pCAG-Cas9-PGK-Venus), U1 (pU6sgh-SMAD4-I-CAG-Cas9-PGK-Venus) or U2 (pU6sgh-SMAD4-II-CAG-Cas9-PGK-Venus) and ssODNs 1 or ssODN 2 (U1+1, U1+2, U2+1, U2+2) (3 replicas). Scale bars = 100 µm.

After 3-4 weeks, I collected the U1+4 bulk populations of R4^{wt} and U1+1, U1+2, U2+1 and U2+2 of R1^{R361H} for DNA isolation and subsequent PCR (Figure 27). I was not able to isolate DNA from the bulk populations of R4^{wt} transfected with U1+3, U2+3 and U2+4 because the organoids did not survive after sorting.

I eluted the PCR products (688 bp) from the agarose gel and sent them for Sanger sequencing.

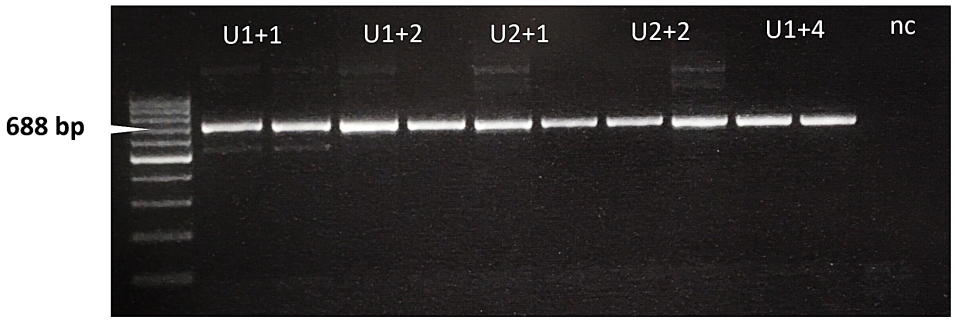

Figure 27: Gel electrophoresis image of PCR products from SMAD4 region of interest (688 bp) from R1^{R361H} and R4^{wt}.
The DNA was isolated from Venus- and BFP-positive cells. SMAD4 region of interest was amplified using corresponding primers. (U1+1/U1+2 = pU6sgh-SMAD4-I-CAG-Cas9-PGK-Venus plus ssODN 1 /ssODN 2, U2+1/U2+2 = pU6sgh-SMAD4-II-CAG-Cas9-PGK-Venus plus ssODNs 1 and ssODN 2, U1+4 = pU6sgh-SMAD4-I-CAG-Cas9-PGK-Venus plus ssODN 4, nc = negative control).

I aligned the sequence of the bulk DNA of both, R4^{wt} and R1^{R361H} to the SMAD4 target area. A representative example is shown in Figure 28. At the position 361 in exon 8 of the SMAD4 gene, I identified a double peak (Figure 28) indicating that a nucleotide exchange (C to T) occurred in R4^{wt}.

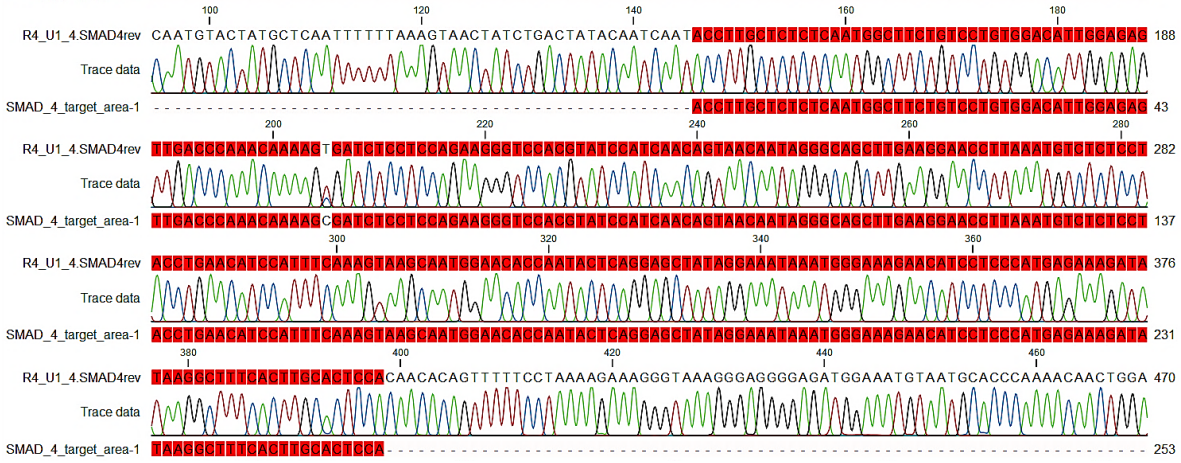

Figure 28: Aligned sequence of SMAD4 region of interest from Venus- and BFP-positive R4^{wt} cells.
Sequence was aligned to the SMAD4 target area using CLC Genome Viewer.

No nucleotide exchange was detected in R1^{R361H} transfected with U1+1, U1+2, U2+1 and U2+2 (Figure 29).

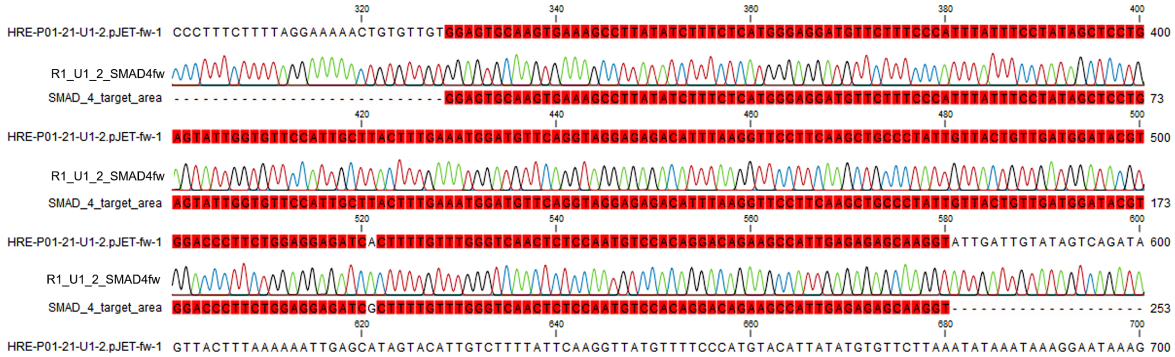

Figure 29: Representative aligned sequence of SMAD4 region of interest from Venus- and BFP-positive R1^{R361H} cells.
Sequence was aligned to the SMAD4 target area using CLC Genome Viewer.

I repeated this approach several times but the correction of the SMAD4 mutation was not successful in R1^{R361H}.

I continued with the Venus- and BFP-positive bulk population of R4^{wt} transfected with U1+4. I performed a pJET cloning to assess the targeting efficacy and to estimate the proportion of clones in the bulk population of R4^{wt}. For this purpose, I cloned the PCR product (688 bp) into a pJET1.27blunt vector. In total, 28 out of 31 clones had the right size of 808 bp (Figure 30A). I aligned the sequences of the SMAD4 region of interest to the target region of the SMAD4 gene (Figure 30B).

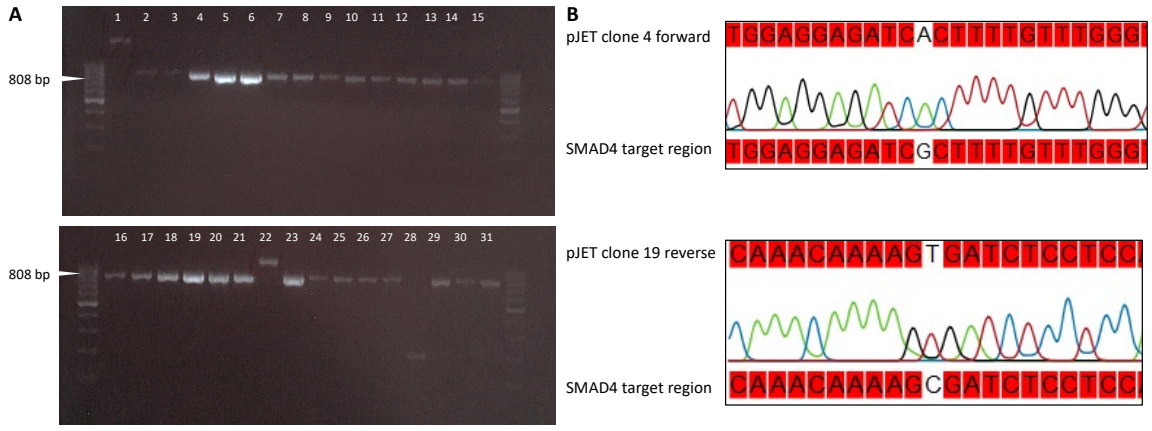

Figure 30: Gel electrophoresis images of PCR products from corresponding pJET clones generated from Venus- and BFP positive R4^{wt} cells.
(A) Gel electrophoresis image of PCR products from SMAD4 region of interest for cloned into the pJET vector (808 bp) from Venus- and BFP-positive R4^{wt} cells. In total 28 of 31 clones showed the correct size of 808 bp. These clones were sequenced and aligned to the target region of the SMAD4 gene. (B) Two representative pJET clones (clone 4 and 19) are shown.

Overall, 15 of 28 clones carried the correct R361H point mutation suggesting that up to 50 % of the bulk population were successfully transfected. I performed a limited dilution to achieve a monoclonal culture (Figure 31).

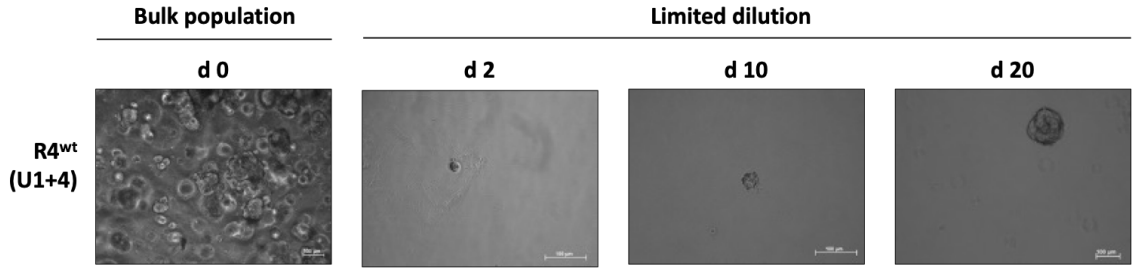

Figure 31: Microscopic images of limited dilution of R4^{wt} (U1+4).
Microscopic images show bulk population of Venus- and BFP positive R4^{wt} (U1+4) on day 0 (d 0) and a representative clone after day 2 (d 2), day 10 (d 10) and day 20 (d 20). Scale bars = 100 µm.

About 50 clones grew from a single cell which I cultured for approximately 20-30 days before digestion and subsequent cultivation. With this approach, I was able to establish three clones (Figure 32).

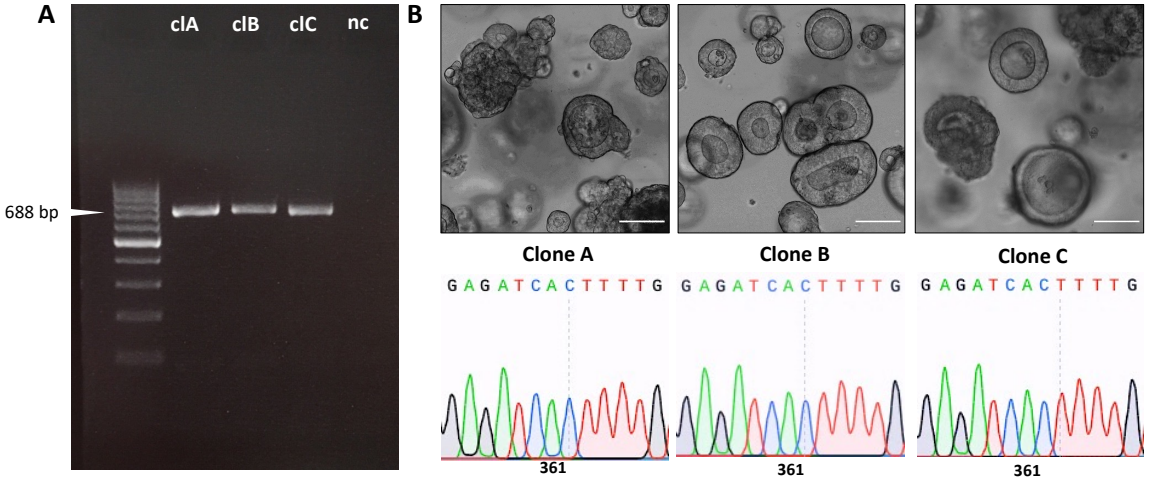

Figure 32: Representative images of three CRISPR-PDOs (clone A, clone B and clone C).
(A) PCR products of SMAD4 region of interest (688 bp) amplified from genomic DNA of clone A (cl A), clone B (cl B) and clone C (cl C) (nc = negative control). (B) Microscopic images of clone A, clone B and clone C and sequences with the nucleotide exchange (G to A) at position 361 in exon 8 of the SMAD4 gene are shown.

The three CRISPR-PDOs (clone A, clone B and clone C) were sequenced via Sanger sequencing (Figure 32B) and CRC panel sequencing [143] to confirm the homozygote SMAD4^{R361H} mutation in each CRISPR-clone (Table 20).

Table 20: Colorectal cancer panel sequencing [143] of R4^{wt} and CRISPR-PDOs (clone A, clone B and clone C).
In total, 94 CRC related genes were sequenced. Variant allele frequencies (VAF) of 12 gene are shown. Clone A, clone B and clone C carry a homozygous SMAD4^{R361H} loss-of-function mutation in comparison to the parental PDO R4^{wt}.

Gene	VAF			
	R4^{wt}	Clone A	Clone B	Clone C
KRAS_c.12 G>D	53	61	57	54
KRAS_c.15 G>A	0	0	0	54
POLE_c.252 A>V	47	42	41	46
TP53_c.242 C>F	100	100	100	100
SMAD4_c.361R>H	0	100	100	100
PI4KA_c.702 Y>*	4	0	0	5
PI4KA_c.2208 N>K	0	0	0	5
MLH1_c.219 I/V	0	0	0	0
PIK3CA_c.1047 H>R	33	0	6	0
KDR_c.472 Q>H	0	0	0	0
HDAC3_c.296 G>V	26	21	0	0
HDAC2_c.81-82 SR>RR	1	0	0	0

The introduction of SMAD4^{R361H} in CRISPR-PDOs (clone A, clone B and clone C) had no influence on the phenotype (Figure 32B). All CRISPR-PDOs showed similar doubling times as R1^{R361H}. They grew significantly faster compared to R4^{wt} (Figure 33).

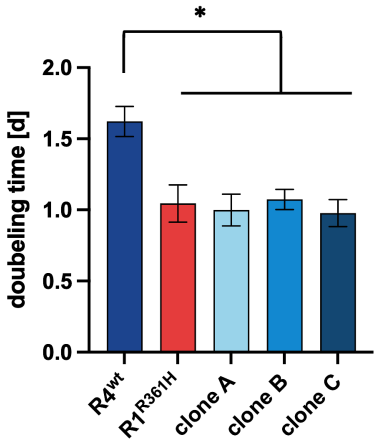

Figure 33: Doubling times of R4^{wt}, R1^{R361H} and CRISPR-PDOs (clone A, clone B and clone C).
The cell density was measured on day [d] 2, 3, 5, and 7 by measuring cellular ATP content using Cell Titer Glow assay. Results from four independent experiments were combined (One-way ANOVA *p < 0.05).

4.1.3. Investigation of the effects of SMAD4 mutation on drug response in CRC patient-derived organoids

4.1.3.1. SMAD4^{R361H} influences MEK inhibition

I treated CRISPR-PDOs (clone A, clone B and clone C) with second-line therapy targeting the MAPK signaling pathway (Figure 20A) and compared them with the original sibling PDOs R4^{wt} and R1^{R361H} (Figure 34).

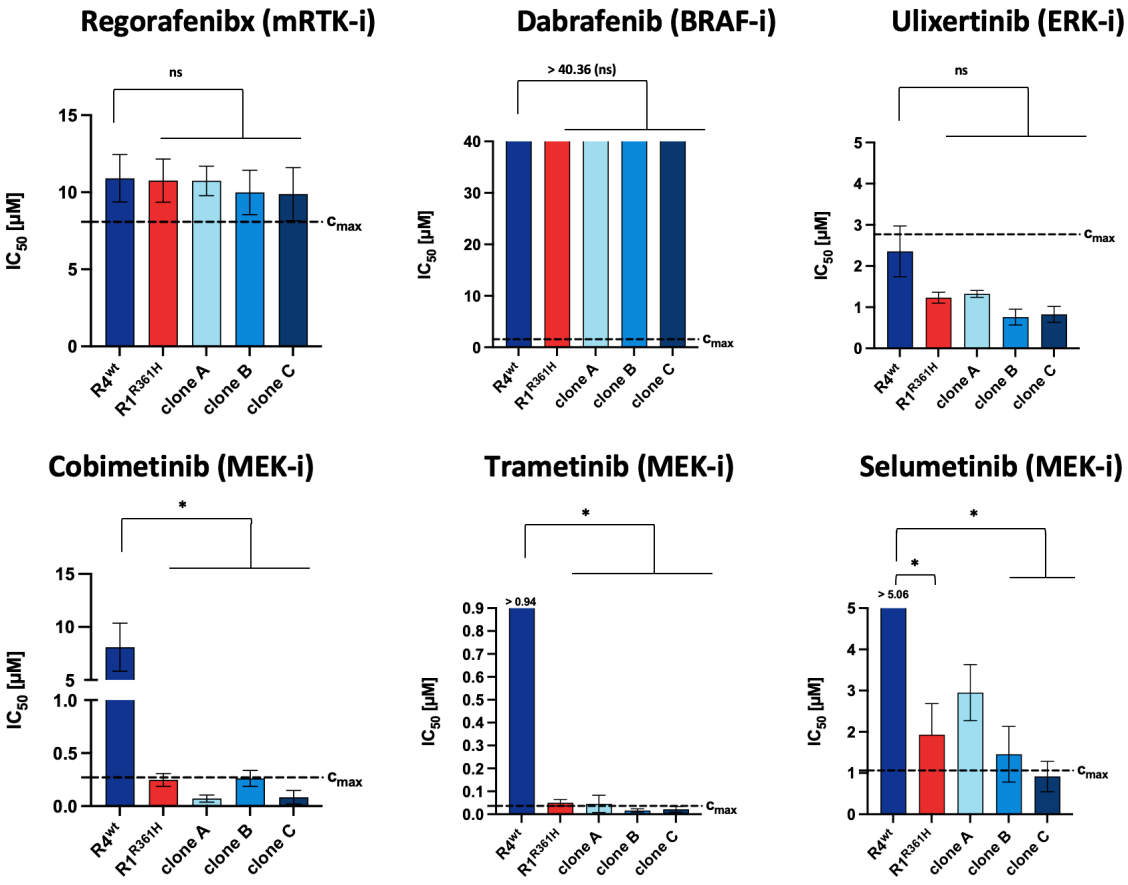

Figure 34: IC$_{50}$ values of R4^{wt} and R1^{R361H} and CRISPR PDOs (clone A, clone B and clone C) treated daily for 4 days with small molecules targeting the MAPK signaling pathway.
Achievable maximal plasma concentrations (c_{max}) are indicated for each drug with dotted lines. The treatment was conducted daily for four days in a 4-point, 12-point and 24-point dilution set-up (combined experiments n=6). When IC_{50} was not reached, the highest concentration of the respective drug tested was used for statistical analysis. (In all panels: bars represent mean ± SEM. One-way ANOVA with Tukey's post-hoc analysis; *p < 0.05).

In the tested concentration range, all CRISPR-PDOs were sensitive to regorafenib and resistant to dabrafenib. However, all CRISPR-PDOs behaved similarly to R1^{R361H} and were significantly more sensitive to MEK-inhibitors cobimetinib, trametinib and selumetinib compared to R4^{wt} (Figure 34, Figure 35). All CRISPR-PDOs were sensitive to ulixertinib without significant difference similar to the original PDOs R4^{wt} and R1^{R361H} (Figure 34, Figure 35).

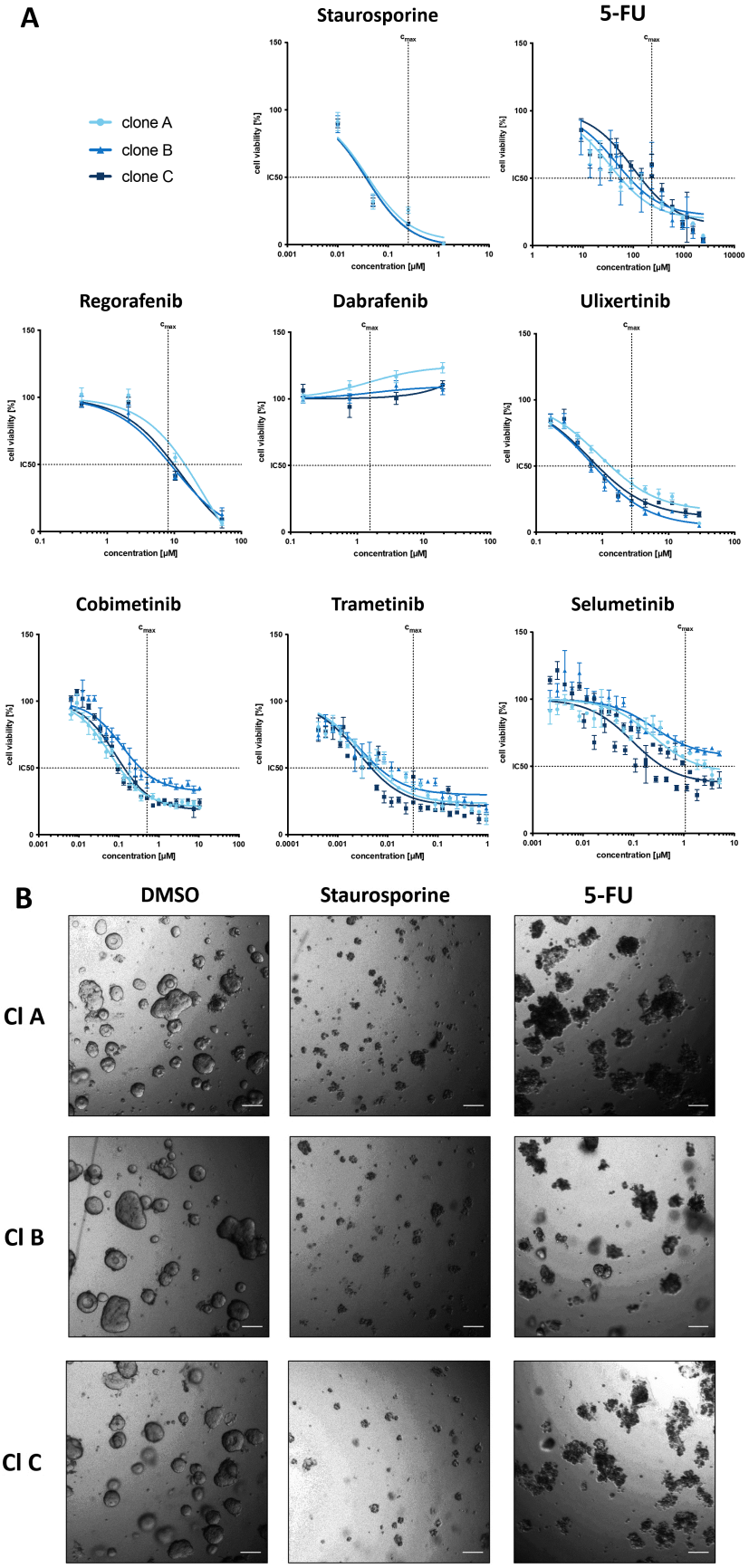
A
clone A
clone B
clone C
Staurosporine
5-FU
Regorafenib
Dabrafenib
Ulixertinib
Cobimetinib
Trametinib
Selumetinib
cell viability [%]
concentration [µM]
IC50
cmax
B
DMSO
Staurosporine
5-FU
Cl A
Cl B
Cl C

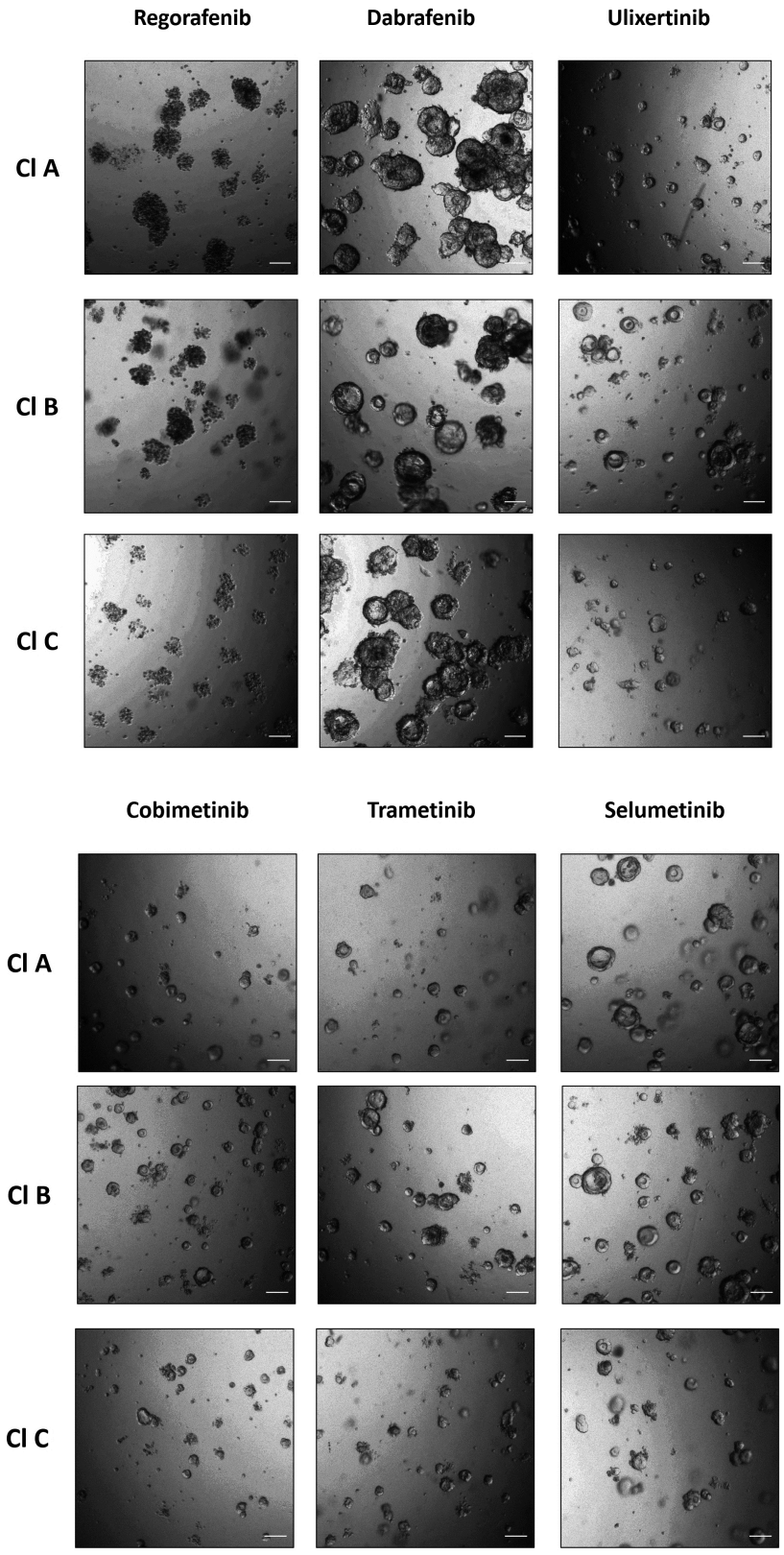

Figure 35: Drug response curves and corresponding microscopic images of CRISPR-PDOs (clone A, clone B and clone C) treated with second-line therapy targeting the MAPK signaling pathway.

(A) Drug response curves of CRISPR-PDOs (clone A, clone B and clone C). There were no significant differences between the three CRISPR-PDOs. (B) Pictures were taken after 4 days of daily treatment with vehicle control: DMSO (0.3%), positive control: staurosporine (0.25 µM), mRTK-inhibitor: regorafenib (10 µM), BRAF-inhibitor: dabrafenib (1.55 µM), MEK-inhibitors: cobimetinib (0,51 µM), trametinib (0.03 µM), selumetinib (1.06 µM), and ERK inhibitor: ulixertinib (2.77 µM). Scale bars = 100 µm.

4.1.3.2. Rescue experiment for the vice versa effect of MEK inhibition

Since the CRISPR/Cas9 genome editing approach was not successful in $R1^{R361H}$, an overexpression of SMAD4 wild-type gene in SMAD4 mutated PDOs should show the opposite effect of MEK inhibition. $R4^{wt}$ was also included as control.

For this approach, I tested all plasmids by restriction digestion before use (Figure 36).

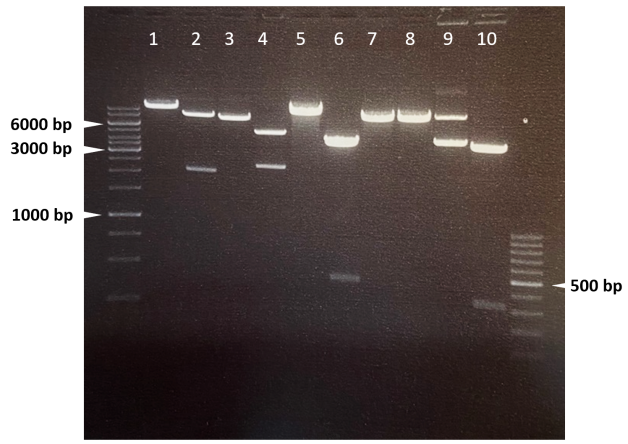

	Gene Ruler	1 kb
1	pHAGE SMAD4 EcoRI-HF	10148 bp
2	pHAGE SMAD4 XhoI	2066 bp + 8082 bp
3	pHAGE puro XhoI	7585 bp
4	pHAGE puro ScaI-HF	2413 bp + 5172 bp
5	pMDLg/pRRE EcoRV	8990 bp
6	pMDLg/pRRE EcoRI-HF	4335 bp + 401 bp + 4254 bp
7	pCMV-VSV-G XbaI	6507 bp
8	pCMV-VSV-G XhoI	1680 bp + 4827 bp
9	pRSV-REV ScaI-HF	4180 bp
10	pRSV-REV EcoRI-HF	311 bp + 3869 bp
	Gene Ruler	100 bp

Figure 36: Gel electrophoresis image of plasmids restriction analysis.
All plasmids were tested by restriction digestion before use.

For virus production, I transfected HEK293T cells with virus packing plasmids, a gfp-plasmid (transfection control) and either SMAD4-plasmid (pHAGE-SMAD4) or empty plasmid (pHAGE-PURO). I collected the virus containing medium after 24 h, 32 h and 48 h (Figure 37).

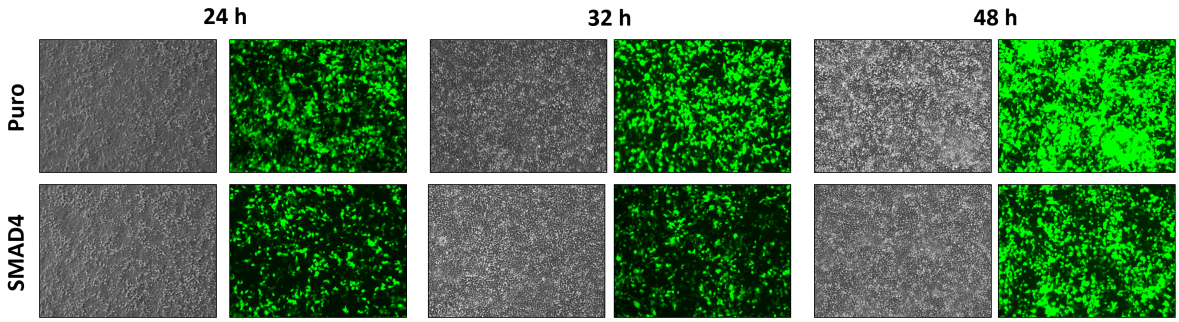

Figure 37: Microscopic images of transfected HEK293T cells.
Microscopic images were taken after 24 h, 32 h and 48 h before medium was collected.

I transduced sibling PDOs ($R4^{wt}$ and $R1^{R361H}$), as well as CRISPR-PDOs (clone A, clone B, and clone C) for 96 h. Since puromycin is toxic to the growth of various eukaryote cells, including mammalian cells [173,174], I used plasmids carrying a puromycin-resistant gene as selection marker gene and selected the PDOs with 2 µg/ml puromycin for 10 days and observed them under the microscope (Figure 38). In parallel non-transduced cells were treated with puromycin (control) and died within two days (Figure 38).

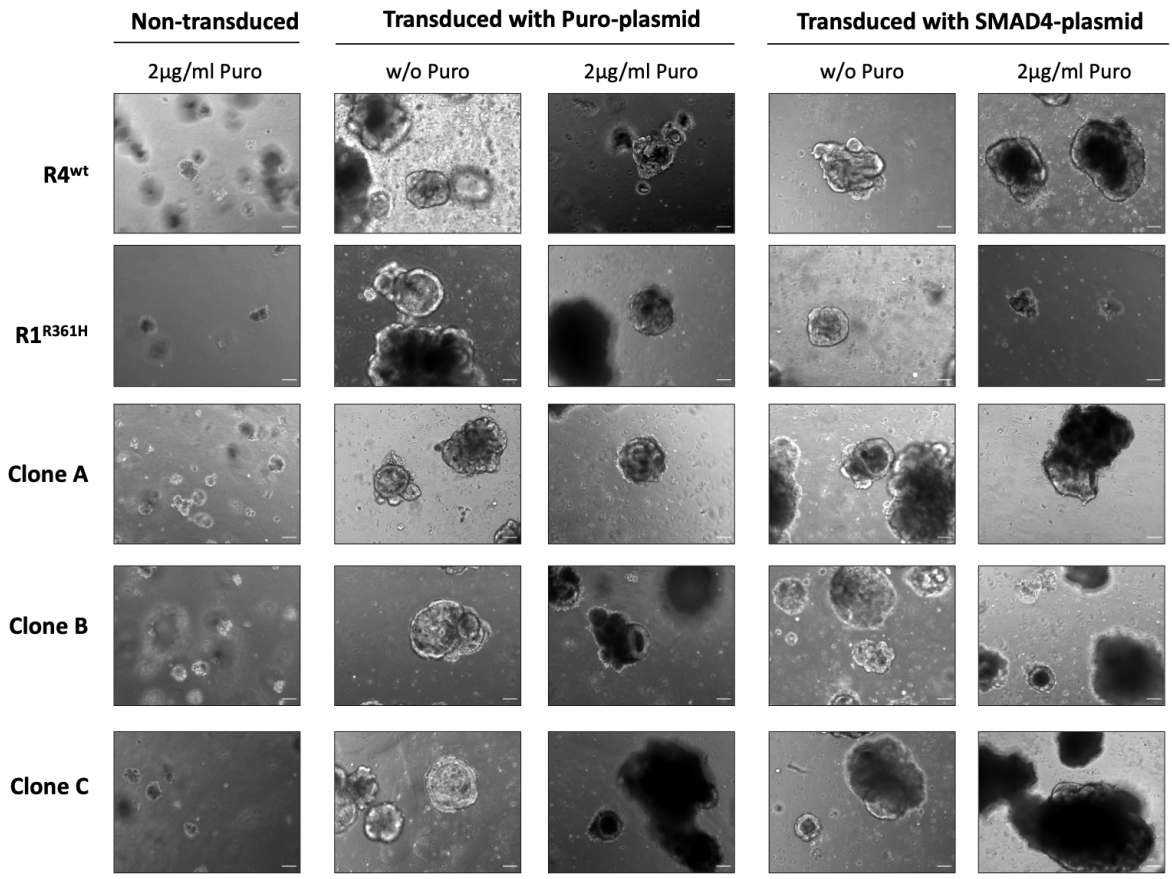

Figure 38: Microscopic images of sibling PDOs (R4^{wt} and R1^{R361H}) and CRISPR-PDOs (clone A, clone B, and clone C).
PDOs were transduced with control plasmid (Puro-plasmid) or SMAD4-plasmid and subsequently selected with 2 µg/ml puromycin (Puro) for 10 days. The non-transduced cells (first raw) died within two days. Scale bars = 100 µm.

I performed a PCR to monitor the outcome of the transduction. The transduction of SMAD4 wild-type gene was only successful for R4^{wt} and clone A (Figure 39).

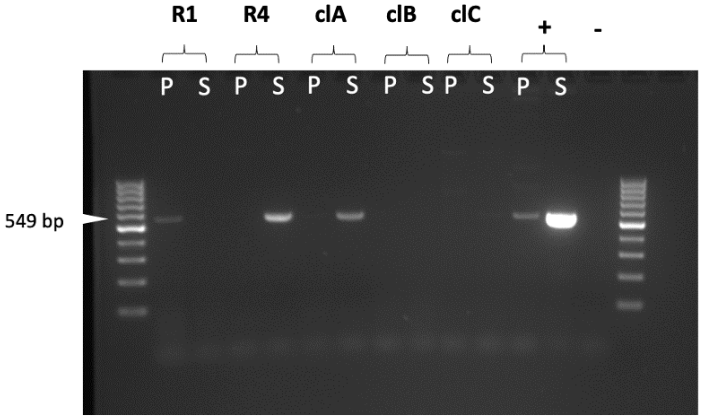

Figure 39: Gel electrophoresis image of PCR products (549 bp) of plasmid-derived SMAD4 from R1^{R361H}, R4^{wt}, clone A (clA), clone B (clB) and clone C (clC).
PCR product was amplified from total DNA isolated from the Puro-plasmid (P) or SMAD4-plasmid (S) transduced and puromycin selected organoids. Purified plasmids were used as positive controls (+), and water was added instead of DNA in the PCR reaction as negative control (-).

I analyzed the genomic DNA for both PDOs. As expected, R4^{wt} carried the SMAD4 wild-type sequence and clone A the R361H mutant sequence (Figure 40).

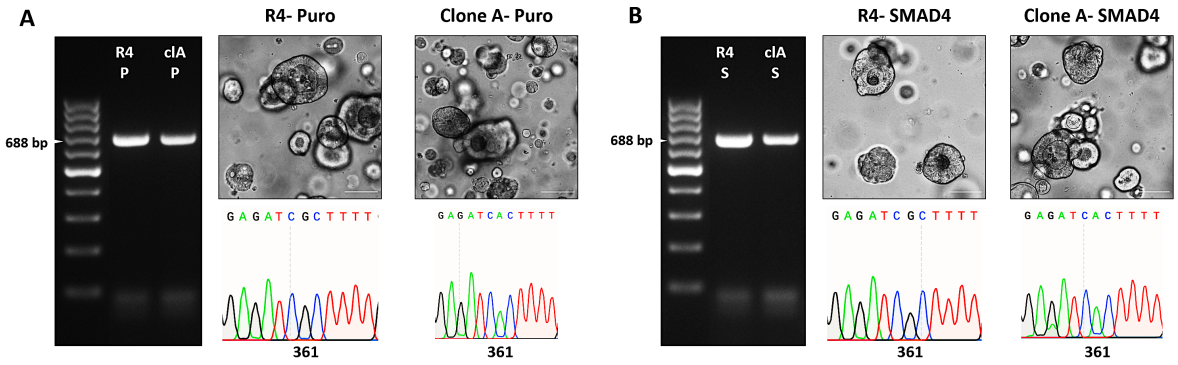

Figure 40: Transduction and puromycin selection did not change SMAD4 mutational status in R4^{wt} and clone A.
(A) Gel electrophoresis image of PCR product of SMAD4 region of interest; representative images and corresponding sequences for (A) Puro transduced R4^{wt} and clone A and (B) for SMAD4 transduced R4^{wt} and clone A.

I used successfully transduced PDOs (R4^{wt} and clone A) for further drug screening and treated them with 5-FU, regorafenib and MEK-inhibitors cobimetinib, trametinib and selumetinib and dabrafenib (Figure 41, Suppl. Figure 2).

The passage-matched counterparts of R4^{wt} and clone A displayed comparable sensitivity to all drugs (Figure 34). As expected, R4^{wt} was resistant to all MEK-inhibitor independent of the transduction.

Indeed, clone A-SMAD4, which expressed SMAD4 wild-type, was more resistant to all MEK-inhibitors, as well as to 5-FU and regorafenib. But the control PDO model clone A-Puro which expressed the empty plasmid showed the same drug response as clone A-SMAD4 (Figure 41).

One possible explanation is that prolonged treatment with puromycin induced a development of multidrug resistance. The experiment was repeated after five more passages in cell culture medium (XY-medium) to ensure that the PDOs recovered completely after puromycin selection. However, the drug test revealed the same results (data not shown).

These results indicate that overexpression of wild-type SMAD4 is possible in PDO models, but the chemical selection using puromycin apparently affects the drug response.

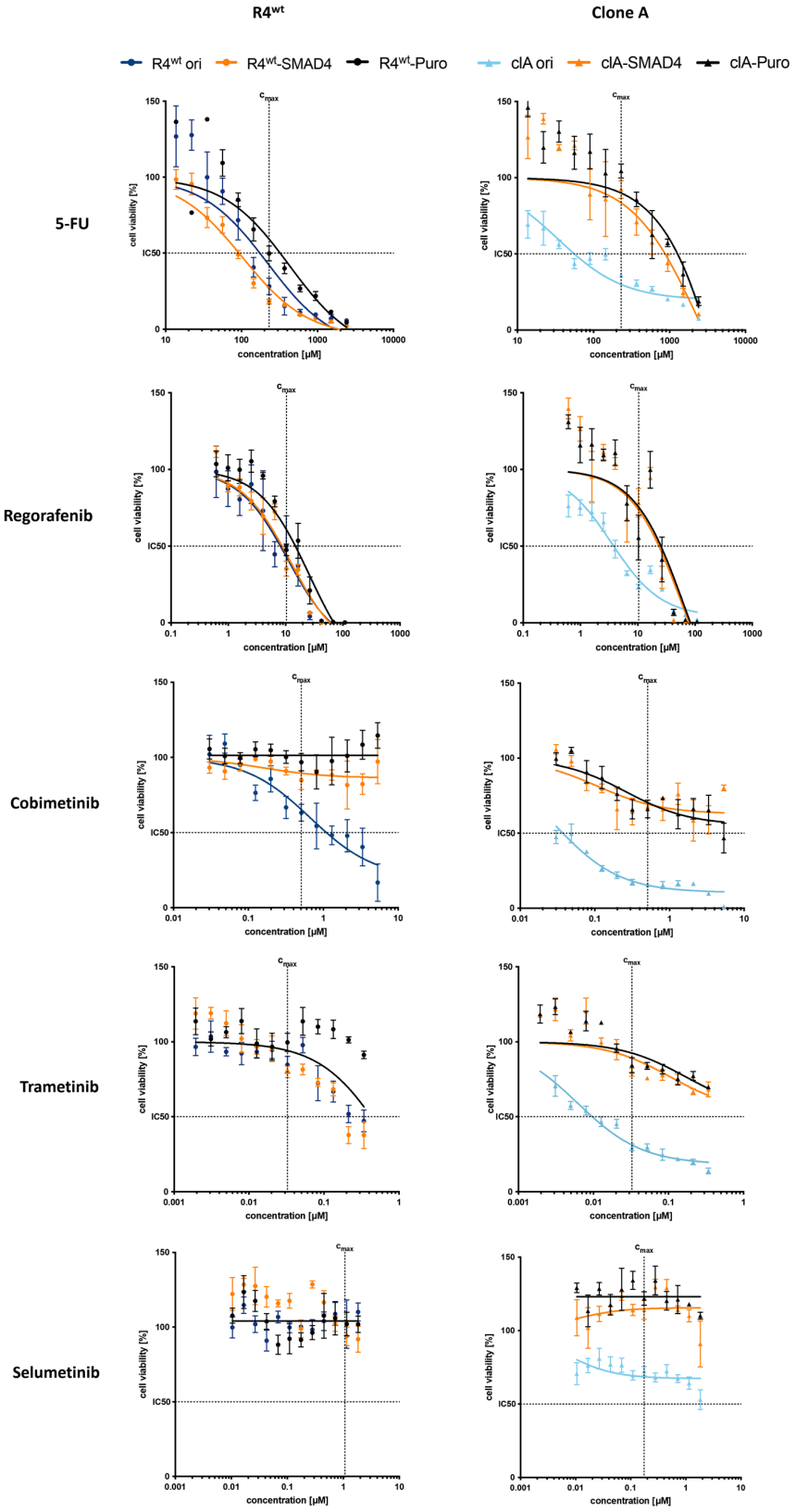

Figure 41: Drug response curves of R4^{wt} and CRISPR-clone A.
The transduced und puromycin selected PDOs (R4^{wt}-SMAD4 and clone A-SMAD4 (orange); R4^{wt}-Puro and clone A-Puro (black)) were compared to the original passage-matched PDO model (blue). For original clone A (clA ori) treated with 5-FU, regorafenib, cobimetinib, trametinib and selumetinib, and for original R4^{wt} (R4^{wt} ori) treated with cobimetinib, fitted curve parameters were significantly different (extra-sum-of-squares F test $p < 0.05$). There were no significant differences between clone A-SMAD4 (clA-SMAD4) and clone A-Puro (clA-Puro), as well as between R4^{wt}-SMAD4 and R4^{w}-Puro detected.

4.1.3.3. De-novo developed drug resistance can affect sensitivity to MEK-inhibitors

In CRC, 5-FU based therapy such as FOLFOX and FOLFIRI is usually considered as the first-line treatment option. MEK-inhibitors are currently not approved for the CRC treatment [175], thus they could be only considered when the first-line therapy fails.

In order to mimic the clinical situation, I established 5-FU resistant sibling- and CRISPR-PDOs. I cultured PDOs in the presence of a sublethal concentration (9.2 µM) of 5-FU. I allowed surviving cells to recover and continued to treat them with 46.1 µM of 5-FU for 4 months. Subsequently, I increased the 5-FU concentration to 230 µM (c_{max}) [134] for another 3 months (Figure 42). I was able to establish 5-FU resistant lines only from PDOs harboring SMAD4^{R361H} (Figure 42). SMAD4^{wt} PDO did not recover from long-term 5-FU treatment in two independent approaches (data not shown).

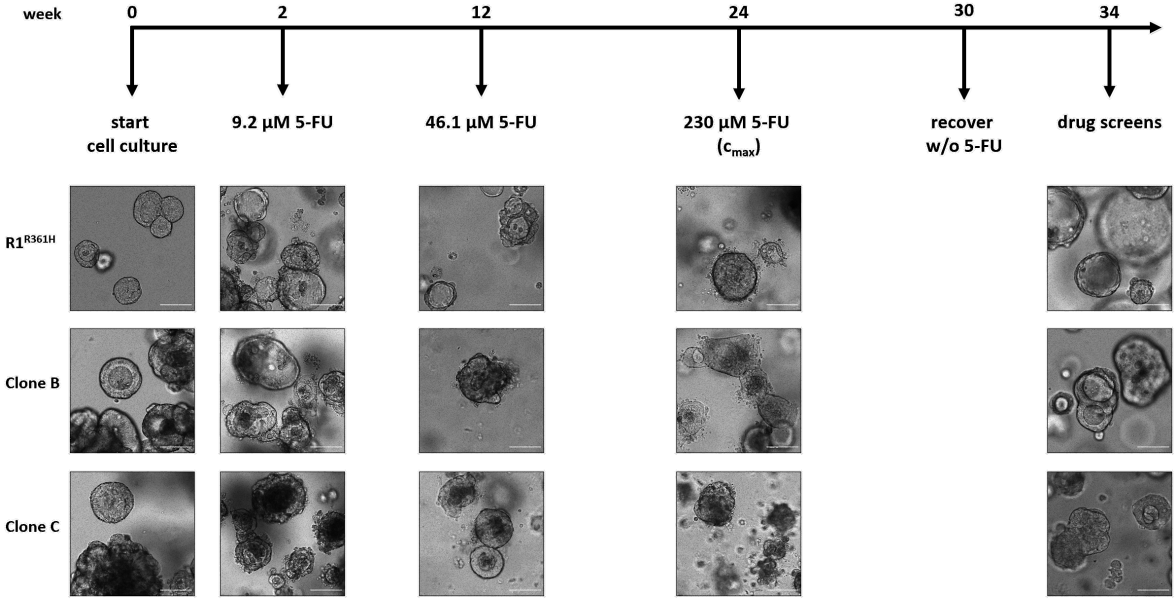

Figure 42: Timeline of establishing 5-FU resistant PDO models (R1^{R316H}, CRISPR-PDOs: clone B and clone C).
Representative microscopic images were taken after cultivating PDOs with 9.2 µM 5-FU, 46.1 µM 5-FU and 230 µM 5-FU. Scale bars = 100 µm.

There were no differences in proliferation between 5-FU resistant PDO models and their passage-matched counterparts (Figure 43).

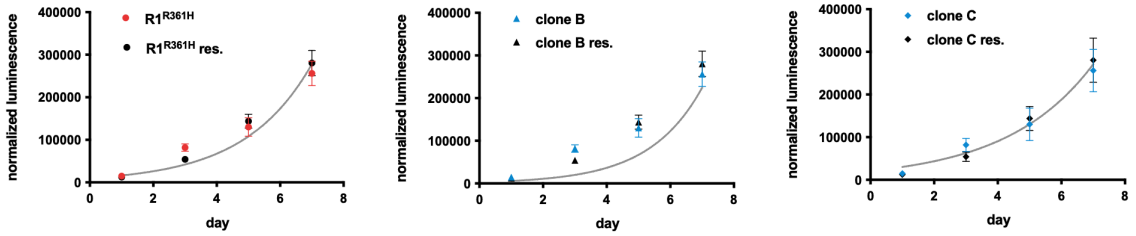

Figure 43: Cell growth curves of 5-FU resistant PDO models (R1^{R361H} res., clone B res. and clone C res.) and their non-resistant counterparts.
The luminescence was measured after day 1, 3, 5, and 7. The fitted curve parameters were not significantly different (extra-sum-of-squares F test $p > 0.05$).

The drug screening revealed a significant increase in 5-FU resistance, as well as increased resistance to the tested targeted therapeutics (regorafenib, cobimetinib and trametinib) (Figure 44).

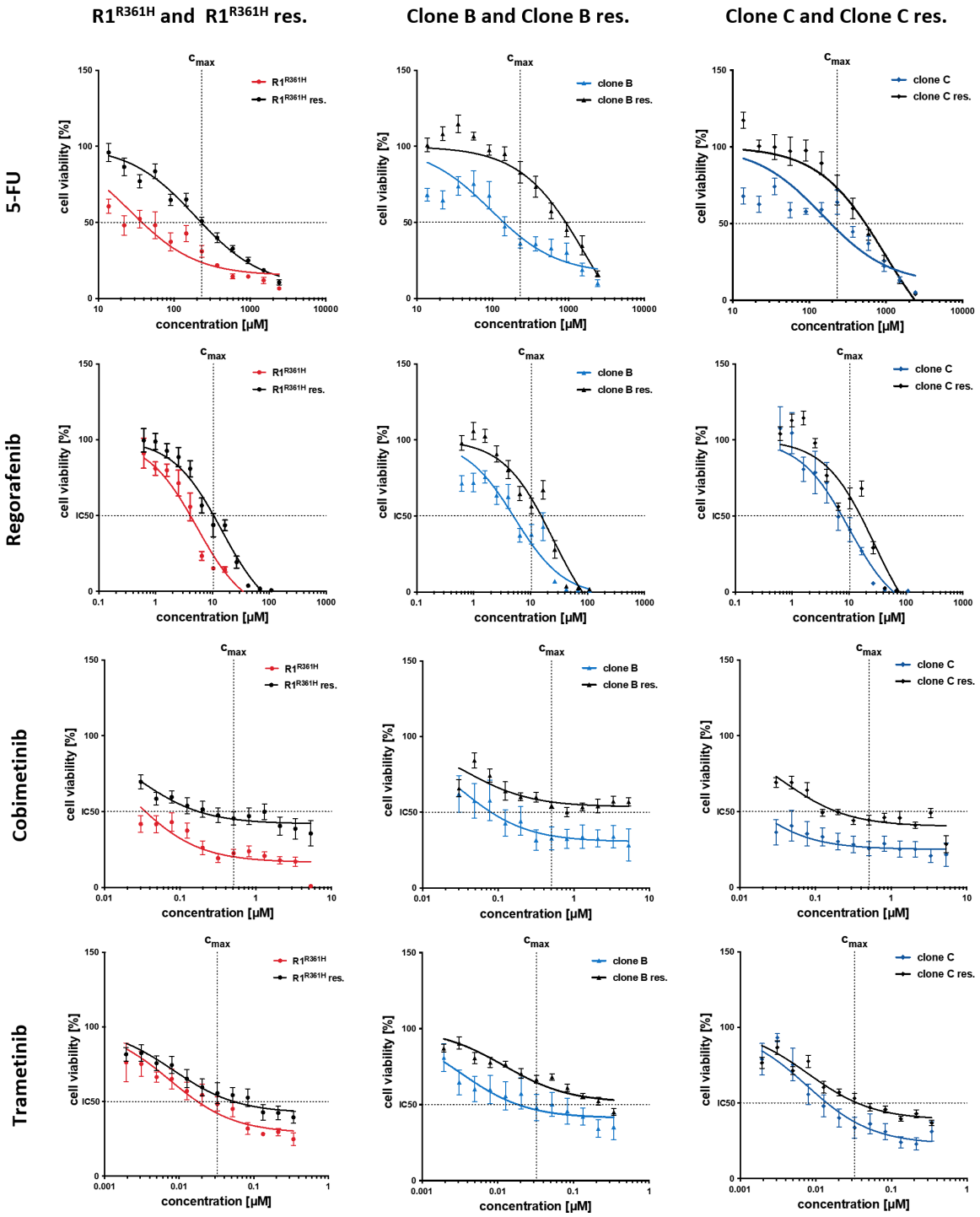

Figure 44: Drug response curves of 5-FU resistant PDO models (R1^{R361H} res., clone B res. and clone C res.) and their non-resistant counterparts after daily treatment with 5-FU, regorafenib, cobimetinib and trametinib.
Achievable maximal plasma concentrations (c_{max}) are indicated for each drug with dotted lines. For all tested drugs, the fitted curve parameters were significantly different (extra-sum-of-squares F test $p < 0.05$).

4.1.4. Examination of molecular signaling pathways that are potentially induced using multi-omics technologies

To investigate the mechanism underlying the differential MEK-inhibitor response, I treated sibling-PDOs ($R4^{wt}$ and $R1^{R361H}$) and CRISPR-PDOs with trametinib (0.03 µM) or DMSO (control) for 24 h and collected cells for transcriptome analysis.

The principal component analysis showed that all CRISPR-PDOs and the model $R1^{R361H}$ clustered together in the untreated group as well as after treatment with trametinib in comparison to $R4^{wt}$ (Figure 45).

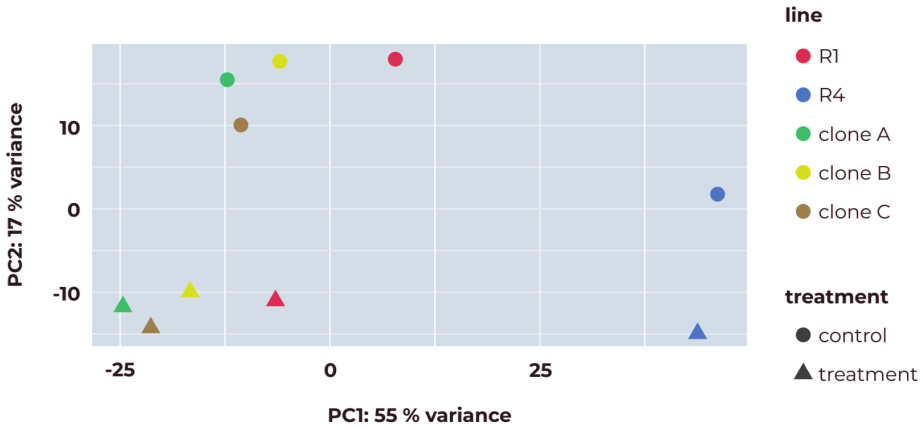

Figure 45: Principal component analysis of mRNA expression from $R4^{wt}$, $R1^{R361H}$ and CRISPR-PDOs (clone A, clone B, clone C).
First component on x-axis contains 55 % of the variance and classifies the samples into two major groups $R1^{R361H}$ / CRISPR-PDOs (treated with 0.03 µM trametinib and untreated) and $R4^{wt}$ (treated with 0.03 µM trametinib and untreated).

There were 618 effected genes overlapping in PDOs with SMAD4 mutation and 222 were unique in $SMAD4^{wt}$ PDO (Figure 46B).

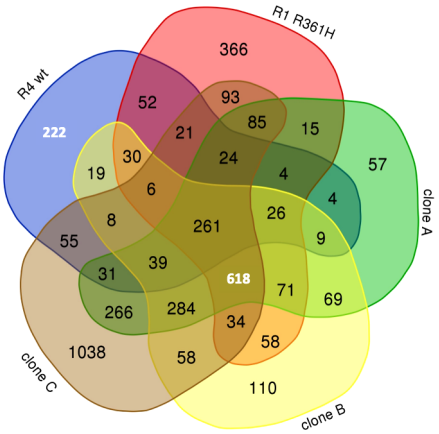

Figure 46: Five-set Venn diagram for genes significantly affected by incubation with trametinib from $R4^{wt}$, $R1^{R361H}$ and CRISPR-PDOs (clone A, clone B, clone C).
The Venn diagram was created using an online tool (https://bioinformatics.psb.ugent.be/webtools/Venn/).

Gene enrichment analysis revealed that in SMAD4 mutated PDOs most of the significantly altered biological processes were processes involved in DNA-replication and cell cycle progression, as it would be expected in case of MEK-inactivation associated growth arrest (Suppl. Table 2). In SMAD4^{wt} PDO affected gene ontology (GO) terms included signal transduction- and TGF-β/BMP signaling-associated, but no DNA-replication or cell cycle progression (Suppl. Table 2).

In addition, I performed a proteome analysis with colleagues from the NMI in Reutlingen, who developed the DigiWest® multiplex protein profiling analysis [166] (Figure 47).

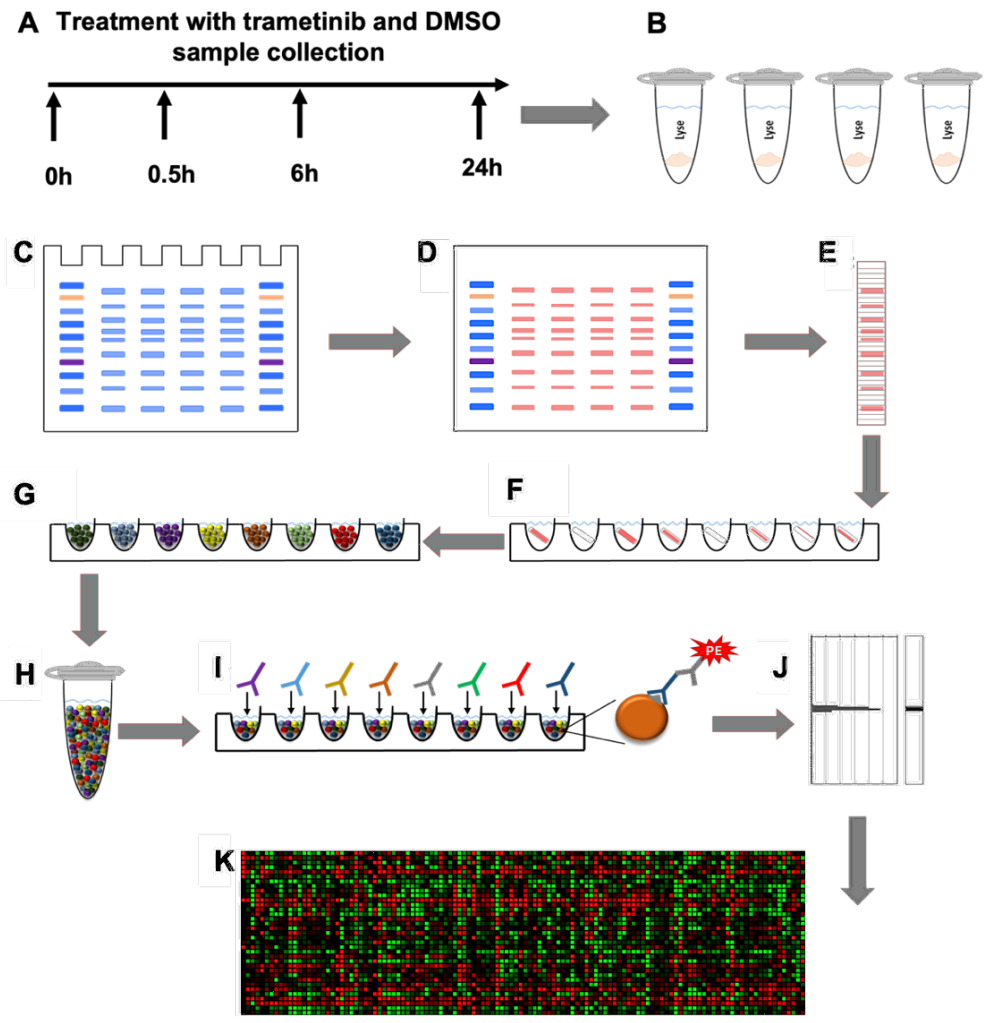

Figure 47: Principle of Digi-West® experiment.
(A) PDOs were treated with DMSO (0.3 %) and trametinib (0.03 µM). After 0.5 h, 6 h and 24 h, samples were collected and (B) lysed. (C) Proteins were separated using SDS-PAGE. (D) Proteins were transferred to a blot membrane and biotinylated. (E) Membrane was cut into 96-membrane strips. (F) Proteins were eluted from the 96-membrane strips in a 96-well plate. (G) Biotinylated proteins were bound to neutravidin-labeled Luminex beads. (H) Beads were pooled. (I) Bead set was incubated with an analyte-specific primary antibody. (J) Amount of bound primary antibody by analyte-specific secondary antibody was quantified. Signals measured in Flexmap 3D were plotted by molecular weight, resulting in a peak resembling the band of a Western blot membrane. (K) Results were summarized in a heat map showing potential clustering between the samples.

For this purpose, I treated PDOs with DMSO (0.3%) or trametinib (0.03 µM) and collected them after 0.5 h, 6 h and 24 h (Figure 47A). The lysed proteins were separated (Figure 47B) via sodium dodecyl sulphate–polyacrylamide gel electrophoresis (SDS-PAGE) (Figure 47C) and stained them for quantification (Figure 48).

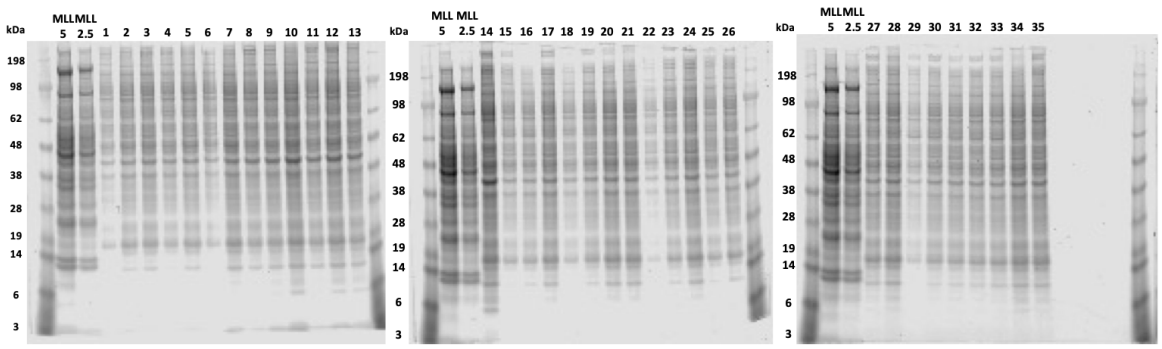

Nr.	Sample name	$C_{Protein}$ [µg/µl]
1	R1 Tra 30 min	0,88
2	R1 Tra 6 h	1,82
3	R1 Tra 24 h	2,16
4	R1 DMSO 30 min	1,55
5	R1 DMSO 6 h	2,09
6	R1 DMSO 24 h	1,16
7	R1 Medium 24 h	2,94
8	R4 Tra 30 min	2,37
9	R4 Tra 6 h	2,74
10	R4 Tra 24 h	4,01
11	R4 DMSO 30 min	3,79
12	R4 DMSO 6 h	2,53
13	R4 DMSO 24 h	2,33

Nr.	Sample name	$C_{Protein}$ [µg/µl]
14	R4 M 24 h	3,70
15	Clone A Tra 30 min	0,75
16	Clone A Tra 6 h	0,79
17	Clone A Tra 24 h	1,75
18	Clone A DMSO 30 min	0,56
19	Clone A DMSO 6 h	1,02
20	Clone A DMSO 24 h	1,78
21	Clone A Medium 24 h	1,72
22	Clone B Tra 30 min	0,34
23	Clone B Tra 6 h	0,98
24	Clone B Tra 24 h	0,89
25	Clone B DMSO 30 min	0,89
26	Clone B DMSO 6 h	1,22

Nr.	Sample name	$C_{Protein}$ [µg/µl]
27	Clone B DMSO 24 h	1,28
28	Clone B Medium 24 h	1,78
29	Clone C Tra 30 min	0,31
30	Clone C Tra 6 h	0,83
31	Clone C Tra 24 h	0,84
32	Clone C DMSO 30 min	0,92
33	Clone C DMSO 6 h	1,03
34	Clone C DMSO 24 h	1,81
35	Clone C Medium 24 h	1,76

Figure 48: Evaluation of the total protein concentration.
Images of the gels stained with Blue BANDit™, as shown, were used for quantification of the protein concentration in samples 1-35. Mouse liver lysates (MLL) 5 µg/µl and 2.5 µg/µl were used as standards.

After blotting, the immobilized proteins (Figure 47D) were biotinylated and each membrane was cut into 96 stripes (Figure 47E). Each stripe represented a unique molecular mass fraction between 15 and 250 kDa. After labeling with Luminex beads the samples were analyzed (Figure 47G-K). About 120 total and (phosphor-)proteins in $R4^{wt}$ and $R1^{R361H}$ and CRISPR-PDOs (clone A, clone B, clone C) were analyzed (Figure 49).

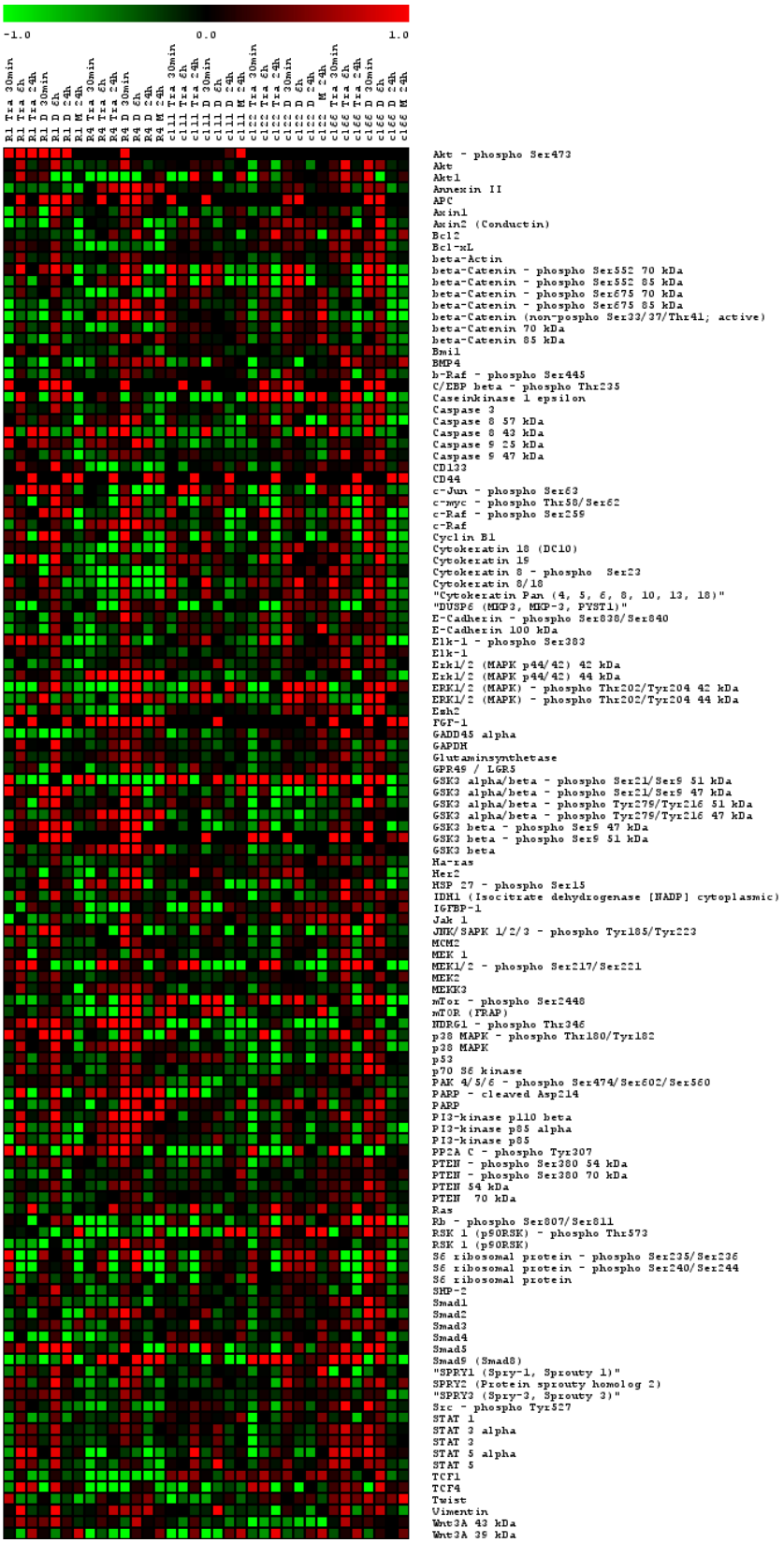

Figure 49: Heatmap (non-clustered) of raw data from DigiWest® experiment.
Heatmap (not-clustered) of differentially expressed total and (phospho-)proteins in $R4^{wt}$, $R1^{R361H}$ and CRISPR-PDOs (cl 11 = clone A, cl 22 = clone B, cl 66 = clone C) untreated (M = medium) and treated with DMSO (D) as vehicle control (0.3 %) and trametinib (Tra) (0.03 µM) (all normalized over streptavidin) is shown. For the color scale, the range was set between -1.0 (green) and 1.0 (red).

After 24 h treatment with DMSO or trametinib, all PDOs harboring SMAD4^{R361H} mutation clustered together (Figure 51) consistent with the principal component analysis (Figure 45).

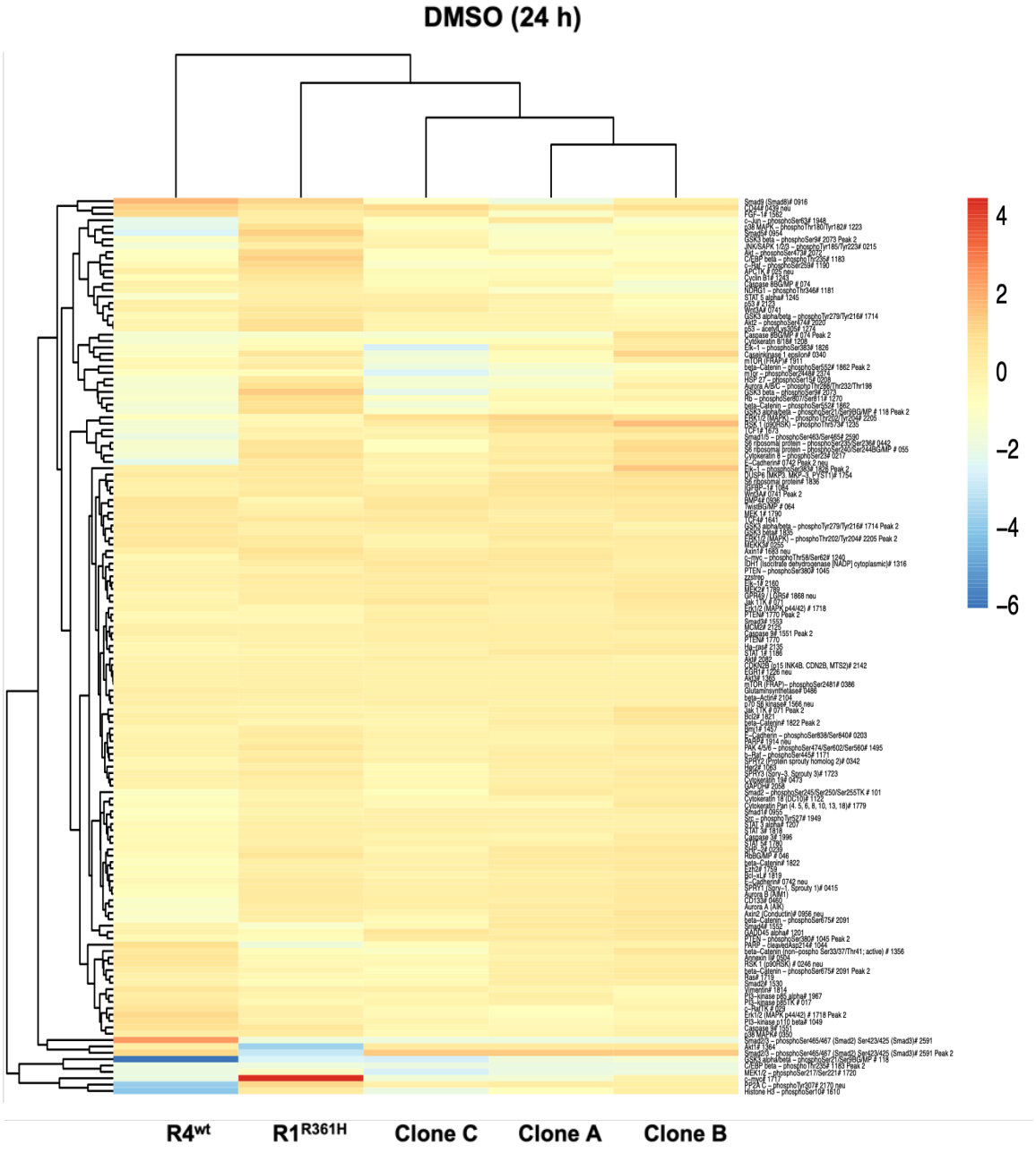

Figure 50: Heatmap of differentially expressed total and (phospho-)proteins in R4^{wt}, R1^{R361H} and CRISPR-PDOs.
Clone A, clone B, and clone C were treated with DMSO as vehicle control (0.3 %) (all normalized over beta actin, log2 fold change trametinib/DMSO. For the color scale, the range was set between -6 (blue) and 4 (red).

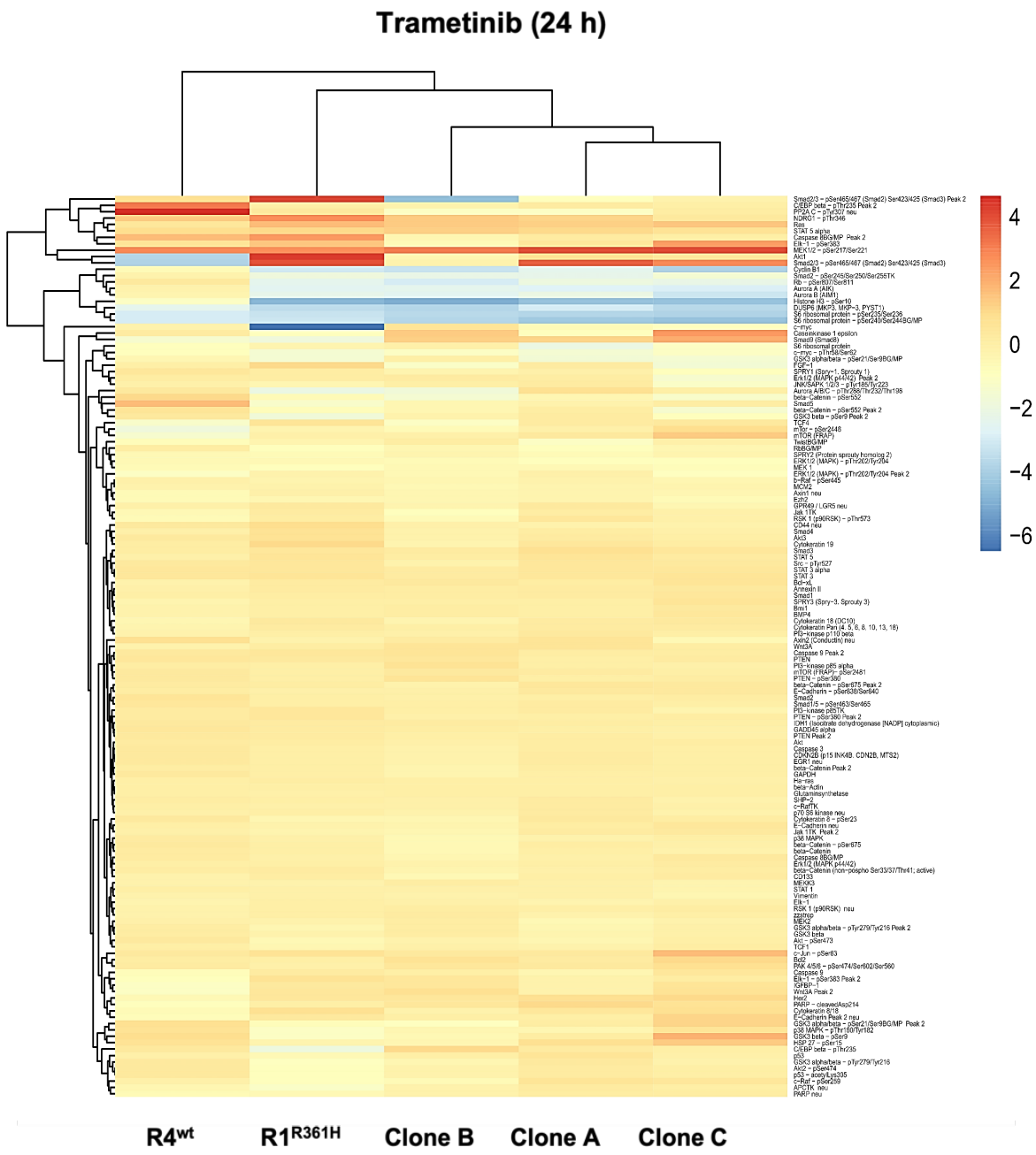

Figure 51: Heatmap of differentially expressed total and (phospho-)proteins in R4^{wt}, R1^{R361H} and CRISPR-PDOs.
Clone A, clone B, and clone C were treated with DMSO as vehicle control (0.3 %) (all normalized over beta actin, log2 fold change trametinib/DMSO. For the color scale, the range was set between -6 (blue) and 4 (red).

In order to investigate differences between SMAD4 wild-type PDOs and SMAD4^{R361H} PDOs, we clustered and compared R4^{wt} with R1^{R361H} (Figure 52A), clone A (Figure 52B), clone B (Figure 52C), and clone C (Figure 52D).

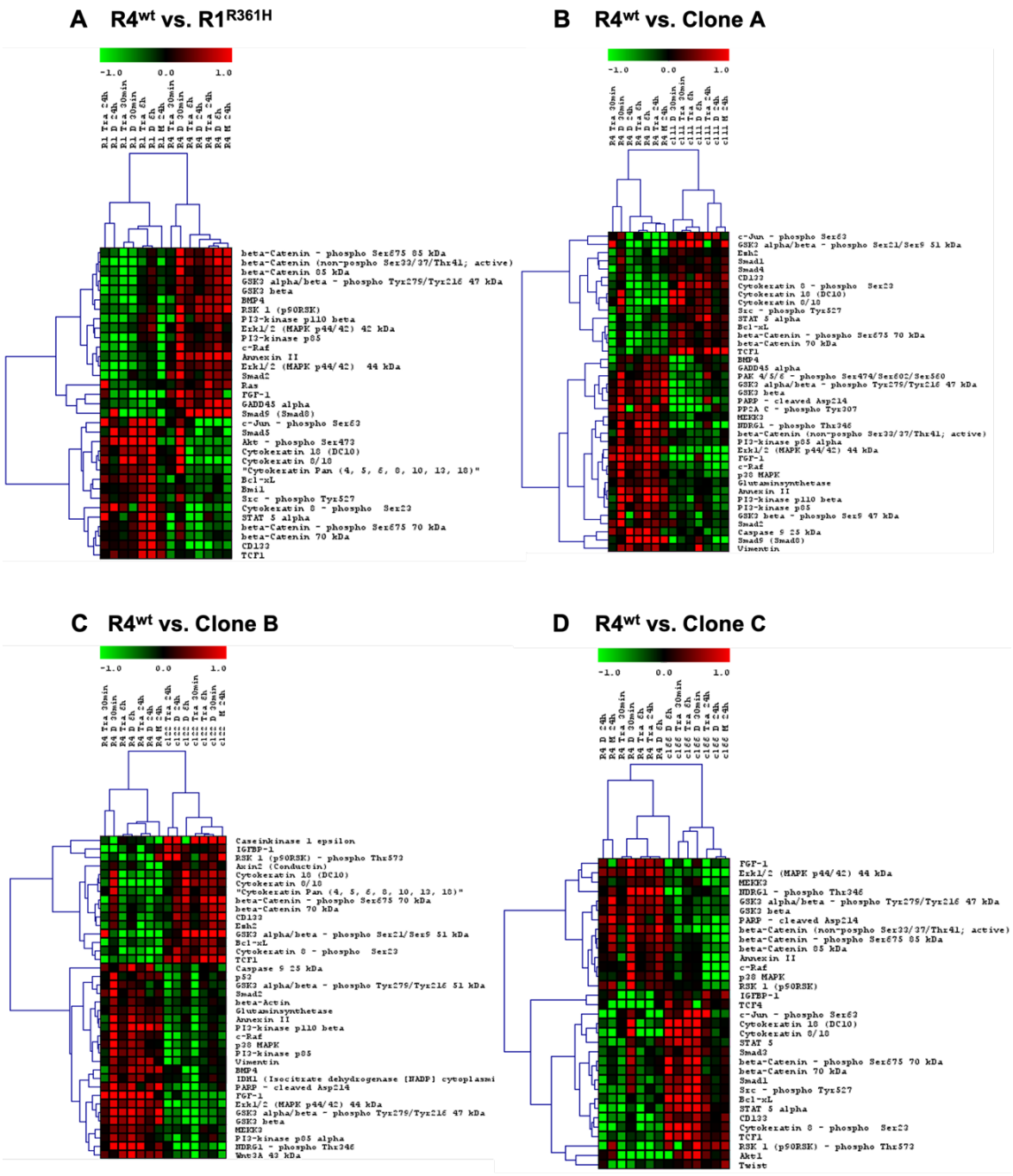

Figure 52: Heatmap (clustered) of significantly expressed total and (phospho-)proteins.
(A) R4^{wt} vs. R1^{R361H} (33 / 120), in (B) R4^{wt} vs. clone A (cl11) (39 / 120) , (C) R4^{wt} vs. Clone B (cl22) (38 / 120) and (D) R4^{wt} vs. Clone C (cl66) (33 / 120) untreated (M = medium) and treated with DMSO (D) as vehicle control (0.3 %) and trametinib (Tra) (0.03 µM) (all normalized over streptavidin). For the color scale, the range was set between -1.0 (green) and 1.0 (red).

For R4^{wt} PDOs, there was a higher WNT signaling activity due to higher expression of β-Catenin and Glycogen synthase kinase 3 (GSK3). There was also a higher expression of RAS, ERK 1/2, the proto-oncogene serine/threonine-protein kinase c-RAF and the acidic fibroblast growth factor FGF-1 in R4^{wt} compared to R1^{R361H} (Figure 52A).

Furthermore, $R1^{R361H}$ exhibited a higher expression of anti-apoptotic marker Bcl-XL (Figure 52A). Similar results were obtained comparing $R4^{wt}$ with clone A (Figure 52B), clone B (Figure 52C) and clone C (Figure 52C).

There was a more pronounced decrease in proliferation markers, such as Aurora kinase A and cyclin B1 in $SMAD4^{R361H}$ PDOs after 24 h treatment with trametinib (Figure 53).

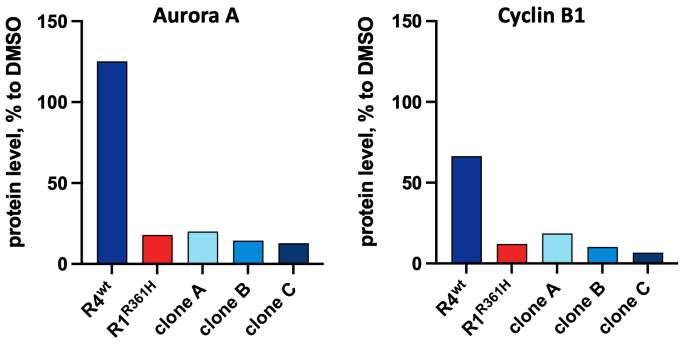

Figure 53: Proliferation markers expression in $R4^{wt}$, $R1^{R361H}$ and CRISPR-PDOs in response to trametinib (0.03 µM).
Protein expression was normalized to beta-actin. Bars represent protein expression levels after 24 h of trametinib exposure in [%] compared to corresponding DMSO controls.

However, there were no changes in proteins and phospho-proteins involved in the MAPK signaling pathway after 24 h treatment with trametinib (Figure 54).

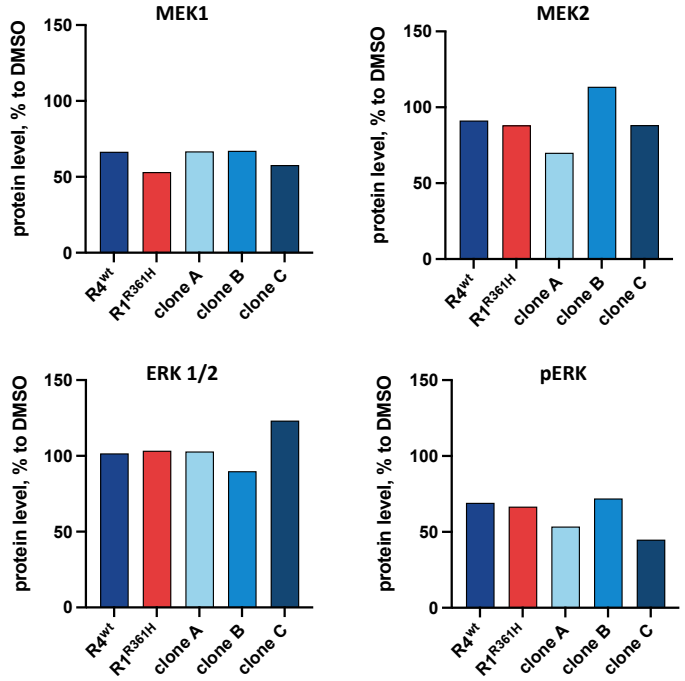

Figure 54: Expression of MEK1/2 and ERK 1/2 in R4, R1 and clones $R4^{wt}$, $R1^{R361H}$ and CRISPR-PDOs in response to trametinib (0.03 µM).
Protein expression was normalized to beta-actin. Bars represent protein expression levels after 24 h of trametinib exposure in [%] compared to corresponding DMSO controls. For pERK (phosphor-ERK), the ratio of phospho-protein level to total protein level was calculated.

I observed a reduction of pS6 for all PDO models, which are both, sensitive and resistant towards trametinib treatment (Figure 55). However, phosphorylated mammalian target of rapamycin (mTOR), which plays an important role in cell proliferation [176] was upregulated in SMAD4^{wt} PDOs after 24 h treatment with trametinib (Figure 55).

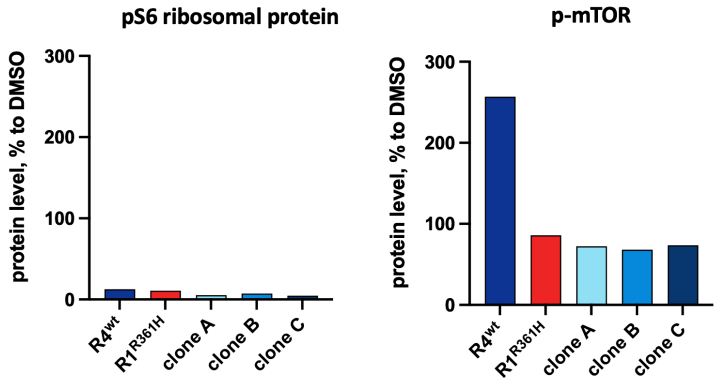

Figure 55: Expression of pS6 and p-mTOR in R4^{wt}, R1^{R361H} and CRISPR-PDOs in response to trametinib (0.03 µM).
Protein expression was normalized to beta-actin. Bars represent protein expression levels after 24 h of trametinib exposure in [%] compared to corresponding DMSO controls. For p-mTOR (phospho-mTOR), the ratio of phospho-protein level to total protein level was calculated.

Since SMAD4^{R361H} is believed to disrupt the TGF-β/BMP signal transduction [102], I analyzed the protein levels and phosphorylation status of receptor-regulated SMADs (SMAD2/3 and SMAD1/5) (Figure 56).

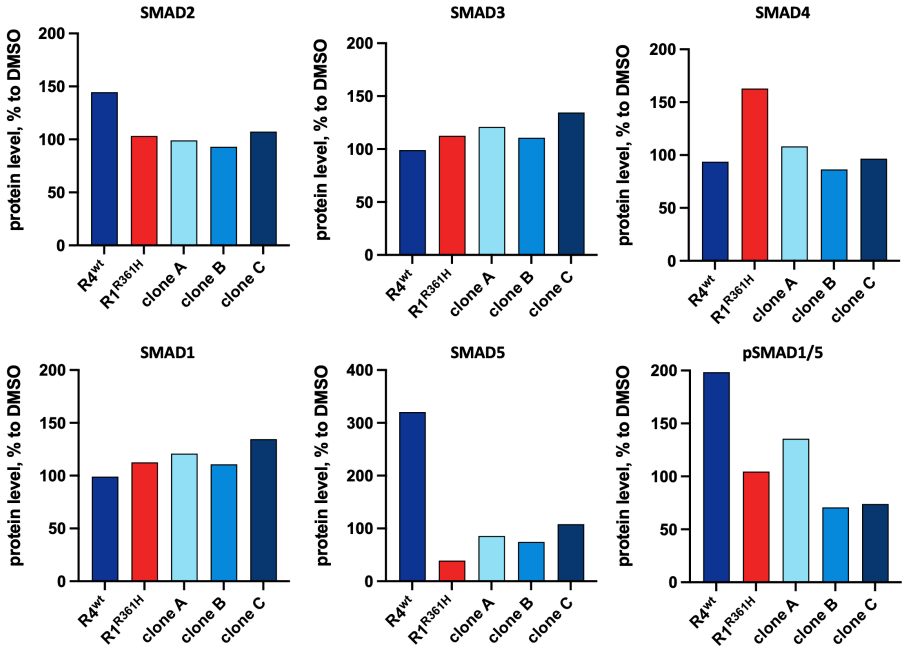

Figure 56: Expression of SMAD2/3, SMAD4 and (p-)SMAD1/5 in R4^{wt}, R1^{R361H} and CRISPR-PDOs in response to trametinib (0.03 µM).
Receptor activated SMAD2 and SMAD3 are involved in the TGF-β signaling pathway. Receptor activated SMAD1 and SMAD5 are involved in the BMP signaling pathway. Co-SMAD SMAD4 is involved in both pathways. Protein expression was normalized to beta-actin. Bars represent protein expression levels after 24 h of trametinib exposure in [%] compared to corresponding DMSO controls. For pSMAD1/5 (phosphor-SMAD1/5), the ratio of phospho-protein level to total protein level was calculated.

Out of all SMADs, only SMAD5 and phosphorylated SMAD1/5 (pSMAD1/5) showed pronounced changes in protein levels and phosphorylation status in response to MEK inhibition only in SMAD4^{wt} organoids (Figure 56). SMAD1 and SMAD5 are receptor-activated SMADs of the BMP signaling pathway [91]. Their upregulation indicates a BMP pathway activation in SMAD4^{wt} organoids.

In conclusion, trametinib treatment stopped proliferation in SMAD4 mutated PDOs and a BMP activation is responsible for the MEK-inhibitor resistance.

4.2. Identification of potential biomarkers for improved treatment outcomes in CRC

4.2.1. SFAB-signature predicts sensitivity to MEK inhibition in CRC PDOs

In order to evaluate feasibility of using SMAD4 mutational status as predictive biomarker, I treated 62 PDOs of CRC with known mutational status (Suppl. Table 12) with MEK-inhibitors cobimetinib, trametinib and selumetinib. About 15 % (9/62) of the PDOs harbored pathogenic SMAD4 mutations according to “The Human Gene Mutation Database” (HGMD®) [177,178] (Suppl. Table 12). All PDOs were sensitive to cobimetinib, about 10 % (6/62) of the models were sensitive to trametinib, and about 8 % (5/62) were sensitive to selumetinib (Figure 57A).

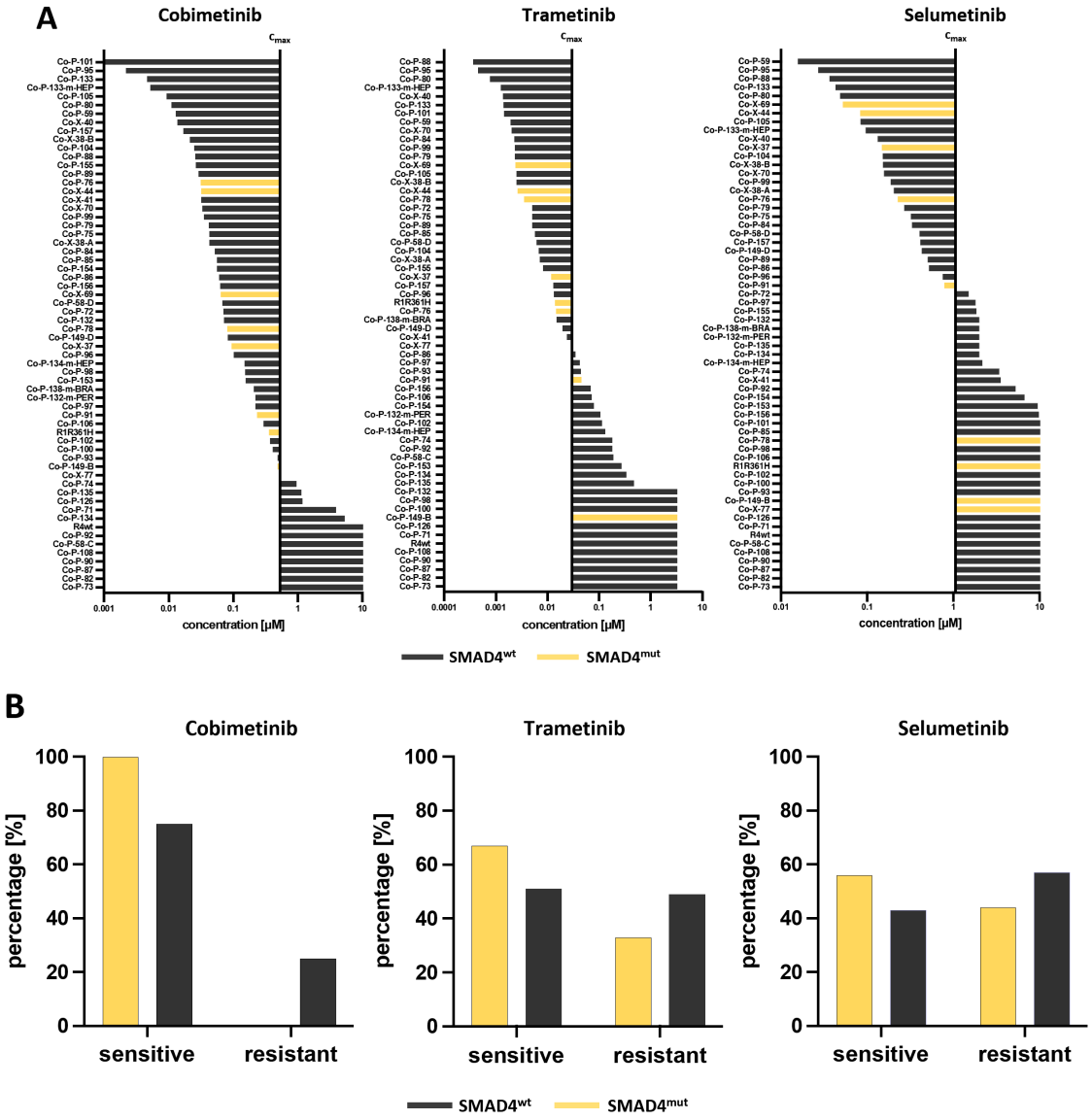

n = 62	Cobimetinib		Trametinib		Selumetinib	
Effect size	**Value**	**95 % CI**	**Value**	**95 % CI**	**Value**	**95 % CI**
Sensitivity	0.1837	0.09976 to 0.3136	0.1818	0.08611 to 0.3439	0.1786	0.07879 to 0.3559
Specificity	1.000	0.7719 to 1.000	0.8966	0.7361 to 0.9642	0.8824	0.7338 to 0.9533
Positive Predictive Value	1.000	0.7009 to 1.000	0.6667	0.3542 to 0.8794	0.5556	0.2667 to 0.8112
Negative Predictive Value	0.2453	0.1493 to 0.3757	0.4906	0.3612 to 0.6212	0.5660	0.4327 to 0.6905
	p 0.1836		p 0.4826		p 0.7192	

Figure 57: PDO models of colorectal cancer (CRC) mutated in SMAD4 gene are sensitive to MEK inhibition.
(A) Waterfall plots of IC_{50} values of CRC PDO models with known SMAD4 status tested with MEK-inhibitors cobimetinib, trametinib and selumetinib. PDO models with IC_{50} values below c_{max} are defined as sensitive, PDO models with IC_{50} values above c_{max} are defined as resistant. (Yellow bars: PDOs harboring pathogenic SMAD4 mutation; gray bars: PDOs harboring non-pathogenic or no SMAD4 mutation.) (B) Contingency analysis for sensitive and resistant models (n=62).

The contingency analysis (Figure 57B) showed that the sensitivity to MEK inhibition within the CRC PDO-cohort harboring SMAD4 pathogenic mutation is drastically increased, however, significant number of unaffected models are also MEK-inhibitor sensitive.

Recently, a third MEK-inhibitor, binimetinib [314], has received FDA approval for clinical use in cancer patients. I treated three PDOs with pathogenic SMAD4 mutation or deletion, and two PDOs with wild-type SMAD4 with binimetinib (Figure 58).

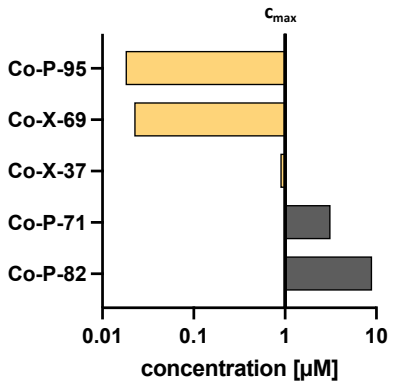

Figure 58: IC_{50} values of CRC PDO models with known SMAD4 status tested with MEK-inhibitor binimetinib.
(A) Waterfall plot of IC_{50} values of CRC PDO models with known SMAD4 status tested with MEK-inhibitors binimetinib. PDO models with IC_{50} values below c_{max} are defined as sensitive, PDO models with IC_{50} values above c_{max} are defined as resistant. (Yellow bars: PDOs harboring pathogenic SMAD4 mutation; gray bars: PDOs harboring non-pathogenic or no SMAD4 mutation.)

PDOs with pathogenic SMAD4 mutation or deletion were sensitive to MEK-inhibitor binimetinib and PDOs that are $SMAD4^{wt}$ or carrying a non-pathogenic SMAD4 mutation were resistant.

In order to find a more comprehensive way to predict MEK-inhibitor sensitivity, I looked for frequently mutated genes in CRC which are associated with the TGF-β/BMP-pathway [179,180] and identified prospective candidates (Figure 59, Figure 60): AT-rich interactive domain-containing protein 1A (ARID1A) [181], bone morphogenetic protein receptor type II (BMPR2) [182] and F-box/WD repeat-containing protein 7 (FBXW7) [183].

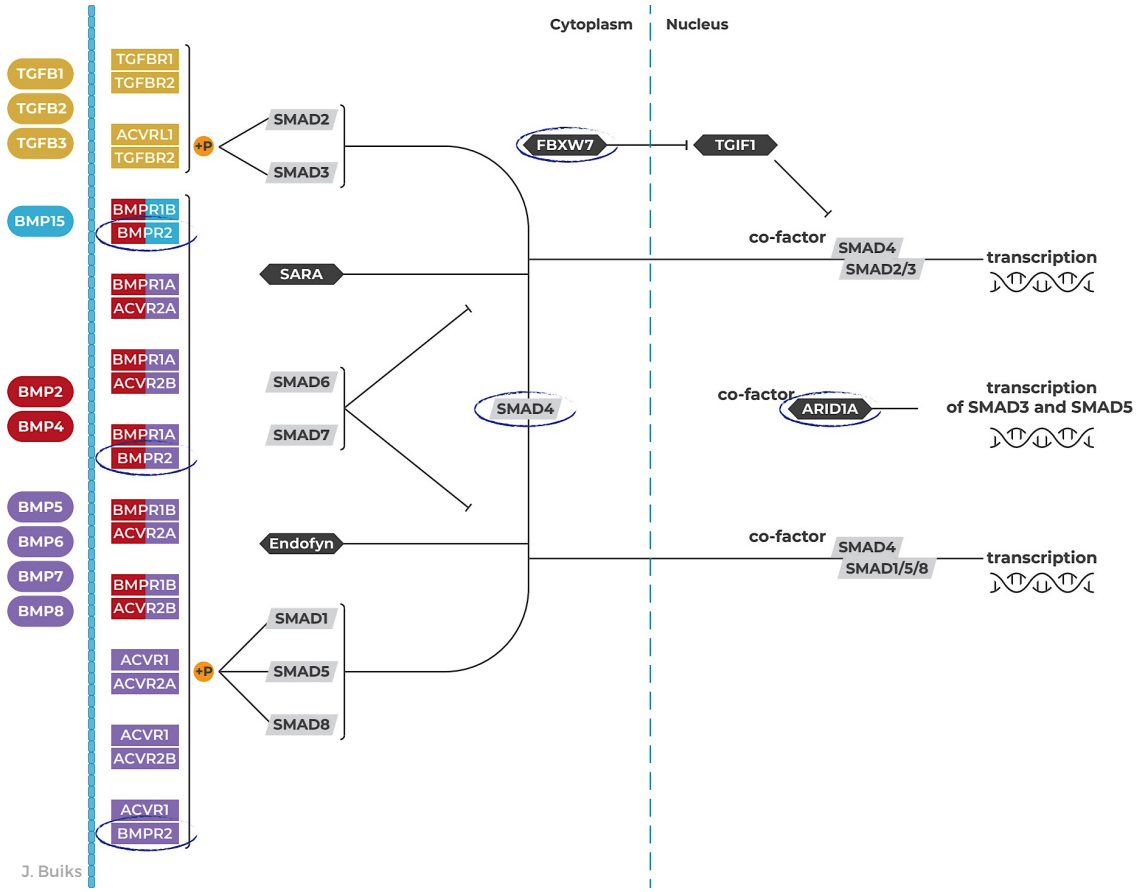

Figure 59: Schematic representation of the TGF-β/BMP-pathway with four frequently mutated genes in colorectal cancer (circled).
ARID1A = AT-rich interactive domain-containing protein 1A, BMPR2 = Bone morphogenetic protein receptor type II, FBXW7 = F-box/WD repeat-containing protein 7, SMAD4 = mothers against decapentaplegic homolog 4.

The Cancer Genome Atlas (TCGA) CRC cohort involving 594 patients revealed that 36 % of the patients had at least one mutation in SMAD4, FBXW7, ARID1A, or BMPR2. 15 % had a SMAD4 mutation, 16 % had a FBXW7 mutation, 10 % had a mutation in ARID1A and 6 % had a mutation in BMPR2 (Figure 60A). I defined the SFAB- (SMAD4, FBXW7, ARID1A, or BMPR2) signature, as a group of at least one mutation in these genes, excluding single non-pathogenic mutations, according to HGMD® [177,178]. The SFAB distribution of CRC PDO models was similar to the TCGA data for CRC patients (Figure 60B, Suppl. Table 12).

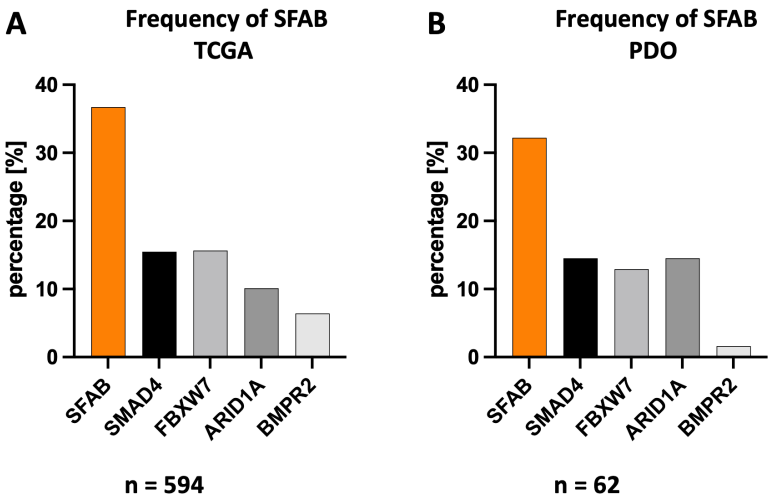

Figure 60: Frequency of SFAB (SMAD4, FBXW7, ARID1A or BMPR2) mutations or deletions in PDOs is similar to CRC patients' frequency.
(A) Frequency of SFAB in CRC patients (TCGA = The Cancer Genome Atlas, PanCancer atlas colorectal adenocarcinomas (n = 594) (cBioPortal, access on 18/08/ 2021)). (B) Frequency of SFAB in CRC PDO models (n = 62). (SMAD4 = mothers against decapentaplegic homolog 4, FBXW7 = F-box/WD repeat-containing protein 7, ARID1A = AT-rich interactive domain-containing protein 1A, BMPR2 = Bone morphogenetic protein receptor type II).

For PDO models with SFAB-signature, there was a 95 % and a 70 % significant positive prediction for sensitivity to cobimetinib and selumetinib, respectively and a 70 % positive prediction for sensitivity trametinib (Figure 61).

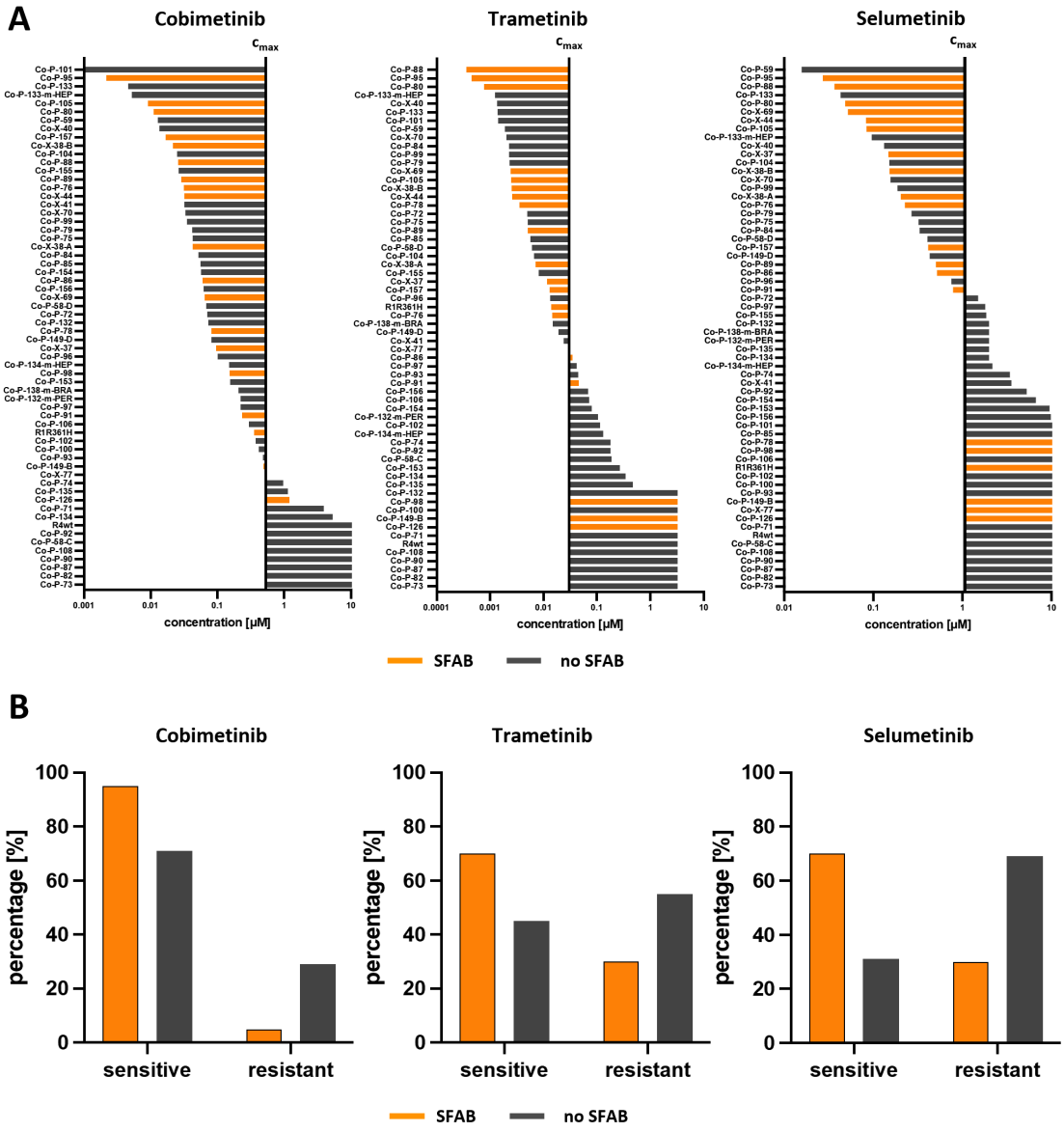

n = 62	Cobimetinib		Trametinib		Selumetinib	
Effect size	**Value**	**95% CI**	**Value**	**95% CI**	**Value**	**95% CI**
Sensitivity	0.3878	0.2643 to 0.5275	0.4242	0.2724 to 0.5919	0.5185	0.3399 to 0.6926
Specificity	0.9231	0.6669 to 0.9961	0.7931	0.6161 to 0.9015	0.8286	0.6732 to 0.9190
Positive Predictive Value	0.9500	0.7639 to 0.9974	0.7000	0.4810 to 0.8545	0.7000	0.4810 to 0.8545
Negative Predictive Value	0.2857	0.1717 to 0.4357	0.5476	0.3995 to 0.6878	0.6905	0.5397 to 0.8093
	p* 0.0451		p 0.1023		p* 0.0059	

Figure 61: CRC PDO models with SFAB- (SMAD4, FBXW7, ARID1A or BMPR2) signature are sensitive to MEK inhibition. (A) Waterfall plots of IC_{50} values of CRC PDO models with known *SMAD4, FBXW7, ARID1A or BMPR2 status* tested with MEK-inhibitors cobimetinib, trametinib and selumetinib. PDO models with IC_{50} values below c_{max} are defined as sensitive, PDO models with IC_{50} values above c_{max} are defined as resistant. (Orange bars: PDOs harboring pathogenic SMAD4 mutation; gray bars: PDOs harboring non-pathogenic or no SMAD4 mutation). (B) Contingency analysis for sensitive and resistant models (n=62).

4.2.2. SFAB-signature predicts sensitivity to MEK inhibition RAS/RAF independent

Here, I performed an additional contingency analysis to investigate whether RAS status can predict sensitivity to MEK inhibition (Figure 62).

About 53 % (33/62) PDO models carry a pathogenic KRAS mutation. This is concordant with published data [184]. The RAS status alone (Figure 62A) and in combination with SFAB-signature (Figure 62B+C) failed to yield better prediction for sensitivity to MEK-inhibitors cobimetinib, trametinib and selumetinib.

About 10 % (6/62) PDO models carry a pathogenic BRAF mutation. This is concordant with published data that approximately 10 % of CRC patients are characterized by a BRAF mutation (cBioPortal, access on 29/11/2021). I investigated whether BRAF status can predict sensitivity to MEK inhibition. BRAF status alone failed to better predict sensitivity to the MEK-inhibitors cobimetinib, trametinib, and selumetinib (Figure 63A).

Apart from one PDO model, all BRAF mutant PDOs have an SFAB-signature (Suppl. Table 12). Therefore, the combination of BRAF mutation and SFAB-signature did not demonstrate a better prediction (Figure 63B) compared with SFAB-signature alone (Figure 61).

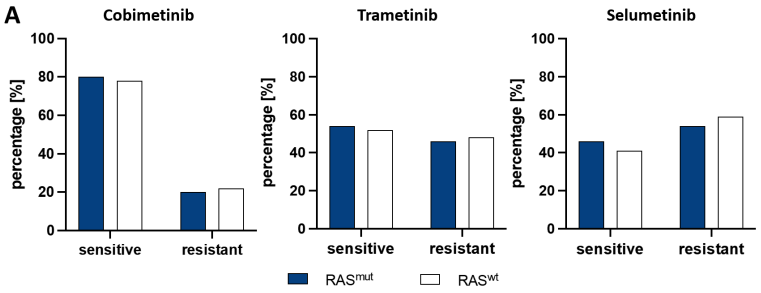

n = 62	Cobimetinib		Trametinib		Selumetinib	
Effect size	**Value**	**95 % CI**	**Value**	**95 % CI**	**Value**	**95 % CI**
Sensitivity	0.5714	0.4327 to 0.6998	0.5758	0.4081 to 0.7276	0.4600	0.3656 to 0.5574
Specificity	0.4615	0.2321 to 0.7086	0.4483	0.2841 to 0.6245	0.5900	0.4920 to 0.6813
Positive Predictive Value	0.8000	0.6411 to 0.8996	0.5429	0.3819 to 0.6953	0.5287	0.4249 to 0.6302
Negative Predictive Value	0.2222	0.1061 to 0.4076	0.4815	0.3074 to 0.6601	0.5221	0.4308 to 0.6120
	p >0.9999		p >0.9999		p 0.5684	

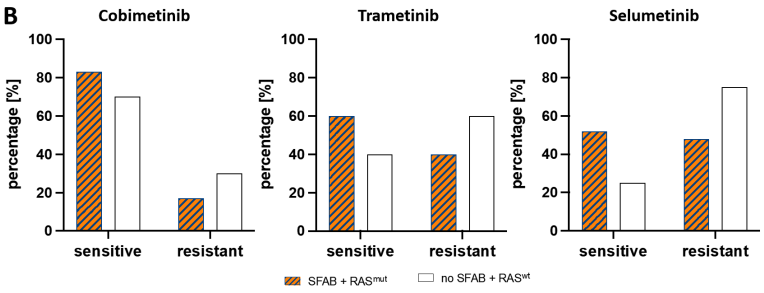

n = 62	Cobimetinib		Trametinib		Selumetinib	
Effect size	**Value**	**95 % CI**	**Value**	**95 % CI**	**Value**	**95 % CI**
Sensitivity	0.7143	0.5759 to 0.8215	0.7576	0.5898 to 0.8717	0.8148	0.6330 to 0.9182
Specificity	0.4615	0.2321 to 0.7086	0.4138	0.2551 to 0.5926	0.4286	0.2798 to 0.5914
Positive Predictive Value	0.8333	0.6940 to 0.9168	0.5952	0.4449 to 0.7296	0.5238	0.3772 to 0.6664
Negative Predictive Value	0.3000	0.1455 to 0.5190	0.6000	0.3866 to 0.7812	0.7500	0.5313 to 0.8881
	p 0.3178		p 0.1806		p 0.0567	

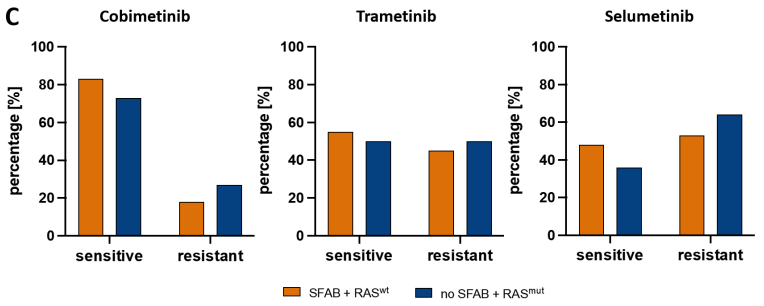

n = 62	Cobimetinib		Trametinib		Selumetinib	
Effect size	**Value**	**95 % CI**	**Value**	**95 % CI**	**Value**	**95 % CI**
Sensitivity	0.6735	0.5338 to 0.7879	0.6667	0.4961 to 0.8025	0.7037	0.5152 to 0.8415
Specificity	0.4615	0.2321 to 0.7086	0.3793	0.2269 to 0.5600	0.4000	0.2555 to 0.5643
Positive Predictive Value	0.8250	0.6805 to 0.9125	0.5500	0.3983 to 0.6929	0.4750	0.3294 to 0.6250
Negative Predictive Value	0.2727	0.1315 to 0.4815	0.5000	0.3072 to 0.6928	0.6364	0.4295 to 0.8027
	p 0.5155		p 0.7929		p 0.4347	

Figure 62: RAS status does not predict sensitivity to MEK-inhibitors.
Contingency analysis for sensitive and resistant models, (A) based on RAS status alone, (B) SFAB-signature + RAS^{mut} vs. no SFAB-signature + RAS^{wt} and (C) SFAB-signature + RAS^{wt} vs. no SFAB-signature + Ras^{mut} (SFAB = SMAD4, FBXW7, ARID1A, BMPR2) (n = 62).

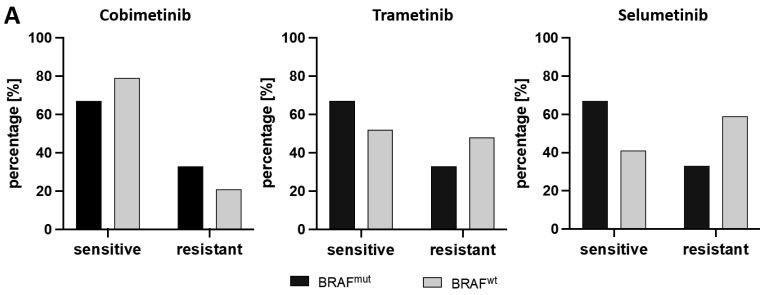

n = 62	Cobimetinib		Trametinib		Selumetinib	
Effect size	**Value**	**95 % CI**	**Value**	**95 % CI**	**Value**	**95 % CI**
Sensitivity	0.0833	0.0328 to 0.1955	0.1212	0.0482 to 0.2733	0.1481	0.0592 to 0.3248
Specificity	0.8571	0.6006 to 0.9746	0.9310	0.7804 to 0.9877	0.9429	0.8139 to 0.9898
Positive Predictive Value	0.6667	0.3000 to 0.9408	0.6667	0.3000 to 0.9408	0.6667	0.3000 to 0.9408
Negative Predictive Value	0.2143	0.1271 to 0.3382	0.4821	0.3567 to 0.6099	0.5893	0.4588 to 0.7083
	p 0.6100		p 0.6757		p 0.3896	

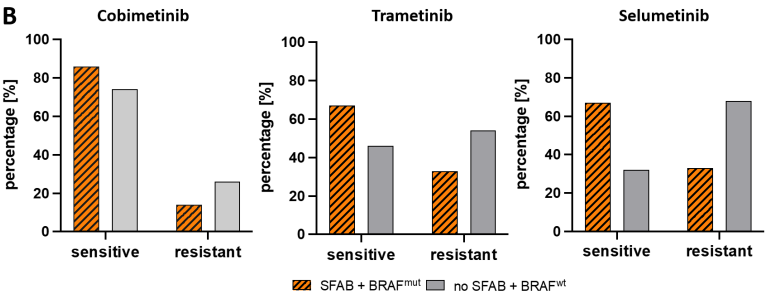

n = 62	Cobimetinib		Trametinib		Selumetinib	
Effect size	**Value**	**95 % CI**	**Value**	**95 % CI**	**Value**	**95 % CI**
Sensitivity	0.3600	0.2414 to 0.4986	0.4242	0.2724 to 0.5919	0.5185	0.3399 to 0.6926
Specificity	0.7857	0.5241 to 0.9243	0.7586	0.5789 to 0.8778	0.8000	0.6411 to 0.8996
Positive Predictive Value	0.8571	0.6536 to 0.9502	0.6667	0.4537 to 0.8281	0.6667	0.4537 to 0.8281
Negative Predictive Value	0.2558	0.1493 to 0.4024	0.5366	0.3875 to 0.6794	0.6829	0.5302 to 0.8044
	p 0.3560		p 0.1803		p* 0.0142	

Figure 63: BRAF status does not predict sensitivity to MEK-inhibitors.
Contingency analysis for sensitive and resistant models, (A) based on BRAF status alone and (B) SFAB-signature + $BRAF^{mut}$ vs. no SFAB-signature + $BRAF^{wt}$ (SFAB=SMAD4, FBXW7, ARID1A, BMPR2) (n = 62).

In summary, I showed that a single gene alteration in the SMAD4 gene leads to differential drug response in CRC. Moreover, SMAD4 loss of function was responsible for sensitivity towards MEK-inhibitors and could, potentially be used as a predictive marker in CRC which was confirmed by syngeneic CRISPR-engineered PDOs.

Transcriptomics and proteomics data support the observation, that MEK inhibition mostly affect $SMAD4^{R361H}$ PDOs. I did show that a BMP-pathway activation in $SMAD4^{wt}$ organoids might be responsible for MEK-inhibitor resistance.

After evaluation of the drug response in 62 PDO models with known mutational status, loss-of-function mutation, or deletion in SMAD4 gene alone did not show a significant positive prediction for MEK inhibition, however, the SFAB-signature (SMAD4, FBXW7, ARID1A, or BMPR2) showed significant positive prediction for two MEK-inhibitors independent of the RAS/RAF status.

5. DISCUSSION

Today, precision oncology aims to match specific tumor mutations with prospective drugs to provide individualized treatment options. Molecular-targeted agents are already included as standard-of-care in combination with traditional chemotherapy [64]. The arsenal of targeted drugs, comprised of currently 89 approved agents [185], has revolutionized the therapeutic landscape of various cancers, especially CRC.

Although there are predictive biomarkers currently used in clinic, only a few percent of CRC patients benefit from them [39]. Therefore, the identification of novel predictive biomarkers is essential to improve the outcomes for cancer patients.

5.1. SMAD4 mutation and its role in intra-tumor heterogeneity

Intra-tumor heterogeneity (ITH) and cancer progression are intertwined. ITH is the main reason for therapy failure and subsequent recurrence [186]. Multi-regional genetic analyses revealed that ITH is present in nearly every solid tumor, interfering with tumor "evolution" over time [115,187]. Schumacher et al. established organoid cultures from multiple regions of a chemo-naïve CRC and its liver metastases. In addition to previous well-described CRC mutations, such as $KRAS^{G12D}$, $PIK3CA^{H1047R}$, and $TP53^{C242F}$ both SMAD4 wild-type and SMAD4 mutant clones have been identified by ultra-deep sequencing [115]. Between the sibling cultures, they observed an up to 30-fold difference in drug response between these clones [115].

The first aim of the present study was to examine the putative clinical relevance of SMAD4 in CRC tumors and its impact on differential drug response. Therefore, I tested two representative PDO models of the previously published models, $R1^{R361H}$ and $R4^{wt}$ [115].

Mutations in SMAD4 have previously been associated with increased metastatic potential and decreased overall survival in several cancer types, including non-small cell lung cancer, head and neck cancer, and CRC [99–103,188–190]. Loss of SMAD4 also promotes tumor development in pancreatic cancer triggered by activation of $KRAS^{G12D}$ [191]. $R1^{R361H}$ and $R4^{wt}$ behaved differently in culture (Figure 17). It has been shown before that SMAD4 loss leads to increased cell proliferation in squamous cell carcinomas [192] and that the R361H mutation is associated with enhanced tumor growth and

metastases [108,112,113]. This may explain the high proliferative potential of $R1^{R361H}$ in comparison to $R4^{wt}$ (Figure 17).

I treated $R1^{R361H}$ and $R4^{wt}$ with six drugs targeting the MAPK-pathway. Since both sibling PDO cultures are $KRAS^{G12D}$ mutated and thereby resistant to an anti-EGFR therapy [193,194], cetuximab was excluded from the analysis. The multi-receptor tyrosine kinase inhibitor regorafenib showed promising results in clinical trials with CRC patients [195]. Although, regorafenib inhibited the cell growth within the tested concentration range, the IC_{50} values for $R1^{R361H}$ and $R4^{wt}$ were comparable to the c_{max} level (Figure 20B). Therefore, regorafenib might not be beneficial for this cancer patient. I treated $R1^{R361H}$ and $R4^{wt}$ with dabrafenib, an ATP-competitive BRAF-inhibitor approved for treatment of malignant $BRAF^{V600E}$ melanoma [196]. The $BRAF^{V600E}$ mutation is an activating mutation that promotes the MAPK signaling, thereby stimulating cell proliferation, while inhibiting apoptosis [197]. Since $R1^{R361H}$ and $R4^{wt}$ lack the $BRAF^{V600E}$ mutation, dabrafenib should have no effect on PDOs. Indeed, both PDOs were resistant to dabrafenib (Figure 20B). However, CRC with $BRAF^{V600E}$ mutation has been shown to be inherently resistant to BRAF-inhibitors due to feedback activation of the epidermal growth factor receptor (EGFR) [198].

MEK-inhibitors have previously been shown to be effective against CRC [82,83,199]. In a preclinical study, trametinib showed high efficacy in xenograft models, derived from the human colon cancer cell line HT-29 [82]. In this HT-29 xenograft model, oral administration of trametinib demonstrated efficacy in inhibiting tumor growth [82]. Similar findings were observed in a xenograft model derived from the A549 cell line (human lung adenocarcinoma) [200]. Cobimetinib has been shown to inhibit cell proliferation and induce apoptosis in HCT116 colorectal cancer cells [83]. Selumetinib was tested in combination with cyclosporine A in patients with metastatic CRC and appeared to be well tolerated, with evidence of activity in metastatic CRC [199].

I treated $R1^{R361H}$ and $R4^{wt}$ with commercially available MEK-inhibitors cobimetinib, trametinib and selumetinib [74,75,77]. In the clinic MEK-inhibitors show efficacy in BRAF wild-type melanomas in combination with chemotherapy and immune checkpoint-inhibitors [201]. Based on the promising results of MEK-inhibitors in BRAF mutated melanoma, researchers are actively engaged in the development of potent MEK-inhibitors to expand their use to other invasive forms of cancer, such as CRC.

Currently, MEK-inhibitors are being evaluated in phase III studies for the treatment of patients suffering from metastatic CRC [61]. MEK-inhibitors are known to cause feedback reactivation of ERK and have shown limited to no activity in KRAS mutant cancers [202]. However, $R1^{R361H}$ and $R4^{wt}$ (both $KRAS^{G12D}$ mutants) showed a significantly different response to MEK-inhibitor treatment (Figure 20B). $R4^{wt}$ was completely resistant, whereas $R1^{R361H}$ was significantly more sensitive to cobimetinib, trametinib, and selumetinib.

A possible mechanism for MEK-inhibitor resistance may be a reactivation of the MAPK-pathway through alterations or mutations in RAS, RAF or MEK [203], but according to the panel sequencing, $R4^{wt}$ carries a $KRAS^{G12D}$ mutation (Table 19) and is wild-type in BRAF and MEK. Consequently, this mechanism can be excluded. Mutations of MEK during or after exposure of cells to MEK-inhibitors is another potential mechanism to induce resistance. This can result either in an overactivation of MEK or in the inability of inhibitors to bind to MEK [204,205]. Additionally, MEK mutation can also lead to reactivation of several receptor tyrosine kinases (RTKs) upstream of the MAPK signaling pathway, which are responsible for initiating the signaling cascade that eventually leads to cell growth and proliferation, resulting in adaptive resistance [206]. RTKs are crucial in signal transduction in multiple pathways which makes them important regulators in cell signaling. Reactivation of RTKs after their inhibition stimulates cell growth through these different pathways [207]. In case of the MAPK signaling pathway, the reactivation occurs because RTKs are normally suppressed by ERK1/2 [208]. When MEK is inhibited, ERK is suppressed and RTKs such as EGFR, ERBB3 (also known as HER3 (human epidermal growth factor receptor 3)), IGF-1R (insulin-like growth factor 1) or PDGFR (platelet-derived growth factor receptor) are rapidly reactivated as an adaptive response [203,209,210]. Previous studies have shown that an upregulation of ERBB3 is a potential factor for resistance to MEK inhibition in KRAS mutated lung and colon cancers [211]. This could be a potential mechanism for MEK-inhibitor resistance, but the upregulation of multiple RTKs would need further investigation as it is not yet fully understood.

I treated $R1^{R361H}$ and $R4^{wt}$ with ulixertinib, an ERK inhibitor that is currently in a phase II clinical trial (recruitment stage) with CRC patients harboring alterations in MEK or BRAF [212]. There was no significant difference between both PDO sibling cultures (Figure 20B).

Based on the panel sequencing, $R1^{R361H}$ carries, in addition to $SMAD4^{R361H}$, a heterozygous mutation in $MLH1^{I219V}$ (MutL homolog 1) and $KLDR^{Q472H}$ (kinase insert domain receptor) while $R4^{wt}$ is wild-type in these genes (Table 19). MLH1 is a tumor suppressor gene involved in DNA mismatch repair [213]. The I291V mutation in MLH1 is a likely benign alteration that showed wild-type-like behavior in HCT116 colorectal cancer cells after transient transfection [214]. The KDR variant Q472H is considered non-pathogenic but has previously been shown to be more proliferative and invasive in comparison to wild-type KDR in melanoma patients [215]. KDR^{Q472H} was reported to be associated with a higher number of lymph node metastases in a CRC patient study [216]. Since, $MLH1^{I129V}$ and KDR^{Q472H} are heterozygous non-pathogenic mutations, I assumed that they do not affect drug response in $R1^{R361H}$, whereas the homozygous pathogenic $SMAD4^{R361H}$ mutation indicates MEK-specificity. The response to MEK-inhibitors has never been associated with SMAD4 alterations. In summary, the SMAD4 mutational status has a clinical relevance and could be a predictive biomarker.

5.2. $SMAD4^{R361H}$ is responsible for sensitivity to MEK inhibition

In order to investigate the $SMAD4^{R361H}$ mutation and its influence on drug response, I used a CRISPR/Cas9 genome engineering approach to introduce R361H into SMAD4 wild-type PDOs (Figure 22). CRISPR/Cas9 is a tool that allows researchers to introduce a double strand break at any location in the genome with high specificity [217].

I was able to introduce the R361H point mutation into $R4^{wt}$ PDOs via homology-directed repair and generated three CRISPR-PDOs (Figure 32). The panel sequencing confirmed the homozygous $SMAD4^{R361H}$ mutation in all syngeneic CRISPR-PDOs (Table 20). However, the three CRISPR-PDOs lost the heterozygous $PI3KCA^{H1047R}$ mutation after clonal selection (Table 20), which was present in both $R1^{R361H}$ and $R4^{wt}$. PIK3CA (Phosphatidylinositol-4,5-bisphosphate 3-kinase, catalytic subunit alpha) is frequently mutated in CRC with up to 32 % [218,219] and is associated with poor prognosis [220,221]. Although, the clones lost $PI3KCA^{H1047R}$, they showed similar behavior to $R1^{R361H}$ in terms of proliferation time and drug response (Figure 33, Figure 34). They were all significantly more sensitive to MEK-inhibitors in comparison to $R4^{wt}$. Thus, I conclude that this $PI3KCA^{H1047R}$ mutation is not involved in MEK-inhibitor response.

The use of CRISPR to investigate effects of single gene mutations on drug responses has been previously reported in the literature [222,223]. Matano et al. generated CRISPR-engineered intestinal organoids to introduce multiple driver pathway mutations, into human normal or adenoma-derived intestinal organoids to examine the influence of various driver pathway mutations on human CRC. They showed that organoids with multiple driver mutations in genes, such as APC, KRAS, TP53, PIK3CA and SMAD4, grew poorly in presence of experimental MEK-inhibitor PD325901 [223]. Based on the increased sensitivity to cobimetinib, trametinib and selumetinib in CRISPR-PDOs, my results support the assumption that SMAD4^{R361H} is indeed responsible for sensitivity to MEK inhibition.

In a *vice versa* approach, I have tried to restore the wild-type phenotype in R1^{R361H}. Despite multiple attempts this approach failed. Control experiments demonstrated successful transfection of cells but this resulted either in a lethal phenotype or failure to restore the wild-type phenotype. This observation could stem from pathway addiction. Pathway addiction is a phenomenon in cancer where cells become highly dependent on specific up-regulated pathways [6,8]. A similar effect was observed in head and neck squamous cell carcinoma PDX tumors in which SMAD4 mutated displaced SMAD4 wild-type cells, leading to the establishment of homogeneous SMAD4 mutated head and neck squamous cell carcinoma (HNSCC) cell lines with partial or complete SMAD4 genomic loss, suggesting a survival advantage of SMAD4 mutated cells [224].

Using a complementary approach based on virus mediated overexpression of SMAD4 wild-type protein in CRISPR-PDOs and R1^{R361H} delivered inconclusive results (Figure 39, Figure 40). I observed a shift in resistance in SMAD4 wild-type-expressed PDOs for all tested drugs, but I was not able to exclude that the acquired puromycin resistance from the selection process in these PDOs was responsible for multi-drug resistance (Figure 41). Other groups that have used a similar CRISPR/Cas9 genome editing with puromycin selection only in 2D cell lines [225] or 2D cell line-derived spheroids of CRC [226] for drug screening, but not in the more complex organoids, while another group claims to have successfully performed a CRISPR knock-out in colon organoids, but without performing a drug screening on those cells [227,228].

How puromycin selection and expression of puromycin N-acetyltransferase can influence multi-drug resistance is still under debate. Two main mechanisms of puromycin-induced

multidrug resistance have been described: (1) classical mutations of genes that metabolize the drug or (2) chromosomal reassortments catalyzed by cancer- and cell line-specific aneuploidy [229].

Less likely possibilities include that the introduction of regular SMAD4 makes the clones less competent and less capable of reproducing and being displaced by non-SMAD4 carriers, or that cells suppress protein expression from a plasmid, which could be investigated in a possible continuation of the project.

In summary, I succeeded in establishing syngeneic PDOs with the $SMAD4^{R361H}$ mutation and investigated its effects on drug response, while the correction of the mutation in the original $R1^{R361H}$ PDOs and the rescue experiment with overexpression of SMAD4 wild-type did not deliver conclusive results.

5.3. 5-FU resistance can affect sensitivity to MEK-inhibitors

5-Fluorouracil (5-FU) based treatment regimen is the standard first-line therapy for CRC patients [64]. 5-FU is a pyrimidine analogue that inhibits the RNA- and DNA-synthesis resulting in inhibition of tumor growth or apoptosis of cancer cells [230].

The sibling cultures $R1^{R361H}$ and $R4^{wt}$ responded to 5-FU, but the absolute IC_{50} values measured for both PDOs were comparable to the c_{max} value of 5-FU [134] (Figure 18), suggesting poor response to 5-FU-based therapies in the clinic.

Cancer patients frequently tend to develop resistance to first-line therapy [231,232] and SMAD4 mutations are associated with acquired chemoresistance [86,102,233].

Multi-drug resistance of cancer cells during chemotherapy may be related to several mechanisms, including increased efflux of drugs, genetic factors (gene mutations, amplifications, and epigenetic changes), growth factors, or increased DNA repair capacity [234], leading to a reduction in the therapeutic efficacy of the administered drugs and thus complicating tumor control [235–237].

Under 5-FU treatment (at plasma concentration level), $R1^{R361H}$ changed their morphology from a round shape to a more mesenchymal cell shape in comparison to $R4^{wt}$ (Figure 19) potentially indicating epithelial to mesenchymal transition (EMT). Mesenchymal cells are associated with tumor cell migration and metastases [238,239]. The transformation into a mesenchymal phenotype may result in increased drug resistance [240]. This could be an explanation for 5-FU related drug resistance. Schumacher et al. described that the

heterogeneous landscape within the same tumor may ensure a very high degree of flexibility in tumor response to chemotherapy, leading to multi-drug resistant disease [115]. Statistical data show that over 90 % of cancer patient's mortality is due to drug resistance in the metastasized setting [241].

$R1^{R361H}$ and $R4^{wt}$ were derived from a tumor that was described as CMS2 (consensus molecular subtype 2) [115]. According to Guinney et al., CMS2 is characterized by WNT and MYC activation and resembles the largest of the 4 molecular subgroups [40]. In addition to CMS classification, CRC intrinsic subtypes (CRIS) were suggested by Isella et al. two years later [242]. One of them is CRIS-B that is associated with TGF-β-pathway activity, EMT, and poor prognosis [242], which applies to this tumor.

In order to recapitulate the clinical situation, I established 5-FU resistant PDOs (Figure 42). Although, $R4^{wt}$ survived sublethal concentration of 5-FU for a short-term, long-term exposure eventually caused cell death. Only SMAD4 mutated PDOs developed a 5-FU resistance (Figure 44), which may likely be a selective event occurring in patients and therefore explains a lower likelihood of successful treatment with successive therapies.

EMT could also be an explanation why only SMAD4 mutated cells would proliferate under 5-FU treatment and developed a multi-drug resistance towards drugs like regorafenib and MEK-inhibitors (trametinib and cobimetinib). Although these mechanisms are far from fully understood, MEK-inhibitors should be considered in addition to first-line chemotherapy in patients with a SMAD4 mutation.

5.4. BMP-pathway activation leads to MEK-inhibitor resistance

The emergence of omics-technologies has improved the ability to characterize biospecimens at the genomic, transcriptomic, proteomic and metabolomic level [243]. High-throughput, biomarker-based analyses are expected to evolve in the coming years, leading to a more individualized tumor treatment [244,245].

In a multi-omics approach using RNA-sequencing (transcriptomics) together with a targeted proteomics approach (DigiWest®), I investigated the mechanisms underlying the MEK-inhibitor response.

Initially, I found an overlap of expression data and DigiWest® data showing that untreated and treated PDOs carrying $SMAD4^{R361H}$ clustered in the respective groups as did $R4^{wt}$ cells in their respective groups (Figure 45, Figure 50, Figure 51). The GO term enrichment

revealed that most of the significantly altered biological processes in SMAD4 mutated PDOs were processes related to DNA replication and cell cycle progression, as would be expected in the case of growth arrest associated with MEK inhibition (Suppl. Table 2, Suppl. Table 4-6).

This corroborates the observation, that trametinib blocked proliferation in $SMAD4^{R361H}$ PDOs. In $SMAD4^{wt}$ PDOs, GO categories included signal transduction and TGF-β/BMP signaling, but not DNA-replication or cell cycle progression (Suppl. Table 3).

The proteomic data revealed an accumulation Bcl-XL which is also used as an anti-apoptotic marker in $SMAD4^{R361H}$ PDOs in comparison to $R4^{wt}$. This points towards the inhibition of proliferation instead of apoptosis (Figure 52). This conclusion is further supported by decreased expression levels of proliferation markers Aurora A and cyclin B1 in $SMAD4^{R361H}$ PDOs (Figure 53). The proliferation of $R4^{wt}$ was unaffected. An investigation of MEK-inhibitor resistance in CRC cell lines showed that mutant PIK3CA contributes to intrinsic MEK-inhibitor resistance by activating AKT to regulate the expression of BCL-XL [246]. In breast cancer, a higher activation of Aurora A led to chemoresistance and cancer progression [247].

None of the tested PDOs displayed changes in MEK and phosphorylated ERK (pERK) protein expression after 24 h of treatment (Figure 54), indicating that this signaling pathway is not involved. As previously reported, a change in pERK was not significantly associated with trametinib sensitivity, only a reduction of phosphorylated ribosomal protein S6 (pS6) [248]. Trametinib resistance in CRC cell lines arises due to upregulation of pS6 [248]. In contrast, the proteomic results showed a reduction of pS6 in cells which are both, sensitive and resistant towards trametinib treatment (Figure 55). Thus, pS6 cannot be responsible for the drug response in these PDO models.

However, I observed an upregulation of p-mTOR in trametinib resistant $R4^{wt}$ PDOs and a decrease for $SMAD4^{R361H}$ PDOs (Figure 55). Several mechanisms of MEK-inhibitor resistance are associated with activation of cellular signaling pathways such as the PI3K/AKT/mTOR-pathway [249]. This finding is consistent with a previously published study showing that an activation of mTOR promotes tumor growth and metastases [250]. Furthermore, I detected a higher expression of SMAD5 and pSMAD1/5 in $R4^{wt}$ (Figure 56). These findings indicate an activation of the BMP signaling pathway that might contribute to resistance towards MEK inhibition.

As previously published, BMP signaling, particularly by SMAD5 promotes cancer cell proliferation and tumor growth [251]. In breast cancer resistance to the tubulin-binding paclitaxel can be reversed by depletion of SMAD5 [247].

The role of the BMP signaling in CRC is historically controversial, potentially due to the differential status of this signaling in different CRC molecular subtypes [40,252]. For instance, there is evidence of BMP-pathway activation in mesenchymal molecular subtype of the CRC, while in others it is suppressed [253].

It is well known that cancer develops from differentiated cells by an increasing degree of de-differentiation [254] and BMP signaling has been shown to lead to a stem-like phenotype associated with a mesenchymal phenotype and drug resistance [255].

From the literature analysis and my observations, it is plausible to assume that functional loss of SMAD4 and thus loss of SMAD5 signaling renders a SMAD4 mutation harboring subpopulation of cells more sensitive to MEK-inhibitors.

5.5. SFAB-signature predicts sensitivity to MEK inhibition

PDO models reflect at least in parts the ITH of the original tumor and faithfully predict its response to drugs as shown before [115]. Organoids obtained from an individual patient's tumor can be used to screen for drug treatment [121]. I discovered the change in MEK-sensitivity in SMAD4 mutated PDOs, but the question remains if this is meaningful to patients.

Our laboratory has developed a suitable tool for prediction of drug response using a high-throughput screening platform for PDOs [122]. The application of this tool in preclinical studies is an important pilar of modern drug discovery. After the initial discovery, nonclinical studies are often conducted with approved drugs to explore opportunities for expanded use and additional disease indications. In order to predict a potential drug response, the concentrations of the tested compounds are adjusted to the therapeutic dosage close to the maximum plasma concentration in humans (c_{max}) [133]. The c_{max} highly depends on the way of administration, compound formulation, and physical properties of the drug [133]. It provides an indication of the highest concentration to which the patient is exposed during therapy. While in *in vitro* studies, drug concentrations can often increase beyond levels that could be achieved *in vivo*, c_{max} should be considered

the highest relevant drug concentration in *in vitro* studies or the highest plasma exposure in *in vivo* studies [133].

However, when targeted agents are tested at concentrations 10- or 100-fold higher than the IC_{50} or K_i (inhibitory concentration) for the molecular target, the possibility increases that off-target activities unrelated to clinical benefit or on-target activities (enzyme inhibition and receptor occupancy) will be introduced that cannot realistically be achieved in the clinic [133]. Either of these situations may lead to misinterpretation of responses in preclinical studies. In addition, c_{max} is only transiently maintained for most agents, and maintained levels may be far below c_{max} to achieve therapeutic efficacy [256]. Furthermore, it is important to note that c_{max} values are an average of large cohorts and do not take individual properties, such as metabolism, into consideration. Therefore, we must be conscious of the risk of false positive or false negative results in preclinical studies.

In our laboratory, we defined achievable IC_{50} values below c_{max} ($IC_{50} < c_{max}$) as sensitive and IC_{50} values above c_{max} ($IC_{50} > c_{max}$) as resistant. In cases where the IC_{50} is close to c_{max} ($IC_{50} \approx c_{max}$), indicating that the drug affects tumor growth *in vitro* but can also result in EMT, as describe before, and may not have a beneficial effect in the clinic beyond stable disease at best.

I applied these criteria to the sequenced PDO models and analyzed their response to MEK-inhibitors and whether it correlated with their SMAD4 status. SMAD4 alone did not show a significant predictive value as several SMAD4 wild-type PDO models that were also sensitive to MEK-inhibitors (Figure 57).

Since the BMP-pathway appeared to play a key role in MEK-inhibitor-resistant cells, I hypothesized that disruption of the BMP-pathway by other genes would lead to sensitivity. I identified three more genes which are frequently mutated in CRC: ARID1A, BMPR2 and FBXW7 [179–183] (Figure 59). The distribution of these pathogenic mutations in the PDOs reflected the distribution of mutations in the TCGA CRC cohort (Figure 60).

The FBXW7 gene regulates TGF-β/BMP-pathway by targeting for degradation co-repressor TGF-β-induced factor 1 (TGIF1), which recruits specific repressor complexes to SMAD2 [257]. FBXW7 is a tumor suppressor and targets transcription factors c-MYC and c-JUN as well as Notch, cyclin E and sterol regulatory element-binding protein 1 (SREBP1), among others, which are degraded in a phosphorylation-dependent manner [258–261].

FBXW7 is commonly deleted in 30 % of human cancers, including CRC [262]. FBXW7 loss has been shown to promote chemoresistance in CRC cell lines [263].

The ARID1A gene participates in the TGF-β/BMP-pathway as a tumor suppressor that interacts with p53 regulating cyclin dependent kinase inhibitor 1A (CDKN1A) and SMAD3 transcription and subsequently tumor growth [264]. It is part of the chromatin remodeling complex and is responsible for the change in chromatin structure required to facilitate various cellular functions such as transcription, DNA synthesis and DNA damage repair [265]. ARID1A has emerged as a candidate “driver gene” tumor suppressor based on its frequent mutations in cancer cells, such as ovarian clear cell and endometroid cancers as well as CRC [265].

The BMPR2 gene is directly involved in BMP-branch signal transduction in the TGF-β/BMP-pathway [266]. It is a transmembrane serine/threonine kinase receptor which is essential for embryogenesis, development, and adult tissue homeostasis [267]. Upon BMP-induced heteromeric complex formation of BMPR2 with BMPR1 (BMP type I receptor), BMPR2 activates BMPR1 by phosphorylation. The activated BMPR1 propagates the signal into the cell by phosphorylation of the SMAD1, SMAD5, and SMAD8 transcription factors [268]. BMPR2 has been reported to play a dual role in regulating tumor growth [269]. For example, a lack of BMPR2 expression in the colon matrix has been shown to lead to epithelial hyperplasia and polyp formation [270]. In CRC lacking SMAD4, BMPR2 can bind to LIM domain kinase 1 to activate the Rho/Rho-associated protein kinase (ROCK) pathway to promote tumor invasion and metastases [271].

I applied the above-described criteria to the PDO models and analyzed whether they correlate with the defined SFAB-signature (SMAD4, FBXW7, ARID1A,or BMPR2) upon MEK inhibition. The SFAB-signature was identified to be significantly highly predictive for the sensitivity to cobimetinib and selumetinib in CRC PDOs (95 % to 70 %, respectively), while trametinib showed a similar trend (70 % positive prediction) but was not statistically significant ($p < 0,05$) (Figure 61).

All three MEK-inhibitors are non-ATP-competitive and allosteric inhibitors, meaning they either occupy the hydrophobic site immediately adjacent to the ATP-binding pocket when the activation loop of a kinase undergoes a conformational change, or they bind at an allosteric site outside the ATP-binding pocket and modulate kinase activity in an allosteric

manner [272]. This explains the high specificity of non-ATP-competitive MEK-inhibitors in comparison to ATP-competitive MEK-inhibitors, such as E6201 and MAP855 [272,273].

All three MEK-inhibitors tested showed different binding affinity to MEK1 and MEK2. Cobimetinib is a potent and highly selective MEK-inhibitor with a biochemical IC_{50} of 0.9 nM against MEK1 and 199 nM against MEK2 [75,274]. Selumetinib is a potent, highly selective inhibitor of MEK1/2 with IC_{50} value of 14 nM for MEK1 and K_D (equilibrium dissociation constant) value of 530 nM for MEK2 [77,275]. Trametinib is an allosteric, non-ATP-competitive inhibitor with sub-nanomolar activity against purified MEK1 and MEK2 kinases IC_{50} of 0.7 nM and 0.9 nM, respectively [70,74,276].

Thus, cobimetinib and selumetinib are more specific for MEK1 than MEK2, so they might follow similar pathways to overcome resistance in the majority of PDOs with SFAB-signature, whereas trametinib equally targets MEK1 and MEK2. Both, cobimetinib and selumetinib increase the interaction between MEK1/2 and c-RAF, which may promote MEK1/2 phosphorylation by c-RAF, leading to a rebound effect in MEK/ERK activity in RAS mutated tumors [272], in contrast trametinib does not activate this feedback loop of MEK/ERK activity in RAS mutated tumors [272].

The SFAB-signature was significantly predictive for the sensitivity to two MEK-inhibitors (cobimetinib and selumetinib) in the CRC PDO cohort (n=62). Trametinib showed a similar trend. However, several PDOs without SFAB-signature were sensitive to trametinib (Figure 61). Future studies are needed to investigate which other possible genetic alterations could be responsible for the sensitivity to trametinib or whether the strong affinity of trametinib to MEK2 plays a role in the sensitivity.

In addition, selected PDOs were tested with the novel cancer approved MEK-inhibitor binimetinib [76] and responded in a similar manner as expected (Figure 58).

In summary, the SFAB signature is highly predictive of response to MEK inhibitors.

5.6. Precision oncology using SFAB as RAS/RAF-independent biomarker

Further stratification of the patients based on the known and novel biomarkers could significantly improve the outcomes and allow for an individually tailored therapeutic approach or precision oncology. Hence the clinical need for diagnostic tests, methods, and biomarkers that will predict patient response to various treatment options in parallel. Despite the clinical success of BRAF-inhibitors in combination with MEK-inhibitors in $BRAF^{V600E}$ melanomas, no biomarker has yet been discovered for predicting therapeutic response in patients treated with MEK-inhibitors [249].

The RAS status is used as a biomarker for clinical decision making [39]. It has been sufficiently demonstrated to interfere with anti-EGFR therapy in CRC [193,194,277], while mutated SMAD4 is an independent factor for resistance to anti-EGFR therapy [102]. A continuous activation of the MAPK pathway due to an activating RAS mutation would also have an influence on downstream genes (RAF, MEK, and ERK) [278].

About half of the CRC PDO models carry pathogenic RAS mutation (Suppl. Table 12). The RAS status by itself could not predict response to MEK inhibition (Figure 62). To determine whether the RAS mutation status could improve the predictive power of the SFAB-signature, I expanded the contingency analysis for SFAB by pathogenic RAS mutations (Figure 62). Addition of the RAS status into the predictor did not improve the power of SFAB-signature. In conclusion, the RAS status is irrelevant for predicting the sensitivity towards MEK inhibition when applying the SFAB-signature.

Since MEK-inhibitors in combination with BRAF-inhibitors are approved for melanomas with BRAF mutations [279], I decided to test whether the BRAF mutational status has an impact on the predictive power of the SFAB-signature. The BRAF status alone and in combination with the SFAB-signature failed to predict sensitivity to MEK inhibition (Figure 63). Thus, the BRAF status is also irrelevant for prediction of sensitivity towards MEK inhibition and SFAB-signature.

Almost 60 % of CRC patients are RAS + SMAD4 + FBXW7 + ARID1A + BMPR2 mutated and approximately 10 % have a BRAF mutation (cBioPortal (access on 20/11/2021)).

The discovered SFAB-signature predicts the response to MEK-inhibitors with high probability. The SFAB-signature could be a new therapeutic option especially for previous non-responders (Figure 64).

Therefore, I propose to treat CRC patients with first-line therapeutics according to current guidelines and to use the SFAB-signature in patients not benefitting from guideline therapies (> 60 %), instead apply MEK-inhibitors to avoid a palliative treatment intention (Figure 64).

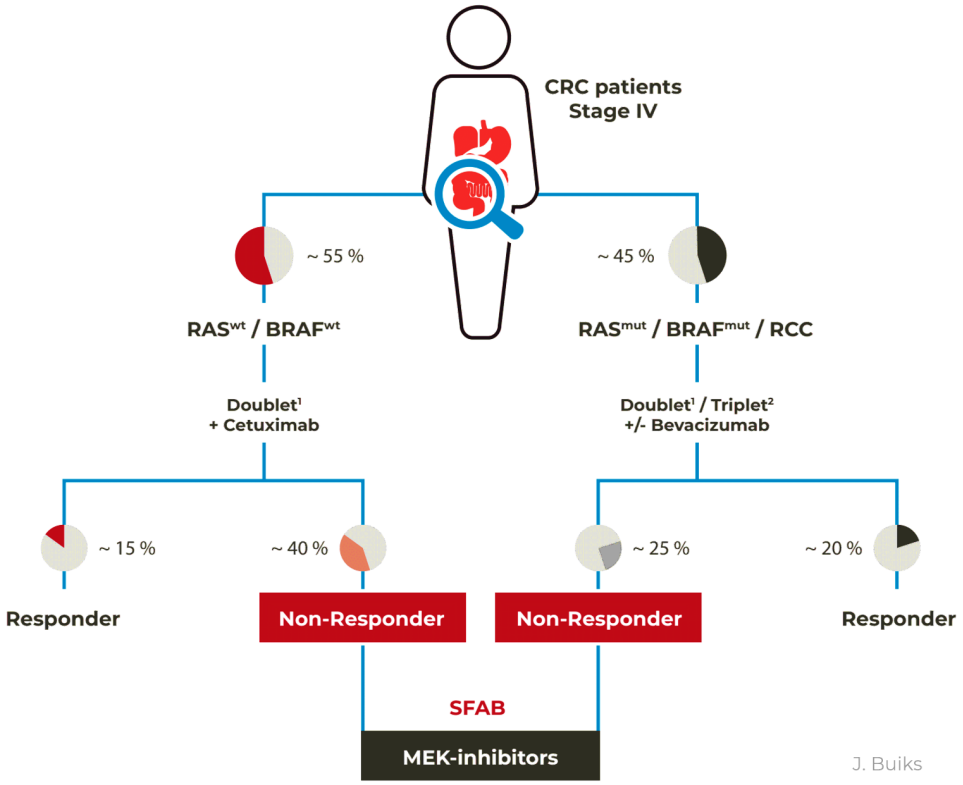

Figure 64: Proposed schematic representation of the therapy structure in colorectal cancer (CRC) stage IV.
RAS mutations have historically been considered "untreatable" despite being very common in colorectal cancer. Mutations in KRAS and BRAF are found in up to a half of CRC patients and occur frequently in right-sided colon cancer (RCC) *[280]*. Therapy regimen for these tumors are combinations of 5-FU-based chemotherapy with and without VEGF-antibody bevacizumab. In case of wild-type RAS/RAF, the anti-EGFR antibody cetuximab is administered to the standard chemotherapy. However, 40 % of eligible CRC patients do not benefit from cetuximab *[128]*. It was shown that only 10-20 % of CRC patients are responsive to anti-EGFR treatment *[48]*. To change the treatment guidelines for CRC patients, it usually takes 5-10 years. Therefore, I propose to treat CRC patients with first-line therapeutics according to current guidelines and to use the SFAB-signature (SMAD4, FBXW7, ARID1A or BMPR2) in non-responders (> 60 %) who do not yet benefit from these treatment guidelines and to administer MEK-inhibitors since they are beyond care. [1]Doublet: combination of 5-FU plus oxaliplatin or irinotecan; [2]Triplet: Combination of 5-FU plus oxaliplatin and irinotecan.

To enhance clinical relevance, models need to be further developed to rebuild more complex cellular interactions with the tumor stroma and the immune system. For further validation of the data, PDX models or inducible CRC mouse models [281–284] could be used. However, as mentioned in the introduction (Figure 11), PDX models are not feasible for studying intra-tumor heterogeneity. First, it would be unethical because excessive numbers of animals would have to be sacrificed for such a study; second, it is logistically difficult; and most importantly, the final implementation would come too late for most cancer patients.

Since the PDO model cohort was representative to the TCGA CRC-cohort (Figure 60) and due to their important features of recapitulating characteristics of the originating tumor [121], these data could be incorporated into clinical decision making. Vlachogiannis and colleagues also compared anticancer drug response in patients with colorectal and gastroesophageal cancer with the corresponding response in organoid cultures. They showed that response *in vitro* mirrors response in patients and suggest integrating functional genomics and drug testing into the decision-making process of early-stage clinical trials [285].

Personalized cancer therapy is gaining increased attention and there are already efforts to make this a clinical reality, for example, through companies offering such personalized PDO models and drug screenings as a service for patients and clinicians. For a wide clinical application, the establishment, maintenance, and screening of such models will need to become highly standardized.

However, after adequate validation of the biomarker signature, PDOs are no longer required in the future and the patient tissue could be directly screened for the SFAB-signature using an appropriate panel sequencing method. The results of SFAB-signature-screening can be directly used for guiding clinical decision making to minimize the use of treatment regimen with high side-effects and potentially little positive impact. Moreover, the stratification of patients and inclusion of MEK-inhibitors into the therapeutic regimen of CRC patients would increase the likelihood of successful treatment, thereby improving the patient's quality of life and maximizing the impact of healthcare resources. However, it may take up to 5-10 years before the SFAB-signature can be integrated into a standard diagnostic algorithm.

5.7. Future promising biomarkers in CRC

An increasing number of drugs is only approved conditionally and requires pretherapeutic biomarker-based patient stratification by companion diagnostics [286]. An evaluation of the indications and contraindications of all EMA approved drugs, found that of 883 European publicly assessable reports only 37 predictive biomarkers were mentioned for 41 drugs [287].

In addition to established CRC biomarkers, there are putative new biomarkers that show promising results and therefore could be applied in clinical decision making for CRC patients, e.g. circulating tumor DNA (ctDNA), tumor sidedness, specific alterations in neurotrophic receptor tyrosine kinase (NTRK), anaplastic lymphoma kinase (ALK) and ROS1 proto-oncogene (ROS), and human epidermal growth factor receptor 2 (HER2) amplification, which were described in detail by Koncina et al. [39] (Table 21).

Table 21: List of promising future biomarkers in colorectal cancer based on Koncina et al. [39].
The newly discovered SFAB-signature, which is predictive for the sensitivity to MEK inhibition could be included in the table but need further investigation. (ALK = anaplastic lymphoma kinase, ctDNA = circulating tumor DNA, CMS = consensus molecular subtypes, EGRF = epidermal growth factor receptor, HER2 = human epidermal growth factor receptor 2, NTRK1-3 = neurotrophic receptor tyrosine kinase 1, P13K = Phosphoinositide 3-kinase, RCC = right-sided colon cancer, ROS1 = ROS proto-oncogene 1, receptor tyrosine kinase, SFAB = pathogenic mutation in SMAD4, FBXW7, ARID1A, or BMPR2, TRK = tropomyosin receptor kinase).

Biomarker	Value	Therapy involved	Target group	References
		Currently translated into daily routine		
ctDNA	Predictive/ prognostic	✓ Targeted therapies ✓ Chemotherapy duration	All CRC	[288]
Tumor sidedness	Predictive/ prognostic	X Anti-EGFR therapy (RCC) Intensive ✓ Chemotherapy (RCC) ✓ Immunotherapy (RCC) (most likely)	All CRC	[289–292]
ALK, ROS1, NTRK1-3 fusions	Predictive	✓ ALK, ROS and TRK inhibitors	All CRC ALK, ROS and NTRK fusions	[293–296]
HER2 amplification	Predictive	✓ Anti-HER2 strategies X Anti-EGFR strategies	All CRC with HER2 amplification	[297,298]
		Need for further investigation		
CMS	Prognostic	Predictive value currently studied	All CRC	[40,242,299]
PI3K	Predictive	X Anti-EGFR therapy X First-line chemotherapy	mCRC All CRC	[300,301]
SFAB	**Predictive**	✓ **MEK-inhibitors**	**All CRC mainly mCRC**	**Novel finding**

Benefit: ✓ ; No benefit: X

One of the biologically most interesting concepts in metastatic CRC is the impact of primary tumor location. It is known that during the gastrointestinal embryogenesis, the parts of the large intestine derive from the midgut for the proximal/ascending colon (also referred to the right-sided colon (RCC)) and hindgut for the distal/descending colon (also referred to the left-sided colon (LCC)) [39,302]. They differ in biological characteristics, blood supply and microbiome population [303]. RCC occurs less frequently (20 – 25 %) but leads to shorter overall survival in stages III and IV, whereas LCC is more common (> 65 %) and shows a better prognosis in later stages [289,290,304,305].

CRC studies suggest an association between primary tumor location and anti-EGFR therapy, showing that KRAS mutated RCC does not apparently benefit from anti-EGFR therapy cetuximab (anti-EGFR antibody) treatment [291,292] and is therefore, only limited to LCC.

CRC biomarkers, such as CMS classification [40,242] or alterations in phosphoinositide 3-kinase (PI3K), need further investigation. Although some recent preclinical studies have highlighted the clinical relevance of CMS and CRIS subtypes by demonstrating differential drug efficacy between the subtypes [306,307], the clinical significance of defining these subtypes remains rather limited. Studies have shown that PI3KCA mutations are linked to clinical resistance of anti-EGFR therapies and first-line chemotherapy [300,301]. Furthermore, it is difficult to assess the significance of PIK3CA as an independent predictive biomarker because PIKC3A mutations often co-occur with RAS or BRAF mutations [308] and is therefore not used for routine testing. Large cohorts, including patients with mutations in PIKC3A but without RAS or BRAF mutations, are needed to elucidate the value of PIKC3A as a biomarker in CRC.

Upon further validation, the newly discovered SFAB-signature is a predictive CRC biomarker for MEK inhibition and can be included in the Table 21.

5.8. Conclusion

I identified a novel SFAB-signature (SMAD4, FBXW7, ARID1A, or BMPR2) that predicts the sensitivity of MEK inhibition with high probability *in vitro*. In a cohort of 62 PDO models, the SFAB-signature significantly predicts with 95 % the sensitivity of cobimetinib and 70 % the sensitivity of selumetinib, respectively, independent of the RAS and RAF status.

In order to identify the SFAB-signature, I used a combinational approach of CRISPR/Cas9 genome editing system, genomic (DNA-sequencing), transcriptomic (RNA-sequencing), and proteomic (DigiWest®) to investigate not only the impact of SMAD4 mutation on drug response but also the mode-of-action (Figure 65).

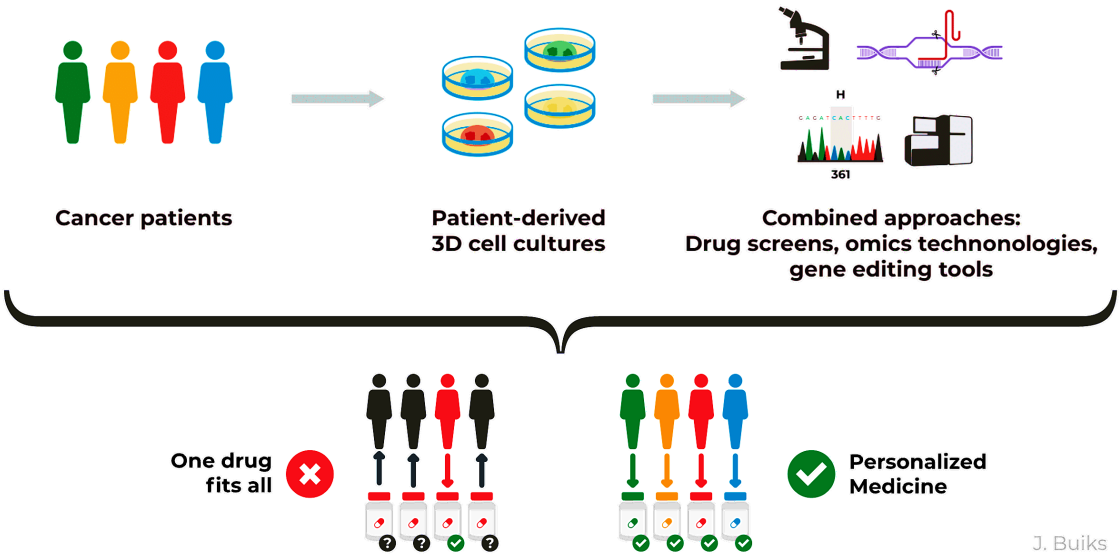

Figure 65: Cancer heterogeneity requires a personalized treatment approach.
An appropriate combination of patient-derived 3D cell culture models and different -omics technologies provides a comprehensive picture of biological processes within a patient's tumor and enables a comprehensive analysis of intra-tumor heterogeneity occurring on multiple levels, including genomic, transcriptomic, epigenomic, and metabolomic. Clinically and molecularly heterogenous tumor is unlikely to be successfully treated with a "one drug fits all" approach but requires a personalized approach specifically targeting its individual dysregulations [309].

This lays the groundwork for later clinical application. Therefore, prospective clinical studies are needed so that cancer patients can benefit as soon as possible.

5.9. Outlook

5.9.1. Scientific outlook

In the present work, I discovered a robust biomarker panel that predicts sensitivity to MEK inhibition. To further understand the underlying biology of RAS/RAF-independent MEK inhibition additional questions need to be addressed in subsequent projects:

1) Experimental validation of proposed BMP-pathway addiction in BMP-pathway naïve organoids by BMP selective inhibition.
2) Establishment of additional syngeneic cell strains for FBXW7, ARID1A or BMPR2, ideally by successful CRISPR/Cas9 based validation of loss or loss-of-function mutations in these genes.
3) Identification of MEK1- and MEK2-specific resistance routs for MEK-inhibitors with distinct binding affinity to these proteins.
4) Investigation of the predictive relevance of the SFAB-signature in other cancer types with high incidence of mutations in the SFAB genes including stomach cancer (43 %), pancreatic cancer (37 %), lung cancer (19.7 %), head and neck cancer (19.5 %) and melanoma (17 %) (cBioPortal, access on 03/12/ 2021).
5) PDOs are recognized as preclinical models for drug discovery. A prospective clinical trial is needed to make the findings of this work accessible to patients.

5.9.2. Clinical outlook

Biomarker discovery and development is more important than ever. The discovery of the SFAB-signature being responsible for sensitivity to MEK-inhibitors has been accomplished. In the next step, it should be further validated for clinical use:

1) Retrospective clinical studies on tumor entities with known mutational status are planned to confirm the novel SFAB-signature that predicts the response to MEK inhibition not only for CRC but also for other entities such as head and neck cancer or malignant melanoma.
2) Prospective clinical trials could be conducted to validate the robustness of the biomarker signature. When SFAB-signature screening is routinely used and MEK-inhibitors are incorporated into existing treatment regimens for CRC,

3) future clinical guidelines should be modified, as proposed in my discussion, however, changing treatment guidelines may take 5-10 years.

5.10. Novelty of these findings

These findings were patented in March 2021 (Nr. DE102020102143B3).

"*A method for determining whether to start or continue a treatment of cancer, a biomarker corresponding to at least one marker gene, and the use of a biomarker in the method of the invention*". "[…] The object of the present invention is to provide a method for determination whether to start or to continue a treatment of cancer, particularly a solid tumor, such as colorectal cancer, which can be carried out by an analysis of the tumor with, preferred simple gene sequencing of nucleic acids isolated from the tumor, such as colorectal tumor cells by using an at least one biomarker to overcome the disadvantages. The said at least one biomarker is also object of the present invention as well as a use of the at least one biomarker in the mentioned inventive method. Preferably, the biological sample comprises a mutation in the coding sequence of an at least one marker gene selected from the group comprising mothers against decapentaplegic homolog 4 (SMAD4) gene, AT-rich inter-active domain-containing protein 1A (ARID1A) gene, F-Box/WD repeat-containing protein 7 (FBXW7) gene, bone morphogenic protein receptor type 2 (BMPR2) gene, Mitogen-activated protein kinase kinase (MEK also known as MAP2K) gene, and combinations thereof. […]" (Nr. DE102020102143B3)

Patent holder: Ulrike Pfohl, Dr. Jürgen Loskutov and Dr. Christian Regenbrecht

6. REFERENCES

1. WHO report on cancer: setting priorities, investing wisely and providing care for all [Internet]. World Health Organization: Geneva; 2020. Available from: https://www.who.int/publications/i/item/who-report-on-cancer-setting-priorities-investing-wisely-and-providing-care-for-all
2. Hood L, Friend SH. Predictive, personalized, preventive, participatory (P4) cancer medicine. Nat Rev Clin Oncol. 2011;8(3):184–7.
3. Malone ER, Oliva M, Sabatini PJB, Stockley TL, Siu LL. Molecular profiling for precision cancer therapies. Genome Med. 2020;12(1):8.
4. Hanahan D, Weinberg RA. Hallmarks of cancer: The next generation. Cell [Internet]. 2011 Jan 1;144(5):646–74. Available from: http://dx.doi.org/10.1016/j.cell.2011.02.013
5. Stratton MR, Campbell PJ, Futreal PA. The cancer genome. Nature. 2009;458(7239):719–24.
6. Bradner JE, Hnisz D, Young RA. Transcriptional Addiction in Cancer. Cell. 2017;168(4):629–43.
7. Weinstein IB. Addiction to Oncogenes--the Achilles Heal of Cancer. Science. 2002;297(5578):63–4.
8. Weinstein IB, Joe AK. Mechanisms of Disease: oncogene addiction—a rationale for molecular targeting in cancer therapy. Nat Clin Pract Oncol. 2006;3(8):448–57.
9. Alberts B, Bray D, Lewis J, Raff M, Roberts K, Watson JD. Molecular biology of the cell (third edition). Vella F, editor. Biochem Educ. 1994;22(3):164.
10. Mocellin S, Provenzano M, Rossi CR, Pilati P, Nitti D, Lise M. DNA Array-Based Gene Profiling: From Surgical Specimen to the Molecular Portrait of Cancer. Ann Surg. 2005;241(1):16–26.
11. Henry NL, Hayes DF. Cancer biomarkers. Mol Oncol. 2012;6(2):140–6.
12. Chen EY, Raghunathan V, Prasad V. An Overview of Cancer Drugs Approved by the US Food and Drug Administration Based on the Surrogate End Point of Response Rate. Jama Intern Med. 2019;179(7):915–21.
13. Gromova M, Vaggelas A, Dallmann G, Seimetz D. Biomarkers: Opportunities and Challenges for Drug Development in the Current Regulatory Landscape. Biomark Insights. 2020;15:1177271920974652.
14. Simon R. Genomic biomarkers in predictive medicine. An interim analysis. Embo Mol Med. 2011;3(8):429–35.
15. M.P.H. BSH, Wilcosky T. Biological Markers in Epidemiologic Research. Archives Environ Heal Int J. 1988;43(2):83–9.
16. Sung H, Ferlay J, Siegel RL, Laversanne M, Soerjomataram I, Jemal A, et al. Global Cancer Statistics 2020: GLOBOCAN Estimates of Incidence and Mortality Worldwide for 36 Cancers in 185 Countries. Ca Cancer J Clin. 2021;71(3):209–49.
17. Rawla P, Sunkara T, Barsouk A. Epidemiology of colorectal cancer: incidence, mortality, survival, and risk factors. Gastroenterology Rev. 2019;14(2):89–103.
18. Xi Y, Xu P. Global colorectal cancer burden in 2020 and projections to 2040. Transl Oncol. 2021;14(10):101174.
19. Vogelstein B, Fearon ER, Hamilton SR. Genetic Alterations During Colorectal-Tumor Development. J Occup Environ Med. 1989;31(10):815.
20. Ewing I, Hurley JJ, Josephides E, Millar A. The molecular genetics of colorectal cancer. Frontline Gastroenterology. 2014;5(1):26.
21. Tariq K, Ghias K. Colorectal cancer carcinogenesis: a review of mechanisms. Cancer Biology Medicine. 2016;13(1):120–35.
22. Schneikert J, Behrens J. The canonical Wnt signalling pathway and its APC partner in colon cancer development. Gut. 2007;56(3):417.

23. Schatoff EM, Leach BI, Dow LE. WNT Signaling and Colorectal Cancer. Curr Colorectal Cancer Reports. 2017;13(2):101–10.

24. Fearon ER, Vogelstein B. A genetic model for colorectal tumorigenesis. Cell [Internet]. 1990 Jun 1;61(5):759–67. Available from: https://linkinghub.elsevier.com/retrieve/pii/009286749090186I

25. Markowitz S, Wang J, Myeroff L, Parsons R, Sun L, Lutterbaugh J, et al. Inactivation of the type II TGF-beta receptor in colon cancer cells with microsatellite instability. Sci New York N Y. 1995;268(5215):1336–8.

26. Thiagalingam S, Lengauer C, Leach FS, Schutte M, Hahn SA, Overhauser J, et al. Evaluation of candidate tumour suppressor genes on chromosome 18 in colorectal cancers. Nat Genet. 1996;13(3):343–6.

27. Samuels Y, Velculescu VE. Oncogenic mutations of PIK3CA in human cancers. Cell Cycle Georget Tex. 2004;3(10):1221–4.

28. Kanthan R, Senger J-L, Kanthan SC. Molecular Events in Primary and Metastatic Colorectal Carcinoma: A Review. Pathology Res Int. 2012;2012:597497.

29. Weisenberger DJ, Siegmund KD, Campan M, Young J, Long TI, Faasse MA, et al. CpG island methylator phenotype underlies sporadic microsatellite instability and is tightly associated with BRAF mutation in colorectal cancer. Nat Genet. 2006;38(7):787–93.

30. Imai K, Yamamoto H. Carcinogenesis and microsatellite instability: the interrelationship between genetics and epigenetics. Carcinogenesis. 2007;29(4):673–80.

31. Boland CR, Goel A. Microsatellite Instability in Colorectal Cancer. Gastroenterology. 2010;138(6):2073-2087.e3.

32. Geiersbach KB, Samowitz WS. Microsatellite Instability and Colorectal Cancer. Arch Pathol Lab Med. 2011;135(10):1269–77.

33. Kang S, Na Y, Joung SY, Lee SI, Oh SC, Min BW. The significance of microsatellite instability in colorectal cancer after controlling for clinicopathological factors. Medicine. 2018;97(9):e0019.

34. Davies RJ, Miller R, Coleman N. Colorectal cancer screening: prospects for molecular stool analysis. Nat Rev Cancer. 2005;5(3):199–209.

35. Vogelstein B, Papadopoulos N, Velculescu VE, Zhou S, Diaz LA, Kinzler KW. Cancer Genome Landscapes. Science. 2013;339(6127):1546–58.

36. Brierley JD, Gospodarowicz MK, Wittekind C. TNM Online. 2020;1–16.

37. Centelles JJ. General Aspects of Colorectal Cancer. Isrn Oncol. 2012;2012:1–19.

38. Güller U, Zettl A, Worni M, Langer I, Cabalzar-Wondberg D, Viehl CT, et al. Molecular investigation of lymph nodes in colon cancer patients using one-step nucleic acid amplification (OSNA): a new road to better staging? Cancer. 2012;118(24):6039–45.

39. Koncina, Haan, Rauh, Letellier. Prognostic and Predictive Molecular Biomarkers for Colorectal Cancer: Updates and Challenges. Cancers. 2020;12(2):319.

40. Guinney J, Dienstmann R, Wang X, Reyniès A de, Schlicker A, Soneson C, et al. The Consensus Molecular Subtypes of Colorectal Cancer HHS Public Access. Nat Med [Internet]. 2015 Jan 1;21(11):1350–6. Available from: http://www.nature.com/authors/editorial_policies/license.html#terms

41. Jin Z, Sinicrope FA. Prognostic and Predictive Values of Mismatch Repair Deficiency in Non-Metastatic Colorectal Cancer. Cancers. 2021;13(2):300.

42. Modest DP, Ricard I, Heinemann V, Hegewisch-Becker S, Schmiegel W, Porschen R, et al. Outcome according to KRAS-, NRAS- and BRAF-mutation as well as KRAS mutation variants: pooled analysis of five randomized trials in metastatic colorectal cancer by the AIO colorectal cancer study group. Ann Oncol. 2016;27(9):1746–53.

43. Nagakubo Y, Hirotsu Y, Amemiya K, Oyama T, Mochizuki H, Omata M. Accurate detection of KRAS, NRAS and BRAF mutations in metastatic colorectal cancers by bridged nucleic acid-clamp real-time PCR. Bmc Med Genomics. 2019;12(1):162.

44. Cunningham D, Humblet Y, Siena S, Khayat D, Bleiberg H, Santoro A, et al. Cetuximab Monotherapy and Cetuximab plus Irinotecan in Irinotecan-Refractory Metastatic Colorectal Cancer. New Engl J Medicine. 2004;351(4):337–45.

45. Cutsem EV, Köhne C-H, Hitre E, Zaluski J, Chien C-RC, Makhson A, et al. Cetuximab and Chemotherapy as Initial Treatment for Metastatic Colorectal Cancer. New Engl J Medicine. 2009;360(14):1408–17.

46. Boccia RV, Cosgriff TM, Headley DL, Badarinath S, Dakhil SR. A Phase II Trial of FOLFOX6 and Cetuximab in the First-line Treatment of Patients With Metastatic Colorectal Cancer. Clin Colorectal Canc. 2010;9(2):102–7.

47. Tveit KM, Guren T, Glimelius B, Pfeiffer P, Sorbye H, Pyrhonen S, et al. Phase III Trial of Cetuximab With Continuous or Intermittent Fluorouracil, Leucovorin, and Oxaliplatin (Nordic FLOX) Versus FLOX Alone in First-Line Treatment of Metastatic Colorectal Cancer: The NORDIC-VII Study. J Clin Oncol. 2012;30(15):1755–62.

48. Bardelli A, Siena S. Molecular Mechanisms of Resistance to Cetuximab and Panitumumab in Colorectal Cancer. J Clin Oncol. 2010;28(7):1254–61.

49. Benvenuti S, Sartore-Bianchi A, Nicolantonio FD, Zanon C, Moroni M, Veronese S, et al. Oncogenic Activation of the RAS/RAF Signaling Pathway Impairs the Response of Metastatic Colorectal Cancers to Anti-Epidermal Growth Factor Receptor Antibody Therapies. Cancer Res. 2007;67(6):2643–8.

50. Fiore FD, Blanchard F, Charbonnier F, Pessot FL, Lamy A, Galais MP, et al. Clinical relevance of KRAS mutation detection in metastatic colorectal cancer treated by Cetuximab plus chemotherapy. Brit J Cancer. 2007;96(8):1166–9.

51. Lièvre A, Bachet J-B, Boige V, Cayre A, Corre DL, Buc E, et al. KRAS mutations as an independent prognostic factor in patients with advanced colorectal cancer treated with cetuximab. J Clin Oncol Official J Am Soc Clin Oncol. 2008;26(3):374–9.

52. Hutchinson L. KRAS wild-type tumors benefit from cetuximab. Nat Rev Clin Oncol. 2009;6(7):374–374.

53. Qin S, Li J, Wang L, Xu J, Cheng Y, Bai Y, et al. Efficacy and Tolerability of First-Line Cetuximab Plus Leucovorin, Fluorouracil, and Oxaliplatin (FOLFOX-4) Versus FOLFOX-4 in Patients With RAS Wild-Type Metastatic Colorectal Cancer: The Open-Label, Randomized, Phase III TAILOR Trial. J Clin Oncol. 2018;36(30):3031–9.

54. Barras D. BRAF Mutation in Colorectal Cancer: An Update. Biomarkers Cancer. 2015;7(Suppl 1):9–12.

55. Saridaki Z, Tzardi M, Sfakianaki M, Papadaki C, Voutsina A, Kalykaki A, et al. BRAFV600E Mutation Analysis in Patients with Metastatic Colorectal Cancer (mCRC) in Daily Clinical Practice: Correlations with Clinical Characteristics, and Its Impact on Patients' Outcome. Plos One. 2013;8(12):e84604.

56. Kopetz S, Grothey A, Tabernero J. Encorafenib, Binimetinib, and Cetuximab in BRAF V600E-Mutated Colorectal Cancer. Reply. New Engl J Medicine. 2020;382(9):877–8.

57. Bläker H, Alwers E, Arnold A, Herpel E, Tagscherer KE, Roth W, et al. The Association Between Mutations in BRAF and Colorectal Cancer-Specific Survival Depends on Microsatellite Status and Tumor Stage. Clin Gastroenterology Hepatology Official Clin Pract J Am Gastroenterological Assoc. 2018;17(3):455-462.e6.

58. Rowland A, Dias MM, Wiese MD, Kichenadasse G, McKinnon RA, Karapetis CS, et al. Meta-analysis of BRAF mutation as a predictive biomarker of benefit from anti-EGFR monoclonal antibody therapy for RAS wild-type metastatic colorectal cancer. Brit J Cancer. 2015;112(12):1888–94.

59. Dhillon AS, Hagan S, Rath O, Kolch W. MAP kinase signalling pathways in cancer. Oncogene. 2007;26(22):3279–90.

60. Jeong W-J, Ro EJ, Choi K-Y. Interaction between Wnt/β-catenin and RAS-ERK pathways and an anti-cancer strategy via degradations of β-catenin and RAS by targeting the Wnt/β-catenin pathway. Npj Precis Oncol. 2018;2(1):5.

61. Kopetz S, Grothey A, Yaeger R, Cutsem EV, Desai J, Yoshino T, et al. Encorafenib, Binimetinib, and Cetuximab in BRAF V600E–Mutated Colorectal Cancer. New Engl J Med. 2019;381(17):1632–43.

62. National NCC. NCCN Guidelines for Patients - Colon Cancer [Internet]. 2021 [cited 2021 Dec 10]. Available from: https://www.nccn.org/patients/guidelines/content/PDF/colon-patient.pdf

63. Thundimadathil J. Cancer Treatment Using Peptides: Current Therapies and Future Prospects. J Amino Acids. 2012;2012:967347.

64. Xie Y-H, Chen Y-X, Fang J-Y. Comprehensive review of targeted therapy for colorectal cancer. Signal Transduct Target Ther. 2020;5(1):22.

65. Douillard J-Y, Oliner KS, Siena S, Tabernero J, Burkes R, Barugel M, et al. Panitumumab–FOLFOX4 Treatment and RAS Mutations in Colorectal Cancer. New Engl J Medicine. 2013;369(11):1023–34.

66. Braicu, Buse, Busuioc, Drula, Gulei, Raduly, et al. A Comprehensive Review on MAPK: A Promising Therapeutic Target in Cancer. Cancers. 2019;11(10):1618.

67. Cremolini C, Schirripa M, Antoniotti C, Moretto R, Salvatore L, Masi G, et al. First-line chemotherapy for mCRC—a review and evidence-based algorithm. Nat Rev Clin Oncol. 2015;12(10):607–19.

68. Ohhara Y, Fukuda N, Takeuchi S, Honma R, Shimizu Y, Kinoshita I, et al. Role of targeted therapy in metastatic colorectal cancer. World J Gastrointest Oncol. 2016;8(9):642–55.

69. Maughan TS, Adams RA, Smith CG, Meade AM, Seymour MT, Wilson RH, et al. Addition of cetuximab to oxaliplatin-based first-line combination chemotherapy for treatment of advanced colorectal cancer: results of the randomised phase 3 MRC COIN trial. Lancet. 2011;377(9783):2103–14.

70. Cheng Y, Tian H. Current Development Status of MEK Inhibitors. Mol Basel Switz. 2017;22(10):1551.

71. Zhao Y, Adjei AA. The clinical development of MEK inhibitors. Nat Rev Clin Oncol. 2014;11(7):385–400.

72. Long GV, Stroyakovskiy D, Gogas H, Levchenko E, Braud F de, Larkin J, et al. Dabrafenib and trametinib versus dabrafenib and placebo for Val600 BRAF-mutant melanoma: a multicentre, double-blind, phase 3 randomised controlled trial. Lancet. 2015;386(9992):444–51.

73. Choo EF, Ng CM, Berry L, Belvin M, Lewin-Koh N, Merchant M, et al. PK-PD modeling of combination efficacy effect from administration of the MEK inhibitor GDC-0973 and PI3K inhibitor GDC-0941 in A2058 xenografts. Cancer Chemoth Pharm. 2013;71(1):133–43.

74. Novartis. MEKINIST® (trametinib) - NDA: 204114 [Internet]. U.S. Food and Drug Administration; 2013 [cited 2021 Dec 9]. Available from: https://www.accessdata.fda.gov/drugsatfda_docs/label/2021/204114s020lbl.pdf

75. Genentech. COTELLIC (cobimetinib) - NDA: 206192 [Internet]. U.S. Food and Drug Administration; 2015 [cited 2021 Dec 9]. Available from: https://www.accessdata.fda.gov/drugsatfda_docs/label/2015/206192s000lbl.pdf

76. Array IB. MEKTOVI® (binimetinib) - NDA: 210498 [Internet]. U.S. Food and Drug Administration; 2019 [cited 2021 Dec 9]. Available from: https://www.accessdata.fda.gov/drugsatfda_docs/label/2018/210498lbl.pdf

77. AstraZeneca. KOSELUGO (selumetinib) - NDA 213756 [Internet]. U.S. Food and Drug Administration; 2020 [cited 2021 Dec 9]. Available from: https://www.accessdata.fda.gov/drugsatfda_docs/label/2020/213756s000lbl.pdf

78. Dummer R, Ascierto PA, Gogas HJ, Arance A, Mandala M, Liszkay G, et al. Overall survival in patients with BRAF-mutant melanoma receiving encorafenib plus binimetinib versus vemurafenib or encorafenib (COLUMBUS): a multicentre, open-label, randomised, phase 3 trial. Lancet Oncol. 2018;19(10):1315–27.

79. Flaherty KT, Infante JR, Daud A, Gonzalez R, Kefford RF, Sosman J, et al. Combined BRAF and MEK Inhibition in Melanoma with BRAF V600 Mutations. New Engl J Medicine. 2012;367(18):1694–703.

80. Long GV, Stroyakovskiy D, Gogas H, Levchenko E, Braud F de, Larkin J, et al. Combined BRAF and MEK Inhibition versus BRAF Inhibition Alone in Melanoma. New Engl J Medicine. 2014;371(20):1877–88.

81. Larkin J, Ascierto PA, Dréno B, Atkinson V, Liszkay G, Maio M, et al. Combined Vemurafenib and Cobimetinib in BRAF-Mutated Melanoma. New Engl J Medicine. 2014;371(20):1867–76.

82. Yamaguchi T, Kakefuda R, Tajima N, Sowa Y, Sakai T. Antitumor activities of JTP-74057 (GSK1120212), a novel MEK1/2 inhibitor, on colorectal cancer cell lines in vitro and in vivo. Int J Oncol. 2011;39(1):23–31.

83. Gong S, Xu D, Zhu J, Zou F, Peng R. Efficacy of the MEK Inhibitor Cobimetinib and its Potential Application to Colorectal Cancer Cells. Cell Physiol Biochem. 2018;47(2):680–93.

84. Nagaraj NS, Datta PK. Targeting the transforming growth factor-β signaling pathway in human cancer. Expert Opin Inv Drug. 2009;19(1):77–91.

85. Liarte S, Bernabé-García Á, Nicolás FJ. Role of TGF-β in Skin Chronic Wounds: A Keratinocyte Perspective. Cells. 2020;9(2):306.

86. Zhao M, Mishra L, Deng CX. The role of TGF-β/SMAD4 signaling in cancer. Int J Biol Sci [Internet]. 2018 Jan 1;14(2):111–23. Available from: ["http://www.ijbs.com", "https://creativecommons.org/licenses/by-nc/4.0/"]

87. Massagué J. TGFβ in Cancer. Cell. 2008;134(2):215–30.

88. Yingling JM, Blanchard KL, Sawyer JS. Development of TGF-β signalling inhibitors for cancer therapy. Nat Rev Drug Discov. 2004;3(12):1011–22.

89. Hao Y, Baker D, Dijke P ten. TGF-β-Mediated Epithelial-Mesenchymal Transition and Cancer Metastasis. Int J Mol Sci. 2019;20(11):2767.

90. Nakao A, Imamura T, Souchelnytskyi S, Kawabata M, Ishisaki A, Oeda E, et al. TGF-β receptor-mediated signalling through Smad2, Smad3 and Smad4. Embo J. 1997;16(17):5353–62.

91. Liu F, Hata A, Baker JC, Doody J, Cárcamo J, Harland RM, et al. A human Mad protein acting as a BMP-regulated transcriptional activator. Nature. 1996;381(6583):620–3.

92. Liu F. Receptor regulated SMADS in TGF beta signaling. Front Biosci. 2003;8(6):s1280-1303.

93. Zhang YE. Non-Smad pathways 128 Non-Smad pathways in TGF-β signaling. Cell Res [Internet]. 2009 Jan 1;19(1):128–39. Available from: www.cell-research.com

94. Zhang Y, Feng X-H, Derynck R. Smad3 and Smad4 cooperate with c-Jun/c-Fos to mediate TGF-β-induced transcription. Nature. 1998;394(6696):909–13.

95. Feng X-H, Liang Y-Y, Liang M, Zhai W, Lin X. Direct Interaction of c-Myc with Smad2 and Smad3 to Inhibit TGF-β-Mediated Induction of the CDK Inhibitor p15Ink4B. Mol Cell. 2002;9(1):133–43.

96. Fearon ER. Molecular Genetics of Colorectal Cancer. Annu Rev Pathology Mech Dis. 2011;6(1):479–507.

97. Samanta D. Alterations in the Smad pathway in human cancers. Front Biosci. 2012;17(1):1281.

98. Yaeger R, Chatila WK, Lipsyc MD, Hechtman JF, Cercek A, Sanchez-Vega F, et al. Clinical Sequencing Defines the Genomic Landscape of Metastatic Colorectal Cancer. Cancer Cell. 2018;33(1):125-136.e3.

99. Miyaki M, Iijima T, Konishi M, Sakai K, Ishii A, Yasuno M, et al. Higher frequency of Smad4 gene mutation in human colorectal cancer with distant metastasis. Oncogene [Internet]. 1999 Jan 1;18. Available from: https://www.nature.com/onc/journal/v18/n20/pdf/1202642a.pdf

100. Alazzouzi H, Alhopuro P, Salovaara R, Sammalkorpi H, Järvinen H, Mecklin J-P, et al. SMAD4 as a Prognostic Marker in Colorectal Cancer. Clin Cancer Res. 2005;11(7):2606–11.

101. Goswami RS, Patel KP, Singh RR, Meric-Bernstam F, Kopetz ES, Subbiah V, et al. Hotspot Mutation Panel Testing Reveals Clonal Evolution in a Study of 265 Paired Primary and Metastatic Tumors. Clin Cancer Res. 2015;21(11):2644–51.

102. Sarshekeh AM, Advani S, Overman MJ, Manyam G, Kee BK, Fogelman DR, et al. Association of SMAD4 mutation with patient demographics, tumor characteristics, and clinical outcomes in colorectal cancer. Plos One [Internet]. 2017 Jan 1;12(3):e0173345–e0173345. Available from: ["http://www.ncbi.nlm.nih.gov/pubmed/28267766", "http://www.pubmedcentral.nih.gov/articlerender.fcgi?artid=PMC5340382"]

103. Mizuno T, Cloyd JM, Vicente D, Omichi K, Chun YS, Kopetz SE, et al. SMAD4 gene mutation predicts poor prognosis in patients undergoing resection for colorectal liver metastases. Eur J Surg Oncol. 2018;44(5):684–92.

104. Hahn SA, Schutte M, Hoque ATMS, Moskaluk CA, Costa LT da, Rozenblum E, et al. DPC4, A Candidate Tumor Suppressor Gene at Human Chromosome 18q21.1. Science. 1996;271(5247):350–3.

105. Lazzereschi D, Nardi F, Turco A, Ottini L, D'Amico C, Mariani-Costantini R, et al. A complex pattern of mutations and abnormal splicing of Smad4 is present in thyroid tumours. Oncogene. 2005;24(34):5344–54.

106. Shi Y, Wang Y-F, Jayaraman L, Yang H, Massagué J, Pavletich NP. Crystal Structure of a Smad MH1 Domain Bound to DNA Insights on DNA Binding in TGF-β Signaling. Cell. 1998;94(5):585–94.

107. Feng X-H, Zhang Y, Wu R-Y, Derynck R. The tumor suppressor Smad4/DPC4 and transcriptional adaptor CBP/p300 are coactivators for Smad3 in TGF-β-induced transcriptional activation. Gene Dev. 1998;12(14):2153–63.

108. Wu JW, Fairman R, Penry J, Shi Y. Formation of a stable heterodimer between Smad2 and Smad4. J Biol Chem [Internet]. 2001 Jun 1;276(23):20688–94. Available from: http://www.ncbi.nlm.nih.gov/pubmed/11274206

109. Houlston R, Bevan S, Williams A, Young J, Dunlop M, Rozen P, et al. Mutations in DPC4 (SMAD4) cause juvenile polyposis syndrome, but only account for a minority of cases. Hum Mol Genet. 1998;7(12):1907–12.

110. Gallione C, Aylsworth AS, Beis J, Berk T, Bernhardt B, Clark RD, et al. Overlapping spectra of SMAD4 mutations in juvenile polyposis (JP) and JP–HHT syndrome. Am J Med Genet A. 2010;152A(2):333–9.

111. Wain KE, Ellingson MS, McDonald J, Gammon A, Roberts M, Pichurin P, et al. Appreciating the broad clinical features of SMAD4 mutation carriers: a multicenter chart review. Genet Med. 2014;16(8):588–93.

112. Liao X, Hao Y, Zhang X, Ward S, Houldsworth J, Polydorides AD, et al. Clinicopathological characterization of SMAD4-mutated intestinal adenocarcinomas: A case-control study. Plos One. 2019;14(2):e0212142.

113. Wan R, Feng J, Tang L. Consequences of Mutations and Abnormal Expression of SMAD4 in Tumors and T Cells. Oncotargets Ther. 2021;Volume 14:2531–40.

114. Zehir A, Benayed R, Shah RH, Syed A, Middha S, Kim HR, et al. Mutational Landscape of Metastatic Cancer Revealed from Prospective Clinical Sequencing of 10,000 Patients. Nat Med. 2017;23(6):703–13.

115. Schumacher D, Andrieux G, Boehnke K, Keil M, Silvestri A, Silvestrov M, et al. Heterogeneous pathway activation and drug response modelled in colorectal-tumor-derived 3D cultures. Plos Genet. 2019;15(3):e1008076.

116. Ozawa H, Ranaweera RS, Izumchenko E, Makarev E, Zhavoronkov A, Fertig EJ, et al. Cancer Therapy: Preclinical SMAD4 Loss Is Associated with Cetuximab Resistance and Induction of MAPK/JNK Activation in Head and Neck Cancer Cells. Clin Cancer Res [Internet]. 2017 Jan 1;23(17):5162–75. Available from: http://clincancerres.aacrjournals.org/

117. Lin L-H, Chang K-W, Cheng H-W, Liu C-J. SMAD4 Somatic Mutations in Head and Neck Carcinoma Are Associated With Tumor Progression. Frontiers Oncol. 2019;9:1379.

118. Gey GO, Coffman WD, Kubicek MT. Tissue culture studies of the proliferative capacity of cervical carcinoma and normal epithelium. Cancer Research. 1952;(12):264–265.

119. Huh D, Matthews BD, Mammoto A, Montoya-Zavala M, Hsin HY, Ingber DE. Reconstituting Organ-Level Lung Functions on a Chip. Science. 2010;328(5986):1662–8.

120. Sajjad H, Imtiaz S, Noor T, Siddiqui YH, Sajjad A, Zia M. Cancer models in preclinical research: A chronicle review of advancement in effective cancer research. Animal Model Exp Medicine. 2021;4(2):87–103.

121. Schütte M, Risch T, Abdavi-Azar N, Boehnke K, Schumacher D, Keil M, et al. Molecular dissection of colorectal cancer in pre-clinical models identifies biomarkers predicting sensitivity to EGFR inhibitors. Nat Commun [Internet]. 2017 Jan 1;8(1):14262–14262. Available from: ["http://www.ncbi.nlm.nih.gov/pubmed/28186126", "http://www.pubmedcentral.nih.gov/articlerender.fcgi?artid=PMC5309787"]

122. Boehnke K, Schumacher D, Iversen PW, Reinhard C, Regenbrecht CRA, Lallena MJ, et al. Assay Establishment and Validation of a High-Throughput Screening Platform for Three-Dimensional Patient-Derived Colon Cancer Organoid Cultures. Slas Discov. 2016 Jan 1;21(9):931–41.

123. Bock C, Boutros M, Camp JG, Clarke L, Clevers H, Knoblich JA, et al. The Organoid Cell Atlas. Nat Biotechnol. 2020;1–5.

124. Pfohl U, Pflaume A, Regenbrecht M, Finkler S, Adelmann QG, Reinhard C, et al. Precision Oncology Beyond Genomics: The Future Is Here—It Is Just Not Evently Distributed. Cells. 2021;10(4):928.

125. Fujii M, Clevers H, Sato T. Modeling Human Digestive Diseases with CRISPR-Cas9-modified Organoids. Gastroenterology. 2018;156(3):562–76.

126. Baddal B. Next-generation technologies for studying host–pathogen interactions: a focus on dual transcriptomics, CRISPR/Cas9 screening and organs-on-chips. Pathog Dis. 2019;77(6).

127. Xu H, Jiao Y, Qin S, Zhao W, Chu Q, Wu K. Organoid technology in disease modelling, drug development, personalized treatment and regeneration medicine. Exp Hematology Oncol. 2018;7(1):30.

128. Parseghian CM, Napolitano S, Loree JM, Kopetz S. Mechanisms of Innate and Acquired Resistance to Anti-EGFR Therapy: A Review of Current Knowledge with a Focus on Rechallenge Therapies. Clin Cancer Res. 2019;25(23):6899–908.

129. Concordet J-P, Haeussler M. CRISPOR: intuitive guide selection for CRISPR/Cas9 genome editing experiments and screens. Nucleic Acids Res. 2018;46(W1):gky354-.

130. Cerami E, Gao J, Dogrusoz U, Gross BE, Sumer SO, Aksoy BA, et al. The cBio Cancer Genomics Portal: An Open Platform for Exploring Multidimensional Cancer Genomics Data. Cancer Discov. 2012;2(5):401–4.

131. Gao J, Aksoy BA, Dogrusoz U, Dresdner G, Gross B, Sumer SO, et al. Integrative Analysis of Complex Cancer Genomics and Clinical Profiles Using the cBioPortal. Sci Signal. 2013;6(269):pl1.

132. Untergasser A, Nijveen H, Rao X, Bisseling T, Geurts R, Leunissen JAM. Primer3Plus, an enhanced web interface to Primer3. Nucleic Acids Res. 2007;35(Web Server issue):W71–4.

133. Liston DR, Davis M. Clinically Relevant Concentrations of Anticancer Drugs: A Guide for Nonclinical Studies. Clin Cancer Res. 2017;23(14):3489–98.

134. Kline CLB, Schiccitano A, Zhu J, Beachler C, Sheikh H, Harvey HA, et al. Personalized Dosing via Pharmacokinetic Monitoring of 5-Fluorouracil Might Reduce Toxicity in Early- or Late-Stage Colorectal Cancer Patients Treated With Infusional 5–Fluorouracil-Based Chemotherapy Regimens. Clin Colorectal Canc. 2014;13(2):119–26.

135. Sullivan RJ, Weber J, Patel S, Dummer R, Carlino MS, Tan DSW, et al. A Phase Ib/II Study of the BRAF Inhibitor Encorafenib Plus the MEK Inhibitor Binimetinib in Patients with BRAFV600E/K-mutant Solid Tumors. Clin Cancer Res. 2020;26(19):5102–12.

136. Waddell JA, Solimando DA. Drug monographs: dabrafenib and trametinib. Hosp Pharm. 2013;48(10):818–21.

137. Novartis. TAFINLAR (dabrafenib) - NDA - 202806 [Internet]. U.S. Food and Drug Administration; 2013 [cited 2021 Dec 9]. Available from: https://www.accessdata.fda.gov/drugsatfda_docs/label/2013/202806s000lbl.pdf

138. Bayer IncPH. STIVARGA (regorafenib) Label - NDA: 203085 [Internet]. U.S. Food and Drug Administration; 2009 [cited 2021 Dec 9]. Available from: https://www.accessdata.fda.gov/drugsatfda_docs/label/2020/203085Orig1s014lbl.pdf

139. Adjei AA, Cohen RB, Franklin W, Morris C, Wilson D, Molina JR, et al. Phase I Pharmacokinetic and Pharmacodynamic Study of the Oral, Small-Molecule Mitogen-Activated Protein Kinase Kinase 1/2 Inhibitor AZD6244 (ARRY-142886) in Patients With Advanced Cancers. J Clin Oncol. 2008;26(13):2139–46.

140. Malsy M, Bitzinger D, Graf B, Bundscherer A. Staurosporine induces apoptosis in pancreatic carcinoma cells PaTu 8988t and Panc-1 via the intrinsic signaling pathway. Eur J Med Res. 2019;24(1):5.

141. Suresh PS, Jairam RK, Chandrasekhar DV, Vinod AB, Hiremath RA, Raj A, et al. Prediction of Human Pharmacokinetics of Ulixertinib, a Novel ERK1/2 Inhibitor from Mice, Rats, and Dogs Pharmacokinetics. Eur J Drug Metab Ph. 2018;43(4):453–60.

142. Mullis K, Faloona F, Scharf S, Saiki R, Horn G, Erlich H. Specific Enzymatic Amplification of DNA In Vitro: The Polymerase Chain Reaction. Cold Spring Harb Sym. 1986;51(0):263–73.

143. Mamlouk S, Childs LH, Aust D, Heim D, Melching F, Oliveira C, et al. DNA copy number changes define spatial patterns of heterogeneity in colorectal cancer. Nat Commun. 2017;8(1):14093.

144. Howe KL, Achuthan P, Allen J, Allen J, Alvarez-Jarreta J, Amode MR, et al. Ensembl 2021. Nucleic Acids Res. 2020;49(D1):gkaa942-.

145. Dobin A, Davis CA, Schlesinger F, Drenkow J, Zaleski C, Jha S, et al. STAR: ultrafast universal RNA-seq aligner. Bioinformatics. 2012;29(1):15–21.

146. Liao Y, Smyth GK, Shi W. The R package Rsubread is easier, faster, cheaper and better for alignment and quantification of RNA sequencing reads. Nucleic Acids Res. 2019;47(8):e47–e47.

147. Liao Y, Smyth GK, Shi W. featureCounts: an efficient general purpose program for assigning sequence reads to genomic features. Bioinformatics. 2014;30(7):923–30.

148. Tarazona S, Furió-Tarí P, Turrà D, Pietro AD, Nueda MJ, Ferrer A, et al. Data quality aware analysis of differential expression in RNA-seq with NOISeq R/Bioc package. Nucleic Acids Res. 2015;43(21):e140–e140.

149. Mortazavi A, Williams BA, McCue K, Schaeffer L, Wold B. Mapping and quantifying mammalian transcriptomes by RNA-Seq. Nat Methods. 2008;5(7):621–8.

150. Robinson MD, Oshlack A. A scaling normalization method for differential expression analysis of RNA-seq data. Genome Biol. 2010;11(3):R25–R25.

151. Lawrence M, Huber W, Pagès H, Aboyoun P, Carlson M, Gentleman R, et al. Software for Computing and Annotating Genomic Ranges. Plos Comput Biol. 2013;9(8):e1003118.

152. Rue-Albrecht K, McGettigan PA, Hernández B, Nalpas NC, Magee DA, Parnell AC, et al. GOexpress: an R/Bioconductor package for the identification and visualisation of robust gene ontology signatures through supervised learning of gene expression data. Bmc Bioinformatics. 2016;17(1):126.

153. Xie Z, Bailey A, Kuleshov MV, Clarke DJB, Evangelista JE, Jenkins SL, et al. Gene Set Knowledge Discovery with Enrichr. Curr Protoc. 2021;1(3):e90.

154. Chen EY, Tan CM, Kou Y, Duan Q, Wang Z, Meirelles GV, et al. Enrichr: interactive and collaborative HTML5 gene list enrichment analysis tool. Bmc Bioinformatics. 2013;14(1):128–128.

155. Jinek M, Chylinski K, Fonfara I, Hauer M, Doudna JA, Charpentier E. A Programmable Dual-RNA–Guided DNA Endonuclease in Adaptive Bacterial Immunity. Science. 2012;337(6096):816–21.

156. Wiedenheft B, Sternberg SH, Doudna JA. RNA-guided genetic silencing systems in bacteria and archaea. Nature. 2012;482(7385):331–8.

157. Fineran PC, Charpentier E. Memory of viral infections by CRISPR-Cas adaptive immune systems: Acquisition of new information. Virology. 2012;434(2):202–9.

158. Gaj T, Gersbach CA, Barbas CF. ZFN, TALEN, and CRISPR/Cas-based methods for genome engineering. Trends Biotechnol. 2013;31(7):397–405.

159. Ran FA, Hsu PD, Wright K, Agarwala V, Scott DA, Zhang F. Genome engineering using the CRISPR-Cas9 system. Nature Protocols. 2013 Jan 1;8(11).

160. Lieber MR. The mechanism of double-strand DNA break repair by the nonhomologous DNA end-joining pathway. Annu Rev Biochem [Internet]. 2010 Jan 1;79(1):181–211. Available from: ["http://www.ncbi.nlm.nih.gov/pubmed/20192759", "http://www.pubmedcentral.nih.gov/articlerender.fcgi?artid=PMC3079308"]

161. Zhang F, Wen Y, Guo X. CRISPR/Cas9 for genome editing: progress, implications and challenges. Hum Mol Genet. 2014;23(R1):R40–6.

162. Sander JD, Joung JK. CRISPR-Cas systems for editing, regulating and targeting genomes. Nat Biotechnol. 2014;32(4):347–55.

163. Maeder ML, Gersbach CA. Genome-editing Technologies for Gene and Cell Therapy. Mol Ther. 2016;24(3):430–46.

164. Wu X, Kriz AJ, Sharp PA. Target specificity of the CRISPR-Cas9 system. Quantitative Biology. 2014;2(2):59–70.

165. Canny MD, Moatti N, Wan LCK, Fradet-Turcotte A, Krasner D, Mateos-Gomez PA, et al. Inhibition of 53BP1 favors homology-dependent DNA repair and increases CRISPR–Cas9 genome-editing efficiency. Nat Biotechnol. 2017;36(1):95–102.

166. Treindl F, Ruprecht B, Beiter Y, Schultz S, Döttinger A, Staebler A, et al. A bead-based western for high-throughput cellular signal transduction analyses. Nat Commun [Internet]. 2016 Dec 1;7(1):12852–12852. Available from: http://www.nature.com/articles/ncomms12852

167. Fleming NI, Jorissen RN, Mouradov D, Christie M, Sakthianandeswaren A, Palmieri M, et al. Molecular and Cellular Pathobiology SMAD2, SMAD3 and SMAD4 Mutations in Colorectal Cancer. Cancer Res [Internet]. 2013 Jan 1;73(2):725–35. Available from: http://cancerres.aacrjournals.org/

168. Lee JJ, Beumer JH, Chu E. Therapeutic drug monitoring of 5-fluorouracil. Cancer Chemoth Pharm. 2016;78(3):447–64.

169. Liu X, Jakubowski M, Hunt JL. KRAS Gene Mutation in Colorectal Cancer Is Correlated With Increased Proliferation and Spontaneous Apoptosis. Am J Clin Pathol. 2011;135(2):245–52.

170. Luke JJ, Ott PA, Shapiro GI. The Biology and Clinical Development of MEK Inhibitors for Cancer. Drugs. 2014;74(18):2111–28.

171. Sullivan RJ, Infante JR, Janku F, Wong DJL, Sosman JA, Keedy V, et al. First-in-Class ERK1/2 Inhibitor Ulixertinib (BVD-523) in Patients with MAPK Mutant Advanced Solid Tumors: Results of a Phase I Dose-Escalation and Expansion Study. Cancer Discov. 2017;8(2):184–95.

172. Paulsen BS, Mandal PK, Frock RL, Boyraz B, Yadav R, Upadhyayula S, et al. Ectopic expression of RAD52 and dn53BP1 improves homology-directed repair during CRISPR–Cas9 genome editing. Nat Biomed Eng. 2017;1(11):878–88.

173. Luna S de la, Soria I, Pulido D, Ortín J, Jiménez A. Efficient transformation of mammalian cells with constructs containing a puromycin-resistance marker. Gene. 1988;62(1):121–6.

174. Vara J, Malpartida F, Hopwood DA, Jiménez A. Cloning and expression of a puromycin N-acetyl transferase gene from Streptomyces alboniger in Streptomyces lividans and Escherichia coli. Gene. 1985;33(2):197–206.

175. National IC. Drugs Approved for Colon and Rectal Cancer [Internet]. 2020 [cited 2021 Dec 10]. Available from: https://www.cancer.gov/about-cancer/treatment/drugs/colorectal

176. Guertin DA, Sabatini DM. Defining the Role of mTOR in Cancer. Cancer Cell. 2007;12(1):9–22.

177. Stenson PD, Ball EV, Mort M, Phillips AD, Shiel JA, Thomas NST, et al. Human Gene Mutation Database (HGMD®): 2003 update. Hum Mutat. 2003;21(6):577–81.

178. Stenson PD, Mort M, Ball EV, Chapman M, Evans K, Azevedo L, et al. The Human Gene Mutation Database (HGMD®): optimizing its use in a clinical diagnostic or research setting. Hum Genet. 2020;139(10):1197–207.

179. Abdullah M-I, Muhammad NAN. Prediction of Colorectal Cancer Driver Genes from Patients' Genome Data. Sains Malays. 2018;47(12):3095–105.

180. Sakai E, Fukuyo M, Ohata K, Matsusaka K, Doi N, Mano Y, et al. Genetic and epigenetic aberrations occurring in colorectal tumors associated with serrated pathway. Int J Cancer. 2016;138(7):1634–44.

181. Mathur R, Alver BH, Roman AKS, Wilson BG, Wang X, Agoston AT, et al. ARID1A loss impairs enhancer-mediated gene regulation and drives colon cancer in mice. Nat Genet. 2017;49(2):296–302.

182. Kodach LL, Wiercinska E, Miranda NFCC de, Bleuming SA, Musler AR, Peppelenbosch MP, et al. The Bone Morphogenetic Protein Pathway Is Inactivated in the Majority of Sporadic Colorectal Cancers. Gastroenterology. 2008;134(5):1332-1341.e3.

183. Iwatsuki M, Mimori K, Ishii H, Yokobori T, Takatsuno Y, Sato T, et al. Loss of FBXW7, a cell cycle regulating gene, in colorectal cancer: Clinical significance. Int J Cancer. 2010;126(8):1828–37.

184. Serebriiskii IG, Connelly C, Frampton G, Newberg J, Cooke M, Miller V, et al. Comprehensive characterization of RAS mutations in colon and rectal cancers in old and young patients. Nat Commun. 2019;10(1):3722.

185. Zhong L, Li Y, Xiong L, Wang W, Wu M, Yuan T, et al. Small molecules in targeted cancer therapy: advances, challenges, and future perspectives. Signal Transduct Target Ther. 2021;6(1):201.

186. Hardin H, Zhang R, Helein H, Buehler D, Guo Z, Lloyd RV. The evolving concept of cancer stem-like cells in thyroid cancer and other solid tumors. Laboratory Investigation J Technical Methods Pathology. 2017;97(10):1142–51.

187. Caravagna G, Giarratano Y, Ramazzotti D, Tomlinson I, Graham TA, Sanguinetti G, et al. Detecting repeated cancer evolution from multi-region tumor sequencing data. Nat Methods. 2018;15(9):707–14.

188. Yamamoto T, Kawada K, Itatani Y, Inamoto S, Okamura R, Iwamoto M, et al. Loss of SMAD4 Promotes Lung Metastasis of Colorectal Cancer by Accumulation of CCR1+ Tumor-Associated Neutrophils through CCL15-CCR1 Axis. Clin Cancer Res. 2017;23(3):833–44.

189. Wang Y, Xue Q, Zheng Q, Jin Y, Shen X, Yang M, et al. SMAD4 mutation correlates with poor prognosis in non-small cell lung cancer. Lab Invest. 2021;101(4):463–76.

190. Malkoski SP, Wang X-J. Two sides of the story? Smad4 loss in pancreatic cancer versus head-and-neck cancer. Febs Lett. 2012;586(14):1984–92.

191. Izeradjene K, Combs C, Best M, Gopinathan A, Wagner A, Grady WM, et al. KrasG12D and Smad4/Dpc4 Haploinsufficiency Cooperate to Induce Mucinous Cystic Neoplasms and Invasive Adenocarcinoma of the Pancreas. Cancer Cell. 2007;11(3):229–43.

192. Hernandez AL, Young CD, Wang JH, Wang X. Lessons learned from SMAD4 loss in squamous cell carcinomas. Mol Carcinogen. 2019;58(9):1648–55.

193. Misale S, Nicolantonio FD, Sartore-Bianchi A, Siena S, Bardelli A. Resistance to Anti-EGFR Therapy in Colorectal Cancer: From Heterogeneity to Convergent Evolution. Cancer Discov. 2014;4(11):1269–80.

194. Emburgh BOV, Sartore-Bianchi A, Nicolantonio FD, Siena S, Bardelli A. Acquired resistance to EGFR-targeted therapies in colorectal cancer. Mol Oncol. 2014;8(6):1084–94.

195. Crona DJ, Keisler MD, Walko CM. Regorafenib. Ann Pharmacother. 2013;47(12):1685–96.

196. Menzies AM, Long GV, Murali R. Dabrafenib and its potential for the treatment of metastatic melanoma. Drug Des Dev Ther. 2012;6:391–405.

197. Croce L, Coperchini F, Magri F, Chiovato L, Rotondi M. The multifaceted anti-cancer effects of BRAF-inhibitors. Oncotarget. 2019;10(61):6623–40.

198. Sanz-Garcia E, Argiles G, Elez E, Tabernero J. BRAF mutant colorectal cancer: prognosis, treatment, and new perspectives. Ann Oncol. 2017;28(11):2648–57.

199. Krishnamurthy A, Dasari A, Lockhart AC, Stein MN, Sanoff HK, Lee JJ, et al. A phase IB study of the combination of selumetinib (AZD6244; ARRY-142886) and cyclosporin A (CsA) in patients with advanced solid tumors with an expansion cohort in metastatic colorectal cancer (mCRC). J Clin Oncol. 2017;35(4_suppl):609–609.

200. Abe H, Kikuchi S, Hayakawa K, Iida T, Nagahashi N, Maeda K, et al. Discovery of a Highly Potent and Selective MEK Inhibitor: GSK1120212 (JTP-74057 DMSO Solvate). Acs Med Chem Lett. 2011;2(4):320–4.

201. Luke JJ. Comprehensive Clinical Trial Data Summation for BRAF-MEK Inhibition and Checkpoint Immunotherapy in Metastatic Melanoma. Oncol. 2019;24(11):e1197–211.

202. Samatar AA, Poulikakos PI. Targeting RAS–ERK signalling in cancer: promises and challenges. Nat Rev Drug Discov. 2014;13(12):928–42.

203. Caunt CJ, Sale MJ, Smith PD, Cook SJ. MEK1 and MEK2 inhibitors and cancer therapy: the long and winding road. Nat Rev Cancer. 2015;15(10):577–92.

204. Emery CM, Vijayendran KG, Zipser MC, Sawyer AM, Niu L, Kim JJ, et al. MEK1 mutations confer resistance to MEK and B-RAF inhibition. Proc National Acad Sci. 2009;106(48):20411–6.

205. Wagle N, Allen EMV, Treacy DJ, Frederick DT, Cooper ZA, Taylor-Weiner A, et al. MAP Kinase Pathway Alterations in BRAF-Mutant Melanoma Patients with Acquired Resistance to Combined RAF/MEK Inhibition. Cancer Discov. 2014;4(1):61–8.

206. Lemmon MA, Schlessinger J. Cell Signaling by Receptor Tyrosine Kinases. Cell. 2010;141(7):1117–34.

207. Nazarian R, Shi H, Wang Q, Kong X, Koya RC, Lee H, et al. Melanomas acquire resistance to B-RAF(V600E) inhibition by RTK or N-RAS upregulation. Nature. 2010;468(7326):973–7.

208. Lake D, Corrêa SAL, Ller • Jü Rgen Mü. Negative feedback regulation of the ERK1/2 MAPK pathway. Cell Mol Life Sci [Internet]. 2016;73(23):4397–413. Available from: https://www.ncbi.nlm.nih.gov/pmc/articles/PMC5075022/pdf/18_2016_Article_2297.pdf

209. Arozarena I, Wellbrock C. Overcoming resistance to BRAF inhibitors. Ann Transl Medicine. 2017;5(19):387.

210. Villanueva J, Vultur A, Lee JT, Somasundaram R, Fukunaga-Kalabis M, Cipolla AK, et al. Acquired Resistance to BRAF Inhibitors Mediated by a RAF Kinase Switch in Melanoma Can Be Overcome by Cotargeting MEK and IGF-1R/PI3K. Cancer Cell. 2010;18(6):683–95.

211. Sun C, Hobor S, Bertotti A, Zecchin D, Huang S, Galimi F, et al. Intrinsic Resistance to MEK Inhibition in KRAS Mutant Lung and Colon Cancer through Transcriptional Induction of ERBB3. Cell Reports. 2014;7(1):86–93.

212. BioMed IDV. Study of Ulixertinib for Patients With Advanced Malignancies Harboring MEK or Atypical BRAF Alterations [Internet]. 2021 [cited 2021 Dec 10]. Available from: https://clinicaltrials.gov/ct2/show/NCT04488003

213. Niv Y. Microsatellite instability and MLH1 promoter hypermethylation in colorectal cancer. World J Gastroentero. 2007;13(12):1867.

214. Abildgaard AB, Stein A, Nielsen SV, Schultz-Knudsen K, Papaleo E, Shrikhande A, et al. Computational and cellular studies reveal structural destabilization and degradation of MLH1 variants in Lynch syndrome. Elife. 2019;8:e49138.

215. Silva IP, Salhi A, Giles KM, Vogelsang M, Han SW, Ismaili N, et al. Identification of a Novel Pathogenic Germline KDR Variant in Melanoma. Clin Cancer Res. 2016;22(10):2377–85.

216. Jauhri M, Gupta V, Shokeen Y, Minhas S, Bhalla S, Aggarwal S. KDR Mutation: A High-Frequency Rare Mutation and its Correlation with other Somatic Mutations in Indian Colorectal Cancer Patients. J Next Generation Sequencing Appl. 2017;4(2).

217. Driehuis E, Clevers H. CRISPR/Cas 9 genome editing and its applications in organoids. Am J Physiol-gastr L [Internet]. 2017 Jan 1;312(3):257–65. Available from: http://ajpgi.physiology.org/content/ajpgi/312/3/G257.full.pdf

218. Hamada T, Nowak JA, Ogino S. PIK3CA mutation and colorectal cancer precision medicine. Oncotarget. 2017;8(14):22305–6.

219. Liao X, Morikawa T, Lochhead P, Imamura Y, Kuchiba A, Yamauchi M, et al. Prognostic Role of PIK3CA Mutation in Colorectal Cancer: Cohort Study and Literature Review. Clin Cancer Res. 2012;18(8):2257–68.

220. Barault L, Veyrie N, Jooste V, Lecorre D, Chapusot C, Ferraz J, et al. Mutations in the RAS-MAPK, PI(3)K (phosphatidylinositol-3-OH kinase) signaling network correlate with poor survival in a population-based series of colon cancers. Int J Cancer. 2008;122(10):2255–9.

221. Wang Q, Shi Y, Zhou K, Wang L, Yan Z, Liu Y, et al. PIK3CA mutations confer resistance to first-line chemotherapy in colorectal cancer. Cell Death Dis. 2018;9(7):739.

222. Drost J, Jaarsveld RHV, Ponsioen B, Zimberlin C, Boxtel RV, Buijs A, et al. Sequential cancer mutations in cultured human intestinal stem cells. Nature [Internet]. 2015;521(7550):43. Available from: https://www.nature.com/nature/journal/v521/n7550/pdf/nature14415.pdf

223. Matano M, Date S, Shimokawa M, Takano A, Fujii M, Ohta Y, et al. Modeling colorectal cancer using CRISPR-Cas9-mediated engineering of human intestinal organoids. Nat Med. 2015;21(3):256–62.

224. Hernandez AL, Wang Y, Somerset HL, Keysar SB, Aisner DL, Marshall C, et al. Inter- and intra-tumor heterogeneity of SMAD4 loss in head and neck squamous cell carcinomas. Mol Carcinogen. 2019;58(5):666–73.

225. Sanson KR, Hanna RE, Hegde M, Donovan KF, Strand C, Sullender ME, et al. Optimized libraries for CRISPR-Cas9 genetic screens with multiple modalities. Nat Commun. 2018;9(1):5416.

226. Ukai S, Sakamoto N, Taniyama D, Harada K, Honma R, Maruyama R, et al. KHDRBS3 promotes multi-drug resistance and anchorage-independent growth in colorectal cancer. Cancer Sci. 2021;112(3):1196–208.

227. Drost J, Boxtel R van, Blokzijl F, Mizutani T, Sasaki N, Sasselli V, et al. Use of CRISPR-modified human stem cell organoids to study the origin of mutational signatures in cancer. Science. 2017;358(6360):234–8.

228. Michels BE, Mosa MH, Streibl BI, Zhan T, Menche C, Abou-El-Ardat K, et al. Pooled In Vitro and In Vivo CRISPR-Cas9 Screening Identifies Tumor Suppressors in Human Colon Organoids. Cell Stem Cell. 2020;

229. Duesberg P, Stindl R, Hehlmann R. Origin of multidrug resistance in cells with and without multidrug resistance genes: Chromosome reassortments catalyzed by aneuploidy. Proc National Acad Sci. 2001;98(20):11283–8.

230. Zhang N, Yin Y, Xu S-J, Chen W-S. 5-Fluorouracil: Mechanisms of Resistance and Reversal Strategies. Molecules. 2008;13(8):1551–69.

231. Sánchez-Gundín J, Fernández-Carballido AM, Martínez-Valdivieso L, Barreda-Hernández D, Torres-Suárez AI. New Trends in the Therapeutic Approach to Metastatic Colorectal Cancer. Int J Med Sci. 2018;15(7):659–65.

232. Jeught KV der, Xu H-C, Li Y-J, Lu X-B, Ji G. Drug resistance and new therapies in colorectal cancer. World J Gastroentero. 2018;24(34):3834–48.

233. Boulay J-L, Mild G, Lowy A, Reuter J, Lagrange M, Terracciano L, et al. SMAD4 is a predictive marker for 5-fluorouracil-based chemotherapy in patients with colorectal cancer. Brit J Cancer. 2002;87(6):630–4.

234. Bukowski K, Kciuk M, Kontek R. Mechanisms of Multidrug Resistance in Cancer Chemotherapy. Int J Mol Sci. 2020;21(9):3233.

235. Luqmani YA. Mechanisms of Drug Resistance in Cancer Chemotherapy. Med Prin Pract. 2005;14(Suppl 1):35–48.

236. Wu Q, Yang Z, Nie Y, Shi Y, Fan D. Multi-drug resistance in cancer chemotherapeutics: Mechanisms and lab approaches. Cancer Lett. 2014;347(2):159–66.

237. Wang J, Seebacher N, Shi H, Kan Q, Duan Z. Novel strategies to prevent the development of multidrug resistance (MDR) in cancer. Oncotarget. 2015;5(0):84559–71.

238. Papaccio F, Paino F, Regad T, Papaccio G, Desiderio V, Tirino V. Concise Review: Cancer Cells, Cancer Stem Cells, and Mesenchymal Stem Cells: Influence in Cancer Development. Stem Cell Transl Med. 2017;6(12):2115–25.

239. Banyard J, Bielenberg DR. The role of EMT and MET in cancer dissemination. Connect Tissue Res. 2015;56(5):403–13.

240. Du B, Shim JS. Targeting Epithelial-Mesenchymal Transition (EMT) to Overcome Drug Resistance in Cancer. Mol Basel Switz. 2016;21(7):965.

241. Si W, Shen J, Zheng H, Fan W. The role and mechanisms of action of microRNAs in cancer drug resistance. Clin Epigenetics. 2019;11(1):25.

242. Isella C, Brundu F, Bellomo SE, Galimi F, Zanella E, Porporato R, et al. Selective analysis of cancer-cell intrinsic transcriptional traits defines novel clinically relevant subtypes of colorectal cancer. Nat Commun. 2017;8(1):15107.

243. Manzoni C, Kia DA, Vandrovcova J, Hardy J, Wood NW, Lewis PA, et al. Genome, transcriptome and proteome: the rise of omics data and their integration in biomedical sciences. Brief Bioinform. 2016;19(2):bbw114.

244. Govindarajan M, Wohlmuth C, Waas M, Bernardini MQ, Kislinger T. High-throughput approaches for precision medicine in high-grade serous ovarian cancer. J Hematol Oncol. 2020;13(1):134.

245. Quezada H, Guzmán-Ortiz AL, Díaz-Sánchez H, Valle-Rios R, Aguirre-Hernández J. Omics-based biomarkers: current status and potential use in the clinic. Boletin Medico Del Hosp Infant De Mexico. 2017;74(3):219–26.

246. Tsubaki M, Takeda T, Noguchi M, Jinushi M, Seki S, Morii Y, et al. Overactivation of Akt Contributes to MEK Inhibitor Primary and Acquired Resistance in Colorectal Cancer Cells. Cancers. 2019;11(12):1866.

247. Opyrchal M, Gil M, Salisbury JL, Goetz MP, Suman V, Degnim A, et al. Molecular targeting of the Aurora-A/SMAD5 oncogenic axis restores chemosensitivity in human breast cancer cells. Oncotarget. 2017;8(53):91803–16.

248. Hirashita Y, Tsukamoto Y, Kudo Y, Kakisako D, Kurogi S, Hijiya N, et al. Early response in phosphorylation of ribosomal protein S6 is associated with sensitivity to trametinib in colorectal cancer cells. Lab Invest. 2021;1–12.

249. Kun E, Tsang YTM, Ng CW, Gershenson DM, Wong KK. MEK inhibitor resistance mechanisms and recent developments in combination trials. Cancer Treat Rev. 2020;92:102137.

250. Hua H, Kong Q, Zhang H, Wang J, Luo T, Jiang Y. Targeting mTOR for cancer therapy. J Hematol Oncol. 2019;12(1):71.

251. Peng J, Yoshioka Y, Mandai M, Matsumura N, Baba T, Yamaguchi K, et al. The BMP signaling pathway leads to enhanced proliferation in serous ovarian cancer-A potential therapeutic target. Mol Carcinogen. 2015;55(4):335–45.

252. Hardwick JC, Kodach LL, Offerhaus GJ, Brink GR van den. Bone morphogenetic protein signalling in colorectal cancer. Nat Rev Cancer. 2008;8(10):806–12.

253. Irshad S, Bansal M, Guarnieri P, Davis H, Zen AAH, Baran B, et al. Bone morphogenetic protein and Notch signalling crosstalk in poor-prognosis, mesenchymal-subtype colorectal cancer. J Pathology. 2017;242(2):178–92.

254. Friedmann-Morvinski D, Verma IM. Dedifferentiation and reprogramming: origins of cancer stem cells. Embo Rep. 2014;15(3):244–53.

255. Zhang L, Ye Y, Long X, Xiao P, Ren X, Yu J. BMP signaling and its paradoxical effects in tumorigenesis and dissemination. Oncotarget. 2016;7(47):78206–18.

256. Singh J, Petter RC, Baillie TA, Whitty A. The resurgence of covalent drugs. Nat Rev Drug Discov. 2011;10(4):307–17.

257. Bengoechea-Alonso MT, Ericsson J. Tumor suppressor Fbxw7 regulates TGFβ signaling by targeting TGIF1 for degradation. Oncogene. 2010;29(38):5322–8.

258. TU K, ZHENG X, YIN G, ZAN X, YAO Y, LIU Q. Evaluation of Fbxw7 expression and its correlation with expression of SREBP-1 in a mouse model of NAFLD. Mol Med Rep. 2012;6(3):525–30.

259. Tu K, Zheng X, Zhou Z, Li C, Zhang J, Gao J, et al. Recombinant Human Adenovirus-p53 Injection Induced Apoptosis in Hepatocellular Carcinoma Cell Lines Mediated by p53-Fbxw7 Pathway, Which Controls c-Myc and Cyclin E. Plos One. 2013;8(7):e68574.

260. Gao J, Azmi AS, Aboukameel A, Kauffman M, Shacham S, Abou-Samra A-B, et al. Nuclear retention of Fbw7 by specific inhibitors of nuclear export leads to Notch1 degradation in pancreatic cancer. Oncotarget. 2014;5(11):3444–54.

261. Cao J, Ge M-H, Ling Z-Q. Fbxw7 Tumor Suppressor: A Vital Regulator Contributes to Human Tumorigenesis. Medicine. 2016;95(7):e2496.

262. Sailo BL, Banik K, Girisa S, Bordoloi D, Fan L, Halim CE, et al. FBXW7 in Cancer: What Has Been Unraveled Thus Far? Cancers. 2019;11(2):246.

263. Li N, Lorenzi F, Kalakouti E, Normatova M, Babaei-Jadidi R, Tomlinson I, et al. FBXW7-mutated colorectal cancer cells exhibit aberrant expression of phosphorylated-p53 at Serine-15. Oncotarget. 2015;6(11):9240–56.

264. Guan B, Wang T-L, Shih I-M. ARID1A, a factor that promotes formation of SWI/SNF-mediated chromatin remodeling, is a tumor suppressor in gynecologic cancers. Cancer Res. 2011;71(21):6718–27.

265. Wu R-C, Wang T-L, Shih I-M. The emerging roles of ARID1A in tumor suppression. Cancer Biol Ther. 2014;15(6):655–64.

266. Rahman MS, Akhtar N, Jamil HM, Banik RS, Asaduzzaman SM. TGF-β/BMP signaling and other molecular events: regulation of osteoblastogenesis and bone formation. Bone Res. 2015;3(1):15005.

267. Wang RN, Green J, Wang Z, Deng Y, Qiao M, Peabody M, et al. Bone Morphogenetic Protein (BMP) signaling in development and human diseases. Genes Dis. 2014;1(1):87–105.

268. Cai J, Pardali E, Sánchez-Duffhues G, Dijke P ten. BMP signaling in vascular diseases. Febs Lett. 2012;586(14):1993–2002.

269. Cao H, Quan S, Zhang L, Chen Y, Jiao G. BMPR2 expression level is correlated with low immune infiltration and predicts metastasis and poor survival in osteosarcoma. Oncol Lett. 2021;21(5):391.

270. Beppu H, Mwizerwa ON, Beppu Y, Dattwyler MP, Lauwers GY, Bloch KD, et al. Stromal inactivation of BMPRII leads to colorectal epithelial overgrowth and polyp formation. Oncogene. 2008;27(8):1063–70.

271. Voorneveld PW, Kodach LL, Jacobs RJ, Liv N, Zonnevylle AC, Hoogenboom JP, et al. Loss of SMAD4 Alters BMP Signaling to Promote Colorectal Cancer Cell Metastasis via Activation of Rho and ROCK. Gastroenterology. 2014;147(1):196-208.e13.

272. Wu P-K, Park J-I. MEK1/2 Inhibitors: Molecular Activity and Resistance Mechanisms. Semin Oncol. 2015;42(6):849–62.

273. Hegedüs L, Okumus Ö, Livingstone E, Baranyi M, Kovács I, Döme B, et al. Allosteric and ATP-Competitive MEK-Inhibition in a Novel Spitzoid Melanoma Model with a RAF- and Phosphorylation-Independent Mutation. Cancers. 2021;13(4):829.

274. Rice KD, Aay N, Anand NK, Blazey CM, Bowles OJ, Bussenius J, et al. Novel Carboxamide-Based Allosteric MEK Inhibitors: Discovery and Optimization Efforts toward XL518 (GDC-0973). Acs Med Chem Lett. 2012;3(5):416–21.

275. Lee C-S, Duesbery NS. Highly Selective MEK Inhibitors. Curr Enzym Inhibition. 2010;6(3):146–57.

276. Gilmartin AG, Bleam MR, Groy A, Moss KG, Minthorn EA, Kulkarni SG, et al. GSK1120212 (JTP-74057) Is an Inhibitor of MEK Activity and Activation with Favorable Pharmacokinetic Properties for Sustained In Vivo Pathway Inhibition. Clin Cancer Res. 2011;17(5):989–1000.

277. Karapetis CS, Khambata-Ford S, Jonker DJ, O'Callaghan CJ, Tu D, Tebbutt NC, et al. K-ras Mutations and Benefit from Cetuximab in Advanced Colorectal Cancer. New Engl J Medicine. 2008;359(17):1757–65.

278. McCubrey JA, Steelman LS, Chappell WH, Abrams SL, Wong EWT, Chang F, et al. Roles of the Raf/MEK/ERK pathway in cell growth, malignant transformation and drug resistance. Biochimica Et Biophysica Acta Bba - Mol Cell Res. 2007;1773(8):1263–84.

279. Tanda ET, Vanni I, Boutros A, Andreotti V, Bruno W, Ghiorzo P, et al. Current State of Target Treatment in BRAF Mutated Melanoma. Frontiers Mol Biosci. 2020;7:154.

280. Etienne-Grimaldi M-C, Formento J-L, Francoual M, François E, Formento P, Renée N, et al. K-Ras Mutations and Treatment Outcome in Colorectal Cancer Patients Receiving Exclusive Fluoropyrimidine Therapy. Clin Cancer Res. 2008;14(15):4830–5.

281. Moser AR, Pitot HC, Dove WF. A Dominant Mutation That Predisposes to Multiple Intestinal Neoplasia in the Mouse. Science. 1990;247(4940):322–4.

282. Bissahoyo A, Pearsall RS, Hanlon K, Amann V, Hicks D, Godfrey VL, et al. Azoxymethane Is a Genetic Background-Dependent Colorectal Tumor Initiator and Promoter in Mice: Effects of Dose, Route, and Diet. Toxicol Sci. 2005;88(2):340–5.

283. Roper J, Tammela T, Akkad A, Almeqdadi M, Santos SB, Jacks T, et al. Colonoscopy-based colorectal cancer modeling in mice with CRISPR-Cas9 genome editing and organoid transplantation. Nat Protoc. 2018 Feb 1;13(2):217–34.

284. Fumagalli A, Suijkerbuijk SJE, Begthel H, Beerling E, Oost KC, Snippert HJ, et al. A surgical orthotopic organoid transplantation approach in mice to visualize and study colorectal cancer progression. Nat Protoc. 2018;13(2):235–47.

285. Vlachogiannis G, Hedayat S, Vatsiou A, Jamin Y, Fernández-Mateos J, Khan K, et al. Patient-derived organoids model treatment response of metastatic gastrointestinal cancers. Science. 2018;359(6378):920–6.

286. García LPO, Ehmann F, Hines PA, Ritzhaupt A, Brand A. Biomarker and Companion Diagnostics—A Review of Medicinal Products Approved by the European Medicines Agency. Frontiers Medicine. 2021;8:753187.

287. Malottki K, Biswas M, Deeks JJ, Riley RD, Craddock C, Johnson P, et al. Stratified medicine in European Medicines Agency licensing: a systematic review of predictive biomarkers. Bmj Open. 2014;4(1):e004188.

288. Reece M, Saluja H, Hollington P, Karapetis CS, Vatandoust S, Young GP, et al. The Use of Circulating Tumor DNA to Monitor and Predict Response to Treatment in Colorectal Cancer. Frontiers Genetics. 2019;10:1118.

289. Meguid RA, Slidell MB, Wolfgang CL, Chang DC, Ahuja N. Is There a Difference in Survival Between Right- Versus Left-Sided Colon Cancers? Ann Surg Oncol. 2008;15(9):2388–94.

290. Moritani K, Hasegawa H, Okabayashi K, Ishii Y, Endo T, Kitagawa Y. Difference in the recurrence rate between right- and left-sided colon cancer: a 17-year experience at a single institution. Surg Today. 2013;44(9):1685–91.

291. Aljehani MA, Morgan JW, Guthrie LA, Jabo B, Ramadan M, Bahjri K, et al. Association of Primary Tumor Site With Mortality in Patients Receiving Bevacizumab and Cetuximab for Metastatic Colorectal Cancer. Jama Surg. 2017;153(1):60.

292. Boeckx N, Koukakis R, Beeck KO de, Rolfo C, Camp GV, Siena S, et al. Effect of Primary Tumor Location on Second- or Later-line Treatment Outcomes in Patients With RAS Wild-type Metastatic Colorectal Cancer and All Treatment Lines in Patients With RAS Mutations in Four Randomized Panitumumab Studies. Clin Colorectal Canc. 2018;17(3):170-178.e3.

293. Sartore-Bianchi A, Ardini E, Bosotti R, Amatu A, Valtorta E, Somaschini A, et al. Sensitivity to Entrectinib Associated With a Novel LMNA-NTRK1 Gene Fusion in Metastatic Colorectal Cancer. Jnci J National Cancer Inst. 2016;108(1):djv306.

294. Amatu A, Somaschini A, Cerea G, Bosotti R, Valtorta E, Buonandi P, et al. Novel CAD-ALK gene rearrangement is drugable by entrectinib in colorectal cancer. Brit J Cancer. 2015;113(12):1730–4.

295. Yakirevich E, Resnick MB, Mangray S, Wheeler M, Jackson CL, Lombardo KA, et al. Oncogenic ALK Fusion in Rare and Aggressive Subtype of Colorectal Adenocarcinoma as a Potential Therapeutic Target. Clin Cancer Res. 2016;22(15):3831–40.

296. Cesi G, Philippidou D, Kozar I, Kim YJ, Bernardin F, Niel GV, et al. A new ALK isoform transported by extracellular vesicles confers drug resistance to melanoma cells. Mol Cancer. 2018;17(1):145.

297. Oh D-Y, Bang Y-J. HER2-targeted therapies — a role beyond breast cancer. Nat Rev Clin Oncol. 2020;17(1):33–48.

298. Lee MKC, Loree JM. Current and emerging biomarkers in metastatic colorectal cancer. Curr Oncol. 2019;26(1):S7–15.

299. Lenz H-J, Ou F-S, Venook AP, Hochster HS, Niedzwiecki D, Goldberg RM, et al. Impact of Consensus Molecular Subtype on Survival in Patients With Metastatic Colorectal Cancer: Results From CALGB/SWOG 80405 (Alliance). J Clin Oncol Official J Am Soc Clin Oncol. 2019;37(22):1876–85.

300. Sartore-Bianchi A, Martini M, Molinari F, Veronese S, Nichelatti M, Artale S, et al. PIK3CA Mutations in Colorectal Cancer Are Associated with Clinical Resistance to EGFR-Targeted Monoclonal Antibodies. Cancer Res. 2009;69(5):1851–7.

301. Wang Q, Shi Y, Zhou K, Wang L, Yan Z, Liu Y, et al. PIK3CA mutations confer resistance to first-line chemotherapy in colorectal cancer. Cell Death Dis. 2018;9(7):739.

302. Kostouros A, Koliarakis I, Natsis K, Spandidos DA, Tsatsakis A, Tsiaoussis J. Large intestine embryogenesis: Molecular pathways and related disorders (Review). Int J Mol Med. 2020;46(1):27–57.

303. Baran B, Ozupek NM, Tetik NY, Acar E, Bekcioglu O, Baskin Y. Difference Between Left-Sided and Right-Sided Colorectal Cancer: A Focused Review of Literature. Gastroenterology Res. 2018;11(4):264–73.

304. Ahmad R, Singh JK, Wunnava A, Al-Obeed O, Abdulla M, Srivastava SK. Emerging trends in colorectal cancer: Dysregulated signaling pathways (Review). Int J Mol Med. 2021;47(3):1.

305. Kearney DE, Cauley CE, Aiello A, Kalady MF, Church JM, Steele SR, et al. Increasing Incidence of Left-Sided Colorectal Cancer in the Young: Age Is Not the Only Factor. J Gastrointest Surg. 2020;24(10):2416–22.

306. Sveen A, Bruun J, Eide PW, Eilertsen IA, Ramirez L, Murumägi A, et al. Colorectal cancer Consensus Molecular Subtypes translated to preclinical models uncover potentially targetable cancer-cell dependencies. Clin Cancer Res. 2017;24(4):clincanres.1234.2017.

307. Berg KCG, Eide PW, Eilertsen IA, Johannessen B, Bruun J, Danielsen SA, et al. Multi-omics of 34 colorectal cancer cell lines - a resource for biomedical studies. Mol Cancer. 2017;16(1):116.

308. Roock WD, Claes B, Bernasconi D, Schutter JD, Biesmans B, Fountzilas G, et al. Effects of KRAS, BRAF, NRAS, and PIK3CA mutations on the efficacy of cetuximab plus chemotherapy in chemotherapy-refractory metastatic colorectal cancer: a retrospective consortium analysis. Lancet Oncol. 2010;11(8):753–62.

309. Sankarasubramanian S, Pfohl U, Regenbrecht CRA, Reinhard C, Wedeken L. Context Matters—Why We Need to Change From a One Size Fits all Approach to Made-to-Measure Therapies for Individual Patients With Pancreatic Cancer. Frontiers Cell Dev Biology. 2021;9:760705.

IX. SUPPLEMENTS

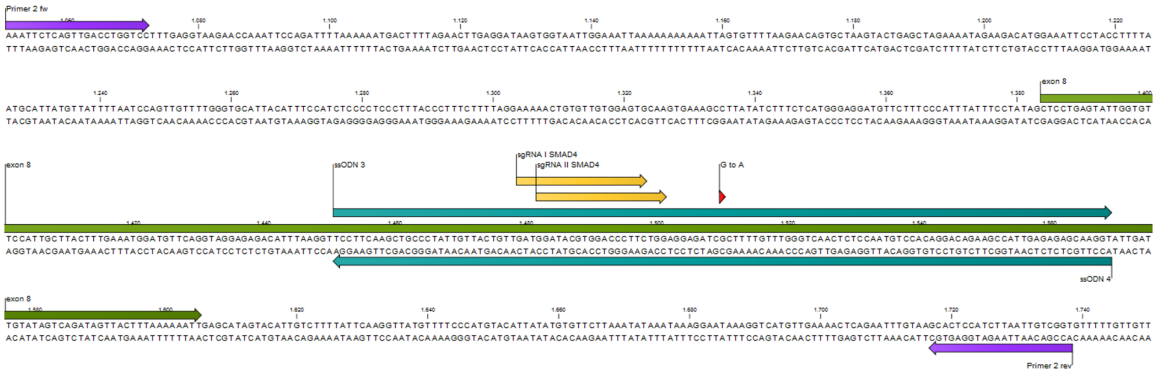

Suppl. Figure 1: Sequence of exon 8 of SMAD4 gene.
Exon 8 of the SMAD4 gene (green) and the position of sgRNA I (SMAD4-I) + sgRNA II (SMAD4-II) (yellow), ssODN 3 (forward) and ssODN 4 (reverse) (petrol) bearing the R361H point mutation (red) and the PCR-primer pair 2 (purple) marks the sequence.

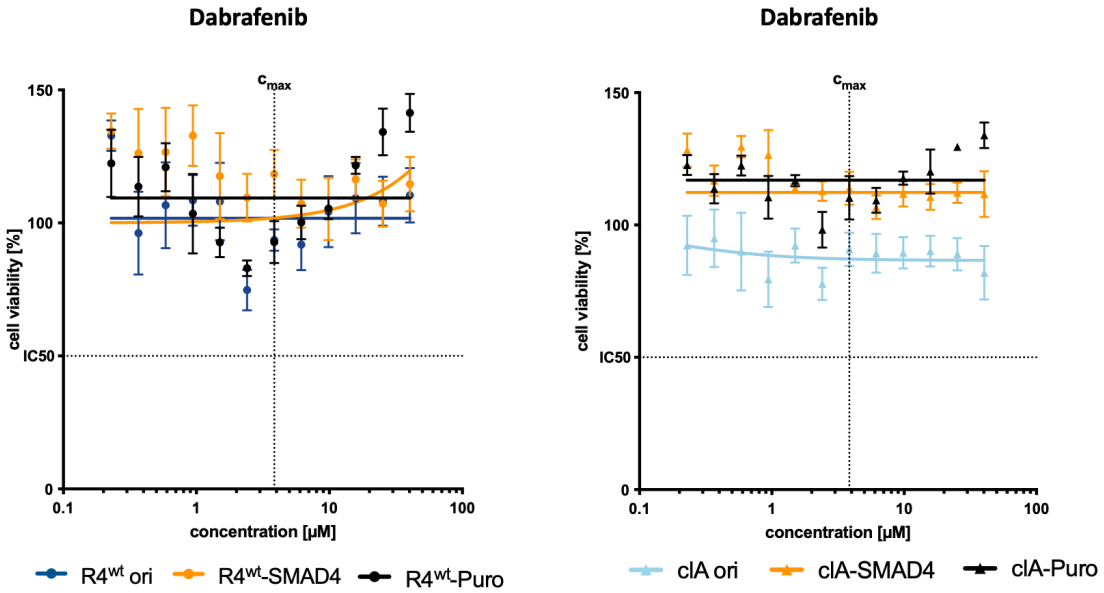

Suppl. Figure 2: Drug response curves of R4^{wt} and CRISPR-clone A treated with dabrafenib.
The transduced und puromycin selected PDOs (R4^{wt}-SMAD4 and clone A-SMAD4 (orange); R4^{wt}-Puro and clone A-Puro (black)) were compared to the original passage-matched PDO model (blue). The IC_{50} was not reached for the original PDOs R4^{wt} and clone A (R4^{wt} ori, clA ori) as well as for R4^{wt}-SMAD4, R4^{w}-Puro, clone A-SMAD4 (clA-SMAD4), and clone A-Puro (clA-Puro).

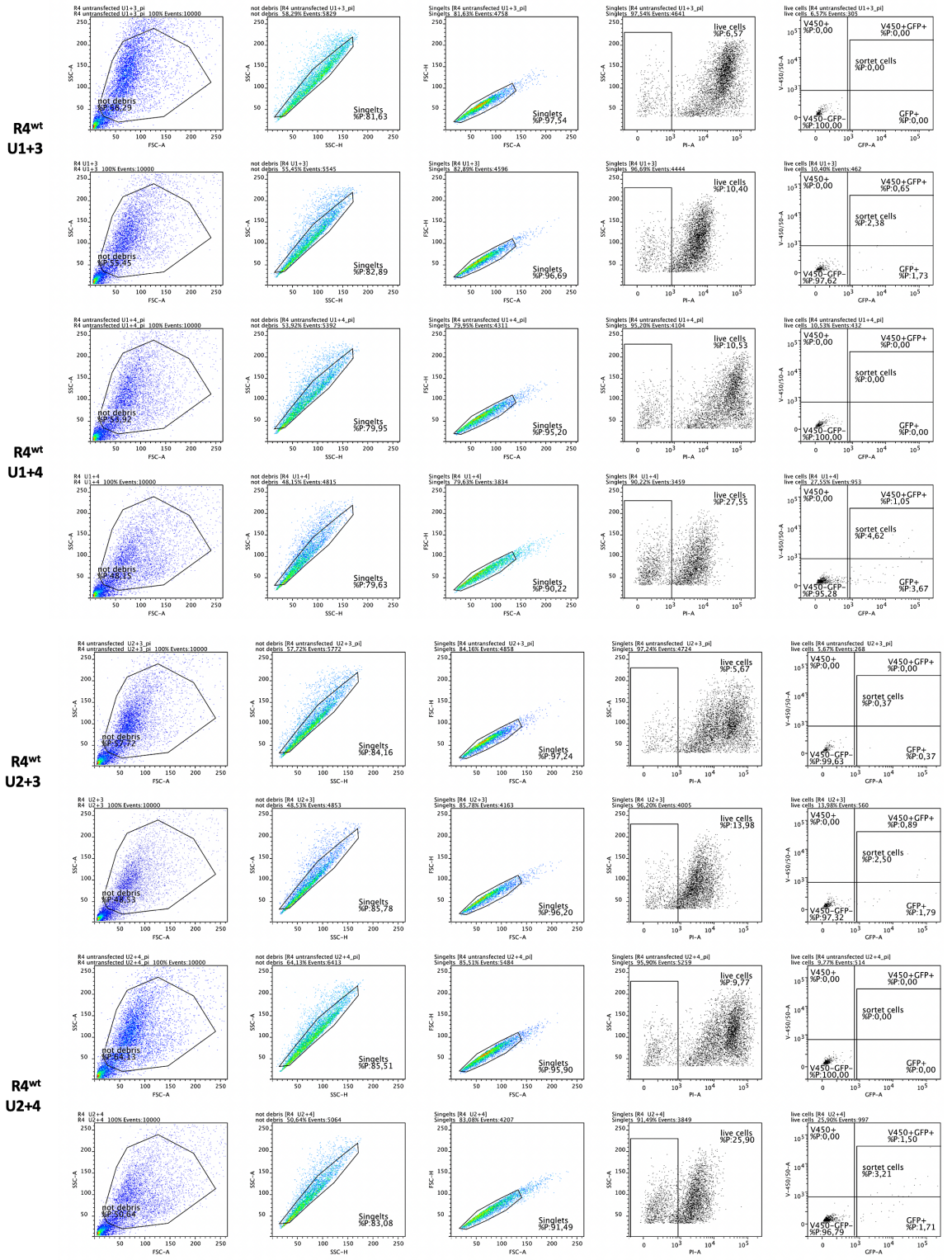

Suppl. Figure 3: Representative FACS images of R4^{wt}.
R4^{wt} cells were transfected with plasmids U1 (pU6sgh-SMAD4-I-CAG-Cas9-PGK-Venus) and U2 (pU6sgh-SMAD4-II-CAG-Cas9-PGK-Venus) and ssODNs 3 and 4 (U1+3, U1+4, U2+3, and U2+4). After 72 h, Venus- and BFP-positive R4^{wt} cells were sorted as bulk population by gating on GFP+/BFP+ (GFP-A/V-450/50-A).

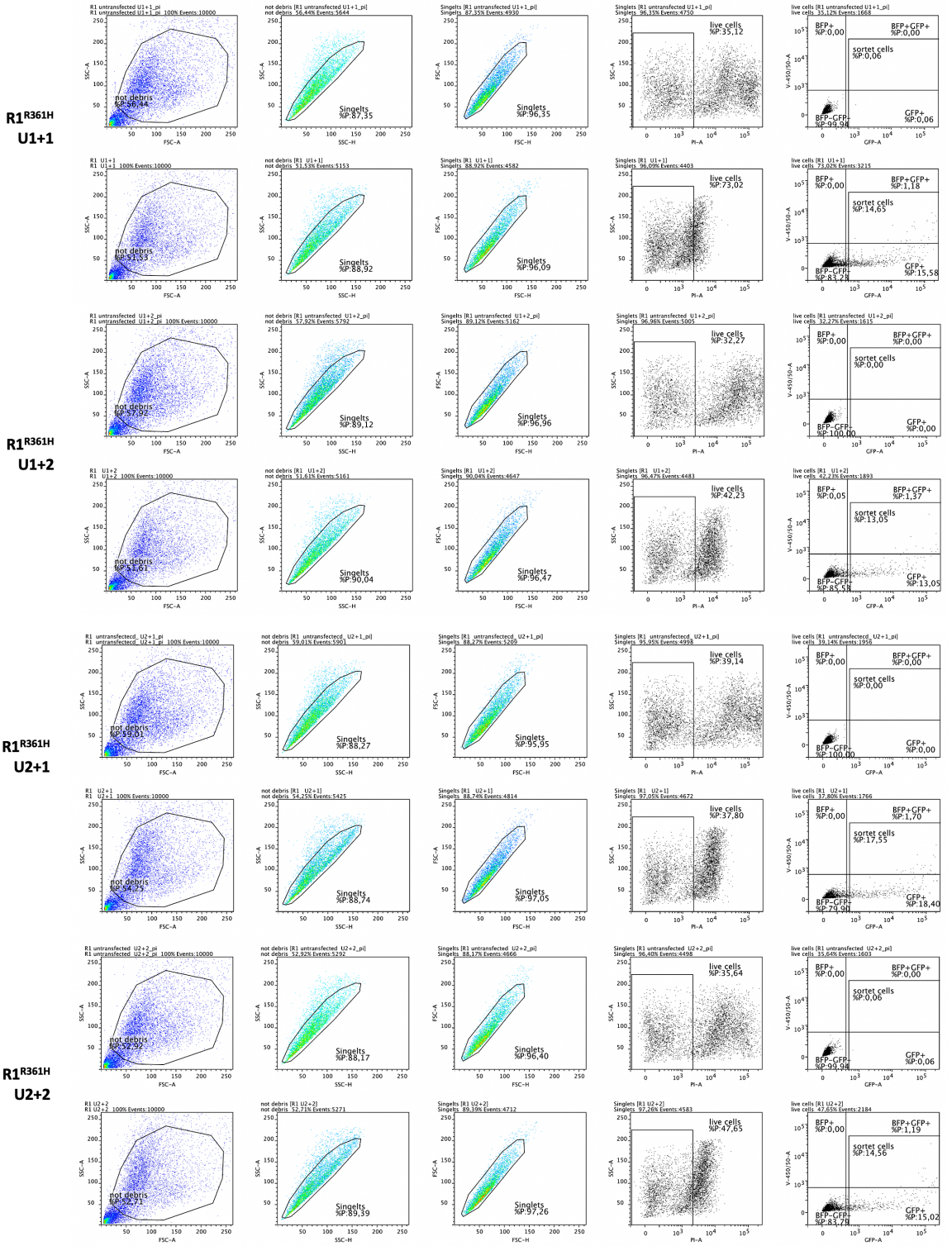

Suppl. Figure 4: Representative FACS images of R1^{R361H}.
R1^{R361H} cells were transfected with plasmids U1 (pU6sgh-SMAD4-I-CAG-Cas9-PGK-Venus) and U2 (pU6sgh-SMAD4-II-CAG-Cas9-PGK-Venus) and ssODNs 1 and 2 (U1+1, U1+2, U2+1, and U2+1). After 72 h, Venus- and BFP-positive R1^{R361H} cells were sorted as bulk population by gating on GFP+/BFP+ (GFP-A/V-450/50-A).

Suppl. Table 1: Colorectal cancer gene panel.
$R1^{R361H}$, $R4^{wt}$ and CRISPR-PDOs were sequenced according to the 94 gene panel *[143]*.

1	ACVR1B	25	EPHA3	49	LAMA1	73	PTPRU
2	ADAM29	26	EPHA4	50	LIFR	74	PXDN
3	APC	27	EPHA5	51	LRP1B	75	ROBO1
4	ARID1A	28	ERBB2	52	LRP2	76	SMAD2
5	ARID2	29	ERBB3	53	LRRK2	77	SMAD4
6	ATM	30	ERBB4	54	MAP2K4	78	SOX11
7	AXIN2	31	ERCC1	55	2 MCF	79	SOX9
8	BMPR1A	32	FAM123B	56	MLH1	80	STK11
9	BRAF	33	FBN2	57	MMP17	81	SYNE1
10	CARD11	34	FBXW7	58	MSH2	82	TCF7L2
11	CBLB	35	FMN2	59	MTOR	83	TENM1
12	CDH11	36	FN1	60	MUC16	84	TET1
13	CDH2	37	GLI3	61	MUTYH	85	TGFBR2
14	CDX2	38	GNAS	62	NOTCH3	86	TIAM1
15	CEP110	39	GPR112	63	NRAS	87	TNRC6B
16	CSMD3	40	GRIA3	64	PAPPA	88	TP53
17	CTNNB1	41	HDAC1	65	PI4KA	89	TPR
18	CUBN	42	HDAC2	66	PIK3CA	90	TRPS1
19	DAPK1	43	HDAC3	67	PLK1	91	UGT1A1
20	DLC1	44	HERC2	68	POLE2	92	VPS13B
21	DNMT1	45	JARID2	69	PREX2	93	WNK3
22	DPYD	46	KALRN	70	PRKD1	94	ZNF521
23	EDNRB	47	KDR	71	PTEN		
24	EIF4A2	48	KRAS	72	PTPRD		

Suppl. Table 2: Gene ontology results of $R1^{R361H}$.
Evaluated with Enrichr - Ma'ayan Laboratory - Computational Systems Biology (https://maayanlab.cloud/Enrichr/) (adjusted p-value < 0.05).

Term	Overlap	P-value	Adjusted P-value
microtubule cytoskeleton organization involved in mitosis (GO:1902850)	52/128	0.0000	0.0000
mitotic spindle organization (GO:0007052)	56/157	0.0000	0.0000
mitotic sister chromatid segregation (GO:0000070)	34/102	0.0000	0.0000
centromere complex assembly (GO:0034508)	18/37	0.0000	0.0000
sister chromatid segregation (GO:0000819)	17/34	0.0000	0.0000
mitotic nuclear division (GO:0140014)	24/74	0.0000	0.0000
chromatin remodeling at centromere (GO:0031055)	15/32	0.0000	0.0000
positive regulation of cell cycle process (GO:0090068)	28/101	0.0000	0.0000
CENP-A containing chromatin organization (GO:0061641)	14/30	0.0000	0.0000
CENP-A containing nucleosome assembly (GO:0034080)	14/30	0.0000	0.0000
DNA metabolic process (GO:0006259)	53/277	0.0000	0.0000
regulation of cell cycle process (GO:0010564)	28/106	0.0000	0.0000
mitotic cell cycle phase transition (GO:0044772)	43/209	0.0000	0.0000
kinetochore organization (GO:0051383)	9/13	0.0000	0.0001
G2/M transition of mitotic cell cycle (GO:0000086)	31/130	0.0000	0.0001
cell cycle G2/M phase transition (GO:0044839)	31/131	0.0000	0.0001
histone exchange (GO:0043486)	15/38	0.0000	0.0001
DNA replication-independent nucleosome assembly (GO:0006336)	15/39	0.0000	0.0001
transport across blood-brain barrier (GO:0150104)	23/86	0.0000	0.0002
DNA replication (GO:0006260)	26/108	0.0000	0.0004
mitotic cytokinesis (GO:0000281)	16/49	0.0000	0.0005
vascular transport (GO:0010232)	22/84	0.0000	0.0005
ribosome biogenesis (GO:0042254)	37/192	0.0000	0.0009
negative regulation of cellular process (GO:0048523)	82/566	0.0000	0.0010
regulation of cell cycle (GO:0051726)	50/296	0.0000	0.0011
negative regulation of mitotic metaphase/anaphase transition (GO:0045841)	10/22	0.0000	0.0012
mitotic chromosome condensation (GO:0007076)	11/27	0.0000	0.0014
neural crest cell migration (GO:0001755)	13/37	0.0000	0.0014
DNA replication initiation (GO:0006270)	13/38	0.0000	0.0019
cation transmembrane transport (GO:0098655)	14/44	0.0000	0.0023
positive regulation of pri-miRNA transcription by RNA polymerase II (GO:1902895)	12/34	0.0000	0.0027
cardiac epithelial to mesenchymal transition (GO:0060317)	9/20	0.0000	0.0030
mitotic metaphase plate congression (GO:0007080)	15/51	0.0000	0.0030
regulation of mitotic sister chromatid separation (GO:0010965)	8/16	0.0000	0.0033
positive regulation of DNA-directed DNA polymerase activity (GO:1900264)	6/9	0.0000	0.0038
regulation of DNA-directed DNA polymerase activity (GO:1900262)	6/9	0.0000	0.0038
sympathetic ganglion development (GO:0061549)	6/9	0.0000	0.0038
mitotic spindle assembly checkpoint signaling (GO:0007094)	9/21	0.0000	0.0040
mitotic spindle checkpoint signaling (GO:0071174)	9/21	0.0000	0.0040
spindle assembly checkpoint signaling (GO:0071173)	9/21	0.0000	0.0040
regulation of cell cycle G2/M phase transition (GO:1902749)	20/85	0.0000	0.0042
regulation of cyclin-dependent protein kinase activity (GO:1904029)	15/54	0.0000	0.0047
rRNA processing (GO:0006364)	32/173	0.0000	0.0047
semaphorin-plexin signaling pathway involved in neuron projection guidance (GO:1902285)	7/13	0.0000	0.0047
positive regulation of cytokinesis (GO:0032467)	12/37	0.0000	0.0050
regulation of cell population proliferation (GO:0042127)	99/764	0.0001	0.0062
maintenance of gastrointestinal epithelium (GO:0030277)	8/18	0.0001	0.0066

nucleotide biosynthetic process (GO:0009165)	8/18	0.0001	0.0066
positive regulation of cell division (GO:0051781)	13/44	0.0001	0.0066
regulation of attachment of spindle microtubules to kinetochore (GO:0051988)	6/10	0.0001	0.0066
L-amino acid transport (GO:0015807)	10/28	0.0001	0.0074
chromosome condensation (GO:0030261)	13/45	0.0001	0.0078
regulation of mitotic nuclear division (GO:0007088)	15/57	0.0001	0.0078
regulation of pri-miRNA transcription by RNA polymerase II (GO:1902893)	13/45	0.0001	0.0078
positive regulation of cell migration (GO:0030335)	43/269	0.0001	0.0081
regulation of mitotic cell cycle phase transition (GO:1901990)	33/188	0.0001	0.0082
negative regulation of blood coagulation (GO:0030195)	12/40	0.0001	0.0092
G1/S transition of mitotic cell cycle (GO:0000082)	19/85	0.0001	0.0095
regulation of axon extension involved in axon guidance (GO:0048841)	9/24	0.0001	0.0095
cytoskeleton-dependent cytokinesis (GO:0061640)	17/72	0.0001	0.0100
DNA-dependent DNA replication (GO:0006261)	25/129	0.0001	0.0100
regulation of apoptotic process (GO:0042981)	95/742	0.0001	0.0100
semaphorin-plexin signaling pathway (GO:0071526)	11/35	0.0001	0.0100
Notch signaling pathway (GO:0007219)	15/60	0.0002	0.0120
regulation of nuclear division (GO:0051783)	8/20	0.0002	0.0121
outflow tract septum morphogenesis (GO:0003148)	9/25	0.0002	0.0121
regulation of cell migration (GO:0030334)	58/408	0.0002	0.0133
mitotic spindle elongation (GO:0000022)	5/8	0.0002	0.0150
mitotic spindle midzone assembly (GO:0051256)	5/8	0.0002	0.0150
positive regulation of cell motility (GO:2000147)	36/221	0.0002	0.0150
regulation of metaphase/anaphase transition of cell cycle (GO:1902099)	5/8	0.0002	0.0150
U4 snRNA 3'-end processing (GO:0034475)	5/8	0.0002	0.0150
purine-containing compound biosynthetic process (GO:0072522)	9/26	0.0002	0.0152
regulation of mitotic metaphase/anaphase transition (GO:0030071)	9/26	0.0002	0.0152
regulation of ubiquitin protein ligase activity (GO:1904666)	8/21	0.0003	0.0156
attachment of mitotic spindle microtubules to kinetochore (GO:0051315)	6/12	0.0003	0.0158
ganglion development (GO:0061548)	6/12	0.0003	0.0158
purine nucleotide biosynthetic process (GO:0006164)	6/12	0.0003	0.0158
regulation of cell division (GO:0051302)	17/76	0.0003	0.0158
L-aspartate transmembrane transport (GO:0070778)	4/5	0.0003	0.0158
negative regulation of plasminogen activation (GO:0010757)	4/5	0.0003	0.0158
amino acid transport (GO:0006865)	13/50	0.0003	0.0165
branching morphogenesis of an epithelial tube (GO:0048754)	12/44	0.0003	0.0168
mitochondrion organization (GO:0007005)	30/175	0.0003	0.0168
mitotic spindle assembly (GO:0090307)	12/44	0.0003	0.0168
regulation of cytokinesis (GO:0032465)	18/84	0.0003	0.0171
ribosomal large subunit biogenesis (GO:0042273)	14/57	0.0003	0.0176
regulation of blood coagulation (GO:0030193)	9/27	0.0003	0.0177
protein localization to chromosome, centromeric region (GO:0071459)	7/17	0.0004	0.0185
peptidyl-threonine dephosphorylation (GO:0035970)	8/22	0.0004	0.0189
neural crest cell development (GO:0014032)	12/45	0.0004	0.0196
organic acid transport (GO:0015849)	20/100	0.0004	0.0198
regulation of exit from mitosis (GO:0007096)	11/39	0.0004	0.0198
rRNA metabolic process (GO:0016072)	28/162	0.0004	0.0206
protein depolymerization (GO:0051261)	9/28	0.0005	0.0223
kinetochore assembly (GO:0051382)	5/9	0.0005	0.0232
tetrahydrofolate interconversion (GO:0035999)	5/9	0.0005	0.0232
epithelial structure maintenance (GO:0010669)	7/18	0.0005	0.0245
microtubule depolymerization (GO:0007019)	7/18	0.0005	0.0245
positive regulation of cell cycle G2/M phase transition (GO:1902751)	8/23	0.0005	0.0245
regulation of chromosome segregation (GO:0051983)	7/18	0.0005	0.0245
regulation of DNA replication (GO:0006275)	13/53	0.0005	0.0245
establishment of mitotic spindle localization (GO:0040001)	9/29	0.0006	0.0273
positive regulation of apoptotic process (GO:0043065)	45/310	0.0006	0.0273
positive regulation of cell differentiation (GO:0045597)	39/258	0.0006	0.0273
regulation of cyclin-dependent protein serine/threonine kinase activity (GO:0000079)	17/82	0.0007	0.0300
amino acid import across plasma membrane (GO:0089718)	8/24	0.0007	0.0304
blood vessel endothelial cell proliferation involved in sprouting angiogenesis (GO:0002043)	4/6	0.0008	0.0304
endocardial cushion morphogenesis (GO:0003203)	7/19	0.0008	0.0304
negative regulation of coagulation (GO:0050819)	6/14	0.0008	0.0304
negative regulation of fibroblast growth factor receptor signaling pathway (GO:0040037)	6/14	0.0008	0.0304
negative regulation of lens fiber cell differentiation (GO:1902747)	4/6	0.0008	0.0304
nuclear polyadenylation-dependent ncRNA catabolic process (GO:0071046)	4/6	0.0008	0.0304
nuclear polyadenylation-dependent rRNA catabolic process (GO:0071035)	4/6	0.0008	0.0304
nuclear polyadenylation-dependent tRNA catabolic process (GO:0071038)	4/6	0.0008	0.0304
protein K29-linked ubiquitination (GO:0035519)	4/6	0.0008	0.0304
purine nucleobase biosynthetic process (GO:0009113)	4/6	0.0008	0.0304
regulation of extrinsic apoptotic signaling pathway via death domain receptors (GO:1902041)	11/42	0.0008	0.0304
tRNA surveillance (GO:0106354)	4/6	0.0008	0.0304
ureteric bud development (GO:0001657)	7/19	0.0008	0.0304
nuclear-transcribed mRNA catabolic process, exonucleolytic, 3'-5' (GO:0034427)	5/10	0.0009	0.0346
negative regulation of cell population proliferation (GO:0008285)	52/379	0.0009	0.0349
epithelium development (GO:0060429)	22/122	0.0009	0.0350
phosphatidylcholine metabolic process (GO:0046470)	16/77	0.0010	0.0355
negative regulation of axon extension involved in axon guidance (GO:0048843)	7/20	0.0011	0.0411
positive regulation of G2/M transition of mitotic cell cycle (GO:0010971)	7/20	0.0011	0.0411
fibrinolysis (GO:0042730)	6/15	0.0012	0.0414
positive regulation of angiogenesis (GO:0045766)	21/116	0.0012	0.0414
positive regulation of endothelial cell migration (GO:0010595)	17/86	0.0012	0.0432

mitotic nuclear membrane organization (GO:0101024)	12/51	0.0013	0.0457
mitotic nuclear membrane reassembly (GO:0007084)	12/51	0.0013	0.0457
positive regulation of programmed cell death (GO:0043068)	41/286	0.0013	0.0464
negative regulation of chemotaxis (GO:0050922)	9/32	0.0014	0.0465
regulation of transcription involved in G1/S transition of mitotic cell cycle (GO:0000083)	9/32	0.0014	0.0465
ameboidal-type cell migration (GO:0001667)	12/52	0.0016	0.0516
negative regulation of homotypic cell-cell adhesion (GO:0034111)	5/11	0.0016	0.0516
negative regulation of sprouting angiogenesis (GO:1903671)	5/11	0.0016	0.0516
sprouting angiogenesis (GO:0002040)	12/52	0.0016	0.0516
tetrahydrofolate metabolic process (GO:0046653)	5/11	0.0016	0.0516
L-alpha-amino acid transmembrane transport (GO:1902475)	8/27	0.0017	0.0532
microtubule polymerization or depolymerization (GO:0031109)	8/27	0.0017	0.0532
negative regulation of platelet activation (GO:0010544)	6/16	0.0017	0.0532
nucleobase-containing small molecule interconversion (GO:0015949)	8/27	0.0017	0.0532
pharyngeal arch artery morphogenesis (GO:0061626)	4/7	0.0017	0.0532
positive regulation of collagen biosynthetic process (GO:0032967)	6/16	0.0017	0.0532
pyrimidine-containing compound biosynthetic process (GO:0072528)	4/7	0.0017	0.0532
regulation of lens fiber cell differentiation (GO:1902746)	4/7	0.0017	0.0532
regulation of sprouting angiogenesis (GO:1903670)	9/33	0.0017	0.0532
sympathetic nervous system development (GO:0048485)	6/16	0.0017	0.0532
positive regulation of cell population proliferation (GO:0008284)	61/474	0.0018	0.0542
positive regulation of smooth muscle cell proliferation (GO:0048661)	11/46	0.0018	0.0542
regulation of endothelial cell migration (GO:0010594)	17/89	0.0018	0.0543

Suppl. Table 3: Gene ontology results of R4^{wt}.

Evaluated with Enrichr - Ma'ayan Laboratory - Computational Systems Biology (https://maayanlab.cloud/Enrichr/) (adjusted p-value < 0.05). GO terms unique for R4^{wt} are highlighted in green.

Term	Overlap	P-value	Adjusted P-value
organic acid transport (GO:0015849)	16/100	0.0000	0.0087
cellular response to oxygen-containing compound (GO:1901701)	31/323	0.0000	0.0127
regulation of cell migration (GO:0030334)	36/408	0.0000	0.0127
transmembrane receptor protein serine/threonine kinase signaling pathway (GO:0007178)	17/133	0.0000	0.0234
regulation of apoptotic process (GO:0042981)	53/742	0.0000	0.0284
regulation of cell adhesion mediated by integrin (GO:0033628)	8/34	0.0001	0.0284
organic hydroxy compound catabolic process (GO:1901616)	5/12	0.0001	0.0328
cardiac epithelial to mesenchymal transition (GO:0060317)	6/20	0.0001	0.0400
positive regulation of intracellular signal transduction (GO:1902533)	41/546	0.0001	0.0400
negative regulation of cellular process (GO:0048523)	42/566	0.0001	0.0400
response to organic cyclic compound (GO:0014070)	10/60	0.0001	0.0400
axon extension involved in axon guidance (GO:0048846)	4/8	0.0002	0.0400
neuron projection extension involved in neuron projection guidance (GO:1902284)	4/8	0.0002	0.0400
positive regulation of epithelial cell proliferation involved in wound healing (GO:0060054)	4/8	0.0002	0.0400
regulation of SMAD protein signal transduction (GO:0060390)	6/23	0.0002	0.0521
transforming growth factor beta receptor signaling pathway (GO:0007179)	12/89	0.0002	0.0521
BMP signaling pathway (GO:0030509)	10/65	0.0003	0.0538
positive regulation of cell-cell adhesion mediated by cadherin (GO:2000049)	4/9	0.0003	0.0542

Suppl. Table 4: Gene ontology results of CRISPR-clone A.

Evaluated with Enrichr - Ma'ayan Laboratory - Computational Systems Biology (https://maayanlab.cloud/Enrichr/) (adjusted p-value < 0.05).

Term	Overlap	P-value	Adjusted P-value
microtubule cytoskeleton organization involved in mitosis (GO:1902850)	54/128	0.0000	0.0000
mitotic spindle organization (GO:0007052)	60/157	0.0000	0.0000
DNA replication (GO:0006260)	43/108	0.0000	0.0000
DNA metabolic process (GO:0006259)	71/277	0.0000	0.0000
mitotic sister chromatid segregation (GO:0000070)	39/102	0.0000	0.0000
centromere complex assembly (GO:0034508)	21/37	0.0000	0.0000
DNA strand elongation involved in DNA replication (GO:0006271)	14/18	0.0000	0.0000
sister chromatid segregation (GO:0000819)	19/34	0.0000	0.0000
DNA replication initiation (GO:0006270)	20/38	0.0000	0.0000
mitotic nuclear division (GO:0140014)	28/74	0.0000	0.0000
chromatin remodeling at centromere (GO:0031055)	18/32	0.0000	0.0000
CENP-A containing chromatin organization (GO:0061641)	17/30	0.0000	0.0000
CENP-A containing nucleosome assembly (GO:0034080)	17/30	0.0000	0.0000
DNA strand elongation (GO:0022616)	13/18	0.0000	0.0000
DNA-dependent DNA replication (GO:0006261)	37/129	0.0000	0.0000
transport across blood-brain barrier (GO:0150104)	29/86	0.0000	0.0000
vascular transport (GO:0010232)	28/84	0.0000	0.0000
histone exchange (GO:0043486)	18/38	0.0000	0.0000
DNA replication-independent nucleosome assembly (GO:0006336)	18/39	0.0000	0.0000
double-strand break repair via break-induced replication (GO:0000727)	10/12	0.0000	0.0000
mitotic DNA replication (GO:1902969)	9/10	0.0000	0.0000
double-strand break repair via homologous recombination (GO:0000724)	29/97	0.0000	0.0000
mitotic cell cycle phase transition (GO:0044772)	46/209	0.0000	0.0000
mitotic cytokinesis (GO:0000281)	19/49	0.0000	0.0000
organic acid transport (GO:0015849)	28/100	0.0000	0.0000
G1/S transition of mitotic cell cycle (GO:0000082)	25/85	0.0000	0.0000

mitotic DNA damage checkpoint signaling (GO:0044773)	20/59	0.0000	0.0000
cholesterol homeostasis (GO:0042632)	22/71	0.0000	0.0000
kinetochore organization (GO:0051383)	9/13	0.0000	0.0000
regulation of cell cycle process (GO:0010564)	28/106	0.0000	0.0000
carbohydrate catabolic process (GO:0016052)	16/41	0.0000	0.0000
regulation of transcription involved in G1/S transition of mitotic cell cycle (GO:0000083)	14/32	0.0000	0.0000
sterol homeostasis (GO:0055092)	22/72	0.0000	0.0000
regulation of apoptotic process (GO:0042981)	110/742	0.0000	0.0001
sterol biosynthetic process (GO:0016126)	15/38	0.0000	0.0001
DNA repair (GO:0006281)	55/298	0.0000	0.0001
secondary alcohol biosynthetic process (GO:1902653)	14/34	0.0000	0.0001
regulation of cyclin-dependent protein kinase activity (GO:1904029)	18/54	0.0000	0.0001
cation transmembrane transport (GO:0098655)	16/44	0.0000	0.0001
negative regulation of mitotic metaphase/anaphase transition (GO:0045841)	11/22	0.0000	0.0001
cholesterol biosynthetic process (GO:0006695)	14/35	0.0000	0.0001
positive regulation of cell cycle process (GO:0090068)	26/101	0.0000	0.0001
mitotic G2/M transition checkpoint (GO:0044818)	16/45	0.0000	0.0002
positive regulation of DNA-directed DNA polymerase activity (GO:1900264)	7/9	0.0000	0.0002
regulation of DNA-directed DNA polymerase activity (GO:1900262)	7/9	0.0000	0.0002
mitotic metaphase plate congression (GO:0007080)	17/51	0.0000	0.0002
mitotic chromosome condensation (GO:0007076)	12/27	0.0000	0.0002
canonical glycolysis (GO:0061621)	11/24	0.0000	0.0003
glucose catabolic process to pyruvate (GO:0061718)	11/24	0.0000	0.0003
mitotic G2 DNA damage checkpoint signaling (GO:0007095)	13/33	0.0000	0.0003
glycolytic process (GO:0006096)	12/29	0.0000	0.0004
glycolytic process through glucose-6-phosphate (GO:0061620)	11/25	0.0000	0.0005
cytoskeleton-dependent cytokinesis (GO:0061640)	20/72	0.0000	0.0005
protein localization to chromosome, centromeric region (GO:0071459)	9/17	0.0000	0.0005
mitotic spindle assembly checkpoint signaling (GO:0007094)	10/21	0.0000	0.0005
mitotic spindle checkpoint signaling (GO:0071174)	10/21	0.0000	0.0005
spindle assembly checkpoint signaling (GO:0071173)	10/21	0.0000	0.0005
regulation of mitotic nuclear division (GO:0007088)	17/57	0.0000	0.0008
nucleotide biosynthetic process (GO:0009165)	9/18	0.0000	0.0009
nuclear DNA replication (GO:0033260)	7/11	0.0000	0.0011
water-soluble vitamin metabolic process (GO:0006767)	20/76	0.0000	0.0011
pre-replicative complex assembly involved in nuclear cell cycle DNA replication (GO:0006267)	6/8	0.0000	0.0012
cholesterol metabolic process (GO:0008203)	20/77	0.0000	0.0013
nitrogen compound transport (GO:0071705)	30/143	0.0000	0.0013
mitotic spindle assembly (GO:0090307)	14/44	0.0000	0.0020
cellular macromolecule biosynthetic process (GO:0034645)	52/314	0.0000	0.0022
protein localization to condensed chromosome (GO:1903083)	7/12	0.0000	0.0022
regulation of nuclear division (GO:0051783)	9/20	0.0000	0.0023
chromosome condensation (GO:0030261)	14/45	0.0000	0.0025
mitotic DNA replication initiation (GO:1902975)	5/6	0.0000	0.0026
nuclear cell cycle DNA replication initiation (GO:1902315)	5/6	0.0000	0.0026
double-strand break repair (GO:0006302)	32/164	0.0000	0.0029
lipid transport (GO:0006869)	24/109	0.0001	0.0034
G2/M transition of mitotic cell cycle (GO:0000086)	27/130	0.0001	0.0036
DNA replication checkpoint signaling (GO:0000076)	8/17	0.0001	0.0039
reverse cholesterol transport (GO:0043691)	8/17	0.0001	0.0039
cell cycle G2/M phase transition (GO:0044839)	27/131	0.0001	0.0039
base-excision repair (GO:0006284)	14/48	0.0001	0.0049
positive regulation of developmental process (GO:0051094)	33/177	0.0001	0.0052
positive regulation of apoptotic process (GO:0043065)	50/310	0.0001	0.0052
regulation of attachment of spindle microtubules to kinetochore (GO:0051988)	6/10	0.0001	0.0057
negative regulation of cellular process (GO:0048523)	80/566	0.0001	0.0061
pyruvate metabolic process (GO:0006090)	15/55	0.0001	0.0061
protein localization to kinetochore (GO:0034501)	7/14	0.0001	0.0065
cellular response to insulin stimulus (GO:0032869)	26/129	0.0001	0.0071
glucose metabolic process (GO:0006006)	16/62	0.0001	0.0072
regulation of cell migration (GO:0030334)	61/408	0.0001	0.0079
replication fork processing (GO:0031297)	12/39	0.0001	0.0079
regulation of cyclin-dependent protein serine/threonine kinase activity (GO:0000079)	19/82	0.0002	0.0081
cellular response to DNA damage stimulus (GO:0006974)	54/350	0.0002	0.0081
monocarboxylic acid transport (GO:0015718)	15/57	0.0002	0.0086
cholesterol transport (GO:0030301)	14/51	0.0002	0.0086
positive regulation of programmed cell death (GO:0043068)	46/286	0.0002	0.0089
establishment of mitotic spindle localization (GO:0040001)	10/29	0.0002	0.0092
tetrahydrofolate metabolic process (GO:0046653)	6/11	0.0002	0.0099
regulation of cell cycle (GO:0051726)	47/296	0.0002	0.0100
response to insulin (GO:0032868)	19/84	0.0002	0.0104
gluconeogenesis (GO:0006094)	12/41	0.0002	0.0120
phospholipid transport (GO:0015914)	15/59	0.0003	0.0120
negative regulation of apoptotic process (GO:0043066)	69/485	0.0003	0.0120
mitotic spindle elongation (GO:0000022)	5/8	0.0003	0.0140
mitotic spindle midzone assembly (GO:0051256)	5/8	0.0003	0.0140
regulation of acetyl-CoA biosynthetic process from pyruvate (GO:0010510)	5/8	0.0003	0.0140
regulation of acyl-CoA biosynthetic process (GO:0050812)	5/8	0.0003	0.0140
DNA unwinding involved in DNA replication (GO:0006268)	7/16	0.0003	0.0142
heme catabolic process (GO:0042167)	7/16	0.0003	0.0142
porphyrin-containing compound catabolic process (GO:0006787)	7/16	0.0003	0.0142
regulation of mitotic sister chromatid separation (GO:0010965)	7/16	0.0003	0.0142

epithelium development (GO:0060429)	24/122	0.0003	0.0145
L-aspartate transmembrane transport (GO:0070778)	4/5	0.0003	0.0149
negative regulation of MAPK cascade (GO:0043409)	20/94	0.0004	0.0149
attachment of mitotic spindle microtubules to kinetochore (GO:0051315)	6/12	0.0004	0.0150
mitotic nuclear membrane disassembly (GO:0007077)	6/12	0.0004	0.0150
negative regulation of hemostasis (GO:1900047)	6/12	0.0004	0.0150
replicative senescence (GO:0090399)	6/12	0.0004	0.0150
purine-containing compound biosynthetic process (GO:0072522)	9/26	0.0004	0.0152
DNA damage response, signal transduction by p53 class mediator resulting in cell cycle arrest (GO:0006977)	14/56	0.0005	0.0195
amino acid transport (GO:0006865)	13/50	0.0005	0.0201
organic hydroxy compound biosynthetic process (GO:1901617)	13/50	0.0005	0.0201
hexose biosynthetic process (GO:0019319)	12/44	0.0005	0.0201
L-alpha-amino acid transmembrane transport (GO:1902475)	9/27	0.0005	0.0201
regulation of protein serine/threonine kinase activity (GO:0071900)	22/111	0.0005	0.0201
sterol metabolic process (GO:0016125)	16/70	0.0006	0.0223
carboxylic acid transport (GO:0046942)	14/57	0.0006	0.0223
phosphatidylcholine metabolic process (GO:0046470)	17/77	0.0006	0.0230
regulation of cytokinesis (GO:0032465)	18/84	0.0006	0.0231
kinetochore assembly (GO:0051382)	5/9	0.0006	0.0231
protein K6-linked ubiquitination (GO:0085020)	5/9	0.0006	0.0231
purine nucleobase metabolic process (GO:0006144)	5/9	0.0006	0.0231
tetrahydrofolate interconversion (GO:0035999)	5/9	0.0006	0.0231
DNA integrity checkpoint signaling (GO:0031570)	11/39	0.0006	0.0231
bile acid and bile salt transport (GO:0015721)	9/28	0.0007	0.0247
L-amino acid transport (GO:0015807)	9/28	0.0007	0.0247
negative regulation of programmed cell death (GO:0043069)	55/381	0.0007	0.0255
carbohydrate derivative transport (GO:1901264)	7/18	0.0008	0.0260
regulation of chromosome segregation (GO:0051983)	7/18	0.0008	0.0260
mitotic cell cycle checkpoint signaling (GO:0007093)	8/23	0.0008	0.0260
positive regulation of cell cycle G2/M phase transition (GO:1902751)	8/23	0.0008	0.0260
mitotic G1 DNA damage checkpoint signaling (GO:0031571)	15/65	0.0008	0.0260
postreplication repair (GO:0006301)	12/46	0.0008	0.0269
organic hydroxy compound transport (GO:0015850)	11/40	0.0008	0.0271
recombinational repair (GO:0000725)	17/79	0.0008	0.0275
epithelial cell differentiation (GO:0030855)	20/101	0.0009	0.0305
cholesterol import (GO:0070508)	4/6	0.0010	0.0305
histone-serine phosphorylation (GO:0035404)	4/6	0.0010	0.0305
negative regulation of lens fiber cell differentiation (GO:1902747)	4/6	0.0010	0.0305
protein K29-linked ubiquitination (GO:0035519)	4/6	0.0010	0.0305
purine nucleobase biosynthetic process (GO:0009113)	4/6	0.0010	0.0305
regulation of neutrophil extravasation (GO:2000389)	4/6	0.0010	0.0305
sterol import (GO:0035376)	4/6	0.0010	0.0305
base-excision repair, gap-filling (GO:0006287)	10/35	0.0010	0.0309
negative regulation of coagulation (GO:0050819)	6/14	0.0010	0.0309
negative regulation of fibroblast growth factor receptor signaling pathway (GO:0040037)	6/14	0.0010	0.0309
nuclear membrane disassembly (GO:0051081)	6/14	0.0010	0.0309
regulation of cell population proliferation (GO:0042127)	97/764	0.0010	0.0309
negative regulation of macromolecule metabolic process (GO:0010605)	32/194	0.0010	0.0309
intrinsic apoptotic signaling pathway (GO:0097193)	20/102	0.0010	0.0309
amino acid import across plasma membrane (GO:0089718)	8/24	0.0011	0.0309
establishment of mitotic spindle orientation (GO:0000132)	8/24	0.0011	0.0309
nucleotide-excision repair, DNA gap filling (GO:0006297)	8/24	0.0011	0.0309
purine nucleotide metabolic process (GO:0006163)	8/24	0.0011	0.0309
anion transmembrane transport (GO:0098656)	15/67	0.0011	0.0312
DNA damage response, signal transduction by p53 class mediator (GO:0030330)	16/74	0.0011	0.0320
folic acid metabolic process (GO:0046655)	7/19	0.0011	0.0320
positive regulation of cell migration (GO:0030335)	41/269	0.0011	0.0329
positive regulation of transferase activity (GO:0051347)	26/148	0.0012	0.0332
negative regulation of mitotic cell cycle (GO:0045930)	12/48	0.0012	0.0338
positive regulation of DNA biosynthetic process (GO:2000573)	14/61	0.0012	0.0338
regulation of extrinsic apoptotic signaling pathway via death domain receptors (GO:1902041)	11/42	0.0013	0.0350
translesion synthesis (GO:0019985)	11/42	0.0013	0.0350
interstrand cross-link repair (GO:0036297)	13/55	0.0013	0.0368
organophosphate ester transport (GO:0015748)	8/25	0.0014	0.0389
regulation of epidermal cell differentiation (GO:0045604)	8/25	0.0014	0.0389
regulation of intracellular signal transduction (GO:1902531)	60/437	0.0015	0.0405
DNA synthesis involved in DNA repair (GO:0000731)	11/43	0.0015	0.0408
DNA-dependent DNA replication maintenance of fidelity (GO:0045005)	11/43	0.0015	0.0408
mitotic intra-S DNA damage checkpoint signaling (GO:0031573)	6/15	0.0015	0.0408
folic acid-containing compound metabolic process (GO:0006760)	7/20	0.0016	0.0408
nucleobase-containing compound biosynthetic process (GO:0034654)	7/20	0.0016	0.0408
organic cation transport (GO:0015695)	7/20	0.0016	0.0408
positive regulation of G2/M transition of mitotic cell cycle (GO:0010971)	7/20	0.0016	0.0408
vitamin transport (GO:0051180)	9/31	0.0016	0.0408
regulation of neuron apoptotic process (GO:0043523)	19/98	0.0016	0.0411
positive regulation of cytokinesis (GO:0032467)	10/37	0.0016	0.0411
cell cycle G1/S phase transition (GO:0044843)	14/63	0.0017	0.0425
organonitrogen compound catabolic process (GO:1901565)	14/63	0.0017	0.0425
cellular response to peptide hormone stimulus (GO:0071375)	20/106	0.0017	0.0434
regulation of reactive oxygen species metabolic process (GO:2000377)	13/57	0.0019	0.0473
regulation of mitotic metaphase/anaphase transition (GO:0030071)	8/26	0.0019	0.0473
negative regulation of cell cycle process (GO:0010948)	14/64	0.0020	0.0488

establishment of centrosome localization (GO:0051660)	4/7	0.0021	0.0515
regulation of lens fiber cell differentiation (GO:1902746)	4/7	0.0021	0.0515
positive regulation of epithelial cell proliferation (GO:0050679)	22/123	0.0021	0.0521
positive regulation of endothelial cell migration (GO:0010595)	17/86	0.0022	0.0538
positive regulation of mitotic cell cycle phase transition (GO:1901992)	13/58	0.0022	0.0540
negative regulation of epithelial cell differentiation (GO:0030857)	6/16	0.0023	0.0546
regulation of ATP biosynthetic process (GO:2001169)	6/16	0.0023	0.0546
transepithelial transport (GO:0070633)	6/16	0.0023	0.0546

Suppl. Table 5: Gene ontology results of CRISPR-clone B.

Evaluated with Enrichr - Ma'ayan Laboratory - Computational Systems Biology (https://maayanlab.cloud/Enrichr/) (adjusted p-value < 0.05).

Term	Overlap	P-value	Adjusted P-value
microtubule cytoskeleton organization involved in mitosis (GO:1902850)	56/128	0.0000	0.0000
mitotic spindle organization (GO:0007052)	60/157	0.0000	0.0000
DNA replication (GO:0006260)	46/108	0.0000	0.0000
DNA metabolic process (GO:0006259)	74/277	0.0000	0.0000
mitotic sister chromatid segregation (GO:0000070)	42/102	0.0000	0.0000
centromere complex assembly (GO:0034508)	22/37	0.0000	0.0000
DNA replication initiation (GO:0006270)	22/38	0.0000	0.0000
sister chromatid segregation (GO:0000819)	20/34	0.0000	0.0000
chromatin remodeling at centromere (GO:0031055)	19/32	0.0000	0.0000
mitotic cell cycle phase transition (GO:0044772)	52/209	0.0000	0.0000
CENP-A containing chromatin organization (GO:0061641)	18/30	0.0000	0.0000
CENP-A containing nucleosome assembly (GO:0034080)	18/30	0.0000	0.0000
DNA-dependent DNA replication (GO:0006261)	38/129	0.0000	0.0000
G2/M transition of mitotic cell cycle (GO:0000086)	38/130	0.0000	0.0000
cell cycle G2/M phase transition (GO:0044839)	38/131	0.0000	0.0000
histone exchange (GO:0043486)	19/38	0.0000	0.0000
DNA replication-independent nucleosome assembly (GO:0006336)	19/39	0.0000	0.0000
DNA strand elongation involved in DNA replication (GO:0006271)	13/18	0.0000	0.0000
mitotic nuclear division (GO:0140014)	26/74	0.0000	0.0000
double-strand break repair via homologous recombination (GO:0000724)	30/97	0.0000	0.0000
positive regulation of cell cycle process (GO:0090068)	30/101	0.0000	0.0000
DNA repair (GO:0006281)	59/298	0.0000	0.0000
double-strand break repair via break-induced replication (GO:0000727)	10/12	0.0000	0.0000
mitotic DNA replication (GO:1902969)	9/10	0.0000	0.0000
regulation of cell cycle process (GO:0010564)	30/106	0.0000	0.0000
sterol biosynthetic process (GO:0016126)	17/38	0.0000	0.0000
secondary alcohol biosynthetic process (GO:1902653)	16/34	0.0000	0.0000
G1/S transition of mitotic cell cycle (GO:0000082)	26/85	0.0000	0.0000
cholesterol biosynthetic process (GO:0006695)	16/35	0.0000	0.0000
regulation of cyclin-dependent protein kinase activity (GO:1904029)	20/54	0.0000	0.0000
regulation of transcription involved in G1/S transition of mitotic cell cycle (GO:0000083)	15/32	0.0000	0.0000
mitotic metaphase plate congression (GO:0007080)	19/51	0.0000	0.0000
DNA strand elongation (GO:0022616)	11/18	0.0000	0.0000
DNA damage response, signal transduction by p53 class mediator resulting in cell cycle arrest (GO:0006977)	19/56	0.0000	0.0000
kinetochore organization (GO:0051383)	9/13	0.0000	0.0000
mitotic G1 DNA damage checkpoint signaling (GO:0031571)	20/65	0.0000	0.0000
regulation of cell cycle (GO:0051726)	52/296	0.0000	0.0000
regulation of cell cycle G2/M phase transition (GO:1902749)	23/85	0.0000	0.0000
negative regulation of mitotic metaphase/anaphase transition (GO:0045841)	11/22	0.0000	0.0001
DNA damage response, signal transduction by p53 class mediator (GO:0030330)	21/74	0.0000	0.0001
mitotic chromosome condensation (GO:0007076)	12/27	0.0000	0.0001
regulation of cyclin-dependent protein serine/threonine kinase activity (GO:0000079)	22/82	0.0000	0.0001
positive regulation of DNA-directed DNA polymerase activity (GO:1900264)	7/9	0.0000	0.0001
regulation of DNA-directed DNA polymerase activity (GO:1900262)	7/9	0.0000	0.0001
cellular macromolecule biosynthetic process (GO:0034645)	53/314	0.0000	0.0001
cholesterol metabolic process (GO:0008203)	21/77	0.0000	0.0001
cellular response to DNA damage stimulus (GO:0006974)	57/350	0.0000	0.0001
canonical glycolysis (GO:0061621)	11/24	0.0000	0.0001
glucose catabolic process to pyruvate (GO:0061718)	11/24	0.0000	0.0001
pyruvate metabolic process (GO:0006090)	17/55	0.0000	0.0002
glycolytic process (GO:0006096)	12/29	0.0000	0.0002
transport across blood-brain barrier (GO:0150104)	22/86	0.0000	0.0002
glycolytic process through glucose-6-phosphate (GO:0061620)	11/25	0.0000	0.0002
mitotic spindle assembly checkpoint signaling (GO:0007094)	10/21	0.0000	0.0002
mitotic spindle checkpoint signaling (GO:0071174)	10/21	0.0000	0.0002
spindle assembly checkpoint signaling (GO:0071173)	10/21	0.0000	0.0002
protein localization to chromosome, centromeric region (GO:0071459)	9/17	0.0000	0.0002
regulation of mitotic nuclear division (GO:0007088)	17/57	0.0000	0.0002
regulation of cell population proliferation (GO:0042127)	101/764	0.0000	0.0004
vascular transport (GO:0010232)	21/84	0.0000	0.0004
mitotic DNA damage checkpoint signaling (GO:0044773)	17/59	0.0000	0.0004
nucleotide biosynthetic process (GO:0009165)	9/18	0.0000	0.0004
nuclear DNA replication (GO:0033260)	7/11	0.0000	0.0006
mitotic cytokinesis (GO:0000281)	15/49	0.0000	0.0006
pre-replicative complex assembly involved in nuclear cell cycle DNA replication (GO:0006267)	6/8	0.0000	0.0006
regulation of apoptotic process (GO:0042981)	97/742	0.0000	0.0009

chromosome condensation (GO:0030261)	14/45	0.0000	0.0009
mitotic G2/M transition checkpoint (GO:0044818)	14/45	0.0000	0.0009
protein localization to condensed chromosome (GO:1903083)	7/12	0.0000	0.0011
positive regulation of mitotic cell cycle phase transition (GO:1901992)	16/58	0.0000	0.0012
DNA unwinding involved in DNA replication (GO:0006268)	8/16	0.0000	0.0012
cholesterol homeostasis (GO:0042632)	18/71	0.0000	0.0012
regulation of G2/M transition of mitotic cell cycle (GO:0010389)	29/149	0.0000	0.0012
regulation of mitotic cell cycle phase transition (GO:1901990)	34/188	0.0000	0.0013
carbohydrate catabolic process (GO:0016052)	13/41	0.0000	0.0013
sterol homeostasis (GO:0055092)	18/72	0.0000	0.0014
mitotic DNA replication initiation (GO:1902975)	5/6	0.0000	0.0014
nuclear cell cycle DNA replication initiation (GO:1902315)	5/6	0.0000	0.0014
negative regulation of cellular process (GO:0048523)	77/566	0.0000	0.0014
organic acid transport (GO:0015849)	22/100	0.0000	0.0016
base-excision repair (GO:0006284)	14/48	0.0000	0.0017
DNA replication checkpoint signaling (GO:0000076)	8/17	0.0000	0.0018
negative regulation of cell population proliferation (GO:0008285)	56/379	0.0000	0.0018
positive regulation of DNA biosynthetic process (GO:2000573)	16/61	0.0000	0.0019
interstrand cross-link repair (GO:0036297)	15/55	0.0000	0.0020
negative regulation of macromolecule metabolic process (GO:0010605)	34/194	0.0000	0.0021
double-strand break repair (GO:0006302)	30/164	0.0000	0.0025
cation transmembrane transport (GO:0098655)	13/44	0.0000	0.0025
mitotic G2 DNA damage checkpoint signaling (GO:0007095)	11/33	0.0001	0.0028
phosphatidylcholine catabolic process (GO:0034638)	6/10	0.0001	0.0029
regulation of attachment of spindle microtubules to kinetochore (GO:0051988)	6/10	0.0001	0.0029
DNA integrity checkpoint signaling (GO:0031570)	12/39	0.0001	0.0030
replication fork processing (GO:0031297)	12/39	0.0001	0.0030
positive regulation of cell cycle G2/M phase transition (GO:1902751)	9/23	0.0001	0.0030
regulation of cytokinesis (GO:0032465)	19/84	0.0001	0.0030
negative regulation of coagulation (GO:0050819)	7/14	0.0001	0.0030
negative regulation of fibroblast growth factor receptor signaling pathway (GO:0040037)	7/14	0.0001	0.0030
protein localization to kinetochore (GO:0034501)	7/14	0.0001	0.0030
positive regulation of cell differentiation (GO:0045597)	41/258	0.0001	0.0033
folic acid metabolic process (GO:0046655)	8/19	0.0001	0.0039
amino acid import across plasma membrane (GO:0089718)	9/24	0.0001	0.0041
negative regulation of apoptotic process (GO:0043066)	66/485	0.0001	0.0041
tetrahydrofolate metabolic process (GO:0046653)	6/11	0.0001	0.0052
positive regulation of transferase activity (GO:0051347)	27/148	0.0001	0.0052
positive regulation of G2/M transition of mitotic cell cycle (GO:0010971)	8/20	0.0001	0.0057
regulation of nuclear division (GO:0051783)	8/20	0.0001	0.0057
regulation of protein serine/threonine kinase activity (GO:0071900)	22/111	0.0001	0.0061
mitotic spindle elongation (GO:0000022)	5/8	0.0002	0.0083
mitotic spindle midzone assembly (GO:0051256)	5/8	0.0002	0.0083
platelet activating factor metabolic process (GO:0046469)	5/8	0.0002	0.0083
amino acid transport (GO:0006865)	13/50	0.0002	0.0084
organic hydroxy compound biosynthetic process (GO:1901617)	13/50	0.0002	0.0084
attachment of mitotic spindle microtubules to kinetochore (GO:0051315)	6/12	0.0002	0.0085
fat-soluble vitamin catabolic process (GO:0042363)	6/12	0.0002	0.0085
mitotic nuclear membrane disassembly (GO:0007077)	6/12	0.0002	0.0085
negative regulation of hemostasis (GO:1900047)	6/12	0.0002	0.0085
organic hydroxy compound catabolic process (GO:1901616)	6/12	0.0002	0.0085
hexose biosynthetic process (GO:0019319)	12/44	0.0002	0.0085
mitotic spindle assembly (GO:0090307)	12/44	0.0002	0.0085
carboxylic acid transport (GO:0046942)	14/57	0.0002	0.0087
negative regulation of cell cycle process (GO:0010948)	15/64	0.0002	0.0090
double-strand break repair via synthesis-dependent strand annealing (GO:0045003)	4/5	0.0002	0.0090
L-aspartate transmembrane transport (GO:0070778)	4/5	0.0002	0.0090
recombinational repair (GO:0000725)	17/79	0.0003	0.0105
steroid biosynthetic process (GO:0006694)	15/65	0.0003	0.0105
regulation of signal transduction by p53 class mediator (GO:1901796)	27/156	0.0003	0.0105
cytoskeleton-dependent cytokinesis (GO:0061640)	16/72	0.0003	0.0105
sprouting angiogenesis (GO:0002040)	13/52	0.0003	0.0112
negative regulation of blood coagulation (GO:0030195)	11/40	0.0004	0.0131
regulation of DNA replication (GO:0006275)	13/53	0.0004	0.0135
mitotic cell cycle checkpoint signaling (GO:0007093)	8/23	0.0004	0.0140
kinetochore assembly (GO:0051382)	5/9	0.0004	0.0140
protein K6-linked ubiquitination (GO:0085020)	5/9	0.0004	0.0140
purine nucleobase metabolic process (GO:0006144)	5/9	0.0004	0.0140
regulation of mitotic centrosome separation (GO:0046602)	5/9	0.0004	0.0140
tetrahydrofolate interconversion (GO:0035999)	5/9	0.0004	0.0140
regulation of cell migration (GO:0030334)	55/408	0.0004	0.0144
regulation of chromosome segregation (GO:0051983)	7/18	0.0004	0.0144
negative regulation of programmed cell death (GO:0043069)	52/381	0.0005	0.0150
positive regulation of developmental process (GO:0051094)	29/177	0.0005	0.0150
gluconeogenesis (GO:0006094)	11/41	0.0005	0.0152
regulation of angiogenesis (GO:0045765)	32/203	0.0005	0.0156
base-excision repair, gap-filling (GO:0006287)	10/35	0.0005	0.0156
negative regulation of mitotic cell cycle (GO:0045930)	12/48	0.0005	0.0168
phospholipid metabolic process (GO:0006644)	16/76	0.0006	0.0174
water-soluble vitamin metabolic process (GO:0006767)	16/76	0.0006	0.0174
nucleotide-excision repair, DNA gap filling (GO:0006297)	8/24	0.0006	0.0178
regulation of extrinsic apoptotic signaling pathway via death domain receptors (GO:1902041)	11/42	0.0006	0.0181

nuclear membrane disassembly (GO:0051081)	6/14	0.0006	0.0189
phosphatidylcholine metabolic process (GO:0046470)	16/77	0.0006	0.0197
sterol metabolic process (GO:0016125)	15/70	0.0007	0.0199
histone-serine phosphorylation (GO:0035404)	4/6	0.0007	0.0199
negative regulation of lens fiber cell differentiation (GO:1902747)	4/6	0.0007	0.0199
positive regulation of tau-protein kinase activity (GO:1902949)	4/6	0.0007	0.0199
protein K29-linked ubiquitination (GO:0035519)	4/6	0.0007	0.0199
protein localization to nucleolus (GO:1902570)	4/6	0.0007	0.0199
cell cycle G1/S phase transition (GO:0044843)	14/63	0.0007	0.0200
DNA synthesis involved in DNA repair (GO:0000731)	11/43	0.0007	0.0209
DNA-dependent DNA replication maintenance of fidelity (GO:0045005)	11/43	0.0007	0.0209
regulation of epithelial cell proliferation (GO:0050678)	18/93	0.0008	0.0215
epithelial cell differentiation (GO:0030855)	19/101	0.0008	0.0222
positive regulation of cytokinesis (GO:0032467)	10/37	0.0008	0.0223
regulation of phosphorylation (GO:0042325)	22/125	0.0008	0.0227
regulation of reactive oxygen species metabolic process (GO:2000377)	13/57	0.0008	0.0227
negative regulation of MAPK cascade (GO:0043409)	18/94	0.0009	0.0237
cardiac epithelial to mesenchymal transition (GO:0060317)	7/20	0.0009	0.0248
folic acid-containing compound metabolic process (GO:0006760)	7/20	0.0009	0.0248
regulation of fibroblast growth factor receptor signaling pathway (GO:0040036)	7/20	0.0009	0.0248
mitotic nuclear membrane organization (GO:0101024)	12/51	0.0010	0.0256
mitotic nuclear membrane reassembly (GO:0007084)	12/51	0.0010	0.0256
nitrogen compound transport (GO:0071705)	24/143	0.0010	0.0259
positive regulation of apoptotic process (GO:0043065)	43/310	0.0010	0.0260
phosphate-containing compound metabolic process (GO:0006796)	32/212	0.0010	0.0272
DNA geometric change (GO:0032392)	8/26	0.0010	0.0272
regulation of mitotic metaphase/anaphase transition (GO:0030071)	8/26	0.0010	0.0272
positive regulation of cell motility (GO:2000147)	33/221	0.0011	0.0274
positive regulation of cell population proliferation (GO:0008284)	60/474	0.0012	0.0312
DNA recombination (GO:0006310)	10/39	0.0012	0.0315
regulation of exit from mitosis (GO:0007096)	10/39	0.0012	0.0315
error-prone translesion synthesis (GO:0042276)	7/21	0.0013	0.0322
glycerol metabolic process (GO:0006071)	5/11	0.0013	0.0325
negative regulation of homotypic cell-cell adhesion (GO:0034111)	5/11	0.0013	0.0325
positive regulation of DNA-dependent DNA replication (GO:2000105)	5/11	0.0013	0.0325
regulation of cysteine-type endopeptidase activity involved in apoptotic signaling pathway (GO:2001267)	5/11	0.0013	0.0325
postreplication repair (GO:0006301)	11/46	0.0013	0.0325
positive regulation of cell migration (GO:0030335)	38/269	0.0013	0.0325
negative regulation of smooth muscle cell proliferation (GO:0048662)	9/33	0.0013	0.0325
regulation of sprouting angiogenesis (GO:1903670)	9/33	0.0013	0.0325
L-alpha-amino acid transmembrane transport (GO:1902475)	8/27	0.0014	0.0330
nucleobase-containing small molecule interconversion (GO:0015949)	8/27	0.0014	0.0330
epithelium development (GO:0060429)	21/122	0.0014	0.0333
negative regulation of cell-substrate junction organization (GO:0150118)	6/16	0.0014	0.0333
negative regulation of epithelial cell differentiation (GO:0030857)	6/16	0.0014	0.0333
negative regulation of focal adhesion assembly (GO:0051895)	6/16	0.0014	0.0333
regulation of mitotic sister chromatid separation (GO:0010965)	6/16	0.0014	0.0333
G-quadruplex DNA unwinding (GO:0044806)	4/7	0.0015	0.0341
pharyngeal arch artery morphogenesis (GO:0061626)	4/7	0.0015	0.0341
regulation of lens fiber cell differentiation (GO:1902746)	4/7	0.0015	0.0341
positive regulation of epithelial cell proliferation (GO:0050679)	21/123	0.0016	0.0360
regulation of DNA binding (GO:0051101)	11/47	0.0016	0.0367
nuclear membrane reassembly (GO:0031468)	12/54	0.0016	0.0369
regulation of epithelial to mesenchymal transition (GO:0010717)	15/76	0.0016	0.0370
negative regulation of extrinsic apoptotic signaling pathway via death domain receptors (GO:1902042)	9/34	0.0017	0.0379
amino acid import (GO:0043090)	7/22	0.0017	0.0383
chaperone-mediated protein complex assembly (GO:0051131)	7/22	0.0017	0.0383
negative regulation of phosphate metabolic process (GO:0045936)	7/22	0.0017	0.0383
positive regulation of angiogenesis (GO:0045766)	20/116	0.0018	0.0389
L-amino acid transport (GO:0015807)	8/28	0.0018	0.0389
neutral amino acid transport (GO:0015804)	8/28	0.0018	0.0389
glucose metabolic process (GO:0006006)	13/62	0.0018	0.0403
regulation of release of cytochrome c from mitochondria (GO:0090199)	10/41	0.0019	0.0403
triglyceride metabolic process (GO:0006641)	12/55	0.0019	0.0413
negative regulation of MAP kinase activity (GO:0043407)	11/48	0.0019	0.0414
modified amino acid transport (GO:0072337)	6/17	0.0020	0.0433
reverse cholesterol transport (GO:0043691)	6/17	0.0020	0.0433
negative regulation of gene expression (GO:0010629)	43/322	0.0021	0.0433
peptidyl-tyrosine dephosphorylation (GO:0035335)	9/35	0.0021	0.0433
cell cycle checkpoint signaling (GO:0000075)	5/12	0.0021	0.0433
negative regulation of cell division (GO:0051782)	5/12	0.0021	0.0433
positive regulation of cellular senescence (GO:2000774)	5/12	0.0021	0.0433
regulation of sister chromatid cohesion (GO:0007063)	5/12	0.0021	0.0433
replicative senescence (GO:0090399)	5/12	0.0021	0.0433
negative regulation of signal transduction (GO:0009968)	37/267	0.0022	0.0442
negative regulation of phosphorylation (GO:0042326)	16/86	0.0022	0.0452
translesion synthesis (GO:0019985)	10/42	0.0023	0.0459
establishment of mitotic spindle localization (GO:0040001)	8/29	0.0023	0.0460
ciliary basal body-plasma membrane docking (GO:0097711)	17/95	0.0025	0.0509
dicarboxylic acid metabolic process (GO:0043648)	12/57	0.0026	0.0529
negative regulation of ERK1 and ERK2 cascade (GO:0070373)	11/50	0.0027	0.0539
meiotic sister chromatid cohesion (GO:0051177)	4/8	0.0028	0.0539

positive regulation of cysteine-type endopeptidase activity involved in apoptotic signaling pathway (GO:2001269)	4/8	0.0028	0.0539
regulation of anion transport (GO:0044070)	4/8	0.0028	0.0539
regulation of metaphase/anaphase transition of cell cycle (GO:1902099)	4/8	0.0028	0.0539
regulation of microvillus organization (GO:0032530)	4/8	0.0028	0.0539
cell migration involved in sprouting angiogenesis (GO:0002042)	6/18	0.0028	0.0543
maintenance of gastrointestinal epithelium (GO:0030277)	6/18	0.0028	0.0543
microtubule depolymerization (GO:0007019)	6/18	0.0028	0.0543
response to axon injury (GO:0048678)	6/18	0.0028	0.0543
triglyceride biosynthetic process (GO:0019432)	6/18	0.0028	0.0543
artery morphogenesis (GO:0048844)	8/30	0.0029	0.0545
phosphatidylcholine acyl-chain remodeling (GO:0036151)	8/30	0.0029	0.0545

Suppl. Table 6: Gene ontology results of CRISPR-clone C.

Evaluated with Enrichr - Ma'ayan Laboratory - Computational Systems Biology (https://maayanlab.cloud/Enrichr/) (adjusted p-value < 0.05).

Term	Overlap	P-value	Adjusted P-value
mitotic spindle organization (GO:0007052)	70/157	0.0000	0.0000
microtubule cytoskeleton organization involved in mitosis (GO:1902850)	61/128	0.0000	0.0000
DNA replication (GO:0006260)	52/108	0.0000	0.0000
DNA metabolic process (GO:0006259)	92/277	0.0000	0.0000
mitotic sister chromatid segregation (GO:0000070)	48/102	0.0000	0.0000
centromere complex assembly (GO:0034508)	24/37	0.0000	0.0000
DNA replication initiation (GO:0006270)	24/38	0.0000	0.0000
mitotic nuclear division (GO:0140014)	35/74	0.0000	0.0000
sister chromatid segregation (GO:0000819)	22/34	0.0000	0.0000
DNA strand elongation involved in DNA replication (GO:0006271)	15/18	0.0000	0.0000
chromatin remodeling at centromere (GO:0031055)	20/32	0.0000	0.0000
CENP-A containing chromatin organization (GO:0061641)	19/30	0.0000	0.0000
CENP-A containing nucleosome assembly (GO:0034080)	19/30	0.0000	0.0000
DNA strand elongation (GO:0022616)	14/18	0.0000	0.0000
histone exchange (GO:0043486)	21/38	0.0000	0.0000
DNA replication-independent nucleosome assembly (GO:0006336)	21/39	0.0000	0.0000
DNA-dependent DNA replication (GO:0006261)	44/129	0.0000	0.0000
regulation of cyclin-dependent protein kinase activity (GO:1904029)	25/54	0.0000	0.0000
G1/S transition of mitotic cell cycle (GO:0000082)	33/85	0.0000	0.0000
DNA repair (GO:0006281)	79/298	0.0000	0.0000
regulation of transcription involved in G1/S transition of mitotic cell cycle (GO:0000083)	18/32	0.0000	0.0000
mitotic cell cycle phase transition (GO:0044772)	60/209	0.0000	0.0000
transport across blood-brain barrier (GO:0150104)	32/86	0.0000	0.0000
double-strand break repair via break-induced replication (GO:0000727)	10/12	0.0000	0.0000
mitotic DNA replication (GO:1902969)	9/10	0.0000	0.0001
vascular transport (GO:0010232)	31/84	0.0000	0.0001
double-strand break repair via homologous recombination (GO:0000724)	34/97	0.0000	0.0001
regulation of cell cycle (GO:0051726)	75/296	0.0000	0.0001
kinetochore organization (GO:0051383)	10/13	0.0000	0.0001
mitotic DNA damage checkpoint signaling (GO:0044773)	24/59	0.0000	0.0002
base-excision repair (GO:0006284)	21/48	0.0000	0.0002
secondary alcohol biosynthetic process (GO:1902653)	17/34	0.0000	0.0002
regulation of cell cycle process (GO:0010564)	35/106	0.0000	0.0002
sterol biosynthetic process (GO:0016126)	18/38	0.0000	0.0002
cholesterol biosynthetic process (GO:0006695)	17/35	0.0000	0.0003
mitotic G1 DNA damage checkpoint signaling (GO:0031571)	25/65	0.0000	0.0003
regulation of cyclin-dependent protein serine/threonine kinase activity (GO:0000079)	29/82	0.0000	0.0003
regulation of nuclear division (GO:0051783)	12/20	0.0000	0.0005
positive regulation of programmed cell death (GO:0043068)	70/286	0.0000	0.0008
mitotic cytokinesis (GO:0000281)	20/49	0.0000	0.0009
DNA damage response, signal transduction by p53 class mediator (GO:0030330)	26/74	0.0000	0.0011
base-excision repair, gap-filling (GO:0006287)	16/35	0.0000	0.0013
cellular response to DNA damage stimulus (GO:0006974)	81/350	0.0000	0.0015
mitotic metaphase plate congression (GO:0007080)	20/51	0.0000	0.0017
interstrand cross-link repair (GO:0036297)	21/55	0.0000	0.0017
positive regulation of apoptotic process (GO:0043065)	73/310	0.0000	0.0019
mitotic spindle assembly (GO:0090307)	18/44	0.0000	0.0022
DNA damage response, signal transduction by p53 class mediator resulting in cell cycle arrest (GO:0006977)	21/56	0.0000	0.0022
carbohydrate catabolic process (GO:0016052)	17/41	0.0000	0.0028
regulation of mitotic nuclear division (GO:0007088)	21/57	0.0000	0.0028
mitotic G2/M transition checkpoint (GO:0044818)	18/45	0.0000	0.0029
mitotic chromosome condensation (GO:0007076)	13/27	0.0000	0.0036
positive regulation of DNA-directed DNA polymerase activity (GO:1900264)	7/9	0.0000	0.0037
regulation of DNA-directed DNA polymerase activity (GO:1900262)	7/9	0.0000	0.0037
nucleotide-excision repair, DNA gap filling (GO:0006297)	12/24	0.0000	0.0042
negative regulation of mitotic cell cycle (GO:0045930)	18/48	0.0001	0.0071
G2/M transition of mitotic cell cycle (GO:0000086)	36/130	0.0001	0.0071
negative regulation of mitotic metaphase/anaphase transition (GO:0045841)	11/22	0.0001	0.0083
mitotic G2 DNA damage checkpoint signaling (GO:0007095)	14/33	0.0001	0.0089
postreplication repair (GO:0006301)	17/46	0.0002	0.0129
epithelial cilium movement involved in extracellular fluid movement (GO:0003351)	10/20	0.0002	0.0160
nucleobase-containing compound biosynthetic process (GO:0034654)	10/20	0.0002	0.0160
regulation of protein serine/threonine kinase activity (GO:0071900)	31/111	0.0002	0.0160

pre-replicative complex assembly involved in nuclear cell cycle DNA replication (GO:0006267)	6/8	0.0002	0.0160
regulation of acetyl-CoA biosynthetic process from pyruvate (GO:0010510)	6/8	0.0002	0.0160
regulation of acyl-CoA biosynthetic process (GO:0050812)	6/8	0.0002	0.0160
regulation of protein localization to cell cortex (GO:1904776)	6/8	0.0002	0.0160
cell cycle G2/M phase transition (GO:0044839)	35/131	0.0002	0.0160
intrinsic apoptotic signaling pathway (GO:0097193)	29/102	0.0002	0.0168
cellular response to fatty acid (GO:0071398)	9/17	0.0002	0.0168
DNA biosynthetic process (GO:0071897)	9/17	0.0002	0.0168
DNA replication checkpoint signaling (GO:0000076)	9/17	0.0002	0.0168
protein localization to chromosome, centromeric region (GO:0071459)	9/17	0.0002	0.0168
canonical glycolysis (GO:0061621)	11/24	0.0002	0.0172
glucose catabolic process to pyruvate (GO:0061718)	11/24	0.0002	0.0172
cilium movement (GO:0003341)	18/52	0.0003	0.0172
nuclear DNA replication (GO:0033260)	7/11	0.0003	0.0181
mitotic spindle assembly checkpoint signaling (GO:0007094)	10/21	0.0003	0.0210
mitotic spindle checkpoint signaling (GO:0071174)	10/21	0.0003	0.0210
spindle assembly checkpoint signaling (GO:0071173)	10/21	0.0003	0.0210
mitotic DNA replication initiation (GO:1902975)	5/6	0.0003	0.0220
nuclear cell cycle DNA replication initiation (GO:1902315)	5/6	0.0003	0.0220
regulation of intracellular signal transduction (GO:1902531)	90/437	0.0004	0.0235
glycolytic process through glucose-6-phosphate (GO:0061620)	11/25	0.0004	0.0238
nucleotide biosynthetic process (GO:0009165)	9/18	0.0004	0.0250
establishment of mitotic spindle localization (GO:0040001)	12/29	0.0004	0.0250
glycolytic process (GO:0006096)	12/29	0.0004	0.0250
cholesterol metabolic process (GO:0008203)	23/77	0.0005	0.0259
cellular macromolecule biosynthetic process (GO:0034645)	68/314	0.0005	0.0259
epithelial cell differentiation (GO:0030855)	28/101	0.0005	0.0259
positive regulation of cell cycle process (GO:0090068)	28/101	0.0005	0.0259
regulation of apoptotic process (GO:0042981)	141/742	0.0005	0.0275
epithelial cilium movement involved in determination of left/right asymmetry (GO:0060287)	6/9	0.0005	0.0299
kinetochore assembly (GO:0051382)	6/9	0.0005	0.0299
motile cilium assembly (GO:0044458)	7/12	0.0006	0.0304
protein localization to condensed chromosome (GO:1903083)	7/12	0.0006	0.0304
cellular response to decreased oxygen levels (GO:0036294)	21/69	0.0006	0.0318
axoneme assembly (GO:0035082)	13/34	0.0006	0.0318
double-strand break repair (GO:0006302)	40/164	0.0006	0.0318
regulation of neuron apoptotic process (GO:0043523)	27/98	0.0006	0.0328
telomere maintenance (GO:0000723)	18/56	0.0007	0.0361
DNA-dependent DNA replication maintenance of fidelity (GO:0045005)	15/43	0.0007	0.0373
negative regulation of MAPK cascade (GO:0043409)	26/94	0.0007	0.0373
replication fork processing (GO:0031297)	14/39	0.0008	0.0389
cilium-dependent cell motility (GO:0060285)	10/23	0.0008	0.0389
positive regulation of cell cycle G2/M phase transition (GO:1902751)	10/23	0.0008	0.0389
cellular response to nutrient levels (GO:0031669)	20/66	0.0009	0.0412
DNA unwinding involved in DNA replication (GO:0006268)	8/16	0.0009	0.0420
organic acid transport (GO:0015849)	27/100	0.0009	0.0423
cholesterol homeostasis (GO:0042632)	21/71	0.0009	0.0427
cation transmembrane transport (GO:0098655)	15/44	0.0010	0.0453
autophagy of mitochondrion (GO:0000422)	14/40	0.0011	0.0487
polyamine metabolic process (GO:0006595)	7/13	0.0011	0.0487
positive regulation of G2/M transition of mitotic cell cycle (GO:0010971)	9/20	0.0011	0.0487
xenobiotic transport (GO:0042908)	9/20	0.0011	0.0487
cytoskeleton-dependent cytokinesis (GO:0061640)	21/72	0.0011	0.0490
sterol homeostasis (GO:0055092)	21/72	0.0011	0.0490
positive regulation of mitotic cell cycle phase transition (GO:1901992)	18/58	0.0011	0.0490
phosphatidylcholine metabolic process (GO:0046470)	22/77	0.0012	0.0502
regulation of attachment of spindle microtubules to kinetochore (GO:0051988)	6/10	0.0012	0.0513
chromosome condensation (GO:0030261)	15/45	0.0013	0.0531
microtubule bundle formation (GO:0001578)	15/45	0.0013	0.0531
unsaturated fatty acid metabolic process (GO:0033559)	17/54	0.0013	0.0531
negative regulation of cellular process (GO:0048523)	109/566	0.0013	0.0531
regulation of cell adhesion (GO:0030155)	33/133	0.0013	0.0531

Suppl. Table 7: Raw data of the DigiWest® experiment - R1^{R361H}.

Relative intensity unit of each analyte tested for R1^{R361H}, which was treated with trametinib [0.03 µM] and DMSO [0.03%] for 0.5 h, 6 h and 24 h.

Analyt	**Trametinib 0.5 h**	**Trametinib 6 h**	**Trametinib 24 h**	**DMSO 0.5 h**	**DMSO 6 h**	**DMSO 24 h**	**Medium only 24 h**
Akt - phosphoSer473# 2072	387	77	81	175	108	117	33.3
Akt# 2082	4921	4594	4018	5458	4317	3899	3677
Akt1# 1364	595	602	678	799	33.3	33.3	592
Akt2 - phosphoSer474# 2020	98	33.3	33.3	33.3	64	62	33.3
Akt3# 1365	70	33.3	54	33.3	33.3	33.3	33.3
Annexin II# 0504	8037	5720	9095	9207	5723	8093	6996
APCTK # 025 neu	33.3	69	33.3	76	84	80	50
Aurora A (AIK)	942	1668	183	792	1555	1060	955
Aurora A/B/C - phosphoThr288/Thr232/Thr198	108	95	33	143	33	121	33
Aurora B (AIM1)	1423	2530	266	1489	2356	1348	966

Axin1# 1683 neu	107	177	238	86	312	266	164
Axin2 (Conductin)# 0956 neu	33.3	70	149	33.3	135	176	33.3
b-Raf - phosphoSer445# 1171	748	923	1018	901	1093	1261	1300
Bcl-xL# 1819	13480	8232	12051	11535	8166	10254	7048
Bcl2# 1821	556	259	498	506	220	489	255
beta-Actin# 2104	236762	211160	218457	241291	214520	226569	233703
beta-Catenin - phosphoSer552# 1862	497	572	403	657	517	643	189
beta-Catenin - phosphoSer552# 1862 Peak 2	239	257	200	380	260	357	107
beta-Catenin - phosphoSer675# 2091	5189	4808	5602	6476	4937	5617	5552
beta-Catenin - phosphoSer675# 2091 Peak 2	2272	2176	3813	2802	2552	3494	3742
beta-Catenin (non-pospho Ser33/37/Thr41; active) # 1356	2033	2789	4221	2445	3914	3606	4016
beta-Catenin# 1822	50864	49681	53281	60759	51915	56298	62140
beta-Catenin# 1822 Peak 2	17207	17341	23471	18879	21015	23221	30763
Bmi1# 1457	9636	6862	8494	10135	6964	8544	7968
BMP4# 0936	363	485	614	447	491	605	412
c-Jun - phosphoSer63# 1948	102	222	226	204	149	140	74
c-myc - phosphoThr58/Ser62# 1240	662	247	199	457	623	615	574
c-myc# 1717	5684	5989	2832	6785	9555	253112	4822
c-Raf - phosphoSer259# 1190	5872	2395	3495	6845	2960	6759	1463
c-RafTK # 029	370	389	418	536	340	452	262
C/EBP beta - phosphoThr235# 1183	293	33.3	33.3	88	61	132	33.3
C/EBP beta - phosphoThr235# 1183 Peak 2	33.3	33.3	33.3	2998	51	33.3	33.3
Caseinkinase 1 epsilon# 0340	33.3	135	80	33.3	62	147	33.3
Caspase 3# 1996	21979	18398	20265	21661	18900	21182	15860
Caspase 8BG/MP # 074	248	177	195	319	130	215	95
Caspase 8BG/MP # 074 Peak 2	255	33.3	173	117	33.3	33.3	98
Caspase 9# 1551	4636	1289	3345	3628	1333	2806	1469
Caspase 9# 1551 Peak 2	714	542	808	609	564	624	376
CD133# 0460	1530	1324	1514	1480	1712	1415	1748
CD44# 0439 neu	33.3	33.3	202	33.3	33.3	109	81
CDKN2B (p15 INK4B, CDN2B, MTS2)# 2142	33.3	33.3	33.3	33.3	33.3	33.3	33.3
Cyclin B1# 1243	25061	17275	2329	41570	19149	19963	16106
Cytokeratin 18 (DC10)# 1122	250773	137025	193990	239129	162853	155100	161439
Cytokeratin 19# 0473	32558	75115	124633	16732	76688	64617	46290
Cytokeratin 8 - phosphoSer23# 0217	146308	95962	156705	65970	119573	212184	126723
Cytokeratin 8/18# 1208	43346	11939	24295	41278	15453	14345	15848
Cytokeratin Pan (4, 5, 6, 8, 10, 13, 18)# 1779	366470	193600	278307	366745	220552	247129	213117
DUSP6 (MKP3, MKP-3, PYST1)# 1754	1564	225	129	1717	1253	1529	1875
E-Cadherin - phosphoSer838/Ser840# 0203	14098	9761	18993	11535	14502	20403	12127
E-Cadherin# 0742 neu	3281	2415	4569	2812	3948	5268	3722
E-Cadherin# 0742 Peak 2 neu	393	167	421	439	163	348	476
EGR1# 1226 neu	33.3	33.3	33.3	33.3	33.3	33.3	70
Elk-1 - phosphoSer383# 1826	390	295	385	372	177	140	33.3
Elk-1 - phosphoSer383# 1826 Peak 2	337	502	867	110	431	542	388
Elk-1# 2160	602	391	543	539	445	549	524
Erk1/2 (MAPK p44/42) # 1718	18548	15252	16953	21366	17322	17002	12242
Erk1/2 (MAPK p44/42) # 1718 Peak 2	7156	6672	8296	8817	6971	7558	6829
ERK1/2 (MAPK) - phosphoThr202/Tyr204# 2205	64	58	95	289	262	143	119
ERK1/2 (MAPK) - phosphoThr202/Tyr204# 2205 Peak 2	33.3	33.3	73	126	33.3	87	33.3
Ezh2# 1759	3923	5321	3110	5538	4274	4151	4054
FGF-1# 1562	88	33.3	150	33.3	33.3	74	33.3
GADD45 alpha# 1201	335	133	352	277	115	304	397
GAPDH# 2058	277169	262041	259568	271379	269941	263567	282206
Glutaminsynthetase# 0486	100756	89887	93900	97598	87646	99944	105428
GPR49 / LGR5# 1868 neu	286	214	388	189	302	324	333
GSK3 alpha/beta - phosphoSer21/Ser9BG/MP # 118	17432	2051	844	1097	3102	2506	17374
GSK3 alpha/beta - phosphoSer21/Ser9BG/MP # 118 Peak 2	1054	219	349	889	350	606	269
GSK3 alpha/beta - phosphoTyr279/Tyr216# 1714	504	371	249	823	499	524	442
GSK3 alpha/beta - phosphoTyr279/Tyr216# 1714 Peak 2	602	579	525	573	620	700	883
GSK3 beta - phosphoSer9# 2073	1439	247	443	1213	345	993	302
GSK3 beta - phosphoSer9# 2073 Peak 2	173	33.3	33.3	263	67	114	33.3
GSK3 beta# 1835	7956	7155	7110	8628	7171	8716	11005
Ha-ras# 2135	524	360	495	534	422	466	390
Her2# 1063	569	307	818	348	385	624	490
Histone H3 - phosphoSer10# 1610	116944	22455	2427	73655	30433	66965	15040
HSP 27 - phosphoSer15# 0208	984	431	890	1710	481	1166	387
IDH1 (Isocitrate dehydrogenase [NADP] cytoplasmic)# 1316	5824	7795	8570	5984	7423	7657	5375
IGFBP-1# 1084	19844	5704	22473	19872	7414	17722	23589
Jak 1TK # 071	3549	6470	6558	234	6456	5516	7356
Jak 1TK # 071 Peak 2	123	137	152	177	169	193	200
JNK/SAPK 1/2/3 - phosphoTyr185/Tyr223# 0215	442	312	200	959	274	274	310
MCM2# 2125	33944	34511	32080	41121	40666	39155	37463
MEK 1# 1790	3760	1808	1378	3351	1854	2684	2746
MEK1/2 - phosphoSer217/Ser221# 1720	988	815	3465	771	166	552	121
MEK2# 1789	2194	1487	1494	2234	1375	1758	1815
MEKK3# 0255	177	145	146	183	107	167	72

mTor - phosphoSer2448# 2374	387	160	264	401	258	345	356
mTOR (FRAP)- phosphoSer2481# 0386	33.3	33.3	33.3	64	33.3	33.3	51
mTOR (FRAP)# 1911	983	670	873	1294	766	979	637
NDRG1 - phosphoThr346# 1181	2291	1777	14368	2747	2063	2337	1458
p38 MAPK - phosphoThr180/Tyr182# 1223	2137	351	476	1636	582	1013	306
p38 MAPK# 0350	527	542	539	608	542	575	336
p53 - acetylLys305# 1274	33.3	33.3	33.3	67	33.3	62	33.3
p53 # 2123	9638	7746	7151	12568	8393	10602	9041
p70 S6 kinase# 1566 neu	6196	4981	4212	6434	4412	4196	5445
PAK 4/5/6 - phosphoSer474/Ser602/Ser560# 1495	736	536	900	926	575	1024	1190
PARP - cleavedAsp214# 1044	84	137	33.3	139	251	33.3	101
PARP# 1914 neu	2378	2961	3539	4171	4600	5497	5200
PI3-kinase p110 beta# 1049	830	931	845	1116	927	847	757
PI3-kinase p85 alpha# 1967	122	198	123	136	147	125	80
PI3-kinase p85TK # 017	417	639	655	589	604	484	470
PP2A C - phosphoTyr307# 2170 neu	1051	33.3	1074	608	33.3	893	1324
PTEN - phosphoSer380# 1045	771	577	642	1010	619	661	870
PTEN - phosphoSer380# 1045 Peak 2	369	313	433	391	352	326	706
PTEN# 1770	2377	1638	2434	3077	1882	2039	2642
PTEN# 1770 Peak 2	1450	1169	1407	1361	1202	1208	1479
Ras# 1719	1116	756	3515	1075	712	1121	1528
Rb - phosphoSer807/Ser811# 1270	4977	2585	1073	4474	3309	6161	1550
RbBG/MP # 046	1039	2151	1269	1419	3071	2272	1139
RSK 1 (p90RSK) - phosphoThr573# 1235	156	80	147	107	33.3	141	314
RSK 1 (p90RSK) # 0246 neu	1801	1135	1769	1430	1458	1747	1615
S6 ribosomal protein - phosphoSer235/Ser236# 0442	25630	2076	1563	19107	6069	16186	1190
S6 ribosomal protein - phosphoSer240/Ser244BG/MP # 055	48149	4321	2969	27723	11972	28207	2309
S6 ribosomal protein# 1836	21898	4707	11546	19140	5707	15107	9481
SHP-2# 0239	2717	2672	3182	3777	2914	3183	3729
Smad1/5 - phosphoSer463/Ser465# 2590	1979	2848	1399	3061	3460	1413	1305
Smad1# 0955	2311	1618	1839	3175	1495	1693	1947
Smad2 - phosphoSer245/Ser250/Ser255TK # 101	436	583	90	614	659	332	174
Smad2/3 - phosphoSer465/467 (Smad2) Ser423/425 (Smad3)# 2591	171	100	436	108	271	33	33
Smad2/3 - phosphoSer465/467 (Smad2) Ser423/425 (Smad3)# 2591 Peak 2	33	83	478	51	200	33	497
Smad2# 1530	1695	1228	1298	2679	1181	1303	1305
Smad3# 1553	339	245	353	480	255	259	533
SMAD4# 1552	1181	1292	1183	1221	1337	753	1581
Smad5# 0954	239	170	157	437	216	415	202
Smad9 (Smad8)# 0916	220	365	760	174	373	2834	90
SPRY1 (Spry-1, Sprouty 1)# 0415	132	156	204	160	148	185	201
SPRY2 (Protein sprouty homolog 2)# 0342	7216	3698	3430	5371	4704	5399	3200
SPRY3 (Spry-3, Sprouty 3)# 1723	90055	44925	75694	89508	52773	74093	66019
Src - phosphoTyr527# 1949	21135	17990	23143	21720	18304	17826	16954
STAT 1# 1186	426	463	405	485	429	452	743
STAT 3 alpha# 1207	7159	8181	12781	8357	8151	9363	8848
STAT 3# 1818	2717	2753	4427	3278	2785	3164	3317
STAT 5 alpha# 1245	457	760	1227	678	644	629	768
STAT 5# 1780	318	372	487	287	324	339	313
TCF1# 1673	1515	1420	1341	1478	1247	1851	2037
TCF4# 1641	5618	9469	13438	288	7292	8946	9599
TwistBG/MP # 064	5862	1257	2245	3420	1123	2803	1961
Vimentin# 1814	389	437	295	338	396	326	332
Wnt3A# 0741	5914	4495	6290	6756	4414	5897	4531
Wnt3A# 0741 Peak 2	4038	1316	6218	4248	1409	4579	7319
zzstrep	3222726	1735692	2988437	3090157	1535089	3118900	3144587

Suppl. Table 8: Raw data of the DigiWest® experiment - R4^{wt}.

Relative intensity unit of each analyte tested for R4^{wt}, which was treated with trametinib [0.03 µM] and DMSO [0.03%] for 0.5 h, 6 h and 24 h.

Analyt	**Trametinib 0.5 h**	**Trametinib 6 h**	**Trametinib 24 h**	**DMSO 0.5 h**	**DMSO 6 h**	**DMSO 24 h**	**Medium only 24 h**
Akt - phosphoSer473# 2072	33.3	33.3	33.3	57	33.3	33.3	33.3
Akt# 2082	2957	3459	3410	3767	3812	3711	3720
Akt1# 1364	33.3	33.3	33.3	669	33.3	565	611
Akt2 - phosphoSer474# 2020	33.3	33.3	33.3	33.3	33.3	33.3	33.3
Akt3# 1365	33.3	33.3	33.3	33.3	33.3	33.3	33.3
Annexin II# 0504	8780	16301	14245	16025	21193	19000	18066
APCTK # 025 neu	33.3	74	33.3	33.3	78	55	33.3
Aurora A (AIK)	494	1085	535	1297	982	548	625
Aurora A/B/C - phosphoThr288/Thr232/Thr198	74	72	33	104	81	33	33
Aurora B (AIM1)	781	832	678	1344	1083	747	686
Axin1# 1683 neu	124	159	95	80	209	186	157
Axin2 (Conductin)# 0956 neu	132	152	110	82	174	79	90
b-Raf - phosphoSer445# 1171	691	1099	763	831	1274	1072	1230
Bcl-xL# 1819	3570	5119	4383	3384	6246	6425	4597

Bcl2# 1821	310	464	478	209	751	565	212
beta-Actin# 2104	170577	214756	189279	219302	250983	243022	221423
beta-Catenin - phosphoSer552# 1862	247	242	238	294	450	146	98
beta-Catenin - phosphoSer552# 1862 Peak 2	236	400	290	248	621	249	252
beta-Catenin - phosphoSer675# 2091	1734	2668	2472	4234	3059	2556	3041
beta-Catenin - phosphoSer675# 2091 Peak 2	2850	4955	4547	3676	6114	4882	7008
beta-Catenin (non-pospho Ser33/37/Thr41; active) # 1356	4678	9465	6842	2670	11376	8258	10464
beta-Catenin# 1822	24837	31566	28472	41154	37993	31530	38370
beta-Catenin# 1822 Peak 2	22117	31333	27340	26518	36378	32746	43763
Bmi1# 1457	5366	6473	4102	3868	6320	6106	4435
BMP4# 0936	422	908	878	945	1116	1315	1263
c-Jun - phosphoSer63# 1948	81	93	33.3	135	33.3	33.3	33.3
c-myc - phosphoThr58/Ser62# 1240	338	371	141	247	639	322	332
c-myc# 1717	3546	4624	3543	7358	8443	3702	3833
c-Raf - phosphoSer259# 1190	2068	2543	1875	2709	3933	2527	1960
c-RafTK # 029	536	678	575	592	858	742	653
C/EBP beta - phosphoThr235# 1183	33.3	33.3	33.3	33.3	33.3	33.3	33.3
C/EBP beta - phosphoThr235# 1183 Peak 2	33.3	33.3	228	33.3	33.3	33.3	33.3
Caseinkinase 1 epsilon# 0340	53	82	53	33.3	63	56	33.3
Caspase 3# 1996	13547	17031	14561	10618	19002	14457	12477
Caspase 8BG/MP # 074	193	245	175	138	306	195	105
Caspase 8BG/MP # 074 Peak 2	78	33.3	83	85	33.3	33.3	33.3
Caspase 9# 1551	2209	2832	1751	881	3421	3776	1212
Caspase 9# 1551 Peak 2	428	562	722	424	796	705	545
CD133# 0460	565	512	385	690	719	556	695
CD44# 0439 neu	33.3	33.3	164	106	33.3	167	52
CDKN2B (p15 INK4B, CDN2B, MTS2)# 2142	33.3	33.3	33.3	33.3	33.3	33.3	33.3
Cyclin B1# 1243	16000	16300	5148	14696	15295	9940	8691
Cytokeratin 18 (DC10)# 1122	102189	67311	62565	154230	88031	111457	80467
Cytokeratin 19# 0473	25988	46744	51498	18146	67364	58858	39609
Cytokeratin 8 - phosphoSer23# 0217	64483	42970	45588	65776	52802	44882	48033
Cytokeratin 8/18# 1208	11865	4599	4324	23154	6084	8928	5183
Cytokeratin Pan (4, 5, 6, 8, 10, 13, 18)# 1779	193703	159496	114551	246661	149923	177424	123145
DUSP6 (MKP3, MKP-3, PYST1)# 1754	1393	450	264	2084	1615	1826	2026
E-Cadherin - phosphoSer838/Ser840# 0203	10154	19980	13351	15196	21481	15527	18796
E-Cadherin# 0742 neu	1905	3746	2624	3410	3968	3375	4553
E-Cadherin# 0742 Peak 2 neu	33.3	134	33.3	33.3	334	70	117
EGR1# 1226 neu	33.3	33.3	33.3	33.3	76	33.3	33.3
Elk-1 - phosphoSer383# 1826	84	124	127	228	120	111	158
Elk-1 - phosphoSer383# 1826 Peak 2	225	462	199	151	372	455	289
Elk-1# 2160	291	418	314	513	509	512	448
Erk1/2 (MAPK p44/42) # 1718	16498	21152	17601	16555	27409	22224	18253
Erk1/2 (MAPK p44/42) # 1718 Peak 2	11173	14591	14175	10603	15656	17110	14497
ERK1/2 (MAPK) - phosphoThr202/Tyr204# 2205	33.3	33.3	63	342	321	115	117
ERK1/2 (MAPK) - phosphoThr202/Tyr204# 2205 Peak 2	33.3	51	33.3	181	206	92	74
Ezh2# 1759	2032	2842	1403	2667	3475	2772	2623
FGF-1# 1562	116	156	117	115	120	142	54
GADD45 alpha# 1201	292	517	451	402	591	428	586
GAPDH# 2058	148876	205068	225977	279193	263154	233546	247145
Glutaminsynthetase# 0486	80842	109128	95826	95639	121531	119827	115162
GPR49 / LGR5# 1868 neu	129	241	178	335	383	238	448
GSK3 alpha/beta - phosphoSer21/Ser9BG/MP # 118	11922	1093	121	5098	2201	210	1076
GSK3 alpha/beta - phosphoSer21/Ser9BG/MP # 118 Peak 2	163	294	165	704	426	124	377
GSK3 alpha/beta - phosphoTyr279/Tyr216# 1714	327	477	311	435	391	321	363
GSK3 alpha/beta - phosphoTyr279/Tyr216# 1714 Peak 2	706	1271	895	969	1223	1021	1610
GSK3 beta - phosphoSer9# 2073	233	400	264	703	560	175	372
GSK3 beta - phosphoSer9# 2073 Peak 2	33.3	33.3	33.3	59	72	33.3	33.3
GSK3 beta# 1835	9583	14041	10603	10849	14593	12011	17027
Ha-ras# 2135	331	454	342	320	492	435	463
Her2# 1063	248	676	289	559	1057	533	655
Histone H3 - phosphoSer10# 1610	41064	24140	2122	23621	35031	3958	2356
HSP 27 - phosphoSer15# 0208	944	1357	487	3846	1528	400	848
IDH1 (Isocitrate dehydrogenase [NADP] cytoplasmic)# 1316	3568	6082	6657	5356	7352	6664	6268
IGFBP-1# 1084	5050	10149	5520	6357	12765	14578	15685
Jak 1TK # 071	1308	2942	2369	452	4440	4228	4316
Jak 1TK # 071 Peak 2	90	136	142	296	262	199	237
JNK/SAPK 1/2/3 - phosphoTyr185/Tyr223# 0215	230	240	67	460	224	90	128
MCM2# 2125	24078	38281	28774	48309	46985	41287	38337
MEK 1# 1790	1956	3118	1795	2072	3505	3463	3709
MEK1/2 - phosphoSer217/Ser221# 1720	232	1626	1690	661	584	301	555
MEK2# 1789	996	1446	1135	1048	1649	1595	2061
MEKK3# 0255	136	209	146	101	207	208	133
mTor - phosphoSer2448# 2374	33.3	479	70	437	2277	324	522
mTOR (FRAP)- phosphoSer2481# 0386	33.3	33.3	33.3	33.3	33.3	33.3	33.3
mTOR (FRAP)# 1911	33.3	635	214	1318	2544	751	1617
NDRG1 - phosphoThr346# 1181	1587	5665	4167	1852	9548	2117	2522

p38 MAPK - phosphoThr180/Tyr182# 1223	344	389	175	698	474	141	194
p38 MAPK# 0350	504	655	543	441	708	578	500
p53 - acetylLys305# 1274	33.3	33.3	33.3	33.3	33.3	33.3	33.3
p53 # 2123	5917	6672	7298	6748	6240	10059	9181
p70 S6 kinase# 1566 neu	2512	3254	3787	5292	5588	5142	3443
PAK 4/5/6 - phosphoSer474/Ser602/Ser560# 1495	514	686	661	775	741	722	999
PARP - cleavedAsp214# 1044	128	165	86	136	195	198	243
PARP# 1914 neu	1570	4463	2601	7079	7694	5104	11492
PI3-kinase p110 beta# 1049	569	1028	1309	1914	1608	1855	1359
PI3-kinase p85 alpha# 1967	142	209	156	161	232	180	143
PI3-kinase p85TK # 017	580	1047	833	577	992	909	865
PP2A C - phosphoTyr307# 2170 neu	442	610	653	512	443	33.3	413
PTEN - phosphoSer380# 1045	581	562	691	931	585	678	889
PTEN - phosphoSer380# 1045 Peak 2	389	509	371	502	563	385	567
PTEN# 1770	1472	1691	2203	2331	2221	2078	2363
PTEN# 1770 Peak 2	1032	1503	1142	1211	1728	1154	1648
Ras# 1719	940	1266	1719	1155	1455	1530	1782
Rb - phosphoSer807/Ser811# 1270	1123	1913	1678	1894	2145	1623	1599
RbBG/MP # 046	830	1594	1476	2931	2087	1146	1326
RSK 1 (p90RSK) - phosphoThr573# 1235	57	33.3	33.3	149	78	68	176
RSK 1 (p90RSK) # 0246 neu	1418	2288	2440	2601	2753	3550	3846
S6 ribosomal protein - phosphoSer235/Ser236# 0442	8170	14059	422	10847	29400	4430	2591
S6 ribosomal protein - phosphoSer240/Ser244BG/MP # 055	17736	33985	834	14052	61413	8501	3215
S6 ribosomal protein# 1836	7338	12744	5393	5777	13092	12892	4726
SHP-2# 0239	1404	1970	1869	2141	2394	2114	2572
Smad1/5 - phosphoSer463/Ser465# 2590	1011	924	841	2528	1123	517	918
Smad1# 0955	1088	1420	910	1855	1390	1179	1732
Smad2 - phosphoSer245/Ser250/Ser255TK # 101	537	424	246	1530	515	251	390
Smad2/3 - phosphoSer465/467 (Smad2) Ser423/425 (Smad3)# 2591	33	33	33	33	33	562	168
Smad2/3 - phosphoSer465/467 (Smad2) Ser423/425 (Smad3)# 2591 Peak 2	33	104	1092	33	127	544	582
Smad2# 1530	2608	2419	2391	3586	2668	2123	2660
Smad3# 1553	201	219	248	344	256	284	310
SMAD4# 1552	742	1253	1120	1294	1593	1535	1853
Smad5# 0954	100	138	83	125	125	33.3	55
Smad9 (Smad8)# 0916	664	2191	1349	297	3424	4701	1827
SPRY1 (Spry-1, Sprouty 1)# 0415	73	114	111	196	217	101	170
SPRY2 (Protein sprouty homolog 2)# 0342	1990	3339	1881	3337	5007	3584	2361
SPRY3 (Spry-3, Sprouty 3)# 1723	33566	48617	37132	47610	64309	57375	44166
Src - phosphoTyr527# 1949	9558	11484	12761	12897	11829	12261	11079
STAT 1# 1186	391	509	367	521	560	455	651
STAT 3 alpha# 1207	5511	7521	7275	6113	8761	6907	7889
STAT 3# 1818	1989	2503	2311	2332	2909	2181	2712
STAT 5 alpha# 1245	169	261	433	274	359	293	334
STAT 5# 1780	151	283	170	154	305	238	164
TCF1# 1673	657	1075	638	922	886	780	1025
TCF4# 1641	1191	3306	2563	473	6395	8319	3675
TwistBG/MP # 064	1517	3387	2051	2491	2959	4375	2030
Vimentin# 1814	243	341	378	228	380	552	309
Wnt3A# 0741	3267	5033	3308	3010	6151	4738	4458
Wnt3A# 0741 Peak 2	1161	2669	1366	1187	3341	3775	4645
zzstrep	2147831	2590959	1929747	1868142	2229972	2813101	2486576

Suppl. Table 9: Raw data of the DigiWest® experiment - clone A.

Relative intensity unit of each analyte tested for clone A, which was treated with trametinib [0.03 µM] and DMSO [0.03%] for 0.5 h, 6 h and 24 h.

Analyt	**Trametinib 0.5 h**	**Trametinib 6 h**	**Trametinib 24 h**	**DMSO 0.5 h**	**DMSO 6 h**	**DMSO 24 h**	**Medium only 24 h**
Akt - phosphoSer473# 2072	33.3	33.3	33.3	33.3	33.3	51	74
Akt# 2082	3535	3944	4304	4401	4620	4472	4251
Akt1# 1364	33.3	33.3	939	552	33.3	610	938
Akt2 - phosphoSer474# 2020	33.3	33.3	33.3	33.3	33.3	33.3	33.3
Akt3# 1365	33.3	33.3	33.3	33.3	33.3	33.3	33.3
Annexin II# 0504	8615	9444	10464	10856	11603	10667	8835
APCTK # 025 neu	65	33.3	33.3	67	33.3	33.3	33.3
Aurora A (AIK)	1661	1937	210	1440	1771	1228	1292
Aurora A/B/C - phosphoThr288/Thr232/Thr198	153	83	56	64	78	33	66
Aurora B (AIM1)	1772	1766	339	1463	1945	1258	1416
Axin1# 1683 neu	110	89	153	112	113	224	214
Axin2 (Conductin)# 0956 neu	90	202	232	151	96	187	190
b-Raf - phosphoSer445# 1171	1127	1143	1033	1136	1131	1404	1334
Bcl-xL# 1819	8997	9179	9946	9031	7636	10777	9110
Bcl2# 1821	338	519	560	443	512	552	261
beta-Actin# 2104	197929	213301	209143	213838	240626	244235	224336
beta-Catenin - phosphoSer552# 1862	582	522	168	652	578	253	256
beta-Catenin - phosphoSer552# 1862 Peak 2	513	381	120	630	410	129	178

beta-Catenin - phosphoSer675# 2091	7083	5880	6643	7232	4864	7026	6728
beta-Catenin - phosphoSer675# 2091 Peak 2	3613	3712	5274	3546	3586	4495	4855
beta-Catenin (non-pospho Ser33/37/Thr41; active) # 1356	5803	5165	5048	5973	5504	6076	7643
beta-Catenin# 1822	66327	60317	61194	63018	55231	71248	71513
beta-Catenin# 1822 Peak 2	27465	27341	33196	27760	27592	36355	37672
Bmi1# 1457	6723	7109	6996	7821	7828	7767	6698
BMP4# 0936	409	552	927	329	956	1041	826
c-Jun - phosphoSer63# 1948	82	253	224	78	116	205	85
c-myc - phosphoThr58/Ser62# 1240	556	230	186	616	604	621	400
c-myc# 1717	5992	4073	3279	6940	6269	4262	5297
c-Raf - phosphoSer259# 1190	4283	2941	2063	2926	3726	1631	1602
c-RafTK # 029	344	379	301	432	483	294	337
C/EBP beta - phosphoThr235# 1183	33.3	76	33.3	55	33.3	33.3	33.3
C/EBP beta - phosphoThr235# 1183 Peak 2	33.3	33.3	33.3	33.3	33.3	33.3	33.3
Caseinkinase 1 epsilon# 0340	33.3	65	33.3	33.3	33.3	72	33.3
Caspase 3# 1996	17394	19228	15635	18880	22384	17003	18964
Caspase 8BG/MP # 074	208	174	141	221	172	174	58
Caspase 8BG/MP # 074 Peak 2	128	33.3	33.3	238	33.3	33.3	33.3
Caspase 9# 1551	1455	1477	978	1418	1695	1555	1510
Caspase 9# 1551 Peak 2	586	766	739	657	643	806	654
CD133# 0460	1021	765	1078	1178	1466	1256	1488
CD44# 0439 neu	33.3	33.3	67	33.3	33.3	91	33.3
CDKN2B (p15 INK4B, CDN2B, MTS2)# 2142	33.3	33.3	33.3	33.3	51	33.3	33.3
Cyclin B1# 1243	20298	17262	1680	26174	13546	10604	14528
Cytokeratin 18 (DC10)# 1122	229037	154995	158995	290055	185582	157576	161834
Cytokeratin 19# 0473	65805	85996	71953	49371	70751	62667	61166
Cytokeratin 8 - phosphoSer23# 0217	156107	130884	150141	91385	154125	135881	138534
Cytokeratin 8/18# 1208	32154	13334	18613	48420	17954	15824	16765
Cytokeratin Pan (4, 5, 6, 8, 10, 13, 18)# 1779	314063	203950	209860	382363	254299	198563	215365
DUSP6 (MKP3, MKP-3, PYST1)# 1754	1375	395	210	1599	901	1931	1715
E-Cadherin - phosphoSer838/Ser840# 0203	10875	20264	16918	14404	19523	15044	15088
E-Cadherin# 0742 neu	2521	5171	4762	3772	5093	4937	5060
E-Cadherin# 0742 Peak 2 neu	133	180	349	301	304	387	290
EGR1# 1226 neu	33.3	33.3	33.3	33.3	33.3	33.3	33.3
Elk-1 - phosphoSer383# 1826	163	226	231	325	194	196	153
Elk-1 - phosphoSer383# 1826 Peak 2	209	334	274	33.3	318	380	370
Elk-1# 2160	343	349	432	391	452	620	424
Erk1/2 (MAPK p44/42) # 1718	22881	24476	20001	23372	34918	22701	21812
Erk1/2 (MAPK p44/42) # 1718 Peak 2	5946	5611	4795	5192	6386	5019	5172
ERK1/2 (MAPK) - phosphoThr202/Tyr204# 2205	84	63	230	322	167	487	238
ERK1/2 (MAPK) - phosphoThr202/Tyr204# 2205 Peak 2	33.3	33.3	78	95	33.3	95	33.3
Ezh2# 1759	4329	4380	3480	4420	4158	5102	4650
FGF-1# 1562	33.3	33.3	33.3	33.3	101	33.3	33.3
GADD45 alpha# 1201	208	337	465	293	371	528	568
GAPDH# 2058	177410	191460	227284	195748	172225	266816	250612
Glutaminsynthetase# 0486	75048	83253	87628	77800	94703	97089	96994
GPR49 / LGR5# 1868 neu	282	194	367	250	295	339	264
GSK3 alpha/beta - phosphoSer21/Ser9BG/MP # 118	27876	12851	1226	5727	29603	4372	11602
GSK3 alpha/beta - phosphoSer21/Ser9BG/MP # 118 Peak 2	272	214	240	193	304	257	450
GSK3 alpha/beta - phosphoTyr279/Tyr216# 1714	495	416	411	551	449	379	467
GSK3 alpha/beta - phosphoTyr279/Tyr216# 1714 Peak 2	348	545	583	339	513	921	707
GSK3 beta - phosphoSer9# 2073	267	248	287	198	164	298	288
GSK3 beta - phosphoSer9# 2073 Peak 2	33.3	33.3	33.3	99	33.3	33.3	33.3
GSK3 beta# 1835	4874	6841	7753	5535	7383	11495	9520
Ha-ras# 2135	477	529	507	539	500	575	584
Her2# 1063	503	620	1086	646	801	709	621
Histone H3 - phosphoSer10# 1610	172535	113885	1758	84581	117431	32180	38368
HSP 27 - phosphoSer15# 0208	521	595	707	729	863	469	470
IDH1 (Isocitrate dehydrogenase [NADP] cytoplasmic)# 1316	4296	6783	8575	4170	7440	8860	7123
IGFBP-1# 1084	5111	5600	18450	7063	6581	24398	18395
Jak 1TK # 071	2878	3503	5018	1320	8841	5255	5585
Jak 1TK # 071 Peak 2	160	168	275	176	229	260	276
JNK/SAPK 1/2/3 - phosphoTyr185/Tyr223# 0215	163	251	123	312	248	125	254
MCM2# 2125	34279	34961	31077	39886	45902	43734	42873
MEK 1# 1790	2096	2150	1546	2444	2515	2703	2600
MEK1/2 - phosphoSer217/Ser221# 1720	687	1695	4064	340	256	317	322
MEK2# 1789	1283	1556	1278	1322	1321	2130	1873
MEKK3# 0255	96	91	131	124	145	161	151
mTor - phosphoSer2448# 2374	1305	662	157	1390	1642	192	389
mTOR (FRAP)- phosphoSer2481# 0386	33.3	33.3	33.3	33.3	33.3	33.3	33.3
mTOR (FRAP)# 1911	1458	909	796	1571	1822	704	1509
NDRG1 - phosphoThr346# 1181	629	718	2212	466	1346	1188	880
p38 MAPK - phosphoThr180/Tyr182# 1223	577	407	168	421	326	260	285
p38 MAPK# 0350	434	401	306	423	472	404	398
p53 - acetylLys305# 1274	33.3	33.3	33.3	33.3	33.3	33.3	33.3
p53 # 2123	10601	9765	10796	12845	12093	8580	11323
p70 S6 kinase# 1566 neu	3727	3236	4239	3994	4107	4316	3890

PAK 4/5/6 - phosphoSer474/Ser602/Ser560# 1495	455	482	925	418	411	814	561
PARP - cleavedAsp214# 1044	33.3	51	190	33.3	82	105	108
PARP# 1914 neu	5407	5162	4723	5243	4919	4954	7916
PI3-kinase p110 beta# 1049	649	495	743	728	975	683	741
PI3-kinase p85 alpha# 1967	130	137	139	178	128	162	186
PI3-kinase p85TK # 017	566	613	702	604	979	697	600
PP2A C - phosphoTyr307# 2170 neu	33.3	33.3	211	33.3	33.3	533	323
PTEN - phosphoSer380# 1045	469	438	876	549	552	1013	977
PTEN - phosphoSer380# 1045 Peak 2	382	446	579	425	504	665	878
PTEN# 1770	1645	1867	2285	2013	1907	2667	2717
PTEN# 1770 Peak 2	1358	1493	1423	1364	1634	1530	1752
Ras# 1719	782	942	3509	980	807	1761	1317
Rb - phosphoSer807/Ser811# 1270	4252	4320	602	4997	4034	2834	3426
RbBG/MP # 046	1134	1686	1253	2472	1816	1918	2258
RSK 1 (p90RSK) - phosphoThr573# 1235	57	60	402	80	69	351	362
RSK 1 (p90RSK) # 0246 neu	2151	2305	2302	2468	2967	2718	2694
S6 ribosomal protein - phosphoSer235/Ser236# 0442	11005	6835	759	12539	13489	12291	9895
S6 ribosomal protein - phosphoSer240/Ser244BG/MP # 055	20968	14362	1232	26109	23238	26858	19922
S6 ribosomal protein# 1836	7731	11792	3450	10559	11474	17740	8412
SHP-2# 0239	2429	2313	3439	2555	2391	3435	2652
Smad1/5 - phosphoSer463/Ser465# 2590	2122	2066	2538	2648	2221	1828	2385
Smad1# 0955	1525	1591	2107	1970	1910	2034	2284
Smad2 - phosphoSer245/Ser250/Ser255TK # 101	664	666	124	809	464	537	625
Smad2/3 - phosphoSer465/467 (Smad2) Ser423/425 (Smad3)# 2591	33	33	368	66	33	33	33
Smad2/3 - phosphoSer465/467 (Smad2) Ser423/425 (Smad3)# 2591 Peak 2	33	95	388	33	33	587	559
Smad2# 1530	1847	1948	1971	2890	1501	2324	2134
Smad3# 1553	250	295	554	313	270	365	449
SMAD4# 1552	2205	2081	2210	2130	2037	2384	2769
Smad5# 0954	200	229	64	290	172	87	108
Smad9 (Smad8)# 0916	601	849	742	396	1119	395	287
SPRY1 (Spry-1, Sprouty 1)# 0415	119	121	147	128	146	181	166
SPRY2 (Protein sprouty homolog 2)# 0342	3251	3162	2751	3146	4678	4899	3669
SPRY3 (Spry-3, Sprouty 3)# 1723	46480	51843	49945	52373	49242	58033	53043
Src - phosphoTyr527# 1949	19201	21251	23406	23488	22858	20172	19963
STAT 1# 1186	545	543	617	585	545	754	866
STAT 3 alpha# 1207	7583	7620	9938	8313	11438	8472	8527
STAT 3# 1818	2635	2574	3846	2893	3969	3154	3204
STAT 5 alpha# 1245	395	512	1171	448	748	652	655
STAT 5# 1780	279	310	429	271	753	337	334
TCF1# 1673	2235	2838	2605	1963	1529	3406	3002
TCF4# 1641	3379	3492	7130	1173	4953	7104	5284
TwistBG/MP # 064	1086	2070	1587	1769	2597	3857	2210
Vimentin# 1814	256	294	236	275	880	295	284
Wnt3A# 0741	3303	2899	4609	3395	3853	3644	3706
Wnt3A# 0741 Peak 2	1326	1288	4256	1682	1787	5576	5938
zzstrep	2179797	2530355	2329644	2574829	2551624	3209437	2718893

Suppl. Table 10: Raw data of the DigiWest® experiment – clone B.

Relative intensity unit of each analyte tested for clone B, which was treated with trametinib [0.03 µM] and DMSO [0.03%] for 0.5 h, 6 h and 24 h.

Analyt	**Trametinib 0.5 h**	**Trametinib 6 h**	**Trametinib 24 h**	**DMSO 0.5 h**	**DMSO 6 h**	**DMSO 24 h**	**Medium only 24 h**
Akt - phosphoSer473# 2072	33.3	33.3	33.3	33.3	33.3	33.3	33.3
Akt# 2082	3568	4357	3946	4244	4551	3659	4036
Akt1# 1364	33.3	685	576	552	547	651	544
Akt2 - phosphoSer474# 2020	33.3	33.3	33.3	33.3	33.3	33.3	33.3
Akt3# 1365	33.3	33.3	33.3	33.3	33.3	33.3	33.3
Annexin II# 0504	11045	11583	15738	11749	15236	12549	11630
APCTK # 025 neu	33.3	33.3	33.3	53	82	33.3	33.3
Aurora A (AIK)	1564	2006	191	1949	1566	1157	1431
Aurora A/B/C - phosphoThr288/Thr232/Thr198	85	131	33	82	33	78	161
Aurora B (AIM1)	1452	1694	193	1749	1662	1335	1630
Axin1# 1683 neu	168	133	170	185	169	196	192
Axin2 (Conductin)# 0956 neu	246	209	348	225	258	252	186
b-Raf - phosphoSer445# 1171	1049	1354	1170	1575	1418	1333	1358
Bcl-xL# 1819	15969	12398	17507	10919	12944	11556	8971
Bcl2# 1821	665	552	1533	471	679	845	226
beta-Actin# 2104	251348	194175	279999	212841	236381	244289	210225
beta-Catenin - phosphoSer552# 1862	334	518	105	572	856	273	327
beta-Catenin - phosphoSer552# 1862 Peak 2	203	494	130	574	645	152	269
beta-Catenin - phosphoSer675# 2091	7076	7606	5820	7699	7854	7595	7867
beta-Catenin - phosphoSer675# 2091 Peak 2	3880	5405	6110	5748	4663	5923	6678
beta-Catenin (non-pospho Ser33/37/Thr41; active) # 1356	5352	7791	7984	10320	7725	8649	11612

beta-Catenin# 1822	69835	63863	62636	67777	68490	77941	75694
beta-Catenin# 1822 Peak 2	29416	33486	41780	38483	34177	43420	49371
Bmi1# 1457	11681	7388	10765	7441	8752	8280	6612
BMP4# 0936	543	720	1247	620	393	1007	736
c-Jun - phosphoSer63# 1948	78	266	90	79	81	61	151
c-myc - phosphoThr58/Ser62# 1240	511	251	244	463	501	465	396
c-myc# 1717	2969	4042	14438	6580	4521	10830	3231
c-Raf - phosphoSer259# 1190	5058	5700	2069	4372	4458	2751	1986
c-RafTK # 029	677	523	443	499	525	413	408
C/EBP beta - phosphoThr235# 1183	58	81	76	83	62	33.3	33.3
C/EBP beta - phosphoThr235# 1183 Peak 2	33.3	33.3	33.3	33.3	33.3	33.3	33.3
Caseinkinase 1 epsilon# 0340	556	194	744	208	33.3	254	150
Caspase 3# 1996	26755	25753	25766	24331	27430	24831	24326
Caspase 8BG/MP # 074	378	272	64	250	205	73	79
Caspase 8BG/MP # 074 Peak 2	88	56	122	33.3	299	142	64
Caspase 9# 1551	1946	2004	2355	1927	2003	2025	1372
Caspase 9# 1551 Peak 2	960	708	1257	766	793	759	439
CD133# 0460	1159	1129	1347	1215	1220	1707	1679
CD44# 0439 neu	33.3	33.3	145	33.3	33.3	130	33.3
CDKN2B (p15 INK4B, CDN2B, MTS2)# 2142	33.3	33.3	33.3	33.3	33.3	33.3	33.3
Cyclin B1# 1243	9959	17789	944	12016	16928	8068	9434
Cytokeratin 18 (DC10)# 1122	284160	224721	211338	226830	312920	224034	216859
Cytokeratin 19# 0473	59224	108202	69446	108577	59421	74141	67182
Cytokeratin 8 - phosphoSer23# 0217	167990	152869	178111	147229	141118	213762	128427
Cytokeratin 8/18# 1208	46090	30584	28920	26931	51525	29927	26797
Cytokeratin Pan (4, 5, 6, 8, 10, 13, 18)# 1779	363736	312702	404635	291435	406410	358419	258987
DUSP6 (MKP3, MKP-3, PYST1)# 1754	2492	551	224	2026	2146	2599	1970
E-Cadherin - phosphoSer838/Ser840# 0203	19318	23404	19064	22698	19421	18074	20875
E-Cadherin# 0742 neu	5501	6702	5529	7188	5389	5921	9924
E-Cadherin# 0742 Peak 2 neu	316	335	638	277	313	535	415
EGR1# 1226 neu	33.3	33.3	33.3	33.3	33.3	33.3	33.3
Elk-1 - phosphoSer383# 1826	195	353	190	315	169	259	196
Elk-1 - phosphoSer383# 1826 Peak 2	445	380	1870	348	181	1130	480
Elk-1# 2160	571	560	751	573	540	692	525
Erk1/2 (MAPK p44/42) # 1718	30147	25064	30266	24581	26715	29352	28161
Erk1/2 (MAPK p44/42) # 1718 Peak 2	9255	7301	8809	7237	7352	6275	6205
ERK1/2 (MAPK) - phosphoThr202/Tyr204# 2205	79	61	292	352	472	393	463
ERK1/2 (MAPK) - phosphoThr202/Tyr204# 2205 Peak 2	33.3	33.3	70	108	101	89	89
Ezh2# 1759	5668	4520	5038	5526	6070	6055	5211
FGF-1# 1562	33.3	33.3	33.3	33.3	33.3	67	33.3
GADD45 alpha# 1201	437	585	838	433	466	665	654
GAPDH# 2058	211879	228060	298650	240001	250832	318937	316554
Glutaminsynthetase# 0486	94163	76855	125132	84190	86033	103962	96195
GPR49 / LGR5# 1868 neu	274	242	434	289	276	462	418
GSK3 alpha/beta - phosphoSer21/Ser9BG/MP # 118	68813	50821	6379	32628	13085	5427	28572
GSK3 alpha/beta - phosphoSer21/Ser9BG/MP # 118 Peak 2	234	356	122	134	144	215	571
GSK3 alpha/beta - phosphoTyr279/Tyr216# 1714	267	427	318	294	427	360	337
GSK3 alpha/beta - phosphoTyr279/Tyr216# 1714 Peak 2	535	467	802	435	343	643	573
GSK3 beta - phosphoSer9# 2073	324	487	262	290	235	339	242
GSK3 beta - phosphoSer9# 2073 Peak 2	106	65	33.3	71	33.3	33.3	33.3
GSK3 beta# 1835	7212	5990	11542	5758	5351	9044	8084
Ha-ras# 2135	640	629	759	609	608	669	757
Her2# 1063	1078	873	1223	881	1063	779	593
Histone H3 - phosphoSer10# 1610	163422	173866	1619	117399	132103	58197	43975
HSP 27 - phosphoSer15# 0208	723	1096	672	483	1238	790	822
IDH1 (Isocitrate dehydrogenase [NADP] cytoplasmic)# 1316	4614	5720	9759	6198	4613	7296	5712
IGFBP-1# 1084	21528	13859	43198	14918	19342	27326	20199
Jak 1TK # 071	11267	6403	4047	5351	2152	6473	6179
Jak 1TK # 071 Peak 2	278	240	324	286	285	389	357
JNK/SAPK 1/2/3 - phosphoTyr185/Tyr223# 0215	214	211	155	184	292	136	159
MCM2# 2125	40255	36309	41336	39602	45183	50244	45647
MEK 1# 1790	3329	2226	2712	2450	2642	3522	1415
MEK1/2 - phosphoSer217/Ser221# 1720	970	3863	3316	503	435	339	244
MEK2# 1789	2149	1466	3023	1406	1679	2323	986
MEKK3# 0255	142	176	221	136	156	179	128
mTor - phosphoSer2448# 2374	849	734	279	604	889	386	681
mTOR (FRAP)- phosphoSer2481# 0386	33.3	33.3	51	33.3	33.3	33.3	33.3
mTOR (FRAP)# 1911	1150	980	1430	805	1259	1346	2721
NDRG1 - phosphoThr346# 1181	1188	1416	3152	1050	796	1033	927
p38 MAPK - phosphoThr180/Tyr182# 1223	517	836	284	493	398	339	328
p38 MAPK# 0350	390	425	361	503	475	448	427
p53 - acetylLys305# 1274	33.3	33.3	33.3	33.3	33.3	33.3	33.3
p53 # 2123	5384	7305	7071	5420	8583	5912	7728
p70 S6 kinase# 1566 neu	4544	3542	4642	4538	5094	4758	4547
PAK 4/5/6 - phosphoSer474/Ser602/Ser560# 1495	997	892	1679	613	711	1053	848
PARP - cleavedAsp214# 1044	33.3	94	170	94	67	106	133
PARP# 1914 neu	4677	6142	6269	6680	8040	6075	7677
PI3-kinase p110 beta# 1049	613	645	830	793	810	795	692

PI3-kinase p85 alpha# 1967	117	154	200	173	151	109	138
PI3-kinase p85TK # 017	670	742	684	736	689	581	719
PP2A C - phosphoTyr307# 2170 neu	1200	33.3	277	33.3	692	516	298
PTEN - phosphoSer380# 1045	568	534	1446	447	629	839	872
PTEN - phosphoSer380# 1045 Peak 2	590	537	851	492	445	760	694
PTEN# 1770	2450	1945	4267	1700	2283	2610	2617
PTEN# 1770 Peak 2	2160	1666	2140	1705	1468	1802	1642
Ras# 1719	1482	1548	5795	1414	1397	2033	2188
Rb - phosphoSer807/Ser811# 1270	5178	6134	548	6124	6204	3648	3769
RbBG/MP # 046	1733	2620	1152	3108	2618	1800	1827
RSK 1 (p90RSK) - phosphoThr573# 1235	124	177	440	122	139	605	481
RSK 1 (p90RSK) # 0246 neu	2117	2727	3541	2868	3090	2895	3031
S6 ribosomal protein - phosphoSer235/Ser236# 0442	24452	10907	2069	15178	18962	21903	9227
S6 ribosomal protein - phosphoSer240/Ser244BG/MP # 055	46358	20966	3751	31244	32679	44709	18310
S6 ribosomal protein# 1836	29927	11613	19443	11875	15023	18258	9737
SHP-2# 0239	2839	2752	4106	3065	3042	3891	3435
Smad1/5 - phosphoSer463/Ser465# 2590	1364	2422	1628	2881	2504	1847	2176
Smad1# 0955	2322	2263	2887	1908	2580	2275	2056
Smad2 - phosphoSer245/Ser250/Ser255TK # 101	352	870	84	806	723	448	471
Smad2/3 - phosphoSer465/467 (Smad2) Ser423/425 (Smad3)# 2591	34	99	33	33	33	33	310
Smad2/3 - phosphoSer465/467 (Smad2) Ser423/425 (Smad3)# 2591 Peak 2	33	33	33	33	33	543	467
Smad2# 1530	2072	2039	2525	2088	2767	2365	1972
Smad3# 1553	309	293	508	270	349	379	473
SMAD4# 1552	2419	1951	2467	2330	2064	2493	2829
Smad5# 0954	191	129	111	122	234	130	192
Smad9 (Smad8)# 0916	4006	1939	4173	2527	878	1481	1134
SPRY1 (Spry-1, Sprouty 1)# 0415	155	147	199	184	178	210	294
SPRY2 (Protein sprouty homolog 2)# 0342	5574	3982	4021	6235	5177	4497	5278
SPRY3 (Spry-3, Sprouty 3)# 1723	71566	57694	82575	58696	60829	72850	61819
Src - phosphoTyr527# 1949	20243	24605	19924	24849	26101	19606	21580
STAT 1# 1186	434	560	733	652	630	692	788
STAT 3 alpha# 1207	6592	7339	11554	8232	7779	8750	9767
STAT 3# 1818	2232	2526	4461	2897	2742	3202	3593
STAT 5 alpha# 1245	390	405	1266	548	383	450	571
STAT 5# 1780	378	377	513	405	310	399	381
TCF1# 1673	3616	3035	3989	2446	2039	3600	3145
TCF4# 1641	18011	11229	4609	6977	2278	8764	5487
TwistBG/MP # 064	4007	3369	5658	2487	3372	4406	2270
Vimentin# 1814	406	263	244	306	306	249	305
Wnt3A# 0741	2028	2599	5048	2577	2508	3004	1845
Wnt3A# 0741 Peak 2	4059	2248	11116	2332	2975	5613	5709
zzstrep	4003681	2579963	4408047	2307196	2730657	3337418	2590807

Suppl. Table 11: Raw data of the DigiWest® experiment - clone C.

Relative intensity unit of each analyte tested for clone C, which was treated with trametinib [0.03 µM] and DMSO [0.03%] for 0.5 h, 6 h and 24 h.

Analyt	**Trametinib 0.5 h**	**Trametinib 6 h**	**Trametinib 24 h**	**DMSO 0.5 h**	**DMSO 6 h**	**DMSO 24 h**	**Medium only 24 h**
Akt - phosphoSer473# 2072	33.3	33.3	33.3	33.3	33.3	33.3	33.3
Akt# 2082	4361	5501	5059	5196	4277	4538	5023
Akt1# 1364	599	631	852	680	33.3	587	762
Akt2 - phosphoSer474# 2020	33.3	33.3	33.3	33.3	33.3	33.3	33.3
Akt3# 1365	33.3	33.3	33.3	33.3	33.3	33.3	33.3
Annexin II# 0504	10652	11640	10769	11737	11206	8538	11763
APCTK # 025 neu	33.3	33.3	33.3	58	69	33.3	33.3
Aurora A (AIK)	1787	2602	136	1876	2352	1046	950
Aurora A/B/C - phosphoThr288/Thr232/Thr198	160	143	33	442	101	33	33
Aurora B (AIM1)	2160	2549	116	2327	2650	1103	1283
Axin1# 1683 neu	127	157	148	127	193	194	212
Axin2 (Conductin)# 0956 neu	164	110	101	116	235	138	171
b-Raf - phosphoSer445# 1171	1167	1011	791	952	1331	1027	1191
Bcl-xL# 1819	12494	9961	12759	10065	11436	8213	10225
Bcl2# 1821	563	559	934	375	657	444	893
beta-Actin# 2104	241380	242405	246532	247192	255622	242405	268561
beta-Catenin - phosphoSer552# 1862	294	315	52	686	460	131	267
beta-Catenin - phosphoSer552# 1862 Peak 2	293	186	33.3	479	375	89	111
beta-Catenin - phosphoSer675# 2091	3661	4552	3833	6169	6020	3961	5171
beta-Catenin - phosphoSer675# 2091 Peak 2	2941	2849	3792	2892	3772	2808	2848
beta-Catenin (non-pospho Ser33/37/Thr41; active) # 1356	3519	2955	3037	2335	5936	2786	2521
beta-Catenin# 1822	44186	47831	44616	51464	61102	51805	60182
beta-Catenin# 1822 Peak 2	22138	19903	25831	20622	28353	24711	24997
Bmi1# 1457	9322	8116	8457	8004	8595	6660	7408
BMP4# 0936	727	1057	1600	669	696	1153	1660

c-Jun - phosphoSer63# 1948	100	477	274	153	89	84	90
c-myc - phosphoThr58/Ser62# 1240	577	209	259	530	469	551	735
c-myc# 1717	6138	4470	2145	6833	10498	3919	4555
c-Raf - phosphoSer259# 1190	3875	4061	2156	6263	2768	1502	2146
c-RafTK # 029	525	481	314	469	464	334	431
C/EBP beta - phosphoThr235# 1183	33.3	64	33.3	73	86	33.3	33.3
C/EBP beta - phosphoThr235# 1183 Peak 2	33.3	33.3	33.3	33.3	33.3	33.3	33.3
Caseinkinase 1 epsilon# 0340	52	105	184	33.3	85	33.3	52
Caspase 3# 1996	21927	22582	18169	20080	22710	17936	18643
Caspase 8BG/MP # 074	221	232	174	262	253	131	122
Caspase 8BG/MP # 074 Peak 2	171	33.3	33.3	117	33.3	33.3	65
Caspase 9# 1551	1974	1737	2468	1592	1858	1693	2055
Caspase 9# 1551 Peak 2	785	932	925	671	897	801	861
CD133# 0460	1126	907	1619	1190	1158	1296	1858
CD44# 0439 neu	33.3	33.3	127	33.3	33.3	142	90
CDKN2B (p15 INK4B, CDN2B, MTS2)# 2142	33.3	33.3	33.3	33.3	33.3	33.3	33.3
Cyclin B1# 1243	14349	14461	634	23863	16074	9250	11443
Cytokeratin 18 (DC10)# 1122	245992	158708	178464	257561	198821	137939	154342
Cytokeratin 19# 0473	51882	71718	54550	32055	94613	47780	51042
Cytokeratin 8 - phosphoSer23# 0217	182249	142549	143175	121004	133457	123132	157715
Cytokeratin 8/18# 1208	37988	16267	24352	43365	20667	14061	18741
Cytokeratin Pan (4, 5, 6, 8, 10, 13, 18)# 1779	361610	220934	235953	376650	263063	193380	210714
DUSP6 (MKP3, MKP-3, PYST1)# 1754	1137	336	115	1177	1655	1367	1587
E-Cadherin - phosphoSer838/Ser840# 0203	12724	16907	20578	16479	15411	15568	16711
E-Cadherin# 0742 neu	3053	3946	6435	3633	4357	4621	4773
E-Cadherin# 0742 Peak 2 neu	290	236	573	262	228	248	548
EGR1# 1226 neu	33.3	33.3	33.3	33.3	33.3	33.3	33.3
Elk-1 - phosphoSer383# 1826	268	180	171	225	223	33.3	33.3
Elk-1 - phosphoSer383# 1826 Peak 2	412	367	364	33.3	439	327	378
Elk-1# 2160	495	561	593	486	561	638	706
Erk1/2 (MAPK p44/42) # 1718	26967	29247	28254	27993	26059	22553	29093
Erk1/2 (MAPK p44/42) # 1718 Peak 2	6347	5901	2413	5627	5988	6336	4884
ERK1/2 (MAPK) - phosphoThr202/Tyr204# 2205	68	86	217	216	333	385	272
ERK1/2 (MAPK) - phosphoThr202/Tyr204# 2205 Peak 2	33.3	33.3	33.3	80	90	63	61
Ezh2# 1759	5517	3791	2868	5136	5620	4351	5000
FGF-1# 1562	76	33.3	33.3	79	33.3	101	85
GADD45 alpha# 1201	372	649	681	422	331	701	714
GAPDH# 2058	186130	198927	195132	206877	250052	193737	246089
Glutaminsynthetase# 0486	98910	101560	96694	96944	106539	92736	103484
GPR49 / LGR5# 1868 neu	320	193	286	286	211	381	288
GSK3 alpha/beta - phosphoSer21/Ser9BG/MP # 118	45827	23113	786	9129	16342	2209	5004
GSK3 alpha/beta - phosphoSer21/Ser9BG/MP # 118 Peak 2	176	220	359	674	197	163	266
GSK3 alpha/beta - phosphoTyr279/Tyr216# 1714	321	411	310	682	384	360	418
GSK3 alpha/beta - phosphoTyr279/Tyr216# 1714 Peak 2	449	569	759	473	527	815	836
GSK3 beta - phosphoSer9# 2073	348	335	376	906	221	94	296
GSK3 beta - phosphoSer9# 2073 Peak 2	81	63	33.3	233	33.3	58	74
GSK3 beta# 1835	6148	6794	9391	5679	6703	10038	10644
Ha-ras# 2135	575	575	498	528	491	509	541
Her2# 1063	512	429	899	396	482	449	514
Histone H3 - phosphoSer10# 1610	137297	145443	661	148981	137196	14813	27289
HSP 27 - phosphoSer15# 0208	867	1305	890	2177	450	351	816
IDH1 (Isocitrate dehydrogenase [NADP] cytoplasmic)# 1316	7661	10345	10695	6479	7862	10136	11913
IGFBP-1# 1084	11873	11631	28886	8721	13302	18827	27670
Jak 1TK # 071	5157	5621	6958	436	6897	7109	6982
Jak 1TK # 071 Peak 2	287	244	271	298	266	212	328
JNK/SAPK 1/2/3 - phosphoTyr185/Tyr223# 0215	294	380	112	529	196	252	245
MCM2# 2125	31520	36699	33561	40752	47536	41284	45853
MEK 1# 1790	2825	3010	1948	2080	2355	3311	3473
MEK1/2 - phosphoSer217/Ser221# 1720	472	3058	3206	1019	451	189	240
MEK2# 1789	1566	1766	1726	1068	1682	1921	2629
MEKK3# 0255	110	124	102	138	99	125	165
mTor - phosphoSer2448# 2374	363	390	205	669	666	105	258
mTOR (FRAP)- phosphoSer2481# 0386	33.3	33.3	33.3	33.3	33.3	33.3	33.3
mTOR (FRAP)# 1911	497	707	1013	821	778	382	1231
NDRG1 - phosphoThr346# 1181	718	1117	2565	1333	696	1933	1349
p38 MAPK - phosphoThr180/Tyr182# 1223	638	858	490	3474	395	323	448
p38 MAPK# 0350	375	425	348	402	427	326	377
p53 - acetylLys305# 1274	33.3	33.3	33.3	55	69	33.3	33.3
p53 # 2123	11737	11226	10400	18659	8878	11224	11236
p70 S6 kinase# 1566 neu	5532	5294	4711	6194	5944	5204	5310
PAK 4/5/6 - phosphoSer474/Ser602/Ser560# 1495	618	512	1263	584	432	733	785
PARP - cleavedAsp214# 1044	70	87	125	56	98	76	101
PARP# 1914 neu	2543	4199	5338	5368	6407	4892	5694
PI3-kinase p110 beta# 1049	895	999	903	953	794	855	937
PI3-kinase p85 alpha# 1967	110	133	114	151	133	120	33.3
PI3-kinase p85TK # 017	654	669	528	653	840	626	568
PP2A C - phosphoTyr307# 2170 neu	2107	33.3	552	33.3	33.3	477	576
PTEN - phosphoSer380# 1045	569	597	1117	824	553	980	902

PTEN - phosphoSer380# 1045 Peak 2	534	440	717	509	462	660	815
PTEN# 1770	2296	2038	3012	2886	2268	2487	2352
PTEN# 1770 Peak 2	1809	1329	1646	1440	1623	1695	1890
Ras# 1719	1033	1037	3254	867	1184	1145	1456
Rb - phosphoSer807/Ser811# 1270	4238	4492	402	7977	5405	1788	2499
RbBG/MP # 046	1552	2332	1018	3625	3720	1419	1611
RSK 1 (p90RSK) - phosphoThr573# 1235	52	97	218	280	131	229	248
RSK 1 (p90RSK) # 0246 neu	2267	1741	2226	1847	2063	1988	2202
S6 ribosomal protein - phosphoSer235/Ser236# 0442	13572	2384	421	20332	12542	6215	11032
S6 ribosomal protein - phosphoSer240/Ser244BG/MP # 055	24011	4127	547	28805	22953	11798	20345
S6 ribosomal protein# 1836	11168	7115	5350	16659	11904	10814	17459
SHP-2# 0239	1632	2018	1990	2099	2230	2180	2803
Smad1/5 - phosphoSer463/Ser465# 2590	2387	3101	1559	5078	3478	1560	1864
Smad1# 0955	2476	2363	2882	3051	2091	2105	2634
Smad2 - phosphoSer245/Ser250/Ser255TK # 101	582	739	86	1156	1237	250	312
Smad2/3 - phosphoSer465/467 (Smad2) Ser423/425 (Smad3)# 2591	78	33	185	107	116	33	33
Smad2/3 - phosphoSer465/467 (Smad2) Ser423/425 (Smad3)# 2591 Peak 2	68	33	509	33	33	584	727
Smad2# 1530	1739	1797	1728	3185	2441	1581	1853
Smad3# 1553	308	357	559	392	304	403	504
SMAD4# 1552	1510	1364	1362	1466	2193	1386	1938
Smad5# 0954	162	194	155	287	255	141	189
Smad9 (Smad8)# 0916	1918	1185	3003	33.3	1242	737	597
SPRY1 (Spry-1, Sprouty 1)# 0415	62	106	84	76	110	153	194
SPRY2 (Protein sprouty homolog 2)# 0342	4511	5229	3589	4095	4937	4402	7031
SPRY3 (Spry-3, Sprouty 3)# 1723	46460	43295	59998	45078	46010	40658	48257
Src - phosphoTyr527# 1949	23960	29119	27538	28377	20590	20457	23772
STAT 1# 1186	450	423	417	435	535	510	533
STAT 3 alpha# 1207	10624	10408	13360	10171	8362	9208	10286
STAT 3# 1818	3690	3453	5081	3872	2782	3446	3929
STAT 5 alpha# 1245	916	806	1230	823	681	763	787
STAT 5# 1780	484	383	419	350	334	340	325
TCF1# 1673	1903	1803	1996	1363	2485	1725	2206
TCF4# 1641	7189	7265	12211	351	9138	9309	10555
TwistBG/MP # 064	3406	3026	4869	3342	2565	4913	7138
Vimentin# 1814	360	380	265	291	367	339	252
Wnt3A# 0741	3635	4778	6062	3503	3136	5227	5810
Wnt3A# 0741 Peak 2	2445	2539	7065	1750	2738	4223	5834
zzstrep	2325528	1805443	3391962	1827915	1860576	3222415	3327252

Suppl. Table 12: Mutational status of colorectal cancer PDO models and the IC_{50} values of MEK-inhibitors [µM].
SFAB-signature (SMAD4, FBXW7, ARID1A, BMPR2) (orange), RAS (blue), and BRAF (green). Mean IC_{50} values [µM] from at least 3 different experiments are shown for cobimetinib (cobi. c_{max} = 0.508 µM), trametinib (tram. c_{max} = 0.03 µM), and selumetinib (selu. c_{max} = 1.062 µM). (Indel = insertion/deletion, mut. = mutations).

Biobank ID	SMAD4	FBXW7	ARID1A	BMPR2	RAS	BRAF	Cobi. IC_{50} [µM]	Tram. IC_{50} [µM]	Selu. IC_{50} [µM]
Co-P-73	wt	wt	wt	wt	wt	wt	> 20.703	> 3.249	> 24.034
Co-P-82	wt	wt	wt	wt	wt	G466R	> 20.704	> 3.249	> 24.034
Co-P-87	wt	wt	wt	wt	G12D	wt	> 20.705	> 3.249	> 24.034
Co-P-90	wt	wt	wt	wt	wt	wt	> 20.706	> 3.249	> 24.034
Co-P-108	wt	wt	wt	wt	G12D	wt	> 20.707	> 3.249	> 24.034
Co-P-58-C	wt	wt	wt	wt	G12D	wt	> 20.708	0.189	> 24.034
Co-P-92	C499Y	wt	wt	wt	G12D	wt	> 20.709	0.180	5.288
$R4^{wt}$	wt	wt	wt	wt	G12D	wt	> 12.299	> 3.249	> 24.034
Co-P-134	I347V	wt	wt	wt	G12D	wt	5.329	0.340	2.000
Co-P-71	wt	wt	wt	wt	wt	wt	3.913	> 3.249	> 24.034
Co-P-126	wt	wt	stopgain SNV	wt	D92, K147Q	R389C	1.197	> 3.249	> 24.034
Co-P-135	I347V, A212T	wt	wt	wt	wt	wt	1.146	0.472	2.000
Co-P-74	wt	wt	wt	wt	wt	wt	0.964	0.179	3.415
Co-X-77	Y353N	wt	wt	wt	G12S	wt	0.526	0.031	> 24.034
Co-P-149-B	R361H	wt	wt	wt	G12D	wt	0.490	> 3.249	> 24.034
Co-P-93	wt	wt	wt	wt	G13D	wt	0.485	0.044	> 24.034
Co-P-100	wt	wt	wt	wt	wt	wt	0.412	> 3.249	> 24.034
Co-P-102	wt	wt	wt	wt	wt	wt	0.372	0.115	> 24.034
$R1^{R361H}$	R361H	wt	wt	wt	G12D	wt	0.356	0.014	> 24.034
Co-P-106	wt	wt	wt	wt	wt	wt	0.295	0.072	> 24.034
Co-P-91	deletion	wt	wt	wt	G13D	wt	0.234	0.045	0.787
Co-P-97	wt	wt	wt	wt	wt	wt	0.222	0.042	1.812
Co-P-132-m-PER	D493H	wt	wt	wt	wt	wt	0.221	0.106	2.000
Co-P-138-m-BRA	I347V	wt	wt	wt	wt	wt	0.207	0.015	2.000
Co-P-153	wt	wt	wt	wt	wt	wt	0.156	0.270	9.548
Co-P-98	wt	wt	Indel	wt	wt	wt	0.153	> 3.249	> 24.034

Co-P-134-m-HEP	I347V	wt	wt	wt	G12D	wt	0.151	0.131	2.172
Co-P-96	wt	wt	wt	wt	wt	wt	0.101	0.013	0.753
Co-X-37	frame-shift variant G80GX	multiple mut.	multiple mut.	multiple mut., non patho-genic	wt	wt	0.095	0.012	0.148
Co-P-149-D	wt	wt	wt	wt	G12D	wt	0.082	0.019	0.431
Co-P-78	D351Y	wt	wt	wt	wt	wt	0.081	0.004	> 24.034
Co-P-132	D493H	wt	wt	wt	G13R	wt	0.073	> 3.249	2.000
Co-P-72	wt	wt	wt	wt	wt /NRAS Q16K	wt	0.071	0.005	1.503
Co-P-58-D	wt	wt	wt	wt	G12D	wt	0.068	0.006	0.404
Co-X-69	deletion	wt	wt	wt	wt	wt	0.064	0.002	0.052
Co-P-156	K385Q	wt	wt	wt	G12S	wt	0.062	0.068	9.821
Co-P-86	wt	L594F	wt	wt	G12V	wt	0.060	0.035	0.520
Co-P-154	wt	wt	wt	wt	G13D	wt	0.056	0.080	6.697
Co-P-85	wt	wt	wt	wt	G12V	wt	0.056	0.006	> 24.034
Co-P-84	wt	wt	wt	wt	wt /NRAS Q16K	wt	0.052	0.002	0.331
Co-X-38-A	wt	multiple mut.	wt	wt	G12D	wt	0.043	0.007	0.204
Co-P-75	wt	wt	wt	wt	G12V	wt	0.043	0.005	0.322
Co-P-79	wt	wt	wt	wt	A146T	wt	0.042	0.002	0.269
Co-P-99	wt	wt	wt	wt	wt	wt	0.035	0.002	0.187
Co-X-70	wt	wt	wt	wt	G12V	wt	0.033	0.002	0.157
Co-X-41	wt	wt	wt	S775N benign	wt	wt	0.032	0.024	3.549
Co-X-44	frame-shift variant G80GX	multiple mut.	multiple mut.	multiple mut., non patho-genic	G13D, I187V	frameshift variants	0.032	0.003	0.083
Co-P-76	142_143 del	wt	wt	wt	G13D	wt	0.031	0.015	0.226
Co-P-89	wt	stopgain SNV	wt	wt	wt	wt	0.029	0.005	0.504
Co-P-155	wt	wt	wt	wt	G12D	wt	0.026	0.008	1.855
Co-P-88	wt	wt	SNV_ splicing	wt	wt	V600E	0.026	0.000	0.037
Co-P-104	wt	wt	wt	wt	G12D	wt	0.025	0.007	0.152
Co-X-38-B	wt	multiple mut.	wt	wt	G12D	wt	0.022	0.003	0.152
Co-P-157	wt	wt	stopgain SNV	wt	wt	wt	0.017	0.013	0.413
Co-X-40	wt	wt	wt	S775N benign	wt	wt	0.014	0.001	0.132
Co-P-59	wt	wt	wt	wt	wt	wt	0.013	0.002	0.016
Co-P-80	wt	G571V	Indel	wt	G12S	wt	0.011	0.001	0.048
Co-P-105	wt	R465H	Indel	wt	wt	G466V	0.009	0.002	0.084
Co-P-133-m-HEP	wt	R385H	wt	wt	G12V	wt	0.005	0.001	0.096
Co-P-133	wt	R385H	wt	wt	G12V	wt	0.005	0.001	0.043
Co-P-95	wt	wt	Indel	Indel	wt	V600E	0.002	0.000	0.027
Co-P-101	wt	wt	wt	wt	G12D	wt	0.000	0.001	> 24.034

X. SELBSTSTÄNDIGKEITSERKLÄRUNG / DECLARATION

Ich versichere hiermit, dass die von mir vorgelegte Dissertation eigenständig und ohne Benutzung anderer als der angegebenen Hilfsmittel angefertigt wurde. Ich versichere, dass alle aus anderen Quellen übernommenen Daten und Konzepte, sowie Ergebnisse aus Kooperationsprojekten unter Angabe der Referenz gekennzeichnet sind.

Außerdem versichere ich, dass mir die aktuelle Promotionsordnung der Johann-Wolfgang von Goethe-Universität Frankfurt am Main von 2015 bekannt ist und ich mich nicht anderwärts um einen Doktorgrad bewerbe, bzw. noch keinen entsprechenden Doktorgrad besitze. Diese Arbeit wurde in gleicher oder ähnlicher Form nicht einer anderen Prüfungsbehörde vorgelegt.

I hereby declare that I have prepared the submitted dissertation independently and without the aid of other than the stated aids. I assure that all data and concepts taken from other sources, as well as results from cooperative projects, are marked with the reference.
Furthermore, I affirm that I am aware of the current doctoral regulations of the Johann-Wolfgang von Goethe-University Frankfurt am Main of 2015 and that I am not applying for a doctoral degree elsewhere or do not yet hold a corresponding doctoral degree. This thesis has not been submitted in the same or similar form to any other examination authority.

Frankfurt am Main, den 13.12.2021

_____

Ulrike Pfohl

XI. CURRICULUM VITAE

For data protection reasons, the *curriculum vitae* is not included in the online version.

XII. PUBLICATION LIST

Patent

Verfahren zur Bestimmung, ob eine Behandlung einer Krebserkrankung begonnen oder fortgesetzt werden soll, ein Biomarker, der mindestens einem Markergen entspricht, und eine Verwendung des Biomarkers in dem erfindungsgemäßen Verfahren

Ulrike Pfohl, Jürgen Loskutov and Christian Regenbrecht
received on 4th March 2021 (Nr. DE10 2020 102 143 B3)
https://register.dpma.de/DPMAregister/pat/basis
International Patent application is submitted and in process

Journal articles

A RAS-Independent Biomarker Panel to Reliably Predict Response to MEK Inhibition in Colorectal Cancer
Ulrike Pfohl, Jürgen Loskutov, Sanum Bashir, Ralf Kühn, Patrick Herter, Markus Templin, Soulafa Mamlouk, Sergei Belanov, Michael Linnebacher, Florian Bürtin, Marcus Vetter, Christoph Reinhardt, Lena Wedeken and Christian R. A. Regenbrecht
Cancers 2022, https://doi.org/10.3390/cancers14133252

Context Matters – Why We Need to Change from a One Size Fits All Approach to Made-To-Measure Therapies for Individual Patients with Pancreatic Cancer
Sushmitha Sankarasubramanian**, Ulrike Pfohl,** Christian R. A. Regenbrecht, Christoph Reinhard, and Lena Wedeken
Frontiers 2021, https://doi.org/10.3389/fcell.2021.760705

Precision Oncology Beyond Genomics: The Future Is Here - It Is Just Not Evenly Distributed.
Ulrike Pfohl, Alina Pflaume, Manuela Regenbrecht, Sabine Finkler, Quirin Graf Adelmann, Christoph Reinhard, Christian R. A. Regenbrecht and Lena Wedeken
Cells 2021, 10, 928. https://doi.org/10.3390/cells10040928

Congress participation

07/05/2019	**Speed Lecture Award XVII. BIONNALE 2019, 1st place** Berlin, Germany "*Taming the beast – What we have learned from patients*"
29/03 – 03/04/2019	**Oral presentation at AACR 2019** Atlanta, USA "*Modulating chemoresistance: Uncovering the role of mutant SMAD4^{R361H} in colorectal cancer using PDO and PDX models*"
21/01 – 22/01/2018	**Oral presentation at 33th German Cancer Congress 2018** Berlin, Germany "*Induced SMAD4 mutation in human colorectal organoids using CRISPR-Cas9-mediated engineering*"

XIII. **PATENT CERTIFICATE**

Bundesrepublik Deutschland

Urkunde

über die Erteilung des
Patents Nr. 10 2020 102 143

Bezeichnung:
Verfahren zur Bestimmung, ob eine Behandlung einer Krebserkrankung begonnen oder fortgesetzt werden soll, ein Biomarker, der mindestens einem Markergen entspricht, und eine Verwendung des Biomarkers in dem erfindungsgemäßen Verfahren

IPC:
C12Q 1/6886

Inhaber/Inhaberin:
Cellphenomics GmbH, 13125 Berlin, DE

Erfinder/Erfinderin:
Regenbrecht, Christian, Dr., 13125 Berlin, DE; Pfohl, Ulrike, 13125 Berlin, DE; Loskutov, Jürgen, Dr., 13125 Berlin, DE

Tag der Anmeldung:
29.01.2020

Tag der Veröffentlichung der Patenterteilung:
04.03.2021

Die Präsidentin des Deutschen Patent- und Markenamts

Cornelia Rudloff-Schäffer

München, 04.03.2021

Den aktuellen Rechtsstand und Schutzumfang entnehmen Sie bitte dem DPMAregister unter www.dpma.de.

XIV. ACKNOWLEDGEMENT

I would like to sincerely thank Prof. Dr. Michaela-McNicoll from the Institute for Molecular Bio Science at Goethe-University Frankfurt am Main for taking over my academic supervision. I thank Prof. Dr. Ritva Tikkanen from the Justus-Liebig-University Giessen for her willingness to be my second reviewer. I thank both for the very friendly and uncomplicated communication.

I am deeply grateful to Dr. Christian Regenbrecht for taking over my lab supervision, for his support, mentorship, and his relentless interest throughout the course of investigation. Thank you for having faith in me when I joined your company CELLphenomics GmbH, for guiding me and giving me the freedom to explore new ideas and interests. Without your guidance and valuable discussions, this thesis would not have been accomplished. Moreover, I gratefully thank CELLphenomics GmbH under the direction of Quirin Graf Adelmann and Dr. Christian Regenbrecht for providing me with all I needed to contribute to cancer research, as well as for financially supporting this project, which even resulted in a patent. I thank Dr. Christoph Reinhard for helpful and stimulating discussions regarding the publication and patent.
I express my earnest gratitude to Dr. Jürgen Loskutov for his great support and cooperation on this project and patent application, his inspiring scientific discussions and for always patiently listening to me and helping me to improve. Sincere thanks go to the entire team from CELLphenomics GmbH: Alina Pflaume, Dr. Katja Herrera Glomm, Dr. Lena Wedeken, Maxine Sil'vestrov, Sushmitha Sankarasubramanian, Alex Herter and Anne-Claire Kröger, as well as to the team of ASC-Oncology GmbH: Dr. Samantha Exner, Dr. Sabine Finkler, Dr. Larissa Ruhe and Melanie Alperstaedt for their work and support in the lab, the lab management, and the always friendly working atmosphere. I also thank Manuela Regenbrecht for her ideas and suggestions from a clinical perspective and Joris Buiks for his help with the graphic design of the figures in the thesis and publication.

Heartfelt thanks go to Dr. Ralf Kühn from the Max Delbrück Center for Molecular Medicine in Berlin for accepting me as a guest and for providing his molecular biology laboratory. My very warm gratitude goes to Dr. Sanum Bashir and her unlimited support during the CRISPR experiment, which would not have been possible without her. Special thanks go to Jana Rossius, Johanna Wolf and Anja Zimmer, for their great and unlimited technical assistance and for the nice breakout time during lunch as well as to Feraye Kocaoglu and Anna Sonsala, for her administrative support at the MDC.

I thank Dr. Markus Templin and his Master student Patrick Herter from the NMI Natural and Medical Sciences Institute at the University of Tübingen for conducting the DigiWest® experiment and Dr. Christoph Sachse, Dr. Gerrit Erdmann and their team from NMI TT GmbH for the Western Blot support.

Furthermore, I would like to acknowlegde Dr. Soulafa Mamlouk and Prof. Dr. Reinhold Schäfer from the Charité Comprehensive Cancer Center for conducting the DNA Panel Sequencing and Dr. Julian Heuberger for helping in the microscope facility at Max Delbrück Center for Molecular Medicine in Berlin.

Many thanks go to Prof. Dr. med. Frauke Alves and her team from the Translational Molecular Imaging group at the Max Planck Institute of Experimental Medicine in Göttingen, especially Dr. Joanna Napp and Dr. Fernanda Ramos-Gomes for helping me with live cell and high-resolution imaging.

I thank very much Dr. Sergei Belanov from the Institute of Biotechnology at the University of Helsinki for RNA sequencing analyses.

Thanks to Dr. Michael Linnebacher and Said Kdimati from the Molecular Oncology and Immunotherapy at the University Medicine Rostock for performing the in vivo *experiments as well as providing me with fresh frozen tumor material.*

I am thankful to Dr. Jens Hoffmann and Prof. Dr. Wolfgang Walther from Experimental Pharmacology and Oncology Berlin-Buch GmbH for their financial support at the beginning of my PhD and their allowance to participate in congresses. I thank the ABINEP International Graduate School funded by the European Structural and Investment Funds (ESF) under the program "Sachsen-Anhalt WISSENSCHAFT Internationalisierung" for a 1-year financial support. I would also like to thank Prof. Dr. Dr. Johannes Haybäck, who was my academic supervisor during that time.

Special thanks go to my former colleagues and friends – Dr. Alessandra Silvestri and Dr. Guido Gambara, who kept the team spirit and exceptionally nice and relaxed atmosphere full of helping hands and ideas. I thank my friends Dr. Magdalena Paterka and Dr. Diana Shah who proofread my thesis and always encouraged me.

I cannot miss to thank all my awesome friends for always being the best motivation and their unlimited support and tolerance during the up and downs of my PhD thesis.

Last but most importantly, I would like to thank my family and my husband Julius Pfohl - I am blessed with their unconditional love. I am eternal grateful for their patience and support these past couple of years. Words will never be enough to express my entire gratefulness! This thesis could not have been completed without your faith and constant encouragement. Thank you!